A minerals research contract report
September 1983

CONTAMINATION OF GROUND AND SURFACE WATERS BY URANIUM MINING AND MILLING

Contract J0295033
University of Colorado

Volume III: Experimental Studies & Analytical Procedures

BUREAU OF MINES
UNITED STATES DEPARTMENT OF THE INTERIOR

50272-101

REPORT DOCUMENTATION PAGE | 1. REPORT NO. | 2. | 3. Recipient's Accession No.

4. Title and Subtitle

Contamination of ground and surface waters due to uranium mining and milling. Vol. III. Experimental studies and analytical techniques.

5. Report Date: September 15, 1983

6.

7. Author(s) D.D. Runnells, C.N. Gerlitz, A. Davis, R.D. Lindberg, R. Meglen, G. Swanson, L. Taylor, R. Sistko, R. McNelly

8. Performing Organization Rept. No.

9. Performing Organization Name and Address

University of Colorado, Department of Geological Sciences, Boulder, 80309, and Center for Environmental Sciences, Denver, 80202.

10. Project/Task/Work Unit No.

11. Contract(C) or Grant(G) No.

(C) J0295033

(G)

12. Sponsoring Organization Name and Address

U. S. Bureau of Mines
Columbia Plaza
2401 E Street, NW
Washington, DC 20241

13. Type of Report & Period Covered: Final: July 25, 1979-September 14, 1981.

14.

15. Supplementary Notes

16. Abstract (Limit: 200 words)

This study focused on the chemical reactions between uranium tailings fluids and cores of subjacent bedrock from the site of the Cotter Corporation uranium mill at Canon City, Colorado. Actual and synthetic tailings fluids were forced through cores of bedrock. The pH of the effluent solutions was the dominant control on the behavior of dissolved species in solution. The pH depended on the presence or absence of calcite cement in the rocks. Calcite neutralized acidic raffinates and caused the precipitation of iron, manganese, aluminum, and possibly uranium. Chloride, sulfate, and sodium were not retarded upon passage through the cores, and sulfate and chloride should be useful as tracers of escaping tailings fluids. Zinc, copper, cobalt, nickel, uranium, and vanadium exhibited high mobility under acidic conditions and were strongly retarded at elevated pH. Calcium was released due to dissolution of calcite and ion-exchange. Magnesium was not retarded in concentrated solutions, but showed moderate retardation in dilute fluids. Potassium and ammonium both showed early retardation followed by breakthrough and mobility. The behavior of molybdenum was strongly dependent on pH, with retardation at low pH and mobility at elevated pH. Selenium was highly mobile under all conditions. Selenium should be a better tracer than molybdenum for many situations. Precipitation of carnotite appears to control the solubility of uranium and, possibly, vanadium. With the exception of the precipitation of aluminum and silica, all reactions were rapid.

17. Document Analysis a. Descriptors

uranium mill tailings, uranium ores, geochemistry, milling waste, waste disposal

b. Identifiers/Open-Ended Terms

ground water, uranium mining, uranium milling, analytical techniques, analysis

c. COSATI Field/Group 8D, 7E

18. Availability Statement: Release unlimited

19. Security Class (This Report): Unclassified

21. No. of Pages: 229

20. Security Class (This Page): Unclassified

22. Price

FOREWORD

This report was prepared by the Department of Geological Sciences, University of Colorado at Boulder, and the Center for Environmental Sciences, University of Colorado, Denver, under USBM Contract Number J0295033. The contract was initiated under the Minerals Environmental Technology Program. It was administered under the technical direction of the Twin Cities Research Center with Daryl R. Tweeton as Technical Project Officer. R.J. Simonich was the contract administrator for the Bureau of Mines. This report is a summary of the work completed as a part of this contract during the period July 25, 1979 to September 14, 1981. Additional work, carried out after the official termination date of the contract, is also summarized in this report. This report was submitted by the authors on September 15, 1983.

No patentable features are included in this report.

The authors thank the personnel of Cotter Corporation, W.A. Wahler and Associates, and the Colorado Department of Health for invaluable cooperation and assistance. The almost superhuman efforts of the personnel of the Central Analytical Laboratory, directed by Dr. Robert Meglen, are also gratefully recognized. Financial support for the computer modeling was provided by the Department of Geological Sciences of the University of Colorado and by John Lankenau and Jim Babcock of Rocky Mountain Energy Corporation.

TABLE OF CONTENTS

LIST OF FIGURES

LIST OF TABLES

INTRODUCTION

Proper handling of tailings and liquid wastes from uranium mining and milling is necessary in order to minimize the impact of potential contaminants upon natural waters. Proper containment is dependent on an understanding of the relationship between the dissolved species and the geochemical environment.

In this study we utilized laboratory experiments and computer models to investigate the interaction between uranium tailings fluids and natural geologic substrates. Our study focused on fluids and subjacent bedrock from the uranium mill operated by Cotter Corporation at Canon City, Colorado. We investigated the chemical reactions that may take place between uranium tailings fluids and bedrock, with special emphasis on the parameters of pH, ionic strength, and bedrock mineralogy. The parameter of Eh was considered only superficially. Our study materials included samples of tailings fluids from active and inactive ponds at Canon City, fresh raffinate from the mill circuit at Canon City, synthetic tailings fluids, and samples of bedrock cores taken from observation wells that were drilled at the site. Eight sampling trips were taken to Canon City during the course of the study. All of the trips were done in cooperation with personnel of Cotter Corporation or their consultants. One trip also involved personnel from the State of Colorado and the Nuclear Regulatory Commission. Our primary objective was to characterize the movement of dissolved species that may be released from a uranium tailings pond in the event of a leak or a spill. Because we worked with both acidic and alkaline tailings fluids, we believe that our results are also applicable to the excursion of fluids from in-situ mining operations. In a broader sense, the work is an attempt to analyze and model the potential mobility of important dissolved species as they interact with calcareous and non-calcareous rocks.

Laboratory experiments were compared and contrasted to modeling results from such computer programs as WATEQFC (Runnells and Lindberg, 1981), EQ3/6 (Wolery, 1979), and PHREEQE (Parkhurst, Thorstenson, and Plummer, 1980).

This report is the third volume in a three-volume set, with the overall title of Contamination of Ground and Surface Waters by Uranium Mining and Milling. Our report, Volume III, is entitled Experimental Studies and Analytical Procedures. Volume I, entitled Biological Processes for Concentrating Trace Elements from Uranium Mine Waters was published by C.G. Brierley and J. A. Brierley in November, 1981. Volume II, entitled Field Sampling and Empirical Modeling was published in December, 1981, by G. Markos and K.J. Bush. Also included in this present report is an appendix, entitled Analytical Procedures, by R. Meglen, G. Swanson, L. Taylor, R. Sistko, and R. McNelly.

Taken as a group, the three volumes in this report cover a broad spectrum of topics related to contamination of natural waters by wastes from uranium mining and milling. In Volume I, Brierley and Brierley present the results of an investigation of the removal of contaminants

from uranium mine waters by biological and sedimentological processes in a series of settling ponds at Kerr-McGee mines in New Mexico. They found that the concentrations of soluble uranium, selenium, and molybdenum were not reduced in the waste waters by passage through the mine water treatment facility. However, the particulate fraction of the uranium, selenium, and molybdenum were reduced by at least 90% upon passage through the water impoundments. The sediments in the ponds were found to be anoxic and enriched in uranium, selenium, and molybdenum. The researchers proposed that the mechanisms for removal of the metals were deposition of particulates and formation of insoluble compounds in the anoxic sediments. It was also found that adsorptive processes resulted in the accumulation of metals in the cells of algae that grow actively in the pond waters, but that this removal was at least partially reversible. The retention of uranium and molybdenum in the sediments of the ponds following the death and decay of the algae was dependent upon maintenance of anoxic conditions.

The research results presented by Brierley and Brierley in Volume I of the report have obvious potential importance in the design and engineering of treatment facilities for the prevention of environmental contamination by waste waters from uranium mines and mills.

In Volume II, Markos and Bush summarize and interpret a large quantity of data on the chemistry and mineralogy of fluids and solids in abandoned uranium mill tailings and the subjacent soils. The data were collected under the sponsorship of the U.S. Department of Energy, as part of the research associated with the Uranium Mill Tailings Remedial Action (UMTRA) Program. Most of the data utilized in Volume II are from investigations of the priority tailings sites at: Salt Lake City, Utah; Canonsburg, Pennsylvania; Riverton, Wyoming; and Grand Junction, Colorado. The data consist of field measurements and laboratory determinations of major and trace cations, dominant anions, pH, and Eh of moist solids, aqueous extracts, and waters from the tailings and surroundings. Evaluation and interpretation of the data were accomplished by using Eh-pH diagrams, various statistical methods, and equilibrium computer modeling.

The study by Markos and Bush shows that the critical areas for investigating the movement of contaminants out of the tailings piles are the interfaces between the tailings and the surrounding environment. The chemical differences at the interfaces appear to act as sinks for the contaminants. The tailings-water-soil system is extremely complex because of chemical and physical heterogeneities. The researchers conclude that pH and Eh are the most important chemical parameters involved in an understanding of the tailings-water-soil system. Neutralization of the acidic tailings fluids by calcite in the subjacent soils is of great importance, in agreement with the conclusions reached in the experimental study summarized in the present volume.

Markos and Bush also found that the most significant reaction occurring at the soil-tailings interface is the precipitation of amorphous iron hydroxides and manganese oxides because of their potential to scavenge trace metals. Also important are the direct precipitation of

compounds of uranium and aluminum and silica gels. Such precipitation is effective in immobilization of contaminants and in decreasing the pore space available for migration of fluids. These conclusions are also in complete agreement with the experiment results summarized in the present report.

The work summarized in Volume II by Markos and Bush should be of interest to a wide variety of scientists and engineers working in the area of containment and treatment of wastes from uranium mines and mills.

It is well known that many chemical, physical, and biological processes may operate in the subsurface to modify the concentrations of toxic substances in ground water (Table 1). Our laboratory studies were designed to evaluate the degree to which some of the more experimentally tractable processes in Table 1 may inhibit movement of dissolved components in tailings fluids.

Table 1. Processes that may operate in the subsurface to modify the concentrations of potential contaminants in ground water (modified from Runnells, 1976).

(1) Dilution

(2) Buffering of pH

(3) Precipitation by reaction with indigenous waters

(4) Loss of mobility due to changes in redox state

(5) Mechanical filtration

(6) Volatilization and loss as a gas

(7) Biological assimilation or degradation

(8) Radioactive decay

(9) Membrane filtration

(10) Sorption-desorption and ion-exchange

(11) Dissolution and reaction of aquifer materials

(12) Formation of complex ions in solution

Several of the processes listed in Table 1 are discussed in Volume I (Brierley and Brierley, 1981) and Volume II (Markos and Bush, 1981) of this set of reports.

Our study was not designed to study the kinetics of reactions between the tailings fluids and the test rocks. However, in some instances in the following report we do mention obvious kinetic effects. In fact, one of the most surprising results of the entire study is the rapidity of reaction which occurred between most dissolved species in the fluids and the test cores.

We attempted to exert control on the Eh of the solutions by adding sodium sulfite, by bubbling nitrogen gas through the fluids, and by adjusting the ratio of ferric to ferrous ion in acidic raffinates. Our efforts met with only limited success. The Eh conditions of our experiments were all relatively oxidizing, ranging from (+)0.32 volts to (+)0.66 volts. Additional work should be done to fully describe the role of this variable.

The initial group of eight experiments (Experiments 6, 8, 9, 14, 17, 18, 19, and 21) was designed primarily to study the behavior of the major dissolved species in acidic tailings fluids (referred to as "raffinates" in the uranium industry). The test fluids were synthetic raffinates, made up in the laboratory, either full-strength or diluted with nine parts of deionized water. A typical "recipe" for the synthetic raffinate is presented in Table 5. The major experimental variables were the pH and ionic strength of the fluids and the mineralogy of the rock cores.

During the first part of the study, attention was focused on the behavior of the following eleven dissolved species: sodium, calcium, magnesium, potassium, ammonium, molybdenum, iron, aluminum, silica, sulfate, and chloride. Five different synthetic acidic raffinates, made up to simulate actual tailings fluids, were used at various times in the study. (Not all of the results for all of the test fluids are reported here.) For some experiments the stock synthetic raffinates were diluted with nine parts of deionized water. The synthetic solutions were then forced through three different sections of core from the Poison Canyon Formation, collected from depths of 41 feet and 105 feet during the drilling of observation wells downgradient from the tailings ponds.

Dissolved sodium, sulfate, and chloride were not attenuated to any significant degree as a result of passage through the rock cores. Computer modeling (using WATEQFC-an acronym for "water equilibrium, FORTRAN, Colorado") of the equilibrium distribution of dissolved species in solution indicates that these three components are present in raffinate chiefly as free ions. Some sodium was no doubt removed as a result of ion-exchange reactions, but because of its very high initial concentrations in the influent solutions, a small amount of removal and retardation would not be detectable in our experiments. Much longer test cores would be necessary to quantitatively evaluate the removal of the abundant sodium.

Magnesium was not significantly retarded during passage of the concentrated raffinates through the rock, but in the diluted raffinates some retardation did occur. The mechanism of retardation of the magnesium is probably adsorption of free Mg^{++} ion on clays and metallic oxyhydroxides in the rock. Based on equilibrium computer modeling, the free magnesium ion predominates in diluted raffinate and is thus available for adsorption. However, in concentrated raffinate, the ion-pair $MgSO_4^o$ is also an important dissolved species and is probably not as strongly adsorbed as Mg^{++} by the clays and metallic oxyhydroxides.

Both potassium and ammonium were slightly retarded when the concentrated raffinate passed through the sandstone, and both were more strongly retarded in the diluted raffinate. This difference in behavior between dilute and concentrated solutions is to be expected from chromatographic theory, in which greater selectivity and affinity are predicted for adsorption and ion-exchange in dilute solutions.

The behavior of calcium varied from core to core. However, the acidic raffinates tend to react strongly with calcite that was present in some of the rocks, causing early "rinse-out" of calcium which was originally present in the rock itself. This rinse-out of indigenous calcium tends to mask any minor retardation of dissolved calcium from the raffinate. A gradual rise in the pH of the effluent raffinate from some of the cores indicated that some of the calcium was being released from calcium carbonate cement, but in other cores the pH remained very low throughout the experimental runs. In these latter cases we must postulate an exchange of hydrogen and sodium ions for adsorbed calcium on the surfaces of clays. Also, in two experiments in which the migrating fluid was alkaline, the concentrations of calcium in the effluent were also much higher than in the influent. Because calcite should not dissolve to any significant degree at the high pH values involved, we attribute the release of calcium from the rock under these conditions to ion-exchange with sodium in the fluids. In the results for calcium, we can identify the movement of a front of exchanged and dissolved calcium ahead of the migrating fluids, similar to the "hardness halo effect" described by Griffin and others (1976) for the migration of calcium ahead of a front of dissolved contaminants migrating out of sanitary landfills.

The behavior of dissolved iron and aluminum appears to be controlled by the prevailing pH. Above a pH of about 8, iron was significantly retarded from the raffinate, probably as a result of precipitation of amorphous iron oxyhydroxide in the pore spaces of the rock. We visually observed precipitates of iron oxyhydroxide in the pore spaces of test cores after passage of acidic tailings fluids. Similarly, in the case of aluminum, maximum retardation occurred between pH values of about 6 and 8. There is some suggestions from the data that the kinetics of precipitation of aluminum may be slow relative to the rate of flow of the test fluids. Under strongly acidic conditions, both iron and aluminum were mobile.

The movement of dissolved silica seems to be mainly a function of the original concentration in the influent fluids, perhaps influenced to some extent by the rate of flow. Significant removal of silica occurred from

solutions in which the initial concentration was high, with relatively less removal from solutions in which the initial concentration was lower.

The behavior of molybdenum is closely linked to the pH regime of the migrating fluids. The pattern of behavior of molybdenum could be due to the precipitation of a new mineral phase; however, computer modeling suggests that the precipitation of a discrete molybdenum mineral is unlikely. We suggest that the solubility of molybdenum is controlled by adsorption, and possibly coprecipitation, of molybdenum on the ferric oxyhydroxide which is precipitated in the pore spaces of the rock. The amount of molybdenum removed during passage of the solutions through the rock decreases at both high pH and low pH, in accord with accepted models of adsorption and coprecipitation of molybdenum on ferric oxyhydroxide (Kaback, 1977; Jones, 1957). In one experiment, the pH of the effluent raffinate fell from an initial value of 8 to a final value near 1.5; the resulting breakthrough curve closely resembles the curve for adsorption and coprecipitation of molybdenum from an aqueous, iron-rich solution, as reported by LeGendre and Runnells (1975). We also found that a greater proportion of dissolved molybdenum was removed from diluted raffinate than from concentrated raffinate, again reflecting the greater selectivity and affinity of exchange reactions in dilute aqueous systems. The reactivity of molybdenum casts doubt on its usefulness as a tracer of escaping tailings fluids.

The second group of experiments (Experiments 22, 23, 24, 25, 26, and 27) was designed primarily to evaluate the chemical behavior of minor and trace elements found in an acidic raffinate from the Canon City mill and alkaline decant fluids collected from the tailings ponds at Canon City. The major experimental parameters in the study of the minor dissolved species were pH, mineralogy of the bedrock, and, to a lesser extent, Eh. The minor and trace elements included the following: uranium, vanadium, selenium, manganese, cobalt, nickel, copper, and zinc.

In the minor-element study, the fluids were all collected at the Canon City mill. The acidic raffinates were collected from the tailings pond and from within the mill circuit itself, prior to discharge to the tailings pond. The alkaline fluids were collected as decant from some of the old tailings ponds near the Canon City mill. The tailings fluids were all diluted with nine parts of deionized water prior to the experimental runs reported here. A summary of the compositions of the test fluids is presented in Table 6. Six core samples, as listed in Tables 8 and 9, were used in minor-element study.

Among the minor and trace elements, uranium and vanadium showed high mobility at low pH, with greatly reduced mobility at intermediate and high pH values. The solubility and movement of uranium through the test cores seems to be controlled by the precipitation of a solid mineral phase, possibly carnotite. The retardation of vanadium may also be controlled by a solid precipitate, but the effect is less clear than in the case of uranium. Both species are probably adsorbed on metallic oxyhydroxides at high pH. Our results suggest that caution should be exercised in attempting to use either uranium or vanadium as a tracer of migrating

tailings fluids.

Selenium was highly mobile under all of the conditions of the experiments, and it may therefore be useful as a tracer of migrating tailings fluids and escaping fluids from the in-situ mining of uranium. It should be noted that our experiments were all relatively oxidizing, and we might expect selenium to be less mobile under more reducing conditions. However, Early and others (1982) have shown that at Eh values below about (-)0.05 volts, selenium is again highly soluble in the form of the HSe^- aqueous ion.

Manganese, like aluminum and iron, is highly soluble and mobile at low pH, with a suggestion of control by a solid precipitate at elevated pH.

Cobalt, nickel, copper, and zinc all show similar behavior in passage through the rock cores, with high mobility under acidic conditions and significant retardation at elevated pH. It appears that the precipitation of solid oxyhydroxides could control the mobility of all four elements at intermediate and high pH. Sorption on the surfaces of oxyhydroxides of iron, aluminum, and manganese may also be important in controlling the movement of these species under neutral to alkaline pH values.

Deionized water was forced through most of the cores prior to passage of the tailings fluids. The purpose of this pre-treatment was to pre-wet the minerals. In five such experiments, the effluent deionized water was collected and analyzed for 11 major components and for 13 trace elements. This information allowed us to estimate the level of natural contamination that might occur in a ground water simply from the passage of rain water through the rock; in other words, we hoped to be able to use the rinse-out data for pure water to estimate the background concentrations that might obtain for many dissolved species in the absence of active migration of tailings fluids. Surprisingly, the initial concentrations observed exceeded various published water quality standards for six major components and seven minor components, including sulfate, magnesium, ammonium, calcium, iron, molybdenum, manganese, lead, zinc, cadmium, chromium, arsenic, and selenium. One unknown factor in this observation is, however, the possibility that some of the samples of rock may have been contaminated by migrating tailings fluid or by contaminated drilling water before they were collected.

Because the cores were wetted with deionized water prior the experiments, there is a possibility that the clays were peptized, with a resulting decrease in hydraulic conductivity. It would certainly have been better to use native ground water for this purpose, but non-contaminated ground water was not available to us at the time of the experiments. Later, when a presumably non-contaminated sample of ground water was obtained (Table 7), it was found to be high in sodium (2650 mg/l). In addition, the tailings fluids contain very high concentrations of sodium. The presence of high concentrations of sodium in the fluids should also be expected to cause swelling and peptization of clay minerals in the rocks, similar to deionized water; this leads us to conclude that

the pre-wetting step with deionized water probably did not significantly reduce the hydraulic conductivities that would have been measured using native ground water.

In several experiments, the cores exerted a strong buffering effect on the pH of the effluent raffinate. For some cores, graphs of the pH versus volume of effluent look very much like normal acid-base titration curves. From such experiments we have found that the solubility and mobility of several of the trace elements show a strong dependency on the pH. As noted above, molybdenum is a good example, with increased mobilization at both high pH and low pH. Nickel, cobalt, zinc, and copper remain relatively immobile until the pH drops below about 4.

The chemical composition of the native ground water collected from a well that was finished at a depth of about 100 meters in an abandoned coal mine beneath the Canon City mill refutes the concept of a "deep flow path" for escaping tailings fluids. This conclusion agrees with that of Murphy and others (1983).

The project has not yet been completed. Our continuing efforts now focus on refining the use of equilibrium and mass-transfer computer models, especially PHREEQE (Parkhurst, Thorstenson, and Plummer, 1980) to predict the precipitation of the oxyhydroxides of iron, aluminum, and manganese under a variety of environmental conditions. We consider these particular solid species to be important because of their role in the adsorption and retardation of potential contaminants. We are continuing to use the data generated in this study to test and calibrate the predictive computer programs.

Scope of Study

In retrospect, it is obvious that the goals and tasks of our study were far too ambitious for the resources and time available. During the two years of the program, we conducted eight sampling trips to Canon City, characterized the chemistry and mineralogy of a wide variety of fluids and solids, designed and built a pressure apparatus for forcing tailings fluids through rock cores, obtained several thousand analytical data points for as many as 24 different species in the test fluids, and utilized three different interpretive computer programs.

Partly as a result of our overly ambitious goals, two weaknesses can readily be identified in our results. First, we did not collect the critical data required to clearly separate the effects of ion-exchange and sorption from those of precipitation and dissolution. And, second, we are not always able to define the role of kinetics in our experimental results. These two areas are deserving of additional study in the future. Our original goal was to characterize, chiefly from an empirical point of view, the overall chemical interactions that may occur between escaping tailings fluids and subjacent rocks at Canon City. Again, in retrospect, it would probably have been better for us to limit the scope of the project to the most important reactions involved in the behavior of a small suite of particularly interesting elements.

GEOLOGIC ENVIRONMENT NEAR CANON CITY URANIUM MILL

As shown on Figure 1, the uranium mill and tailings ponds of the Cotter Corporation are located 2.5 km south-southwest of the Lincoln Park section of Canon City, Colorado. Because of the close proximity of the milling complex to Canon City, much concern has been expressed, both by scientists and by the general public, about the possibility of contamination of native ground waters by seepage of tailings fluids. Unfortunately, no reliable analyses are known to exist of ground water prior to the initiation of uranium milling in the area, leaving open the question of natural background concentrations for dissolved species in the ground water (Wahler, 1978b).

The Canon City area is underlain by a thick sequence of Paleozoic, Mesozoic, and early Tertiary sedimentary rocks above a Precambrian crystalline basement complex. The geology of the area, mapped by Scott (1977), reflects the deformation and faulting which occurred in the area in conjunction with late Mesozoic and Cenozoic orogeny. The geologic relationships are summarized in the map and key of Figure 1, and the stratigraphy is summarized in Table 2.

This page deliberately left blank
(See reverse side)

Figure 1. Map Units in the Canon City study site (modified from Scott, 1977).

Qpp	Post-Piney Creek Alluvium (Holocene)
Qp	Piney Creek Alluvium (Holocene)
Ql	Louviers Alluvium (Bull Lake Glaciation)
Qs	Slocum Alluvium (Sangamon interglaciation or Illinoisian glaciation)
Qs_1	
Qs_2	
Qv	Verdos Alluvium (Yarmouth interglaciation or Kansan glaciation)
Qv_1	
Qv_2	
Qrf	Rocky Flats Alluvium (Aftonian interglaciation or Nebraskan glaciation)
Qrf_1	
Qrf_2	
Qn	Nussbaum Alluvium (Nebraskan glaciation)
Tpc	Poison Canyon Formation (Paleocene)
TKr	Raton Formation (Paleocene and Upper Cretaceous)
Kv	Vermejo Formation (Upper Cretaceous)
Kt	Trinidad Sandstone (Upper Cretaceous)
Kp	Pierre Shale (Upper Cretaceous)
	Niobrara formation (Upper Cretaceous) including:
Kns	Smoky Hill Shale Member
Knf	Fort Hays Limestone Member
Kcgg	Benton Group (Upper Cretaceous) including:
Kc	Carlile Shale
Kgh	Greenhorn Limestone
Kdp	Dakota Sandstone and Purgatoire Formation (Lower Cretaceous)
Jmr	Morrison and Ralston Creek Formation (Upper Jurassic)
Xgn	Migmatitic biotite gneiss (Precambrian X)

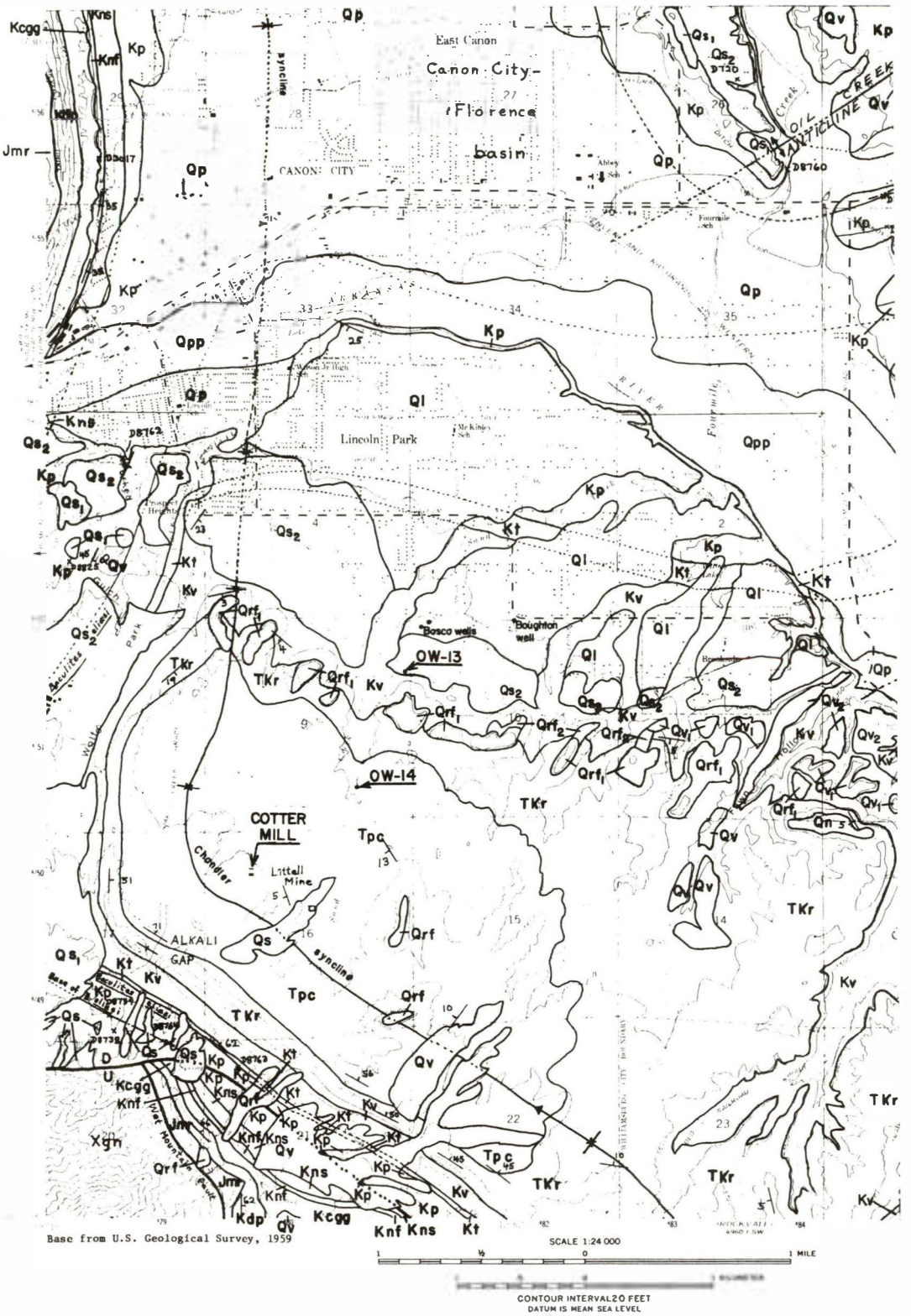

Figure 1. Map Units in the Canon City study site (modified from Scott, 1977).

Era	Period	Formation	Estimated thickness (feet)	Description
Cenozoic	Quaternary	Alluvium	---	Silt, sand and gravel along the Arkansas River and small tributaries.
		Terrace deposits	---	Mixed silt, sand, gravel and boulders above and along the Arkansas River and on nearby pediments.
	Early Tertiary	Poison Canyon	840	Yellowish-brown to medium-gray, cross-stratified sandstone and conglomerate with interbedded gray claystone and siltstone.
		Raton	240-500	Yellowish-gray, medium- to coarse-grained, cross-stratified, massive, cliff-forming sandstone; contains shaley sandstone layers.
Mesozoic	Cretaceous	Vermejo	150-750	Light gray or yellowish-orange, fine- to medium-grained sandstone and interbedded sandy shale and bituminous coal.
		Trinidad Sandstone	40-90	Light gray to yellowish-gray friable, micaceous, fine- to medium-grained, cross-stratified, cliff-forming sandstone with carbonaceous shale layers.
		Pierre Shale	3900	Olive-gray, clayey, silty, sandy shale containing bentonite beds and marine fossils.
		Niobrara	610	Smoky Hill Shale Member: fossiliferous chalk, chalky shale, shale, limestone. Fort Hays Limestone Member: gray, hard, fossiliferous, ledge-forming limestone.
		Benton Group	480	Includes the Carlile Shale, Greenhorn Limestone and Graneros Shale.
		Dakota Sandstone and Purgatoire	300	Yellowish-brown, cross-bedded, fine-grained, thin bedded sandstone (Dakota), and shale, clay and white fine- to coarse-grained sandstone (Purgatoire).
	Jurassic	Morrison; Ralston Creek	360	Varicolored siltstone, claystone, and thin beds of sandstone, limestone and conglomerate.

Table 2. Stratigraphy of the Canon City area (modified from Scott, 1977).

Samples of rock used in our laboratory studies were all obtained from drill holes, emplaced for purposes of environmental monitoring, to the north (down the ground water gradient) from the mill site (Fig. 1). The rock samples were taken from the Poison Canyon Formation and Raton Formation, both of Tertiary age, and from the Cretaceous Vermejo Formation (Table 2). These sedimentary units consist generally of arkosic sandstones interbedded with pebbly conglomerates, claystones, siltstones, and shales (Scott, 1977). Coal is locally abundant, and abandoned coal mine workings underlie the mill site.

Uranium milling operations began at the Canon City site in the late 1950's. Since that time several attempts have been made to determine the extent to which mill waters may have impacted ground waters in the area. A very complete summary of past studies is given by Murphy and others (1983). Most of the water analyses in the past studies include just a few major and minor dissolved species, making them of limited value.

In 1977 Wahler and Associates were retained by Cotter Corporation to design a new tailings impoundment and to study the problem of seepage from existing ponds. A network of drill holes and observation wells was constructed to evaluate and monitor possible seepage out of the ponds and to obtain fundamental data on the movement of ground water in the area.

Core hole data and pump tests suggest that observed large variations in quantity, occurrence, and movement of ground water at the mill site are controlled primarily by fracture permeability in the shallow Poison Canyon Formation bedrock. Measured interstitial permeabilities for Poison Canyon sandstone units are generally very low, but in the presence of fractures, field permeabilities are often several orders of magnitude higher (Wahler, 1978a). Pump tests show that fractures in the near-surface portion of the Poison Canyon Formation (upper 50 to 100 feet) allow water from overlying alluvial deposits to enter the bedrock and also provide an interconnection between individual water-bearing zones of the Poison Canyon Formation. Water-level measurements within the drill holes indicate that ground water flow is north to northeast from the mill location, and that there is a subparallel relationship between the potentiometric surface and the bedrock surface (Wahler, 1978b). The bedrock surface is essentially the present ground surface.

Early tailings ponds at the Cotter mill were unlined catchment basins which held the waste fluids from the acidic processing methods. Use of these ponds was gradually discontinued, and the tailings are now being reworked and moved to a new lined pond. An example analysis of the waste raffinate fluid contained in an old tailings pond is given in Table 3. As compared to the values in Table 3, we have obtained other analyses of fresh raffinate directly from the mill circuit at Canon City that show a pH of 1.8 and much higher concentrations of such species as Fe, Al, Mn, and Zn. The new mill at Canon City uses an alkaline circuit.

Table 3. Analysis of tailings fluid from tailings pond No. 2 at the Cotter Corporation millsite. Canon City, Colorado. All concentrations in mg/l (from non-copyrighted report by Wahler, 1978b).

Field pH	3.1	Cr	0.5
Alkalinity	<1	Co	5.2
Acidity	1,250	Cu	16
Electrical Conductivity	60,600 umho/cm	Fe	150
TDS	98,800	Mn	32
Ca	550	Pb	0.020
Mg	1,020	Hg	0.003
Na	15,000	Mo	170
K	ND	Se	14
SO_4	61,000	W	0.008
Cl	5,100	V	0.018
F	>6.6	Zn	3.3
Al	76	As	1.2
Br	24	Gross alpha	27,300 +/- 2,600 pci/l
N	200	Gross beta	17,500 +/- 900 pci/l
P	1.6	Ra^{226}	1,505 +/- 5.9 pci/l
Cd	0.042		

Sample collection date was October 22, 1975. A check of electrical balance on the above data (using WATEQFC to account for ionic speciation, such as HSO_4^-), shows an excess of anionic charge; possible explanations include analytical errors for the major ions, unknown species in solution, and unknown valence states on the elements. ND = not determined.

The analysis in Table 3 was used as a model for the laboratory preparation of the synthetic raffinates used in our experiments on major dissolved species. Mr. John Litz of Hazen Research, Golden, Colorado, suggested that for a raffinate of this pH and TDS, nitrogen should be converted to NH_4^+ and, based on the Na/K ratio of 13.6, potassium can be estimated at about 1000 mg/l; these modifications will result in an acceptable electrical balance. According to Mr. Litz, the concentration of SiO_2 is 1300-1900 mg/l for a water near 100,000 mg/l TDS, and the solution is very oxidizing, with a measured Eh in the range of 0.64-0.69 volts.

Comparison of the values in Table 3 with various drinking water standards (van der Leeden, 1975) shows that the concentrations of several species exceed recommended or permissible levels, including arsenic, chromium, copper, fluorine, iron, manganese, mercury, molybdenum, nitrogen, selenium, radium-226, gross-alpha, and gross-beta activity. The fluid is strongly acidic and contains high concentrations of sulfate and chloride.

Based on ground water analyses by Wahler and Associates in April, 1978, it was determined that plumes of anomalously high electrical conductivity, molybdenum, selenium, natural uranium, gross-alpha, and gross-beta extend northeastward from the mill (Wahler, 1978b). The probability that the old tailings ponds were the source of the potential contaminants raises important questions about the rate and direction of flow of potentially dangerous fluids in the subsurface. Specifically, what effect might the interaction with bedrock have on the composition of the migrating fluids? Might the natural aquifers, under certain conditions, afford some protection against the spread of contaminants through the rocks that underlie a leaking pond? Similarly, are some dissolved species more likely than others to be useful as tracers of escaping tailings fluids? Finally, what effect might barren aquifer rocks have on the excursion of dissolved contaminants in fluids associated with in-situ mining operations?

CHARACTERIZATION OF SUBSURFACE SOLUTE TRANSPORT

Geochemical Processes

Retardation of ionic species in solutions migrating through porous media results primarily from sorption and precipitation. These processes are, in turn, strongly influenced by acid-base equilibria, changes in redox conditions, and complexing of ions. We have used the equilibrium water chemistry computer model WATEQFC (Runnells and Lindberg, 1981) to aid us in determining the form of ions in solution and to evaluate the state of saturation of the aqueous fluids with respect to various possible solid precipitates (see the publication by Runnells and Lindberg for a discussion of WATEQFC, and Volume II of this report, by Markos and Bush, for additional examples of the use of our model). It is necessary to have such information in order to understand and interpret the observed changes in the chemistry of the uranium tailings fluids after reaction with the native bedrock. We are also utilizing a new mass-transfer program, PHREEQE (Parkhurst, Thorstenson, and Plummer, 1980), to help us predict the series of precipitation and dissolution reactions that may occur in laboratory experiments when a uranium tailings fluid passes through a sample of reactive bedrock.

Precipitation Reactions

Direct precipitation from solution, or coprecipitation within a host solid, may provide a significant retardation mechanism for some dissolved potential contaminants. Minerals and other solid compounds precipitated by interaction of tailings fluids with the bedrock substrate may also inhibit movement of potential contaminants by clogging the pore spaces in the rock. Using thermodynamic predominance diagrams, acid extraction techniques, and x-ray diffraction analyses, Markos and Bush (Volume II of this report, 1981) demonstrated the significance of precipitation reactions in the chemistry of abandoned tailings. They found that precipitated compounds of iron, manganese, aluminum, and silica are particularly important in retarding the movement of contaminants out of abandoned uranium tailings ponds.

Ion-exchange and Sorption

Krauskopf (1979) emphasizes that our present understanding of adsorption and ion exchange is based primarily on empirical observation, without a completely satisfactory theoretical basis. Because so many variables are involved, simple rules governing adsorption cannot be formulated. Some of the important variables include chemical composition of the solution and solid substrate, particle size, aging of the substrate, as well as the type and abundance of other species in solution.

Recently, a comprehensive model of the double-layer and adsorption at the oxide/solution interface has been proposed by Davis and others (1978) and by Davis and Leckie (1978, 1979, 1980). Net interactions of all species at the oxide surface are considered, as well as the effect of a change in concentration or composition of the supporting electrolyte on

the development of surface charge. These workers demonstrate that calculated results based on the model are in good agreement with experimental data for adsorption of cations, anions, and metal-ligand complexes.

Adsorption of ions may take place on all materials which make up the porous medium through which a solution moves. However, colloid-size particles (such as clays and metal oxyhydroxides) are of overwhelming importance in regulating the chemical composition of the surrounding solutions because of the large surface area of such small particles (Stumm and Morgan, 1981).

Cation exchange may be represented by the reaction:

$$y(A^{+}R^{-}) + B^{y+} = (B^{y+}R^{-}_{y}) + yA^{+} \qquad (1)$$

where R^{-} represents a negatively charged exchange substrate and A and B represent ions in solution.

A selectivity coefficient Q may be used to describe the exchange equilibrium:

$$Q_{(AR \rightarrow BR)} = (X_{BR}[A^{+}]^{y})/(X_{AR}[B^{y+}]) \qquad (2)$$

where X is the equivalent counterion fraction on the exchanger. In contrast to such thermodynamic constants as solubility products, the selectivity coefficients for ion-exchange reactions are neither constant nor well-defined. The composition of the exchanger affects the equilibrium distribution because the activities of the ions in the solid phase vary from one material to another (Stumm and Morgan, 1981). A substrate may also have more than one type of exchange site involving, for example, both specific adsorption and general electrostatic attraction (Fang and others, 1962; Garrels and Christ, 1965).

Distribution coefficient and breakthrough curves

The equilibrium distribution coefficient, kd, is an empirical parameter often used in discussions of ion-exchange reactions (Tamura, 1972):

$$kd = \frac{S}{C} = \frac{\text{mass of ion sorbed per gram solid}}{\text{mass of ion in solution per ml solution}} \qquad (3)$$

Under favorable circumstances, the velocity of chemical species dissolved in ground water, relative to the velocity of the water itself, may be approximated by employing kd in the retardation equation (Tamura, 1972):

$$V(\text{relative}) = \frac{V(\text{ion})}{V(\text{water})} = \frac{1}{1 + ((\rho/\theta)kd)} \qquad (4)$$

where θ is the porosity and ρ is the bulk density of the porous medium through which the water is flowing.

Equation (4) assumes that kd is a constant, which is generally not true under such conditions as changing water composition, variations in solid substrates, and variations in the rates of flow. Reardon (1981) has discussed some of the serious problems associated with the use of kd in predictive modeling of the transport of dissolved contaminants. However, for specific and relatively constant conditions, the use of kd is valuable and justified, as shown by Valocchi and others (1981).

Ketelle and Boyd (1947) showed that kd values may be obtained from column experiments involving frontal chromatography. In frontal chromatography a so-called "breakthrough curve" is produced when the concentration of an ion in the effluent solution, relative to the original concentration in the influent solution, is plotted against the number of pore volumes of fluid that have passed through the column (Freeze and Cherry, 1979), as shown in Figure 2. This is the type of column experiment that we used in our study.

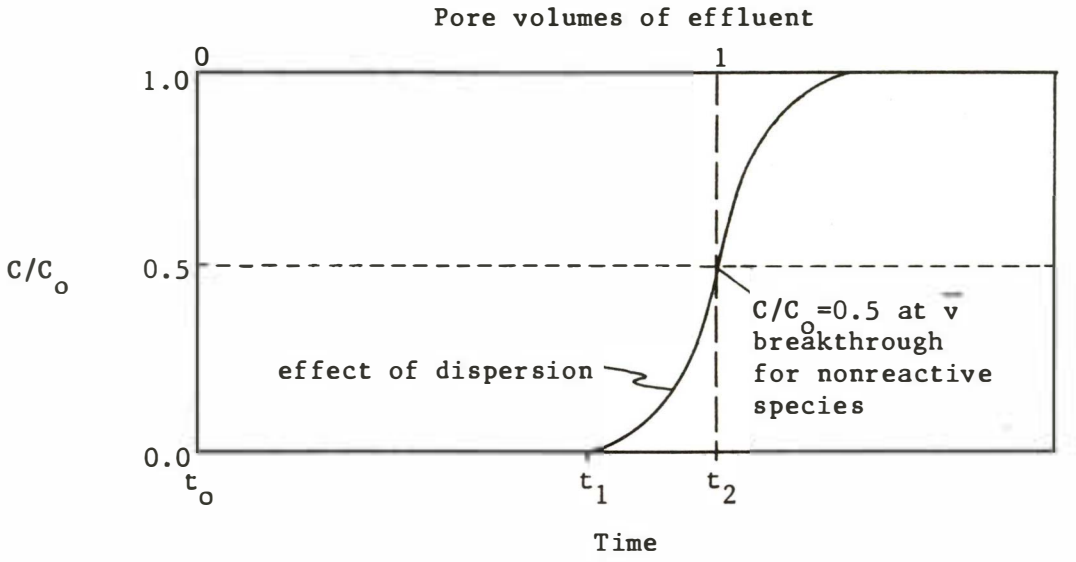

Figure 2. Typical breakthrough curve for frontal chromatography for non-reactive solute in column effluent. Vertical dashed line represents "plug-flow" in the absence of mechanical mixing and molecular diffusion (from the non-copyrighted thesis by Gerlitz, 1982).

The frontal breakthrough curve shown in Figure 2 would correspond to the continuous introduction and passage of a solute through a homogeneous, granular column, with no chemical reaction. The spreading of the observed curve away from the vertical dashed line in Figure 2 is due to mechanical mixing and molecular diffusion. Most of our experimental results are shown later in this report in the form of breakthrough curves, similar to Figure 2.

The ordinate in Figure 2 is expressed as C/Co, where C is the concentration of a dissolved species at any stage in the experiment, and Co is the original composition of the same species in the influent solution. Breakthrough is usually defined as having occurred when the value of C/Co = 0.5. Ketelle and Boyd (1947) demonstrated that the following relationship is valid for frontal chromatography:

$$kd = (V-1)(\theta / \rho) \qquad (5)$$

in which V is the number of pore volumes corresponding to C/Co = 0.5, θ is the bulk porosity of the column, and ρ is the bulk density of the column. Freeze and Cherry (1979) point out that kd properly describes partitioning between solid and liquid over a range of conditions only if the reaction is fast and reversible, and only if the corresponding adsorption isotherm is linear. Freeze and Cherry (1979) also note that if a partitioning reaction is reversible, adsorbed contaminants may be remobilized as a result of changes in the environmental conditions.

A good example of the potential usefulness of kd values (and the closely related selectivity coefficients) can be found in the work of Valocchi and others (1981). Using laboratory measurements of the selectivity coefficients and the cation exchange capacities, as well as basic hydrogeologic parameters, these workers demonstrated a remarkable agreement between their transport model and actual field data for movement of dissolved species away from the point of injection of municipal wastewaters into an alluvial aquifer near Palo Alto, California.

For our experiments involving major dissolved species (Experiments 6 through 21, Table 8), we have computed the distribution coefficients (kd values) and relative velocities of movement (RV), using Equations (4) and (5) above. A summary of the values is presented in Table 4.

Table 4. Summary of distribution coefficients (kd) and relative velocities (RV) of migration of major dissolved species in raffinate through cores of Poison Canyon Formation in selected experiments. The kd values were computed from Equation (5) in the text, and the relative velocities (RV) from Equation (4) in the text. No kd values are reported for Ca because the concentration of this component in the effluent always exceeded its concentration in the effluent. No values are given for Al because breakthrough did not occur in any of the experiments reported here, and only one value was estimated for Fe for the same reason. ND = not determined. a = approximately.

	Experiment Number											
	6-C		9-C		14-C		17-C		19-C		21-C	
Component	kd	RV	kd	RV	kd	RV	kd	RV	kd	RV	kd	RV
Na	.06	.59	0	1	.01	.91	0	1	0	1	0	1
Mg	.03	.77	0	1	ND	ND	.02	.83	0	1	0	1
K	.07	.56	.04	.67	.31	.22	.18	.37	.19	.38	.5	.71
SiO_2	.25	.25	ND	ND	>.86	<.09	ND	ND	ND	ND	0	1
Fe	ND	ND	ND	ND	a.03	ND	ND	ND	ND	ND	ND	ND
NH_4	0	1	.03	.71	.28	.24	.03	.77	.12	.5	.4	.77
Mo	.46	.16	ND	ND	.58	.13	>.85	<.11	ND	ND	0	1
Cl	a.01	a.9	0	1	ND	ND	0	1	0	1	0	1
SO_4	.09	.50	0	1	.01	.91	0	1	0	1	.1	.91

From Table 4 we see that for sodium, sulfate, and chloride, the kd values are usually near 0, indicating that these species passed through the rock cores without significant retardation. At first glance, the fact that the positively-charged sodium ion was apparently as mobile as the negatively-charged chloride and sulfate ions is surprising, possibly suggesting that the exchange sites in the rocks were initially saturated with respect to sodium. However, as shown by the typical fluid analysis in Table 3, sodium was initially present in such overwhelmingly high concentrations in the test fluids that any minor loss or retardation due to exchange with other cations initially present on the exchange sites in the rocks would not be at all obvious in the effluent solutions. In fact, as will be shown later in the report, there is very good evidence that calcium ion was initially present on the exchange sites in the rocks and was consistently displaced by sodium and hydronium ions during the experiments.

For most of the other major dissolved components (Table 4) we found a wide range of kd values, generally restricted to values less than 1, depending on the species and the particular conditions of the experiment. The wide range of kd values is particularly striking for Mo, SiO_2, and Mg.

The kd values for NH_4 and K in Table 4 both fell within a relatively narrow range of values, from about 0 to 0.8 ml/gm. As a result, the relative velocities for NH_4 and K are very similar.

From Table 4, it is also seen that neither Al nor Fe showed any significant mobility in the major-ion experiments. This is clearly the result of precipitation of solid compounds of these ions, and would result in very large apparent kd values.

Field Complexities of Geologic Materials

In a heterogeneous aquifer system, such as the sedimentary bedrock at Canon City, a number of geologic formations are layered together with a resulting change in hydraulic conductivity, K, from one unit to another. Freeze and Cherry (1979) note that variations in hydraulic conductivity larger than an order of magnitude can result from an almost imperceptible variation in the texture and size of grains in the rock. This may partially explain the variations in hydraulic conductivity which we observed in the laboratory (as listed in Table 8 later in this report). It also makes us believe that our use of deionized water, rather than native ground water, for pre-wetting the core samples probably introduced errors that are minor compared to the enormous range of hydraulic conductivities that exist in the field situation. Osiensky (1983) presents the results of a study of the escape of fluids from uranium tailings ponds in central Wyoming, with emphasis on the role played by the heterogeneities in the hydraulic conductivities of the rock units.

We measured the vertical hydraulic conductivity, Kv, in cores that were generally cut at an acute angle to the bedding planes of the rock. However, in the field, the horizontal hydraulic conductivity, Kh, may dictate the direction and rate of movement of subsurface fluids.

According to Freeze (1972), it is not uncommon for Kh to exceed Kv by two or three orders of magnitude. Fracturing of the rocks presents yet another complication in modeling the transport of solutes by ground water. Work by Grisak and others (1976) has shown that at shallow depths (less than about 1000 meters), intergranular flow is generally subordinate to fracture flow, even though intergranular voids comprise the bulk of the porosity. This suggests that the subsurface flow of tailings fluids, or the escape of fluids from in-situ mining operations, may be governed by the very high permeabilities afforded by the system of fractures. This may be the case at Canon City (Wahler, 1978b).

EXPERIMENTAL APPROACHES

Introduction

Laboratory experiments were designed to simulate the intergranular flow of a uranium tailings fluid through a sandstone aquifer. An experimental apparatus was constructed to allow us to force tailings fluids through the sections of rock core that had been collected from the observation wells at the Canon City site. A description of the apparatus is given in a later section.

The purpose of the experiments was to identify and characterize the interaction between migrating tailings fluids and the natural bedrock that underlies the Canon City millsite, with the focus of the work being on those reactions that might serve to retard the movement of potential contaminants relative to the flow of the fluid. The reactions and processes that were expected to be most important include neutralization, precipitation, dissolution, ion exchange, and sorption.

Our experiments were restricted to intergranular flow of the tailings fluids through the rocks. No attempt was made to model fracture flow. Therefore, in any extrapolation of our experimental results to a field situation, proper consideration should be given to the probability that reaction and retardation of the dissolved species due to reactions along fracture surfaces in the bedrock will certainly be less than for the intergranular flow in our laboratory studies.

Fluids Used in Experiments

Synthetic raffinates

The term "raffinate" refers to the strongly acidic solution used in some uranium mills to leach and free the uranium from the raw ore. Raffinate is essentially a concentrated solution of sulfuric acid with various chemical additives to enhance the leaching process. After contact with the uranium ore the raffinate contains a wide and variable suite of major and minor elements released during the leaching process.

For Experiments 6, 8, 9, 14, 17, 18, 19, and 21, in which the behavior of the major dissolved species was of primary interest, we made up a series of five synthetic raffinates in the laboratory, utilizing reagent-grade chemicals and sulfuric acid. The concentrations of the eleven major dissolved components were generally based on a 1975 analysis of the actual fluid from Tailings Pond No. 2 at the Canon City site (analysis in Table 3). The "recipe" used in the laboratory to synthesize a typical test raffinate is given in Table 5.

Table 5. Recipe used for making Synthetic Raffinate No. 5 (concentrated). This particular solution was used in Experiment No. 21, and it was diluted 1:9 with deionized water for use in Experiment No. 19. The reagents are listed here in the order in which they were added to the solution. After preparation, chemical analysis showed that a significant amount of silica had been lost from solution (1,200 mg/l in recipe compared to 627 mg/l by analysis).

		Resulting Concentrations	
Reagent	Grams reagent per liter solution	Component	mg/liter
NaCl	4.7325	Ca	550
KCl	1.8902	Mg	1,020
Na_2SO_4	36.8042	Na	14,694
$MgSO_4$	5.0524	K	1,100
$KAl(SO_4)_2 \cdot 12\ H_2O$	1.3186	SO_4	29,720*
$Fe_2(SO_4)_3 \cdot 5.2\ H_2O$	0.0309 } poised at Eh=0.66	Cl	5,200
$FeSO_4 \cdot 7\ H_2O$	0.7118 } volts	NH_4	259
NH_4Cl	0.6897	Al	75
$(NH_4)_6Mo_7O_{24} \cdot 4\ H_2O$	0.3129	Fe	150
$Na_2SiO_3 \cdot 9\ H_2O$	5.6761	Mo	170
$CaCl_2$ (anhydrous)	1.5232	SiO_2	1,200

Concentrated H_2SO_4 added to lower pH as desired.

*Lowering the pH by addition of concentrated sulfuric acid increased the SO_4 concentration to 31,710 mg/l by analysis, for a final pH of 3.2

A total of five synthetic raffinates were prepared. The raffinates were centrifuged and filtered through 0.8 micrometer membrane filters. The centrifugation and filtration were necessary to remove a flocculent silica-rich precipitate that formed in all solutions following the addition of the sodium metasilicate component. (Raffinate No. 2, used for Experiment No. 6, was filtered only through an 8.0 micrometer filter because of the large amount of flocculent silica present.) Chemical analyses of the first synthetic raffinate showed that about one-third of the silica originally added was removed by the clarification steps. The amount of sodium metasilicate was therefore reduced by about one-third for all subsequent formulations.

The Eh was poised at (+)0.66 volts in the synthetic stock raffinates by adjusting the amounts of ferrous and ferric salts added. Diluted raffinates were made up by adding one volume of stock concentrated raffinate to nine volumes of deionized water. Complete analyses of all test solutions, as well as additional details about the experimental procedures, can be found in the Appendices to the Master's Thesis by Carol N. Gerlitz (Gerlitz, 1982), available from the Earth Sciences Library, Department of Geological Sciences, University of Colorado, Boulder, 80309

Actual Tailings Fluids

The fluids used in the experiments on trace and minor dissolved species, Experiments 22 through 27, were collected from several different tailings ponds and the mill circuit, prior to discharge, at Canon City. The solutions were stored in sealed linear polyethylene containers in the laboratory. The containers had been previously washed with detergent, acid, and deionized water. Because the solutions were collected from systems that were open to the atmosphere and were highly saline, no special precautions were taken in the laboratory to preserve or protect them from the atmosphere. The fluids were filtered, and some were diluted as mentioned above for the synthetic raffinates, prior to use in experiments.

To lower the Eh in the tailings fluids, sodium sulfite was added. This reagent lowered the Eh by about 0.3 volts, but it also had the undesirable effect of raising the pH by nearly 4 units; the results of this treatment can be seen by comparing solutions UW-429 (treated) with UW-536 (non-treated) in Table 6. Because of the high initial values of sodium and sulfate in UW-536, the addition of the sodium sulfite did not significantly alter the original values of these components.

Table 6. Summary of initial compositions of test fluids used in minor-ion experiments, Nos. 22-27. R = raffinate collected from mill circuit. RR = same as R, but with sodium sulfite added to lower the Eh. TF = fluid from tailings ponds at Canon City. (0.1) = dilution factor, 9 parts deionized water to 1 part raw fluid.

	Experiment and Solution Number					
	22	23	24	25	26	27
	UW429	UW468	UW446	UW394	UW348	UW536
Component	(0.1RR)	(0.1TF)	(0.1TF)	(0.1R)	(0.1TF)	(0.1TF)
Fe	5.2	0.18	0.03	175	0.02	290
Mn	6.7	0.12	0.12	7.3	0.06	16
Mg	350	84	89	350	85	228
Ca	51	27	29	47	26	55
Al	0.7	1.8	1.5	310	1.4	120
Si	8.4	1.3	0.4	14	0.4	11
Na	4400	1680	1840	163	1700	689
Co	0.25	<0.03	<0.03	0.30	<0.01	0.21
Cr	<0.01	0.06	<0.02	0.27	0.04	0.22
Ni	0.32	<0.04	0.07	0.20	<0.02	0.30
Sr	0.61	0.63	0.66	0.92	0.61	0.58
V	2.5	0.84	0.78	18	0.89	22
U	<0.4	8.2	<0.8	<0.4	5.8	5.6
Mo	0.12	43	44	0.16	40	7.0
Cu	0.11	0.13	0.06	2.7	<0.06	1.8
Pb	0.14	<0.2	<0.2	0.43	<0.1	0.42
Zn	1.6	0.25	0.01	3.6	0.01	3.7
Se	0.34	0.06	<0.6	0.54	<0.3	0.15
Cd	0.03	<0.02	<0.02	0.13	<0.01	0.04
As	0.03	<0.4	<0.4	0.3	<0.2	0.4
K	78	11	12	82	10	33
NH_4	745	11.0	9.0	680	25	256
F	ND	5.1	1.4	3.2	0.8	3.6
Cl	<10.	260	290	18	245	140
SO_4	12,500	3420	3510	6760	3550	4090
pH	6.0	7.7	7.5	3.0	8.3	2.3
Eh	0.38	0.44	0.58	0.60	0.30	0.37

ND = not determined.

Native Ground Water

On November 24, 1981, in conjunction with personnel of Wahler and Associates, water samples were taken from a drillhole that penetrates the 300-foot level of an abandoned coal mine beneath the mill site. The samples were collected during a pumping test of the well. The objective of the sampling was to determine whether or not contaminants might have migrated from the tailings ponds into the water that was present in the abandoned coal mine. This particular question, concerning a "deep flow path", has often been raised about the Canon City site because of the infinite permeability that would be provided by the abandoned workings beneath the mill ponds (Wahler, 1978b).

Pumping from the 300-foot level was done with a head of 150 feet through 5-inch casing. Samples were taken after about six hours of pumping, corresponding to about six full exchanges of water in the well. Measurements of Eh and pH were made using a sealed, flow-through cell. Depending on the species of interest, the samples were either acidified with nitric or hydrochloric acid or brought back to the laboratory raw. The same day as they were collected the waters were taken to our Central Laboratory and stored at $4^{o}C$.

The results of the analysis of the ground water are given in Table 7.

Table 7. Analysis of ground water collected from 300-foot depth in test well adjacent to tailings ponds at Canon City, Colorado. The well intercepted the workings of an abandoned coal mine. All concentrations in mg/l.

Species	Concentration
Na	2650 mg/l
Ca	44
Mg	123
K	23
Sr	8.5
Si	23
Fe	372
Mn	4.4
Al	0.33
Zn	9.9
As	0.01
Th	<0.25
Cu	<0.01
Se	<0.01
Pb	<0.01
Co	<0.13
Ni	<0.02
Cd	<0.1
U	<0.37
V	<0.02
Mo	<0.03
Cl	20
SO_4	7150
NO_3	145
F	<1.0
HCO_3	ND
pH	5.5
Eh	(+)0.12 volts

ND = not determined

Examination of the values in Table 7 show that the native ground water is a relatively saline sodium-sulfate water, with an unusually low pH and distinctively high concentrations of zinc, nitrate, manganese, strontium, and iron. There is an absence of those contaminants that should be present if tailings fluids had migrated downward from the ponds and contaminated this ground water, such as molybdenum, selenium, vanadium, ammonium, and uranium. It is our conclusion that the chemistry of the water is controlled by reaction with the coal and iron sulfides exposed in the workings of the old mine, not by contamination from leaky tailings ponds. The chemistry of the water from the mine is therefore not consistent with the concept of a "deep flow path" often postulated for escaping tailings fluids at Canon City (Wahler, 1978b), in agreement with the conclusions reached by Murphy and others (1983).

Rock Cores Used in Experiments

The rock cores that were used in the experiments were collected at the site, from boxes of core stored in a small building during the drilling of Observation Well 14 (OW-14) and Observation Well 13 (OW-13). (There were actually three separate wells, 13A, 13B, and 13C, drilled just a few feet apart at site OW-13, but because the three wells were so close together the samples of rock can reasonably be considered to have come from the same drillhole.) We are grateful to Cotter Corporation, the Colorado Department of Health, and personnel of Wahler and Associates for assisting us in the selection and collection of the samples.

Samples were generally taken from the units of arkosic sandstone, rather than from the shaley beds, simply to insure that the cores would have adequate hydraulic conductivity to pass the test fluids in the laboratory experiments. We also avoided fractured or conglomeratic sections. Based on drill-logs provided by Cotter Corporation and Wahler Associates, samples were collected from the Raton, Vermejo, and Poison Canyon formations (Table 2).

Calipers were used to measure the diameters of sample cores. Cores about 10 cm long were then mounted with epoxy resin in 2-inch I.D. PVC pipe. The ends were cut at right angles to the length, and the final lengths were measured with calipers. The assemblies were then glued into PVC couplings and threaded onto the nitrogen pressure chamber.

Small pieces of core were taken adjacent to the experimental sections for determination of porosity, pore volume, and bulk density. The porosity was measured by the Kobe method of mercury injection, using a Ruska Instrument Corporation[1] apparatus.

The physical and experimental parameters of the rock cores are summarized in Table 8. Important experimental parameters corresponding to the rock cores in Table 8 are summarized in Table 9.

---

1. Reference to specific brands, equipment, or trade names in this report is made to facilitate understanding and does not imply endorsement by the Bureau of Mines.

Table 8. Summary of physical properties and sources of rock cores used in experiments.

Core site, geologic formation, and depth	Experiment number	Core length (cm)	Core cross-sectional area (cm^2)	Bulk density (g/cc)	Percent Porosity	Pore Volume (ml)	Calcite in core	Log hydraulic conductivity using test fluids
OW-14, PC, 26.4 ft.	6	4.6	17.5	2.2	19	14.9	yes	-7.1
OW-14, PC, 26.0 ft.	9	11.1	17.5	2.2	19	36.2	yes	-7.0
	8 (deionized water)							-6.1
OW-14, PC, 41.4 ft.	14	10.1	17.6	2.2	19	34.3	yes	-6.6
OW-14, PC, 104-104.3 ft.	17	9.8	17.6	2.1	22	38.0	no	-4.2
OW-14, PC, 105.2-105.5 ft.	19	9.2	17.6	2.1	24	39.4	no	-4.9
	18 (deionized water)							-4.9
OW-14, PC, 104.9-105.2 ft.	21	7.3	17.6	2.1	24	31.4	no	-6.1
OW-14, R, 508.4 ft.	22	5.0	17.4	1.9	29	24.3	no	-4.0
OW-13, V, 119 feet	23	2.7	17.4	2.1	18	8.4	yes	-4.5
OW-13, V, 68.1 ft.	24	4.7	17.4	2.1	24	19.3	no	-3.6
OW-14, R, 409 ft.	25	1.5	17.4	2.1	21	5.6	no	-3.8
OW-13, V, 118 ft.	26	4.9	17.4	2.1	18	15.4	yes	-3.1
OW-14, PC, 54 ft.	27	4.5	17.4	2.1	20	15.6	yes	-4.1

NR = not recorded. PC = Poison Canyon Formation. R = Raton Formation. V = Vermejo Formation.

Table 9. Summary of important parameters in experiments utilizing rock cores of Table 8.

Experiment number	Influent solution	Imposed nitrogen pressure (psi)	Influent pH	pH, first effluent pore volume	Final effluent pH	Eh, first effluent pore volume (volts)	Final effluent Eh(volts)	Total volume through core(ml)	Number Pore volumes through core	Length of leaching experiment (hours)	Average flow rate (ml/hr)
6	1.0 MR	29	1.1	7.6	1.4	NR	NR	216	14.6	98.5	2.2
8	DI	30	NR	NR	NR	NR	NR	662	18.3	73.3	9.0
9	1.0 MR	30	3.6	7.8	8.4	NR	NR	493	13.6	427.	1.2
14	0.1 MR	30	3.4	7.2	8.1	+0.44	+0.40	368	10.7	120.	3.1
17	0.1 MR	30	3.4	3.4	3.7	+0.66	+0.65	361	9.5	0.4	903
18	DI	15	6.0	3.4	6.8	NR	NR	509	12.9	6.6	77
19	0.1 MR	15	3.8	3.7	3.9	+0.56	+0.55	756	19.2	8.9	85
21	1.0 MR	15	3.4	3.7	3.6	+0.55	+0.55	212	6.8	35.4	6.0
22	0.1 RR	50	6.0	3.7	3.6	+0.38	+0.32	291	12.0	9.2	32
23	0.1 TF	40	7.7	8.2	8.1	+0.40	+0.47	410	48.8	6.5	63
24	0.1 TF	NR	7.5	4.5	7.5	+0.58	+0.45	415	21.5	NR	NR
25	0.1 R	5	3.0	3.2	2.9	+0.60	+0.68	117	20.9	2.3	51
26	0.1 TF	40	8.3	8.3	8.1	+0.32	+0.36	154	10.0	NR	NR
27	0.1 TF	NR	2.3	8.0	3.4	+0.37	+0.63	170	10.9	20.0	8.5

DI = deionized water. NR = not recorded. MR = synthetic major ion raffinate. R = raffinate taken from mill circuit. RR = reduced raffinate (same as R, but with added Na_2SO_3 to lower Eh). TF = tailings fluids collected from ponds in field.

The data in Tables 8 and 9 are of fundamental importance in understanding and interpreting the results of our experiments, particularly the information in the eighth column of Table 8 concerning the presence or absence of calcite cement. As will be emphasized later, the change in pH of the acidic tailings fluids as a result of reaction with calcite cement in the cores is of great importance in determining the mobility or immobility of many of the dissolved species. This observation is in complete agreement with information from field studies of abandoned tailings piles, reported by Markos and Bush (1981) in Volume II of this report. It is also important to note, from Tables 8 and 9, that the cores which lacked calcite cement usually showed the highest hydraulic conductivities and fluid flow rates. Hydraulic conductivity was measured by the falling head method for Experiments 1 through 21, and by Darcy's method for Experiments 22 through 27.

Mineralogy of rock cores

The mineralogy of a rock is of overwhelming importance in controlling the chemical behavior of potentially toxic substances dissolved in migrating fluids. Rocks which contain reactive materials, such as calcite or clay, may be effective in retarding such species, whereas in non-reactive rocks the dissolved contaminants may migrate nearly as fast as the fluids.

Thin-sections of both non-leached and leached segments of core were prepared by the Rudolf von Huene Laboratory, Pasadena, California. Some of the rocks were impregnated with blue epoxy to facilitate recognition of pores. Oil was used as a carrier in the grinding process to prevent loss of water-soluble minerals, such as gypsum.

An electron microprobe (MAC Model 400S, Department of Geological Sciences, University of Colorado) was used to analyze the perthitic feldspar and a sample of clay from a depth of 54 feet in Observation Well 14.

Experimental Procedures

The flow of tailings fluids through the bedrock cores was controlled in the laboratory by using nitrogen gas to force the liquids through core segments. The experimental apparatus, shown schematically in Figure 3, utilizes a pressure chamber and holder constructed from PVC pipe and connectors. Core segments were mounted with epoxy, cemented into threaded PVC couplings, and attached to the pressure chamber. Pressures up to three atmospheres were applied using a tank of purified nitrogen gas. At these pressures adequate amounts of fluid moved through the samples in times that were experimentally reasonable (see Table 9). In some instance, minor clay layers completely prevented flow of fluids through the cores, highlighting the potential importance of the horizontal component of hydraulic conductivity.

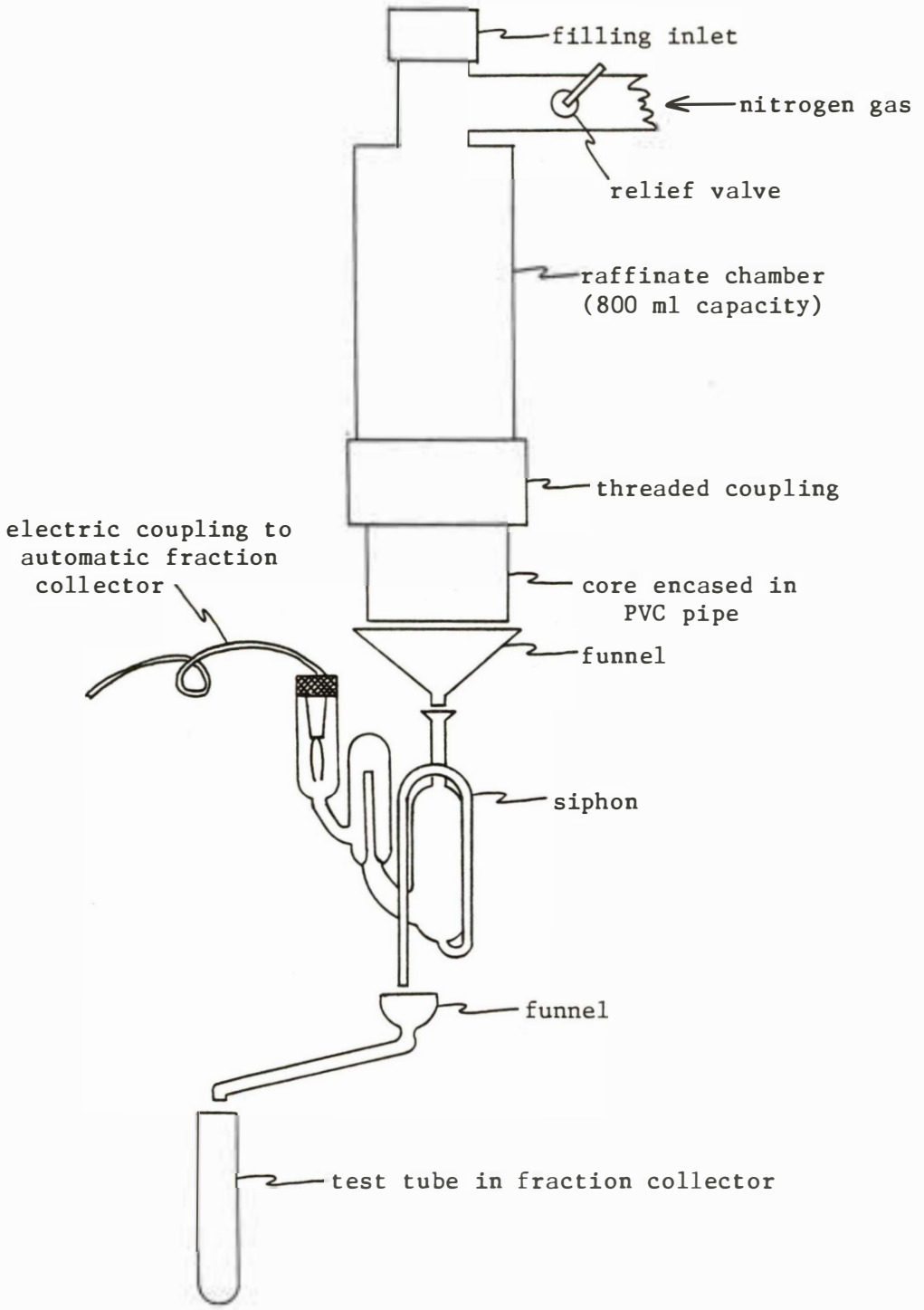

Figure 3. Schematic drawing of the nitrogen pressure apparatus used in the experiments.

From the values given in Tables 8 and 9 for the average volumetric flow rates, the cross-sectional areas, and the porosities, one can compute the average intergranular velocities of the test fluids as they moved through each of the cores (v = (volumetric flow rate)/(area)(porosity)). The volumetric flow velocities range from a minimum of 0.36 cm/hr (0.09 m/day) in Experiment 9 to a maximum of 233 cm/hr (56 m/day) in Experiment 14. Most of the intergranular velocities fall in the range from about 1 cm/hr to 20 cm/hr (about 0.2 to 4.8 m/day); such velocities correspond reasonably well to velocities to be expected for natural ground waters.

Aliquots of the effluent fluids were collected continuously using a 10-ml siphon and an automatic fraction collector (SMI Industries, Model 10263). The samples were stored in plastic containers and taken to the Central Analytical Laboratory within a few days of collection. Because our experimental fluids were generally very high in concentration, we did not encounter the severe problems usually associated with collecting and preserving natural waters. The flow rates were somewhat variable with time, and only overall averages were recorded, as shown in Table 9.

The nitrogen gas was applied directly to the test solution in the pressure chamber; because of this direct contact, it is possible that the nitrogen gas might have dissolved in the test fluid, later coming back out of solution under conditions of reduced pressure to form bubbles within the pore spaces of the test core. If such bubbles were to form, the hydraulic conductivity would be significantly reduced. However, we did not observe any bubbles on the surface of the outlet end of the cores as the effluent fluids flowed out, suggesting that amount of nitrogen which dissolved in the tailings fluids was insufficient to affect the hydraulic conductivity of the test cores.

The hydraulic conductivities (K) of the rock cores in Experiments 6, 9, 14, 17, 19, and 21 were measured by the falling head method using the test fluids. The equation employed was (Todd, 1980, p. 74):

$$K = (r_t^2 L / r_c^2 t) \ln(h_o / h_f) \qquad (6)$$

where:

r_c = radius of core

r_t = radius of pressure chamber

L = length of core sample

h_o = original total head

h_f = final total head

t = time interval for fluid level in chamber to fall from original height to final height.

In the falling-head calculations h_o and h_f both include the head imposed by the nitrogen pressure, as well as the gravitational head to the bottom of the core. For example, h_o = pressure head (33.4883 feet H_2O/14.5038 PSI at 60°F; Weast, 1978, p. F308), plus the gravitational head (original fluid height above the core in the raffinate chamber plus the core length).

For Experiments 22 through 27, the hydraulic conductivities were calculated from Darcy's Law (Todd, 1980). The results are summarized in Table 8.

Chemical Analyses

Extensive chemical analyses were required for the fluids used in this study. The analyses were carried out by Dr. Robert Meglen and other personnel of the Central Analytical Laboratory of the Center for Environmental Sciences, University of Colorado, Denver. The report by Meglen and others is included in this report as Appendix A. The species of interest, together with the detection limits of the various procedures employed, are summarized in Table 10.

Table 10. Analytical techniques and corresponding detection limits for species in tailings fluids. See Appendix A for details.

Analytical method	Species	Detection limit (mg/l)
ARL Model 35000C inductively coupled plasma emission spectrophotometer	aluminum	0.15
	arsenic	0.1
	barium	0.002
	cadmium	0.02
	calcium	0.1
	chromium	0.02
	cobalt	0.02
	copper	0.01
	iron	0.02
	lead	0.2
	magnesium	0.25
	manganese	0.02
	molybdenum	0.04
	nickel	0.04
	potassium	0.2
	selenium	0.2
	silicon	0.1
	sodium	0.2
	strontium	0.001
	uranium	0.4
	vanadium	0.04
	zinc	0.06
Perkin-Elmer Model 5000 atomic absorption spectrophotometer with Model 500 graphite furnace (nickel matrix modification)	arsenic	0.01
	selenium	0.01
Colorimetric method (sulfate-methylthymol blue on Technicon Auto Analyzer; chloride--mercuric thiocyanate method or ion chromatography using Dionex Model 12-S Ion Chromatograph)	chloride	1.0
	sulfate	10.0
Allex Model 532154 in selective electrode, used with Corning Model 120 pH meter	ammonium	10.0

The error-bars which appear on several of the graphs in this report include the analytical chemical error reported to us by Dr. Meglen. He estimates that for all species the error of accuracy is (+/-) 5% of the value reported, at the 95% confidence level. Full details of the analytical procedures and quality control can be found in Appendix A to this report.

Measurements made in the laboratory soon after elution of the fluids from the cores included temperature, pH, Eh, and specific conductance.

Computer Graphics

Computer programs were written to automatically plot all column breakthrough data. The data were tabulated and plotted using FORTRAN programs written for a Cromemco Z-2D microcomputer system with a Cromemco 3355A printer. The plotting software, Microplot, was obtained commercially from MICAH, Inc., Kentfield, California. This software enabled the Cromemco 3355A printer to function as a pen-plotter. Listings of the plotting programs are included in the Master's thesis by C.N. Gerlitz, available from the Earth Sciences Library, University of Colorado, Boulder, Colorado, 80309.

The raw data for all of the experiments, from which the plots in this report were prepared, are available from Dr. Donald D. Runnells, Department of Geological Sciences, University of Colorado, Boulder, Colorado, 80309.

Rationale for Major and Minor Ion Experiments

The chief purpose of our study was to measure, characterize, and interpret the chemical reactions that take place between uranium tailings fluids and samples of bedrock from beneath the Canon City uranium mill. We recognize that many of our results and conclusions may be specific to the Canon City fluids and lithologies, but many aspects of our work should also be applicable to other situations and environments.

We felt that the most logical starting point would be to study the interactions between bedrock and the major dissolved species in a relatively "clean" synthetic raffinate. After gaining knowledge about the chemistry of major dissolved species, we could move into a study of the minor and trace components. The difficulties of interpreting the chemistry of minor and trace dissolved species in saline aqueous solutions are well known. The discussion which follows in this report roughly follows the dual approach used in the experimental program. We will first present and discuss the experimental results for the major ions, followed by a discussion of the results and computer modeling of the minor and trace elements. The experiments numbered 6 through 21 consider the major dissolved species in synthetic acidic raffinate, and Experiments 22 through 27 focus on the minor and trace components in both acidic and alkaline tailings fluids.

EXPERIMENTAL RESULTS

Rock Cores

The samples of rock used in the study were from Observation Wells 13 (OW-13) and 14 (OW-14). Sections of core were taken from OW-13 at depths below the surface of 68, 118, and 119 feet, and from OW-14 samples were collected at depths of approximately 26, 41, 54, 104, 105, 179, 409, and 508 feet. Most of the cores came from either the Poison Canyon Formation or the Vermejo Formation, except for those from depths of 409 and 508 feet, which came from the Raton Formation (see the listing of stratigraphic names in Table 2). The physical properties of the samples are summarized in Table 8.

Mineralogy

Studies of thin-sections of sandstone cores from the Poison Canyon Formation show that the rocks consist primarily of detrital quartz and feldspars (microcline and plagioclase), with minor muscovite, biotite, sericite (alteration of plagioclase), perthitic feldspar, chlorite, garnet, epidote, opaque minerals, and clays (identified by heating and x-ray diffraction as consisting partly of kaolinite). Calcite occurs as fragments of limestone and as fine-grained cement in some samples.

Analysis by electron microprobe yielded a stoichiometry of $K_{0.5}Na_{0.5}AlSi_3O_8$ for the perthitic feldspar and a formula of $(Mg_{.08}Al_{1.48}Fe_{.38}K_{.06})O_{10} \cdot 0.5\ H_2O$ for some of the clay.

Test Fluids

In most of the leaching experiments we passed deionized water through the cores before introducing the tailings fluids. This was done to pre-wet the rocks. In some cases we analyzed the deionized water after it had passed through the core; such analyses gave us a measure of the background concentrations of dissolved species that might be expected in uncontaminated ground water as a result of normal rock-water interaction.

The initial compositions of the tailings fluids employed in the experiments are given in Table 5 and Table 6. The range in pH of the test fluids was from about 1 to about 8. The Eh ranged from (+)0.32 to (+)0.66 volts.

Hydraulic Conductivity and Flow Rate

As shown in Tables 8 and 9, generally high hydraulic conductivities and high flow rates were recorded in Experiments 17, 18, 19, 22, 23, 24, 25, and 26. Note also, in the eighth column of Table 8, that these same cores generally did not contain any calcite cement. The high hydraulic conductivities and flow rates could therefore be due to dissolution and

removal of the calcite cement from the rocks, possibly by contaminating fluids, prior to the time that we collected our core samples.

Upon conclusion of the experiments with synthetic raffinate, we observed a thin coating of an orange precipitate at the inlet end of several of the rock cores. This suggests that at least part of the loss of permeability evidenced in Table 7 may be due to plugging of the pore spaces by flocculent precipitates, probably of silica and iron oxyhydroxide. This suggestion is in agreement with the observations of precipitation of flocculent materials in inactive tailings piles reported by Markos and Bush (1981) in Volume II of this report.

Rinse-out of Contaminants by Deionized Water

As mentioned earlier, in several of the experiments we passed deionized water through the core before introducing the tailings fluid. In some cases the effluent water was then analyzed. Our purpose was to gain some information on the concentrations of dissolved species that might be expected in uncontaminated ground water as a result of normal water-rock interaction. A surprising result of such experiments was that, for at least two cores from different locations (105 feet in OW-14 and 68 feet in OW-13), the effluent deionized water contained high concentrations of some of the ions that are characteristic of fluids from the tailings ponds. We interpret this result to indicate that some of the cores had been contaminated in the field prior to our sampling, either by leakage of fluids from the tailings ponds or through the use of contaminated water by the drillers when they constructed the observation wells. The result of one of these experiments (Experiment No. 18) is summarized in Table 11, together with the more typical chemical composition of effluent deionized water from a core that had apparently not been contaminated prior to sampling (Experiment No. 8).

Table 11. Composition of effluent deionized water after passage through two different samples of rock core. The pH and composition of the water in Experiment 18 strongly suggest that the core had been contaminated by subsurface fluids in the field prior to sampling. All values in mg/l except where indicated. See Tables 8 and 9 for details of experimental parameters.

Species	Experiment 8	Experiment 18
pH	ND	3.4
Mg	47	650
Al	1	330
Fe	<0.02	220
NH_4	5	50
Mo	0.3	1.2
SO_4	1570	6400
Co	<0.02	17.
Cr	<0.02	0.85
Mn	0.15	10.
Ni	<0.004	17.
Zn	0.24	8.4
Se	ND	2.0
As	ND	1.0

ND = not determined.

Many of the values listed in Table 11 for Experiment 18 greatly exceed the standards that have been established for drinking water (van der Leeden, 1975). It was obviously important for us to recognize these anomalies in our efforts to interpret our other experimental data. However, because we do not know how the presumed contamination actually occurred in the field, we cannot offer any particular environmental interpretation of the results. If the contaminating fluid flowed through the rocks from the overlying tailings ponds, the results would be very interesting and important. On the other hand, if the cause was the use of contaminated fluids by the drillers, the results are of no particular environmental concern. Based on a number of inquiries that we made, it does indeed appear that the drillers used a mixture of tailings fluid and river water.

Effect of Acidic Tailings Fluids on Calcite Cement

The amount and appearance of calcite was compared in thin-sections of rocks from depths of 26 and 41 feet in Observation Well 14 (OW-14), before and after passage of the raffinate through the samples. Sample 26.4 (non-leached, from a depth of 26.4 feet) contains about 3 volume percent calcite, entirely in the form of granular cement between the framework grains of silicate minerals. About one-third of the intergranular calcite cement lies adjacent to open pore spaces in the rock (upper photo, Fig. 4). In contrast, after leaching with strongly acidic raffinate, the same sample contains less than 1 volume percent calcite, most of which is isolated from the open pore spaces (lower photo, Fig. 4). We interpret this to mean that much of the calcite cement formerly present in the rock was rapidly and easily leached by the raffinate as the acidic fluid flowed through the core. As will be emphasized later, the leaching of calcite cement, with a consequent rise in pH and neutralization of some of the acidity of the raffinate, is a major chemical control on the mobility and retardation of dissolved species in the acidic tailings fluids. In fact, the single most important chemical reaction that we have been able to identify in our work is the rise in pH caused by the reaction of the raffinate with the indigenous calcite. The neutralization of the raffinate causes several important reactions to occur in the interstices of the rock, especially the precipitation of iron oxyhydroxides, with its resulting influence on the behavior of other metals.

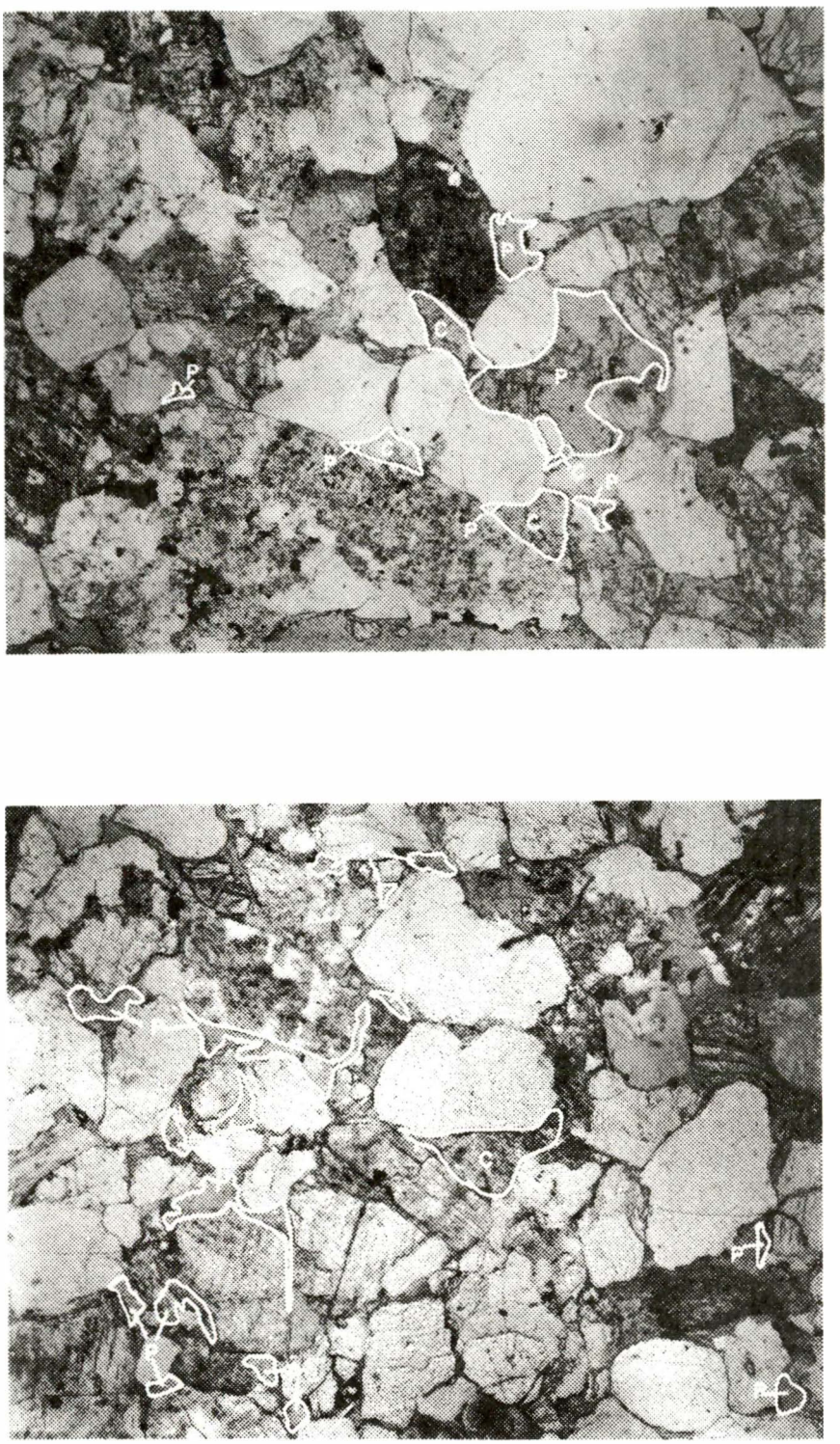

Figure 4. Photomicrographs of Poison Canyon Formation from a depth of 26.4 feet in OW-14. Outlined areas indicate pore space (P) and calcite (C). Upper photograph is unleached, showing calcite adjacent to pore spaces. Lower photograph is leached sample, with no calcite adjacent to pore spaces. Width of view is 3.3 mm.

Change in pH of Effluent Fluids

The effect on pH of the chemical interaction between rock and synthetic raffinate is illustrated by the curves shown in Figures 5, 6, and 7. It seems clear that dissolution of the calcite cement causes neutralization of the acidic raffinates; this is in agreement with the petrographic observations discussed earlier.

In Experiment 6 (Fig. 5), in which a short core from a depth of 26.4 feet in CW-14 (Poison Canyon Formation) was leached, the neutralizing capacity of the rock was quickly exhausted by the concentrated raffinate. The pH of the effluent in this experiment dropped rapidly from 8 to less than 2. Longer cores from the 26-foot level (Experiment 9, Fig. 5) and from a depth of 41.4 feet (Experiment 14, Fig. 6) were both leached by less acidic raffinates. Effluent pH values for these experiments remained near 8, indicating that there was enough calcite in the rocks to continue the neutralization of the raffinates through the length of the experiments.

Cores used in Experiments 17, 19, and 21 (Figs. 6 and 7) all came from approximately the same depth in OW-14, near 105 feet. Effluent pH for experiments on these cores all remained near the original value of the influent raffinate, from 3.35 to 3.80. The lack of neutralization of the raffinates by these cores indicates that there is no significant amount of calcite cement present in the rocks. There are two possible explanations for this. First, acidic fluids from the tailings ponds may have already passed through this rock in the field, leaching out the calcite that was present. Or, second, the rocks may have never contained calcite cement. We believe that the first explanation, previous leaching by raffinate, is a likely possibility. Our evidence for this conclusion is based on the results of measurements of the pH and composition of deionized water after passage through the cores. For the cores from a depth of 41 feet and a depth of 179 feet in OW-14 (Experiment 10, not used for later raffinate leaching), the pH of the effluent deionized water remained near neutral pH for the length of the experiments. This is the result that we would expect for an unaltered sandstone. However, for the same type of rinsing experiment, the cores from a depth of 105 feet yielded effluent deionized water with a pH between 3.5 and 4.0. We take this to indicate that acidic tailings fluids or contaminated drilling water had previously contaminated this rock. A lowering of the effluent pH, indicative of prior contamination, also occurred in minor-ion experiments Nos. 22 and 24 (Table 9).

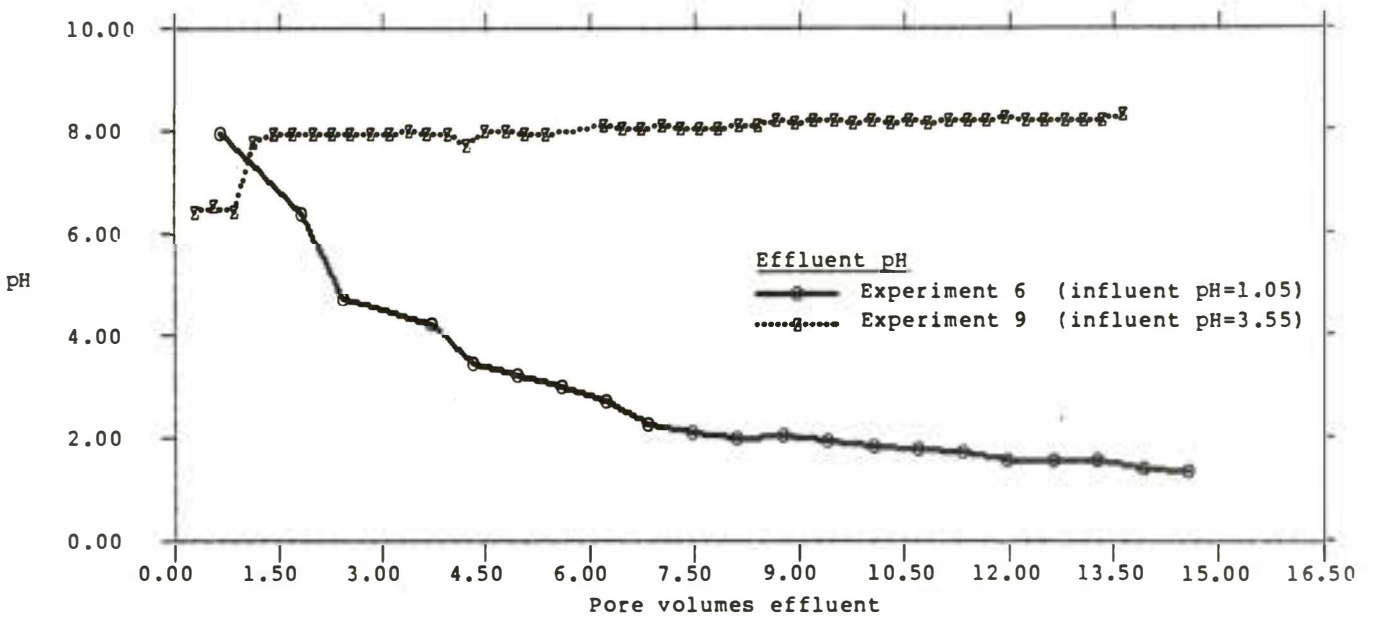

Figure 5. Observed pH of effluent in Experiments 6 and 9. Experiment 6: Concentrated synthetic raffinate. Pore volume = 14.9 ml. Total effluent volume = 216.3 ml. Core from 26.4 feet in OW-14. Experiment 9: Concentrated synthetic raffinate. Pore volume = 36.2 ml. Total effluent volume = 493.2 ml. Core from 26.0 feet in OW-14. This core was about twice as long as the one used in Experiment 6. See Tables 8 and 9 for additional data.

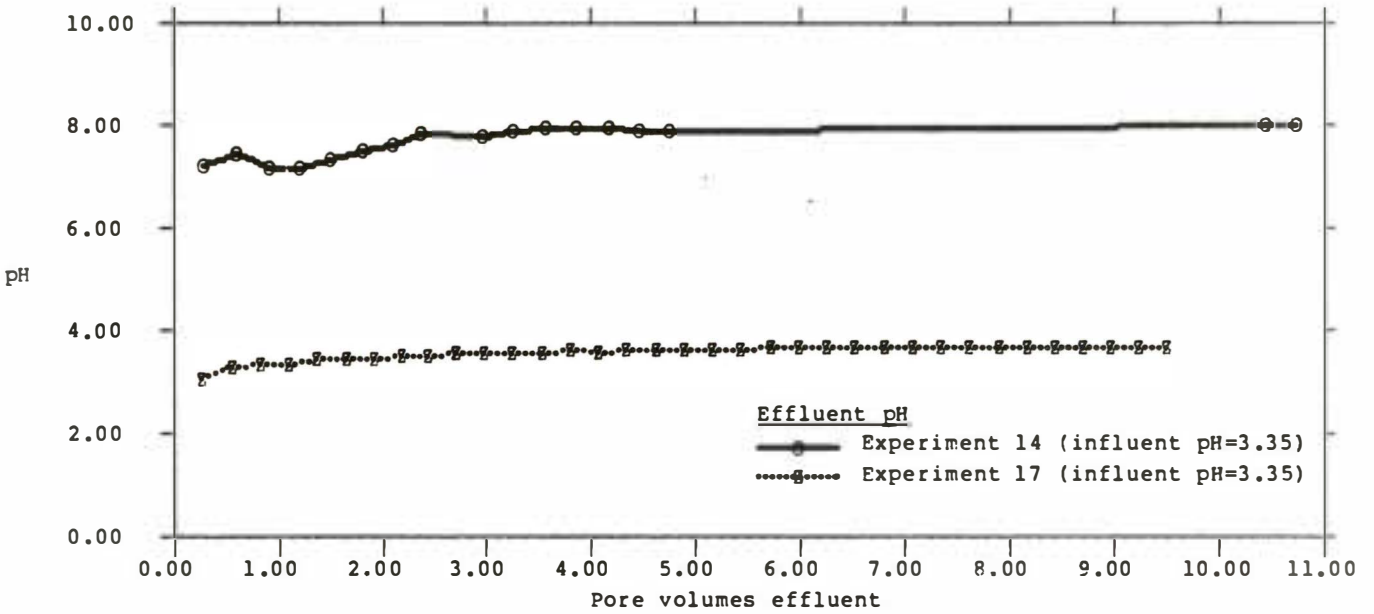

Figure 6. Observed pH of effluent in Experiments 14 and 17. Experiment 14: Dilute synthetic raffinate. Pore volume = 34.3 ml. Total effluent volume = 368.2 ml. Core from 41.4 feet in OW-14. Experiment 17: Dilute synthetic raffinate. Pore volume = 38.0 ml. Total effluent volume = 360.8 ml. Core from depth of 104.0-104.3 feet in OW-14.

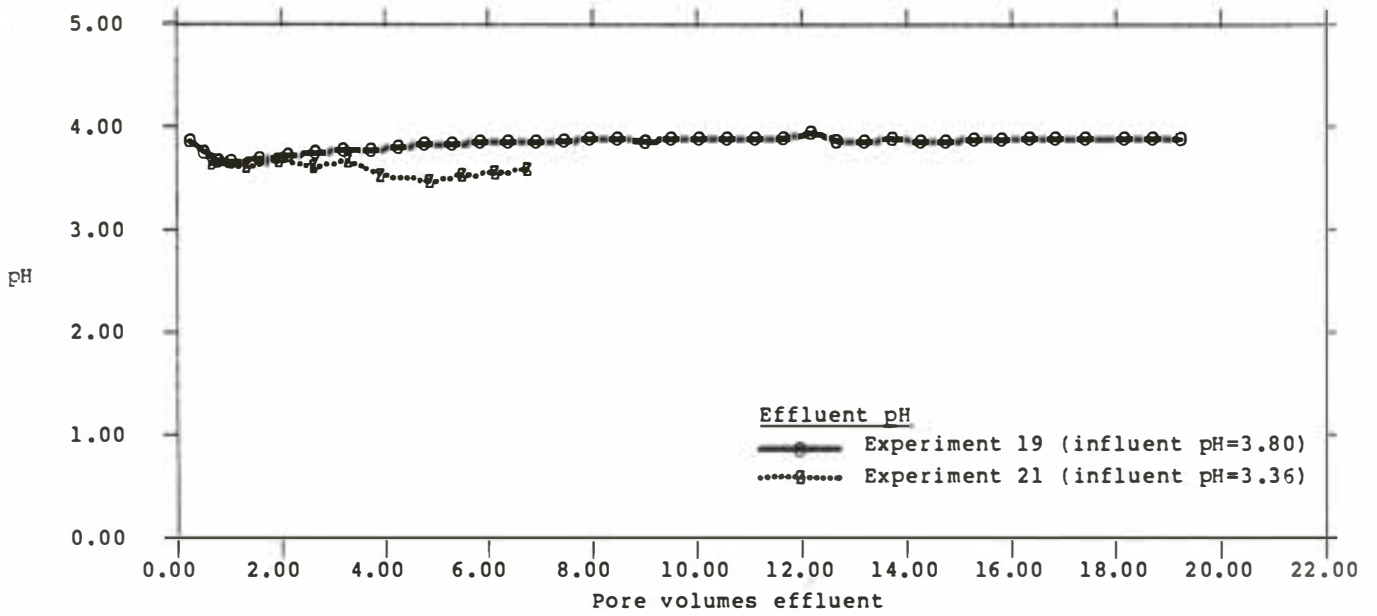

Figure 7. Observed pH of effluent in Experiments 19 and 21. Experiment 19: Dilute synthetic raffinate. Pore volume = 39.4 ml. Total effluent volume = 756.5 ml. Core from depth of 105.2-105.5 feet in OW-14. Experiment 21: Concentrated synthetic raffinate. Pore volume = 31.4 ml. Total effluent volume = 212.4 ml. Core from depth of 104.9-105.2 feet in OW-14. Lack of neutralization in these experiments suggests that calcite is absent from core.

Behavior of Major Species

Sulfate and chloride

There was no significant retardation of sulfate or chloride during passage of the synthetic raffinate through the rock cores, as indicated by kd values near 0 in Table 4. Typical breakthrough curves are shown for chloride and sulfate in Figures 8 and 9, with breakthrough (C/Co = 0.5) occurring at approximately one pore volume. Use of the model WATEQFC (Runnells and Lindberg, 1981) suggests that the predominant forms of sulfate and chloride in solution in most of the raffinates is as the free ions, SO_4^{--} and Cl^-. However, for synthetic raffinate No. 2 (pH = 1.05, used in Experiment No. 6), WATEQFC predicts that the principal form of the dissolved sulfur is bisulfate, HSO_4^-. Several workers have shown (Carritt and Goodgal, 1954; Davis and Leckie, 1979) that bisulfate ion is much more strongly sorbed on reactive substrates than free sulfate ion, probably as a result of hydrogen bonding. This may account for the slight amount of retardation exhibited by the sulfate in the experiment in which we used the synthetic raffinate No. 2 (Fig. 9, Experiment 6).

Concerning possible retardation of chloride, Hingston and others (1972) demonstrated that adsorption of free chloride ion is unlikely on such substrates as aluminum hydroxide and iron oxyhydroxide. Benjamin and Leckie (1982) have shown that substantial quantities of chloride and sulfate may be adsorbed in the form of metal-ligand complexes, but generally only at elevated pH values.

In general, sulfate and chloride should be useful as tracers of migrating raffinate solutions in the subsurface. The only exception seems to be the instance in which the pH is so low (near 1.5) that bisulfate ion becomes the predominant dissolved component of the total dissolved sulfur.

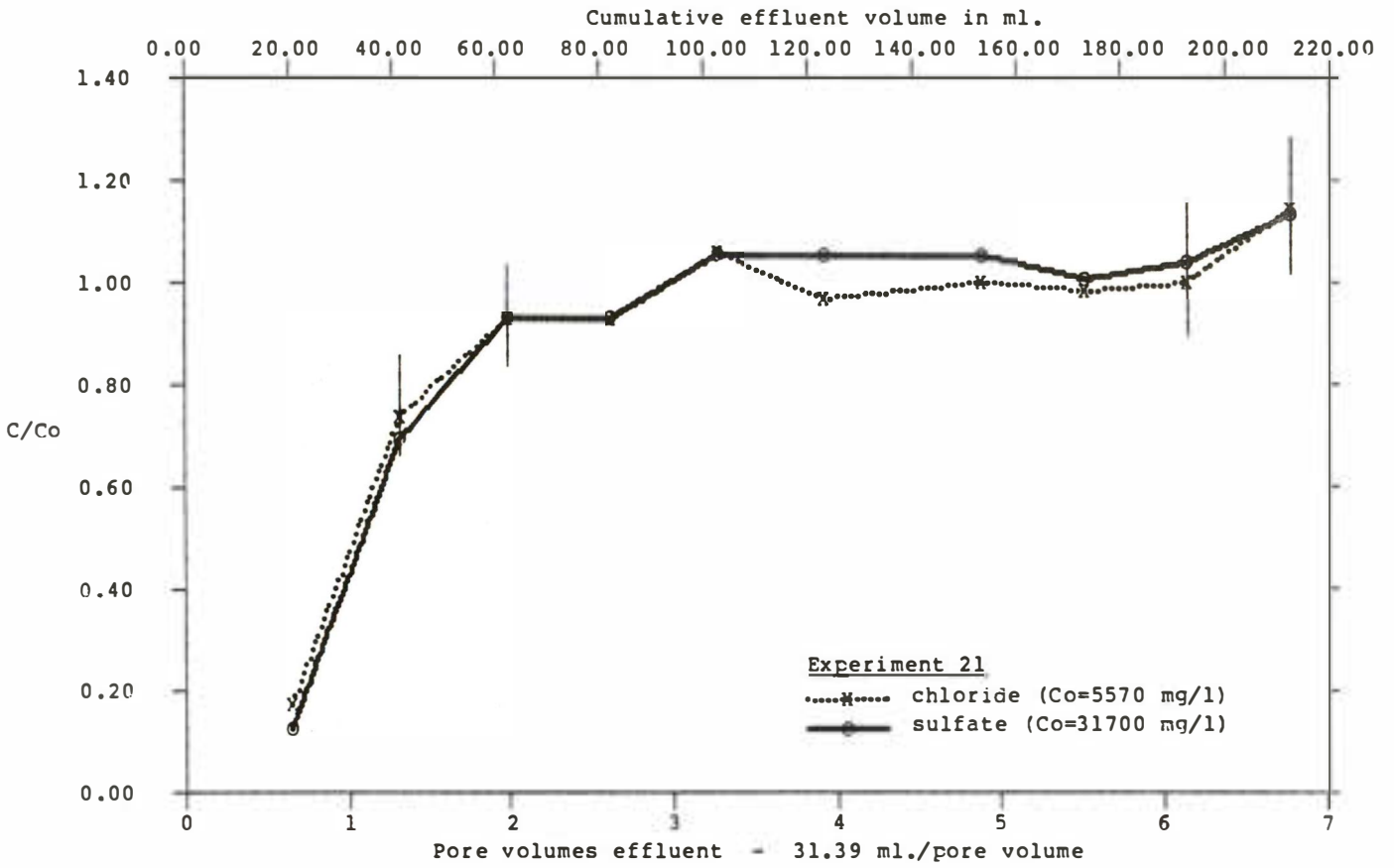

Figure 8. Breakthrough curves for sulfate and chloride in Experiment 21. Concentrated synthetic raffinate, uniformly acidic during experiment. See Tables 8 and 9 for experimental parameters.

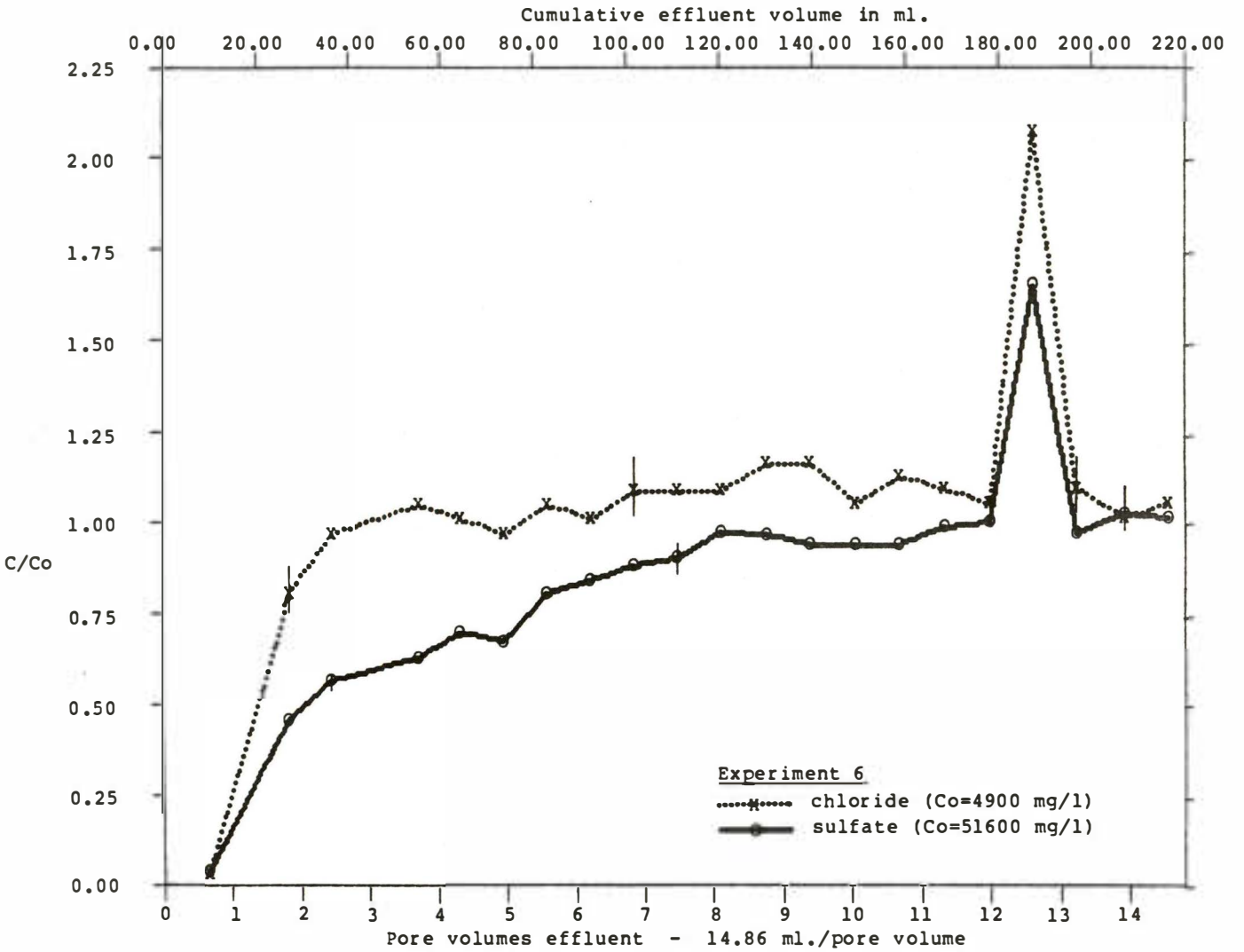

Figure 9. Breakthrough curves for sulfate and chloride in Experiment 6. Concentrated synthetic raffinate, initial pH = 1.05. Effluent changed from alkaline to acidic during run. See Tables 8 and 9 for experimental parameters.

Sodium and Magnesium

During the passage of the concentrated synthetic raffinates, neither sodium nor magnesium was significantly retarded, as shown in Figure 10. However, in diluted raffinate, some minor retardation of magnesium does occur, as shown in Figure 11. As noted earlier, the affinity and selectivity of ion-exchange and sorption reactions tend to increase with greater dilution. The retarding mechanism for magnesium in dilute raffinate is probably adsorption of free Mg^{++} ion on clays and metallic oxyhydroxides within the sandstone. Computer modeling of the ionic species of magnesium shows that free Mg^{++} ion is the predominant species in dilute raffinate, but in the concentrated raffinate the aqueous complex $MgSO_4^o$ predominates.

Criteria for cation exchange suggest that sodium, because of its large hydrated radius and monovalent charge, is less likely to be adsorbed than are most competing cations. In our test raffinates, the high concentration of sodium ion probably prevented detection of minor exchange with other ions over the short lengths of the test cores.

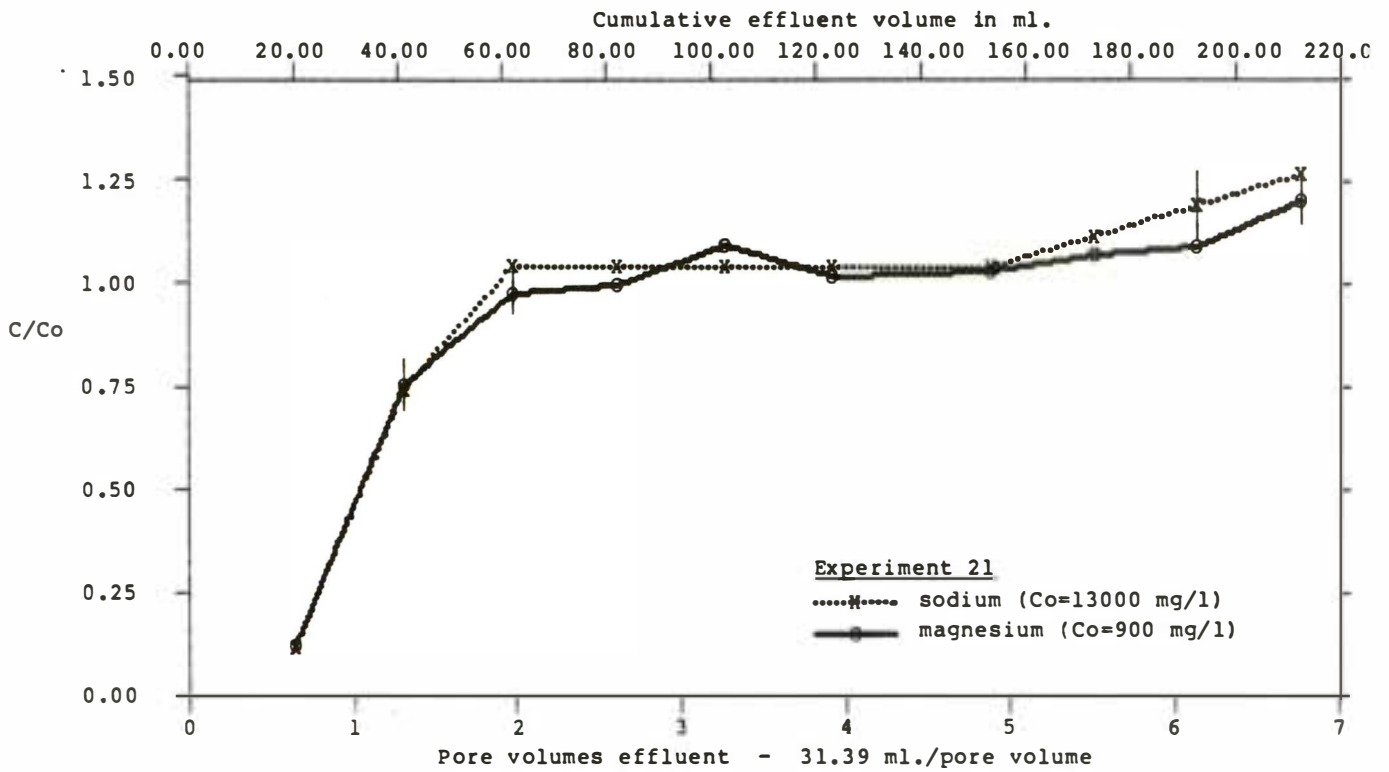

Figure 10. Breakthrough curves for sodium and magnesium in Experiment 21. Concentrated synthetic raffinate, remaining acidic during run. Initial pH = 3.35. See Tables 8 and 9 for experimental parameters.

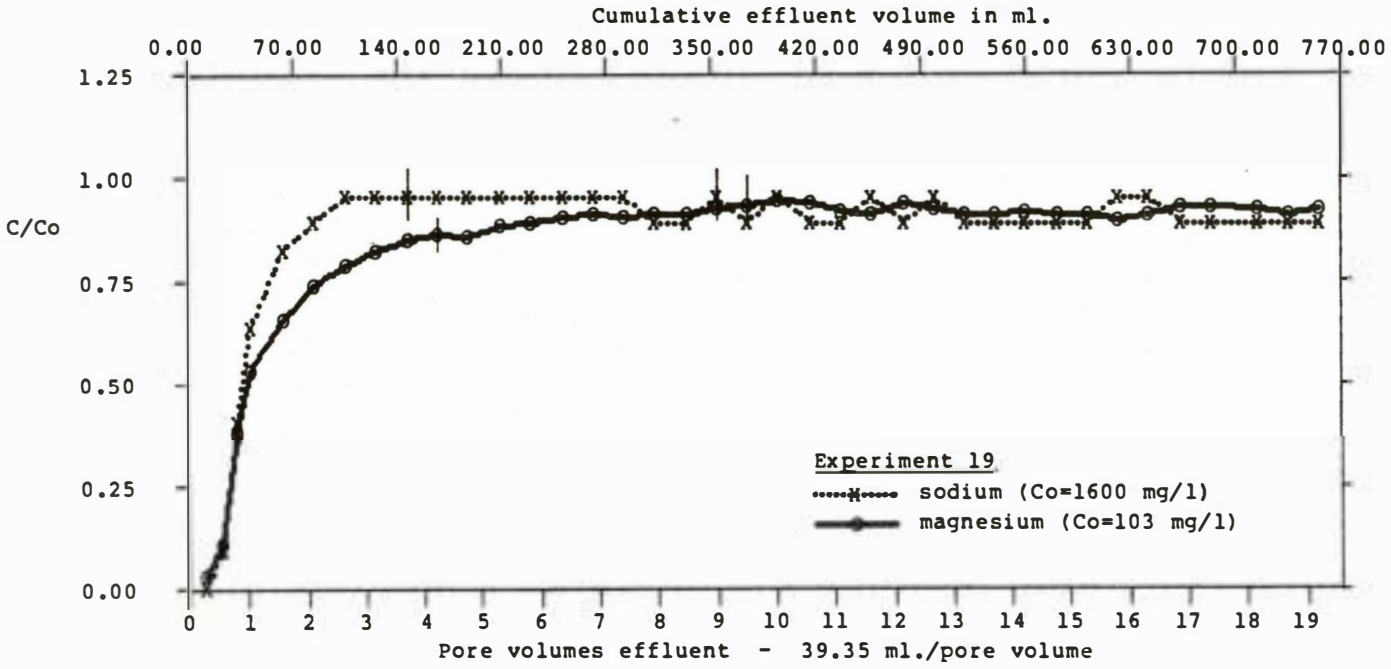

Figure 11. Breakthrough curves for sodium and magnesium in Experiment 19. Dilute synthetic raffinate, remaining acidic during run. Initial pH = 3.8. See Tables 8 and 9 for experimental parameters.

Potassium and Ammonium

Typical breakthrough curves for potassium and ammonium are shown in Figures 12 (Experiment 19) and 13 (Experiment 21). These two species behave in a fashion similar to each other in all experiments, as shown by the similarity of kd values in Table 4. Both are slightly retarded during passage of concentrated raffinate (Fig. 13), with increased attenuation in dilute raffinate (Fig. 12).

We believe that the retardation of these two species is caused by ion-exchange on clays and metallic oxyhydroxides in the rocks. The basis for this conclusion is the fact that neither of these two ions forms insoluble precipitates in nature, whereas both are known to be readily involved in ion-exchange reactions (Grim, 1968). The valence and the ionic radii are the same for potassium and ammonium (Nightingale, 1959), which probably accounts for the similarity in behavior in the column experiments. The difference in behavior of potassium and ammonium between the diluted raffinate (Experiment 19, Fig. 12) and in the concentrated raffinate (Experiment 21, Fig. 13) probably reflects the expected increase in affinity and selectivity of ion-exchange and sorption in dilute systems.

Use of WATEQFC to model the solution chemistry shows that the dominant forms of K^+ and NH_4^+ are the free ions in all test solutions, with KSO_4^- and $NH_4SO_4^-$ of secondary importance. The proportion of free ions increases with dilution, in turn favoring increased adsorption in the dilute raffinates.

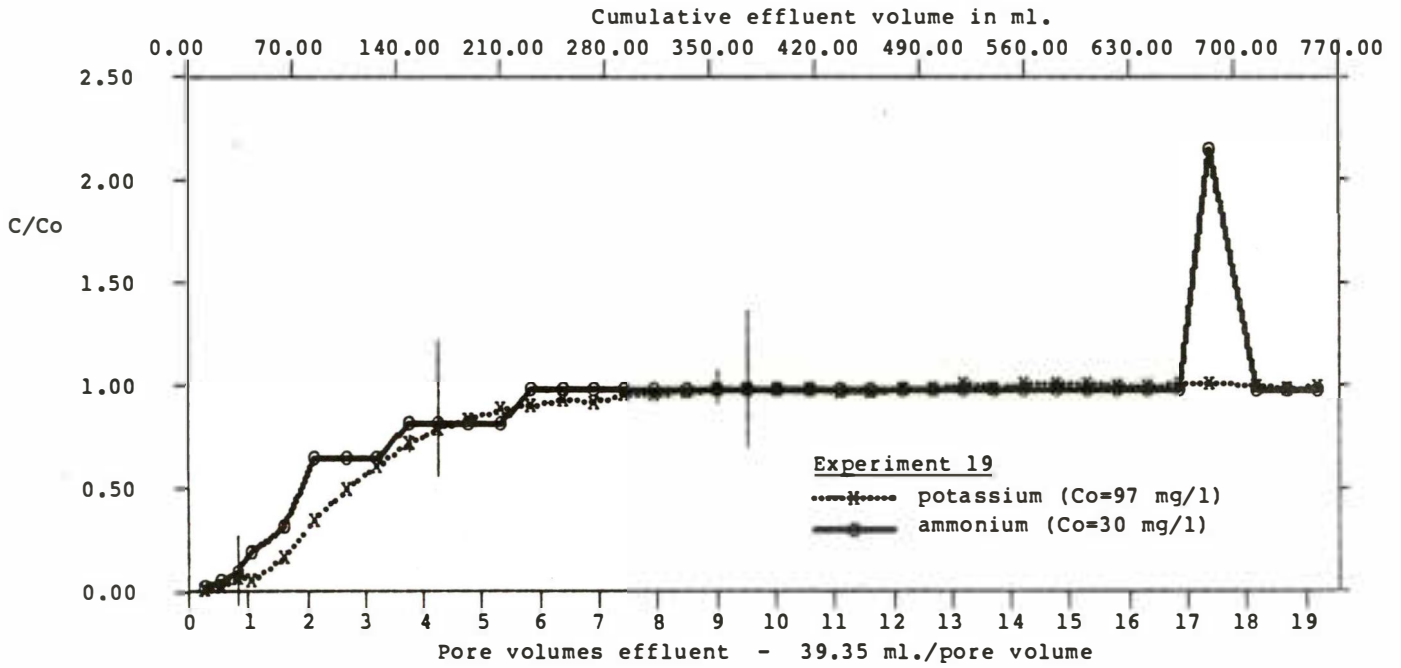

Figure 12. Breakthrough curves for potassium and ammonium in Experiment 19. Dilute synthetic raffinate, remaining acidic during run. Initial pH = 3.8. See Tables 8 and 9 for experimental parameters.

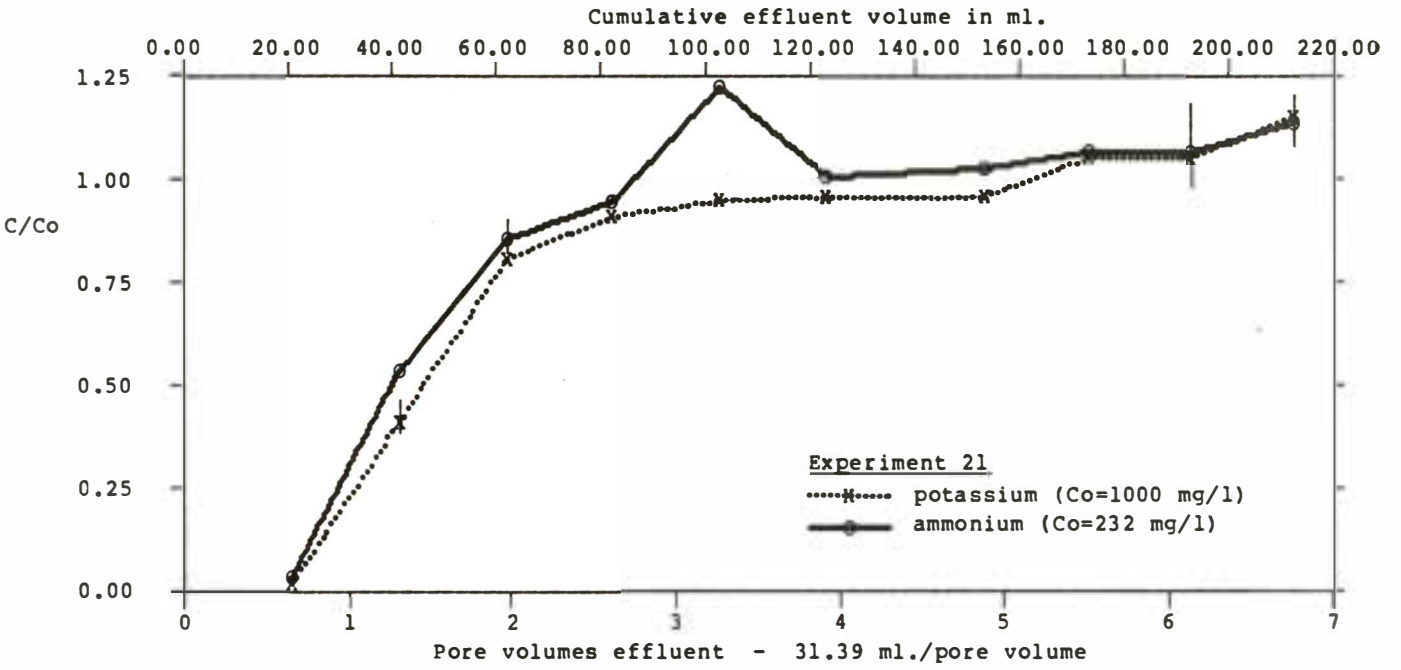

Figure 13. Breakthrough curves for potassium and ammonium in Experiment 21. Concentrated synthetic raffinate, remaining acidic during run. Initial pH = 3.35. See Tables 8 and 9 for experimental parameters.

Calcium

No attenuation of calcium was observed in any of the experiments involving the acidic raffinate solutions; instead, significant rinseout of calcium (C/Co > 1) occurred in all experiments. Figures 14 through 16 illustrate the calcium response observed for six major-ion experiments involving acidic fluids. A high initial peak is observed in several of the curves, and in most instances there is a later gradual decline to a C/Co value near 1. In Experiment No. 9 (Fig. 14) and Experiment No. 14 (Fig. 15) the value of C/Co failed to stabilize and level off near a value of 1.0, indicating that slow leaching of some calcium-rich mineral occurred for the entire duration of these experiments.

Calcite cement was observed in thin-sections of rocks from depths of 26 and 41 feet in OW-14, leached in Experiments No. 6, 9, and 14 (Figs. 14 and 15, respectively). Effluent pH curves for these experiments (shown in Figures 5 and 6) clearly suggest that dissolution of calcite occurred, with consequent neutralization of the effluent raffinates. This reaction must account for the release and significant rinseout of calcium observed in the effluent solutions in these experiments.

There was apparently no calcite present in the samples of core from depths of 104-105 feet in OW-14, which were leached in Experiments 17, 19, and 21. Petrographic examination failed to reveal calcite, and the pH curves (Figs. 6 and 7) show that the acidic raffinates passed through the rock without neutralization. However, the breakthrough curves (Figs. 15 and 16) show that calcium was also rinsed out of these rocks, as well as those that contained calcite, with initial C/Co values as great as 2.5. This must represent ion-exchange and desorption of calcium from the surfaces of clays in the rock, similar to the so-called "hardness halo effect" described by Griffin and others (1976) in their studies of the movement of contaminants in calcium-rich soils adjacent to sanitary landfills in Illinois.

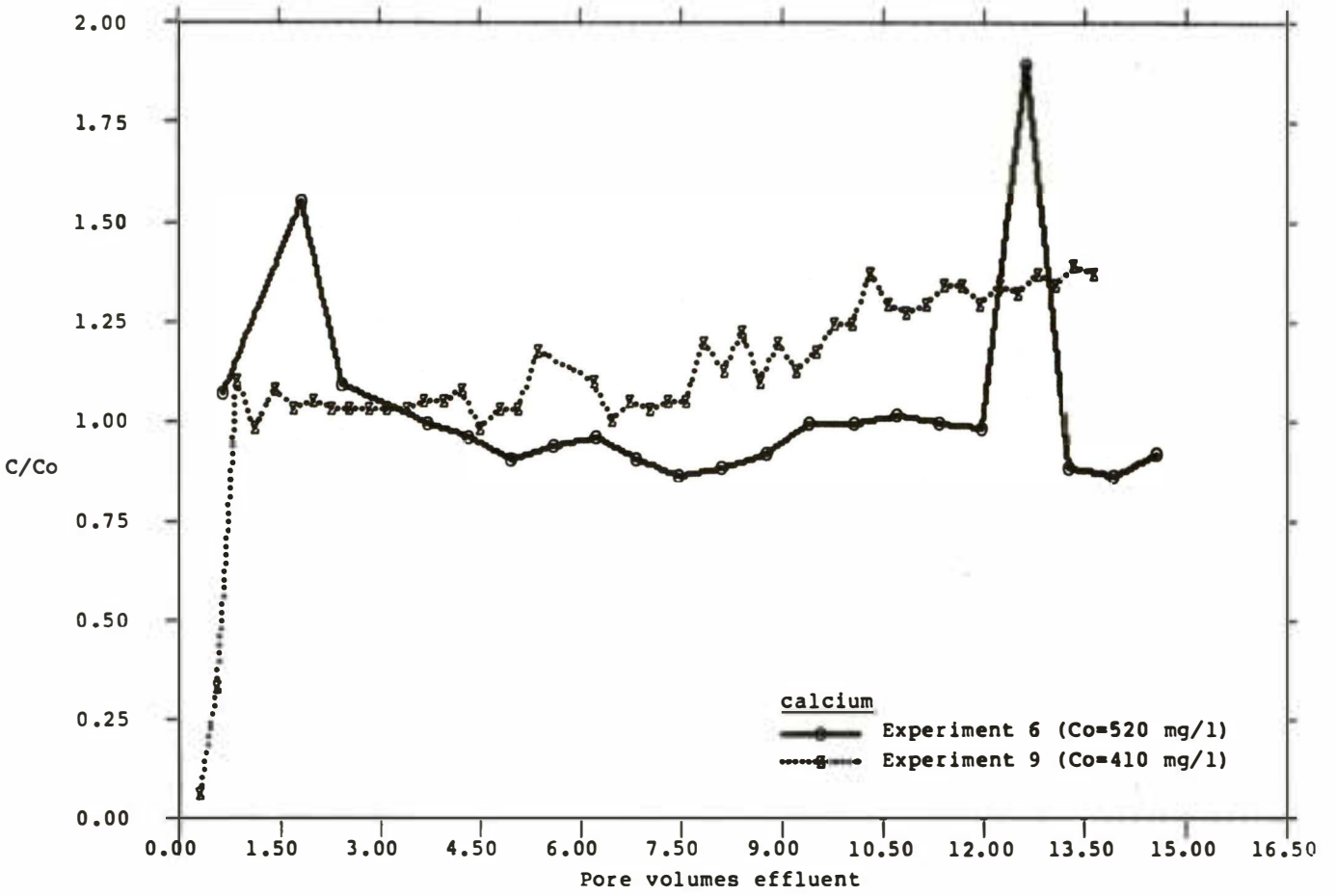

Figure 14. Breakthrough curves for calcium in Experiments 6 and 9. Experiment 6: Concentrated synthetic raffinate influent. Effluent changed from alkaline to acidic during run. Initial pH = 1.05. Experiment 9: Concentrated synthetic raffinate, initial pH = 3.55. Alkaline effluent. See Tables 8 and 9 for experimental parameters.

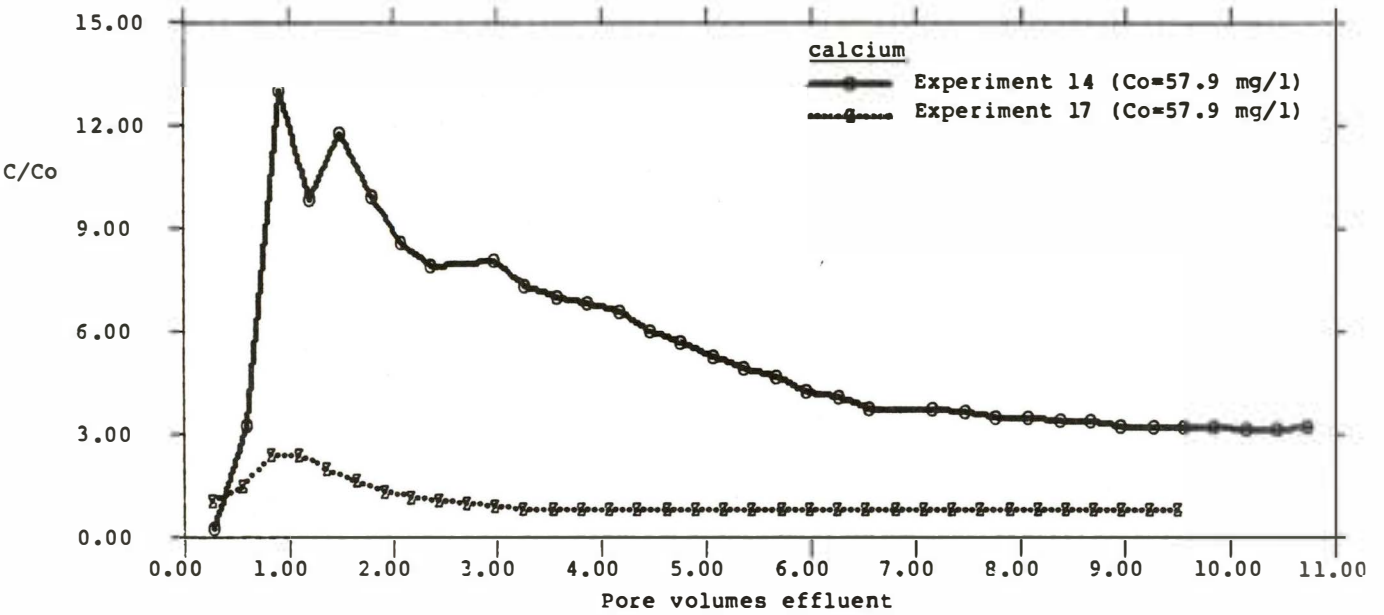

Figure 15. Breakthrough curves for calcium in Experiments 14 and 17. Experiment 14: Dilute synthetic raffinate, initial pH = 3.35. Alkaline effluent. Experiment 17: Dilute synthetic raffinate, remaining acidic during run. Initial pH = 3.35. See Tables 8 and 9 for experimental parameters.

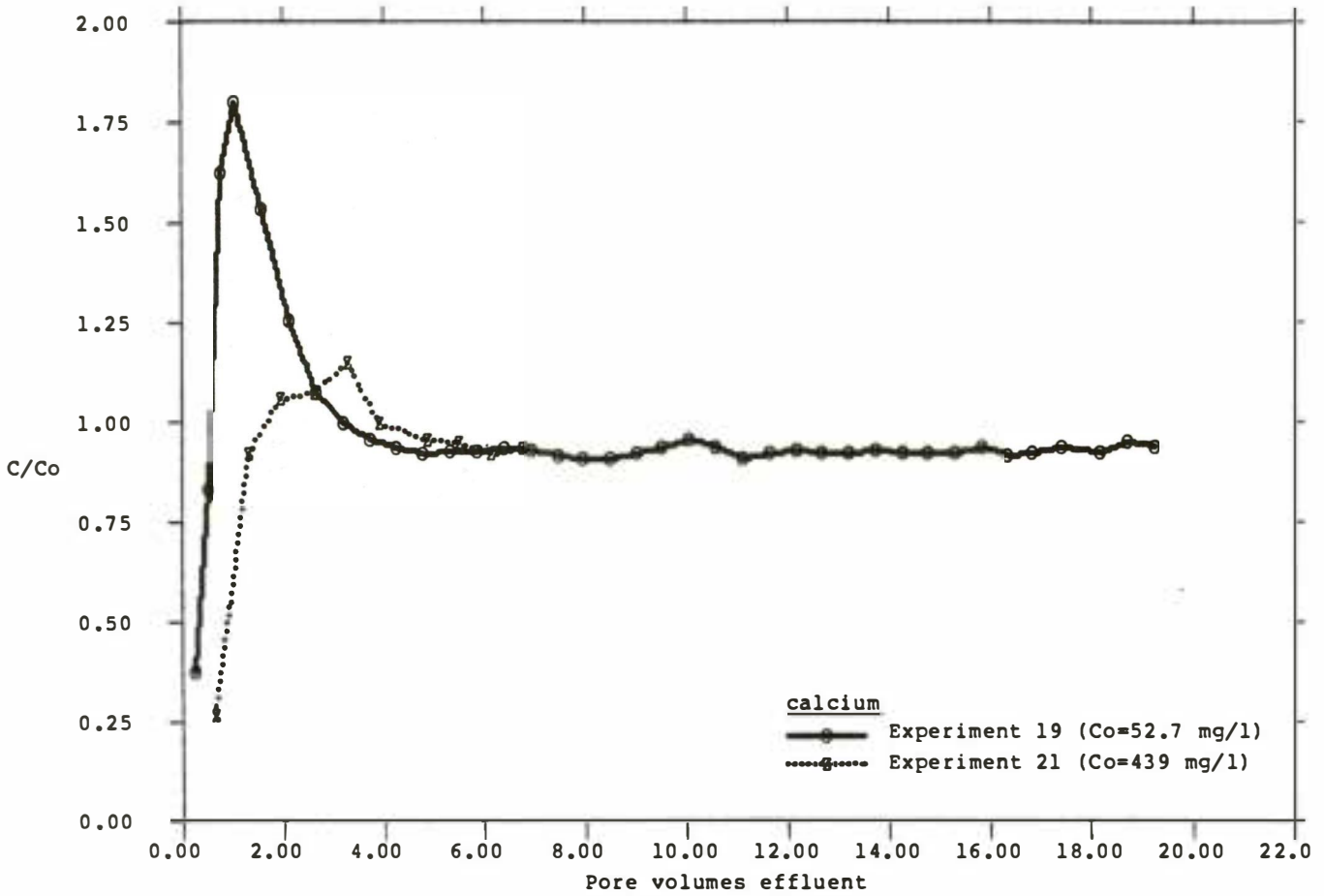

Figure 16. Breakthrough curves for calcium in Experiments 19 and 21. Experiment 19: Dilute synthetic raffinate, remaining acidic during run. Initial pH = 3.8. Experiment 21: Concentrated synthetic raffinate, remaining acidic during run. Initial pH = 3.35. See Tables 8 and 9 for experimental parameters.

In our experiments, the high concentrations of sodium and hydronium ion in the raffinates would be very effective in displacing calcium from exchange sites on clay minerals. For Experiment 21, a very rough computation of the mass balance shows that about 17 microequivalents of Na were retarded per gram of rock (estimated from Fig. 10), compared to about 4 microequivalents of Ca released per gram of rock (estimated from Fig. 16); the difference presumably was due to other ions released from the exchange sites, such as magnesium and potassium. It is interesting to speculate on the possibility of using the enrichment of calcium in the ground water (the "hardness halo effect"; Griffin and others, 1976), ahead of a migrating front of tailings fluid, as an indicator of the up-gradient contamination.

Figure 17 shows the results for minor-element Experiments 23 and 26, in which splits of the same alkaline fluid were passed through adjacent samples of core. In both Experiments 23 and 26 there was a significant rinse-out of calcium. Because the pH of the fluids was approximately 8, intergranular calcite would probably not dissolve in these fluids. The rinse-out illustrated in Figure 17 must therefore have been the result of ion-exchange by sodium for calcium on mineral surfaces in the rock.

Because the two experiments shown in Figure 17 were duplicates, involving splits of the same fluid and adjacent samples of core, they offer an indication of the total experimental variance to be expected in our experiments.

In summary, all of the experiments revealed essentially the same behavior of calcium, in which calcium was mobilized and rinsed out of the rock in the early parts of the experiments. The experiments show that the calcium can be derived either from the dissolution of calcite cement or by ion-exchange with dissolved sodium and hydronium ions in the fluid.

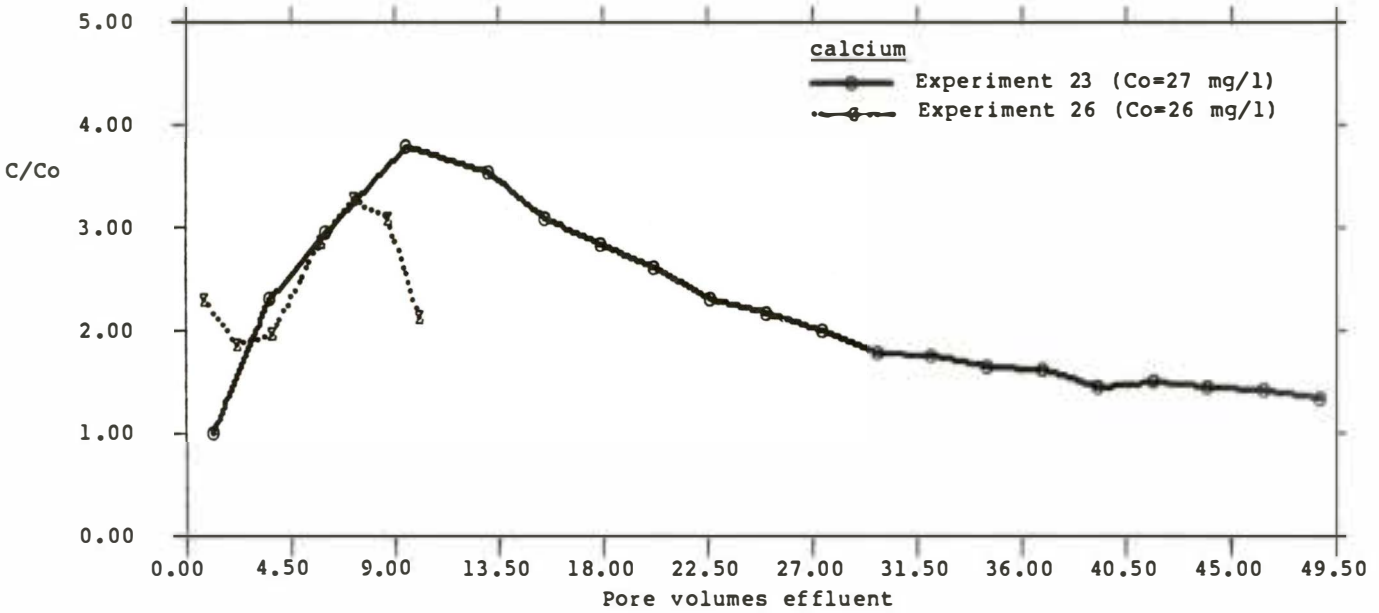

Figure 17. Breakthrough curves for calcium in Experiments 23 and 26. These two experiments used splits of the same dilute, alkaline tailings fluid, and adjacent samples of core. Effluents remained alkaline during runs. See Tables 8 and 9 for experimental parameters.

Aluminum and Iron

Aluminum and iron showed strong similarities in behavior during the passage of tailings fluids through the rock cores. Behavior of the aluminum in these experiments was very clearly related to pH, with maximum solubility observed at pH values below 6. This is in agreement with the study of aluminum solubility by Hem and Roberson (1967), who demonstrated that aluminum hydroxide shows a minimum solubility near pH 6, increasing rapidly at both higher and lower pH values.

Figure 18 shows the behavior of aluminum (and iron) in Experiment 6. In this experiment the pH of the originally acidic influent was neutralized and rose to a value near 8 in the early effluent (see Figure 5 for pH curve). As discussed earlier, the neutralization was caused by reaction of the acidic raffinate with the interstitial calcite cement. Corresponding to this early neutralization of the raffinate, the aluminum was retarded by about 3 pore volumes relative to the velocity of the effluent fluid. This retardation is to be expected on the basis of the known solubility of aluminum hydroxide as a function of pH (Hem and Roberson, 1967; Morgan, 1967). However, after the calcite cement in the rock of Experiment 6 was exhausted and the pH began to fall back toward the original influent value of 1.5, aluminum was again solubilized and traveled with the raffinate.

Effluent concentrations of aluminum were also initially far below influent concentrations for Experiments 9 and 14 (see Fig. 19 for Experiment 9; the data for Al were not plotted for Experiment 14 because the effluent concentrations were below detection limits). The effluent pH was near pH 8 for the entire length of these runs, without the return to acidity observed in Experiment 6. Corresponding to this constancy of alkaline pH, aluminum was strongly retarded for the entire experiment. Flow rates were also slower in Experiments 9 and 14 than for most other runs (Table 9), thus allowing more time to overcome any kinetically slow steps in the precipitation of aluminum-bearing compounds.

In contrast to the rock cores used in Experiments 6, 9, and 14, in which the synthetic raffinate was neutralized by calcite cement in the rock, the rocks used in major-ion Experiments 17, 19, and 21 (Figures 20, 21, and 22) did not contain calcite (Table 8); as a result, these rocks had little neutralizing capacity and the pH of the effluent raffinates was nearly as low as the influent. As a result of the consistently low pH of the migrating fluid, aluminum was mobile and moved with the fluid. In fact, in most cases additional aluminum was leached from minerals in the cores ($C/Co > 14$), as shown in Figures 20, 21, and 22.

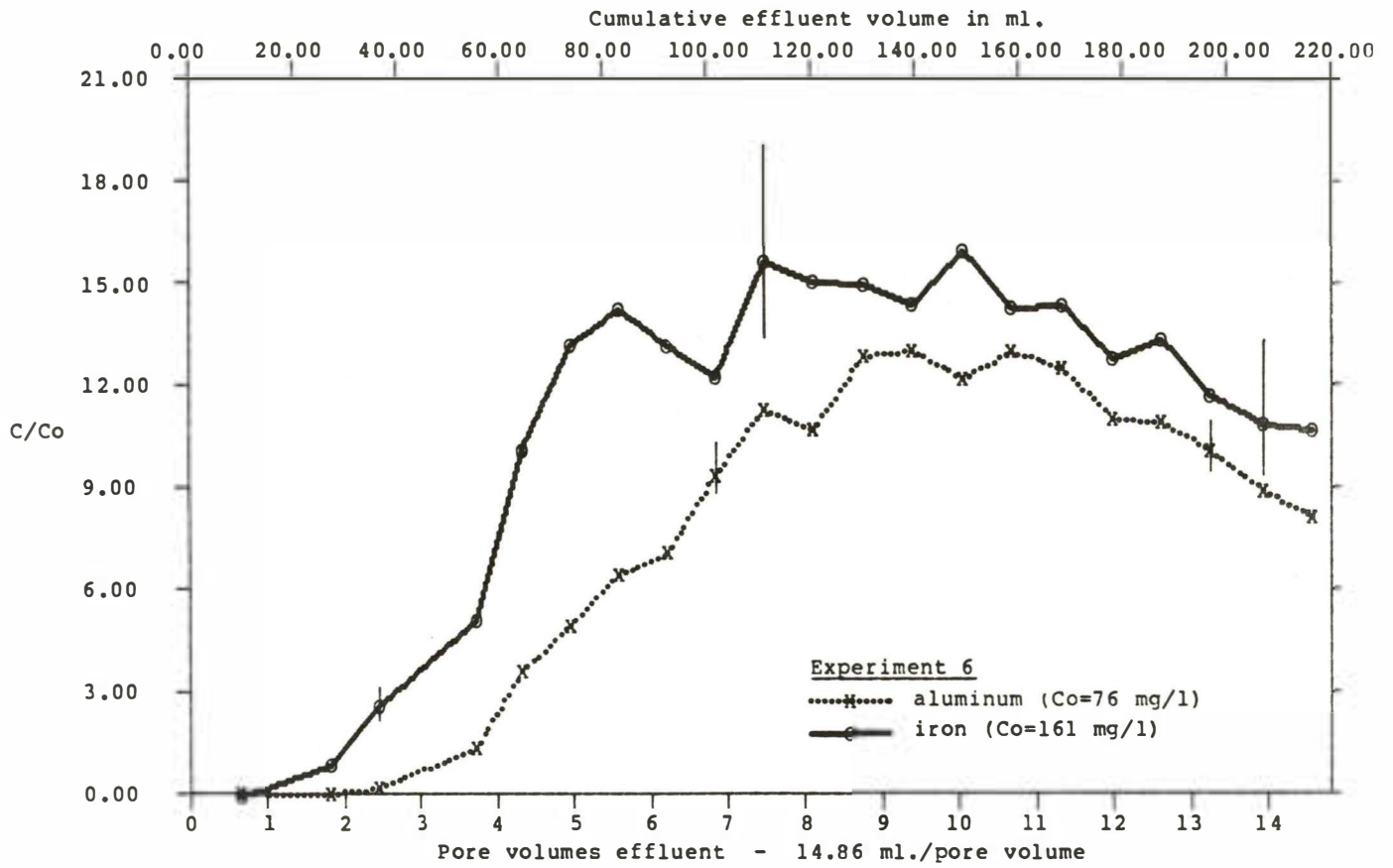

Figure 18. Breakthrough curves for aluminum and iron. Experiment 6: Concentrated synthetic raffinate. Effluent pH initially near 8, dropping gradually to original value near 1.05. See Figure 5 for details of pH variation during the run.

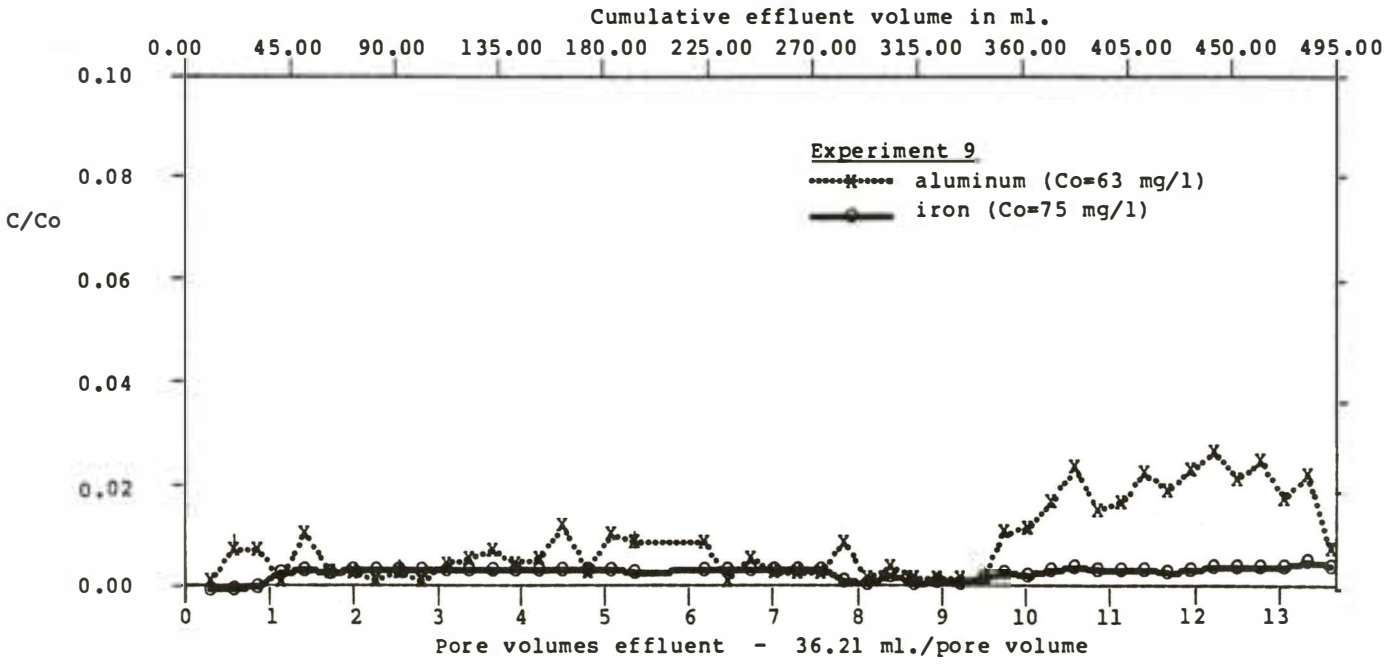

Figure 19. Breakthrough curves for aluminum and iron. Experiment 9: Concentrated synthetic raffinate, neutralized by reaction with calcite in rock. Effluent pH remained near 8 for entire experiment. See Figure 5 for details of pH variation during the run.

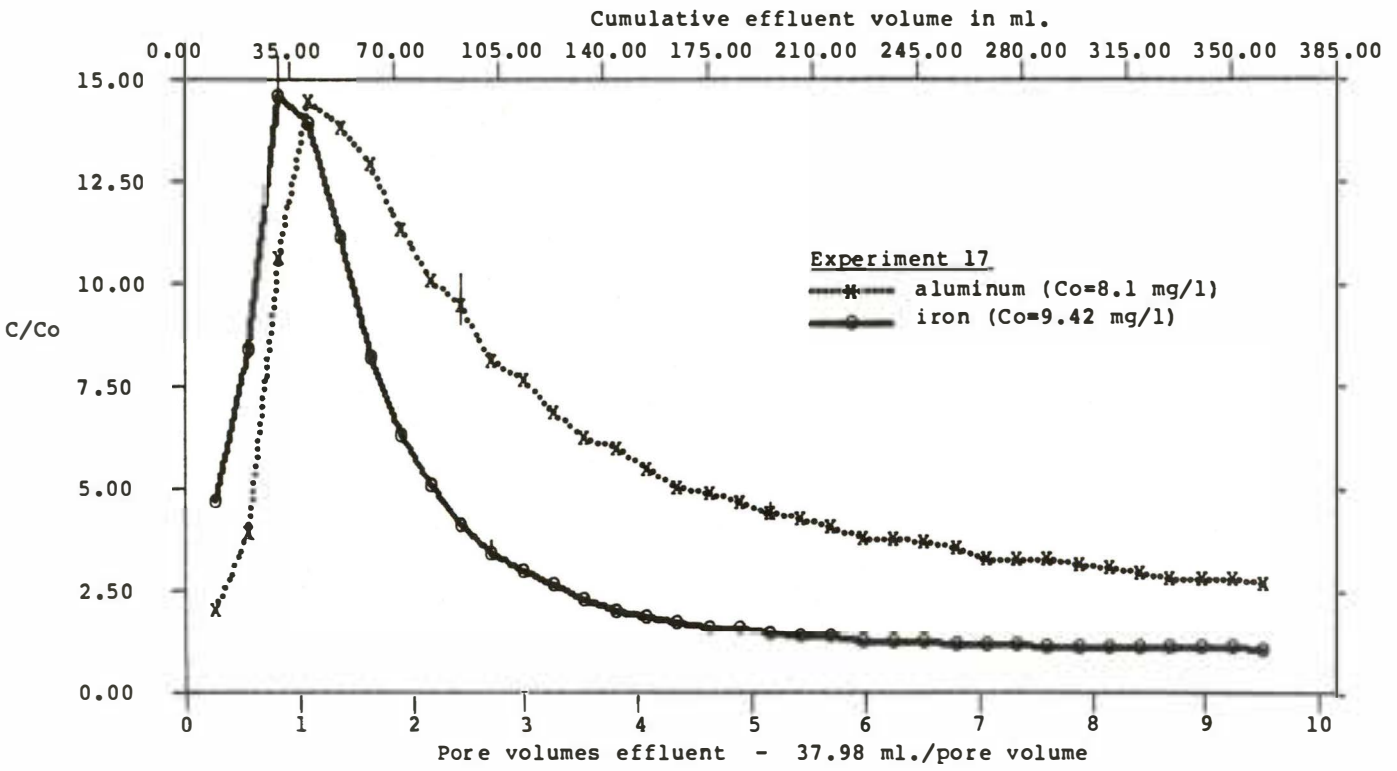

Figure 20. Breakthrough curves for aluminum and iron. Experiment 17: Dilute synthetic raffinate, with initial pH = 3.35. pH remained acidic for entire experimental run, reflecting absence of calcite in the rock. See Figure 6 for details of pH variation during the run.

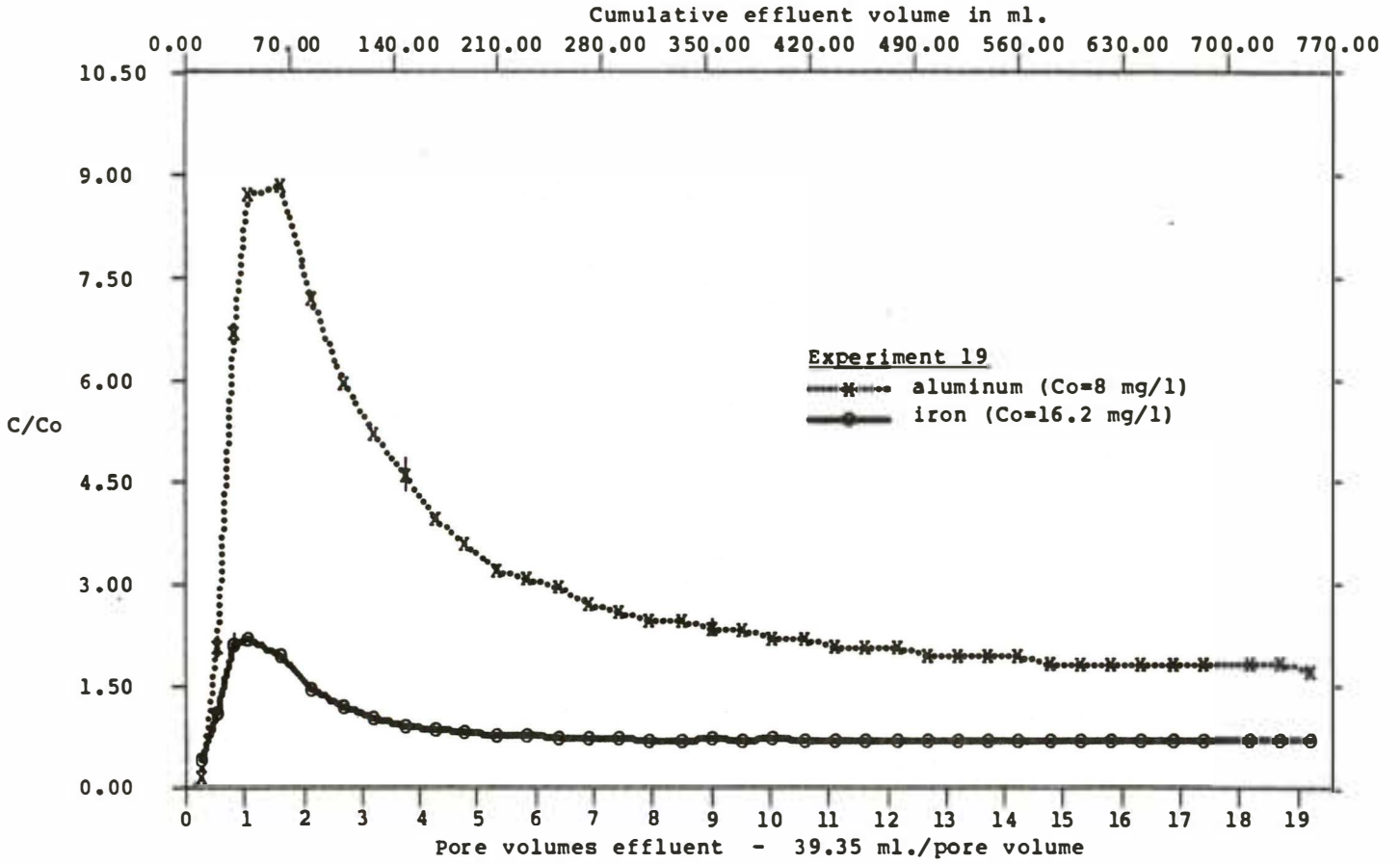

Figure 21. Breakthrough curves for aluminum and iron. Experiment 19: Dilute synthetic raffinate, with initial pH = 3.35. Effluent pH remained acidic for duration of experiment, reflecting absence of calcite in rock. See Figure 7 for details of pH variation during experiment.

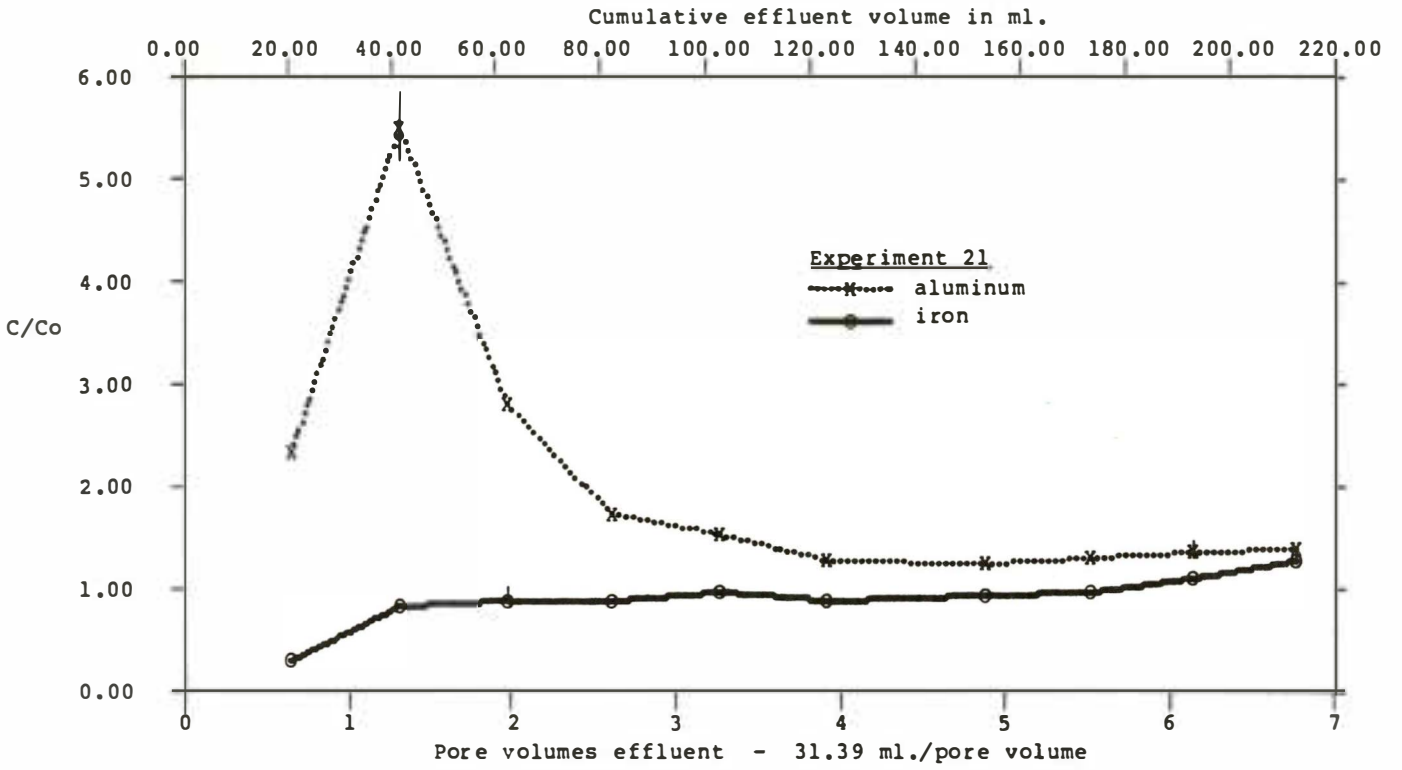

Figure 22. Breakthrough curves for aluminum and iron. Experiment 21: Concentrated synthetic raffinate, with initial pH = 3.36. Effluent pH remained acidic for duration of experiment, reflecting absence of calcite in rock. See Figure 7 for details of pH variation during experiment.

Markos and Bush, in Volume II of this report, suggest that complexing of dissolved aluminum by dissolved sulfate ion plays a significant role in controlling the solubility of aluminum in tailings fluids. In our studies, however, because sulfate ion was not retarded, the concentration of dissolved sulfate was essentially constant throughout the course of any given experiment. As a result, the formation of stable aqueous complexes of sulfate with aluminum cannot be called upon to explain the differences in mobility and retardation of aluminum that we observed during the course of any given experiment, except as the stability of such complexes might be influenced by the observed changes in pH.

In summary, the chemical behavior of aluminum in reactions between acidic tailings fluids and bedrock seems to clearly reflect the solubility of aluminum oxyhydroxide, as controlled by the pH of the migrating fluid. There is also some evidence that greater removal occurs under conditions of slow flow; this suggests that the precipitation of the aluminum is kinetically slow relative to the rates of flow of the fluids in the experiments.

The behavior of iron also appears to be mainly a function of pH, with possibly a minor role played by Eh. Unfortunately, the range of Eh values in our experiments was not great enough to unambiguously define the role of this parameter.

Figure 23 is an Eh-pH diagram showing the fields of thermodynamic stability of potentially important solid species of iron (also see summary studies of iron stability relationships by Garrels and Christ, 1965; Hem, 1970; Lindsay, 1979). The values of dissolved sulfur and iron used to construct Figure 23 are representative of the concentrations observed in the effluent solutions for Experiment 27.

The most important solid phase in Figure 23 is $Fe(OH)_3$; we believe that a similar phase controls the solubility of iron in our experiments. The precipitation of ferric oxyhydroxide seems to occur easily and quickly during the passage of tailings fluids through the rocks. We have observed the precipitation of a yellow-brown solid on the ends of many of the rock cores after completion of the experiments, and in some cases (Figure 24, for example) we were able to see precipitates of solid ferric oxyhydroxide in thin-sections of the cores after completion of the experimental runs. Although our study was not designed to obtain kinetic data, it is very obvious that the precipitation of ferric oxyhydroxide is extremely fast relative to the rates of intergranular flow of the test fluids through the cores. And, importantly, the intergranular velocities of our test fluids were geologically reasonable.

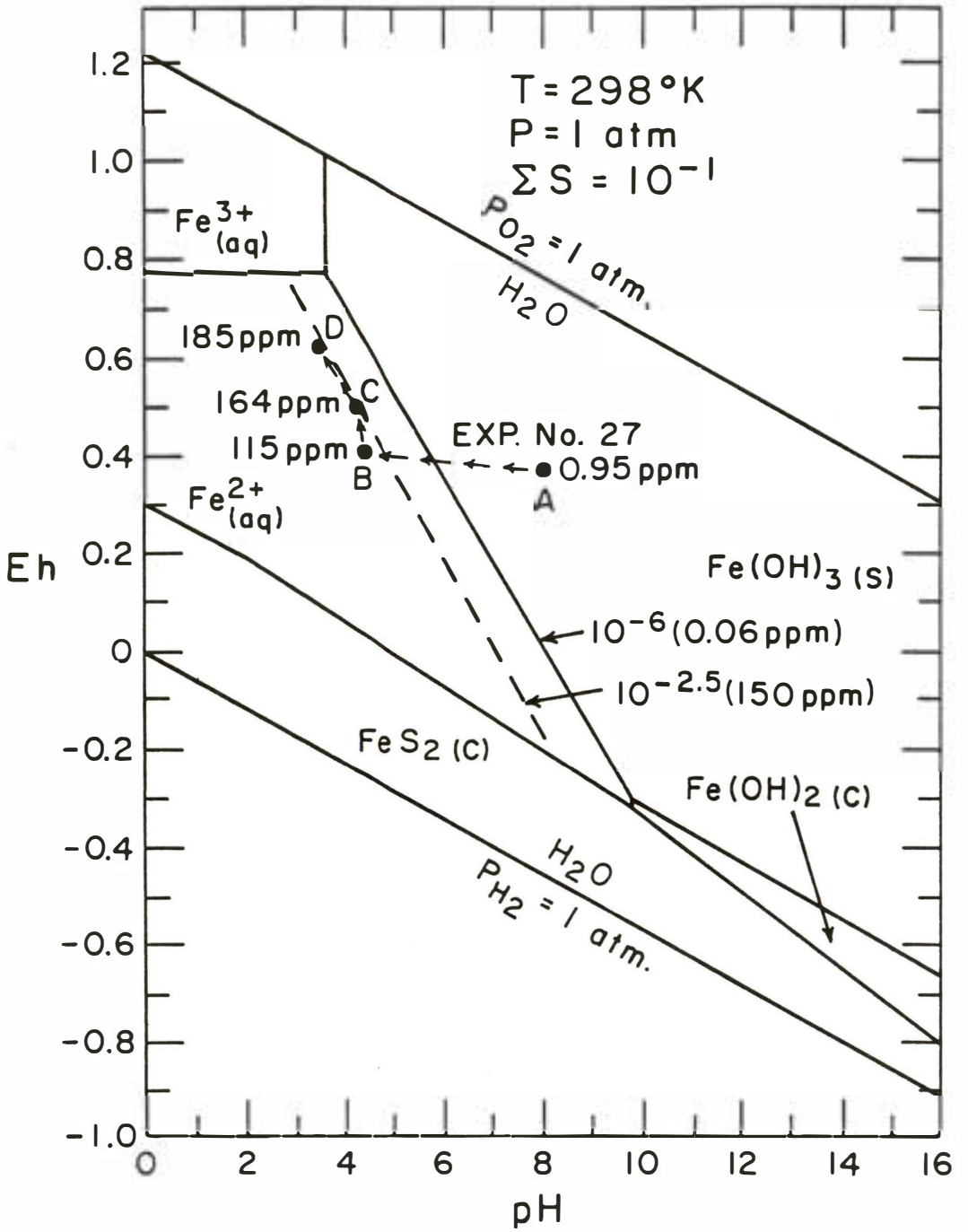

Figure 23. Thermodynamic stability diagram for iron. Concentrations based on observed values of sulfate and total iron in effluent solutions from column experiments. Constructed from free energy data in Naumov and others, 1974.

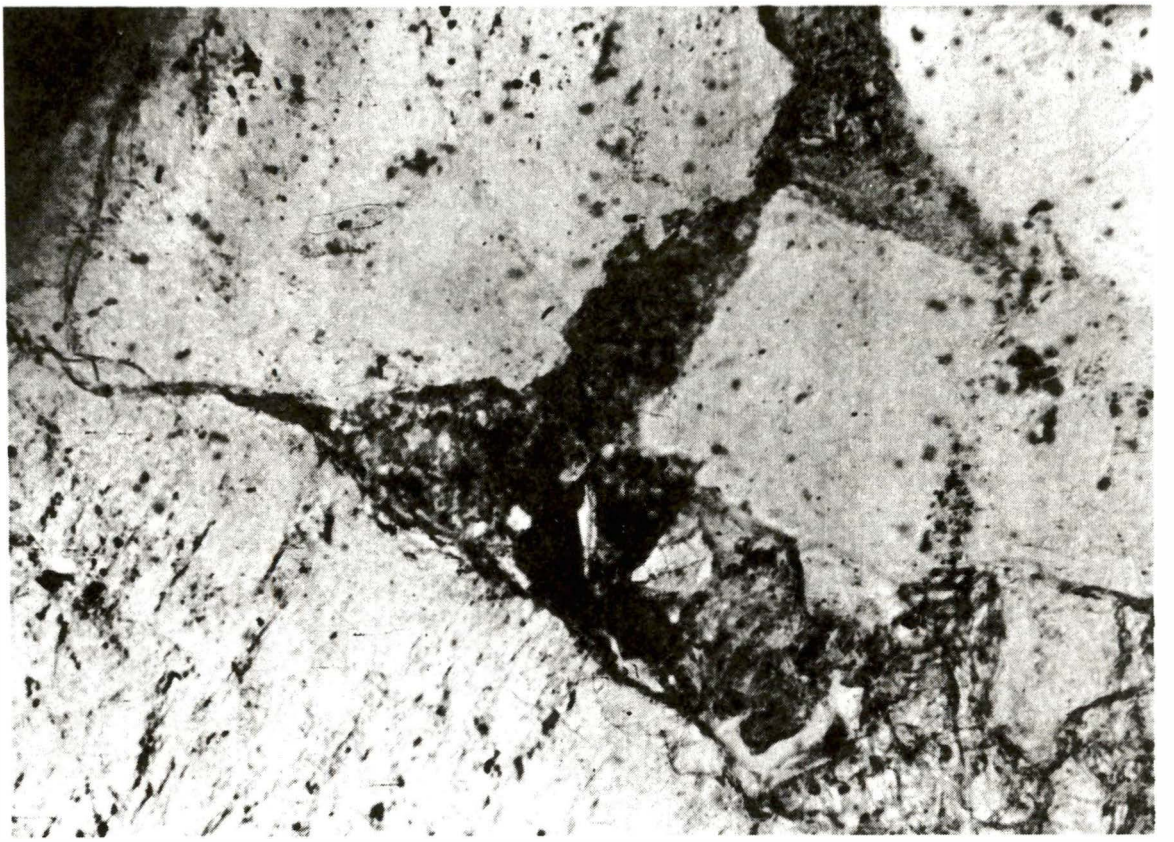

Figure 24. Thin-section of core after completion of experiment. Note precipitate of ferric oxyhydroxide (dark material in center of photograph). Depth of 53.5 feet in CW-14. Width of view is approximately 0.1 mm.

The precipitation of solid ferric oxyhydroxide during our experiments could be important in several ways. For example, formation of such a precipitate is probably one of the causes for a general decrease in hydraulic conductivity which we observed upon passage of raffinate solutions through the rock cores. In addition, such precipitates offer active sites for ion-exchange and adsorption of minor components from the migrating tailings fluids.

We have traced the compositional history of the effluent solutions in Experiment 27 by means of the arrow on Figure 23. The initial pH of the influent solution was 2.3, with an Eh of 0.3 volts and a content of total dissolved iron of 290 mg/L. Point A on Figure 23 represents an early effluent from the core, showing a pH near 8 and a content of iron of only 0.95 mg/L. The change from the initial acidic, iron-rich influent solution to the alkaline, iron-poor effluent represented by Point A was due chiefly to a rapid initial reaction with calcite in the rock, with the resulting rise in pH causing the rapid precipitation of solid ferric oxyhydroxide. As Experiment 27 progressed, the composition of the effluent solution moved from Point A to Point B in Figure 23, with a drop in pH, a rise in Eh, and an increase in total dissolved iron to 115 mg/L. Continuing through Points C and D, the effluent showed a continuing fall in pH and rise in Eh. The content of iron was 164 mg/L at Point C and 185 mg/L at Point D. The remarkable feature about the experimental path in Figure 23 is that Points B, C, and D fall almost perfectly on the theoretical isopleth for 150 mg/L ferrous ion in equilibrium with ferric hydroxide. We take this agreement between the observed values of total dissolved iron in the effluent solutions and the theoretical position of the 150 mg/L ferrous iron isopleth to be good evidence for equilibrium between the solution and reactive ferric oxyhydroxide in the core.

In Experiments 9 and 14, the effluent pH remained near 8 throughout the runs (shown in Figs. 5 and 6), and the movement of iron was strongly retarded in these experiments, with C/Co values consistently less than about 0.03 (Figs. 19 and 25). Within the Eh range of these experiments (0.32 volts to 0.66 volts) conditions within the cores were well within the field of $Fe(OH)_3$, as shown in Figure 23. This indicates that the lack of mobility of iron in the alkaline fluids was probably due to the precipitation of solid ferric oxyhydroxide within the core.

Experiments 17 and 19 (Figs. 20 and 21) show quite a different behavior pattern for the movement of iron. In both of these experiments the pH of the effluent remained acidic. Iron was initially strongly leached from the rock, as evidenced by values of C/Co greater than 1, followed by C/Co values that gradually declined and approached 1. The gradual decline in C/Co probably reflects the leaching and exhaustion of any easily soluble iron that might have initially been present in the rock, as was also the case for the aluminum results shown on the same graphs.

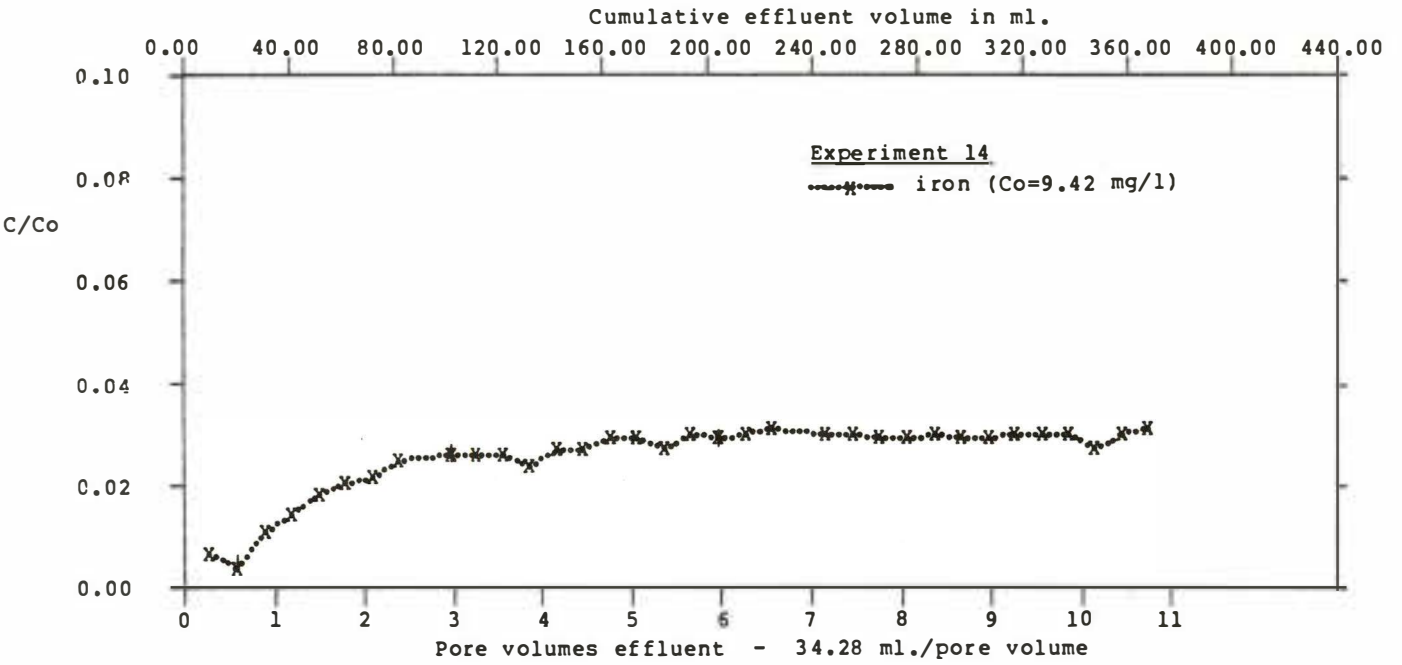

Figure 25. Breakthrough curve for iron. Experiment 14: Dilute synthetic raffinate. Initial pH = 3.35. Effluent pH remained near 8 for duration of experiment. See Figure 6 for details of pH variation during experiment.

In contrast, in Experiment 21 (Fig. 22) there was no initial high peak of rinseout of iron; in this experiment, immediate breakthrough (C/Co = 1) was observed. The pH in this experiment was nearly the same as in those which showed high initial rinseout. We do not have an explanation for this different behavior; it is possible that this particular rock sample simply did not contain any significant amount of leachable iron, or that the iron was in a form which could not be leached in the time available during the passage of the fluid.

The results for Experiment 26, involving an alkaline (pH = 8.1) and relatively reducing (Eh = 0.36 volts) tailings fluid, are also somewhat surprising, as shown in Figure 26. In this experiment we saw a very significant amount of initial rinseout of iron from the rock core (C/Co > 7), in spite of the fact that the fluid was consistently alkaline. This is in sharp contrast to our other experiments in which the iron was relatively immobile in alkaline fluids. Two explanations seem possible. First, the rock core may have been earlier contaminated by acidic, iron-rich fluids in the field, and our experiment simply rinsed out some highly soluble salt of iron. This possibility is supported by the observation that the pH of deionized water dropped to low values as the water was forced through this core. Or, second, and less likely, the Eh of 0.36 volts was sufficiently low as to reduce and mobilize a portion of the iron from solid ferric oxyhydroxides in the core. The Eh of 0.36 volts was one of the lowest used in our studies, well below the value of 0.66 volts in some of the experiments. This subject deserves more study.

One of the most important aspects of our consideration of the behavior of iron and aluminum is the tendency of these metals to form flocculent precipitates of oxyhydroxides. Other dissolved species may then be adsorbed on such precipitates, with the result that iron and aluminum may play a significant role in the attenuation and retardation of dissolved contaminants in natural waters (Parks, 1965; Hingston and others, 1972; LeGendre and Runnells, 1975; Kaback, 1977; Davis and others, 1978; Davis and Leckie, 1978, 1979, 1980; Benjamin and Leckie, 1982). We will discuss this point in some detail later in this report.

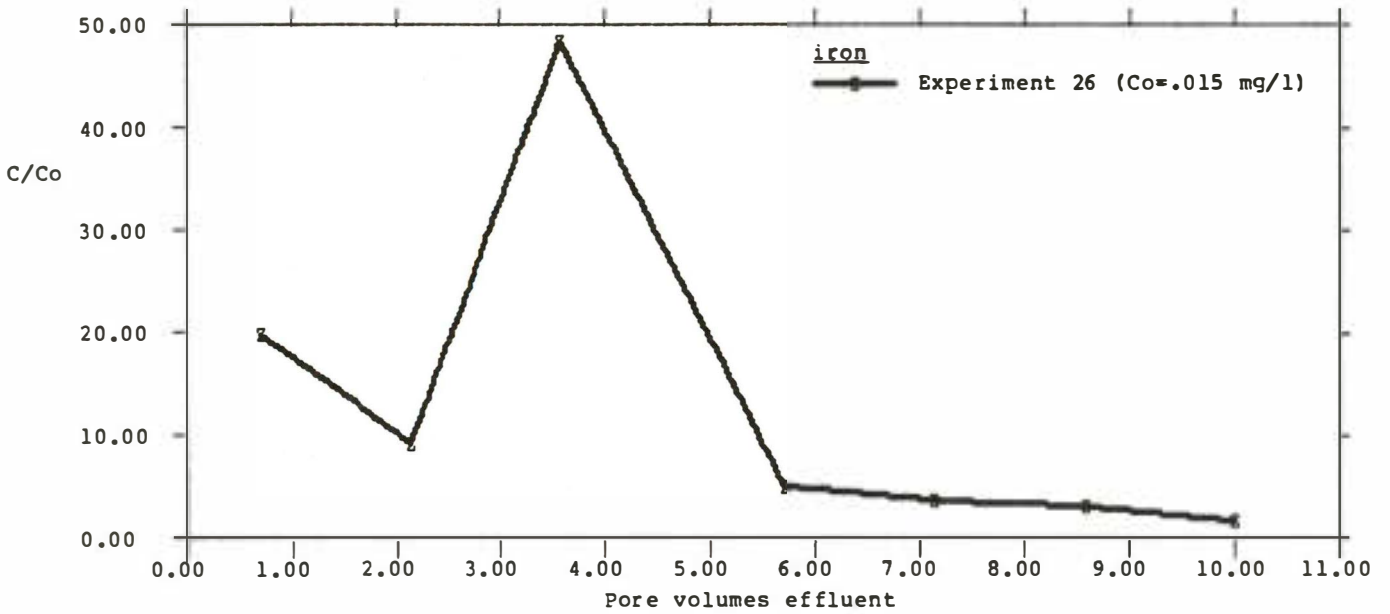

Figure 26. Breakthrough curve for iron. Experiment 26: Initial pH = 8.0. pH remained constant for duration of run. Sample from 118 feet in OW-13. Pore volume = 15.4 ml. Total effluent volume = 154 ml. The Eh of the effluent was relatively reducing, at 0.36 volts.

Silica

Considerable variation in the behavior of silica was observed in our experiments. This seems to be due in large part to differences in the original content of silica in each test solution. In many of the test raffinates a gray, translucent precipitate formed upon standing. Such solutions were centrifuged and filtered prior to passing the test solutions through the cores. Analyses of the solutions after centrifugation and filtration showed that as much as one-third of the silica originally added had been removed. The amount of dissolved and colloidal silica remaining in the test solutions varied from run to run, undoubtedly leading to some of the variation observed in the results. This problem was not experienced in Experiments 22 through 27, for which the fluids were collected in the field.

Another parameter which appeared to be important in the observed results for silica was the rate of flow of the fluid through the core. The slow kinetics of precipitation of solid silica are well known (Morey and others, 1964), and it seems possible that in our longer-term runs the silica had a greater opportunity to precipitate within the cores.

Experiment 6 (Fig. 27) reflects the general dependence on pH of the mobility of silica in the raffinates. In this experiment the value of C/Co gradually rose from zero to about 1.5 as the pH of the effluent fluid dropped from 8 to near 1.5. This behavior is consistent with attack and decomposition of the feldspars in the rock by the strongly acidic raffinate, with rapid kinetics. We presume that the loss and retardation of silica in the early portion of Experiment 6 (Fig. 27) was due to the formation of an amorphous precipitate in the pore spaces of the rock. Similarly, in Experiment 14 (Fig. 27) (and in Experiment 9, not illustrated) silica was initially strongly removed from solution. In these experiments the effluent pH remained near 8 for the entire duration of the run. It is also worth noting that the rate of flow was very slow in these two experiments (Table 9), allowing more time for polymerization and precipitation of the dissolved silica.

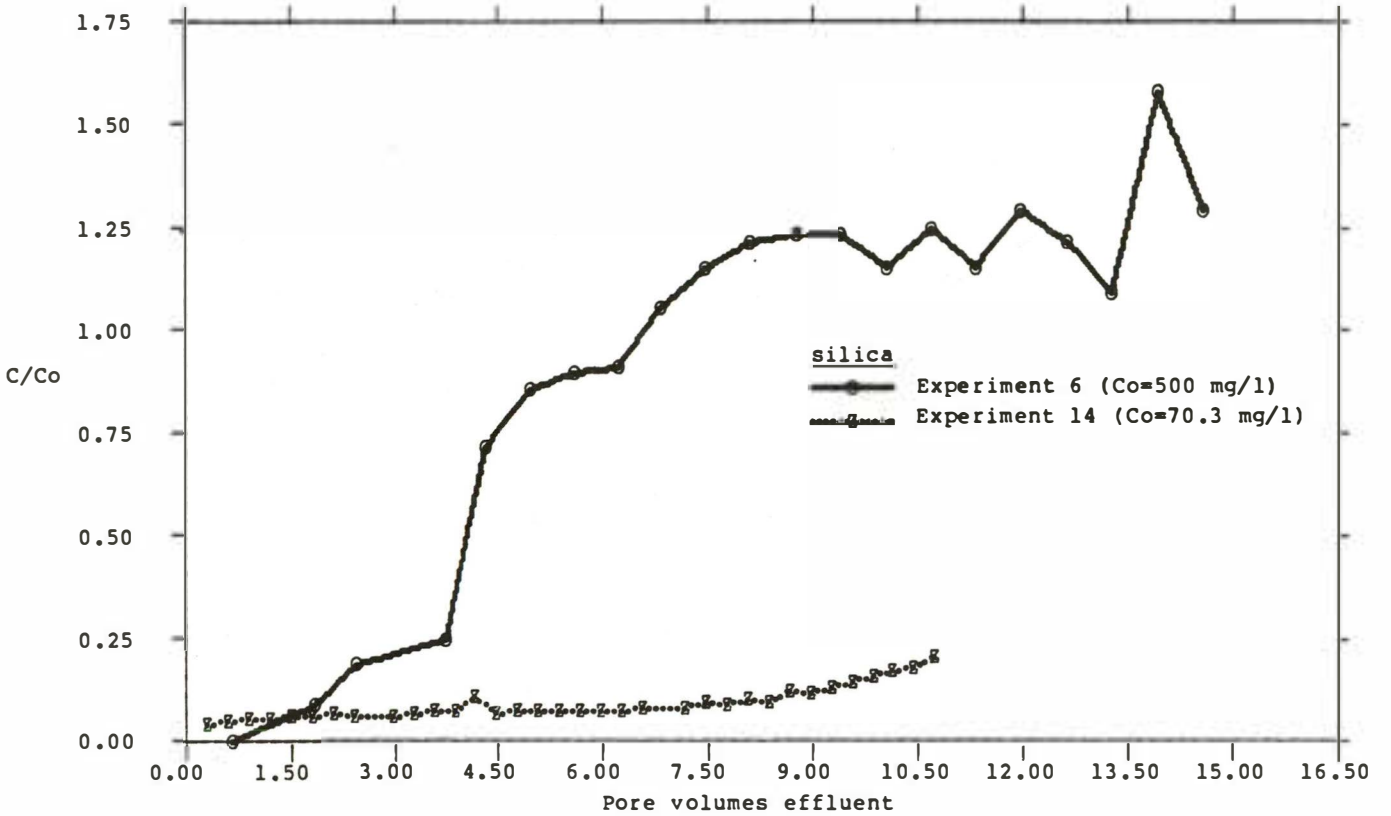

Figure 27. Breakthrough curves for silica. Experiment 6: Concentrated synthetic raffinate. Effluent pH changing from alkaline to acidic during course of run. See Figure 5 for details of pH variaton. Experiment 14: Dilute synthetic raffinate. pH of effluent remained near 8 for duration of run. See Figure 6 for details of pH.

In Experiments 19 and 23 (Fig. 28), the dissolved silica broke through early in the experiment, with minimal removal. The pH of the effluent in Experiment 19 was acidic, whereas the pH of the effluent in Experiment 23 was alkaline. And, from Table 9, it is seen that the average volumetric flow rate was identical for these two experiments. Based these observations, we conclude that neither pH nor kinetics were the controlling factors involved in determining the mobility of silica in the migrating fluids in Experiments 19 and 23. Examining the initial concentrations of silica in the four experiments summarized in Figures 27 and 28, we see that for those fluids that had high initial concentrations of silica (500 mg/L in Experiment 6 and 70 mg/L in Experiment 14), the extent of retardation was much greater than for the fluids with lower initial concentrations of silica (1.3 mg/L in Experiment 23 and 35 mg/L in Experiment 19). It thus appears that the initial concentration of dissolved silica is more important than either the pH or the rate of flow in determining the mobility of silica through the rocks. Results from the minor-ion experiments (22 through 27) further support this conclusion.

In summary, we conclude that the behavior of silica in migrating uranium-rich fluids will depend strongly on the initial concentrations. In those fluids with high initial values the silica will show significant removal and retardation due to precipitation as amorphous silica, whereas in those fluids with low initial concentrations the silica will probably move essentially with the bulk fluid. Kinetic factors appear to be less important than the initial concentrations. Our results suggest that in a field situation it might be possible to selectively regulate the plugging of the porosity in an aquifer by controlling the concentration of silica in a migrating fluid.

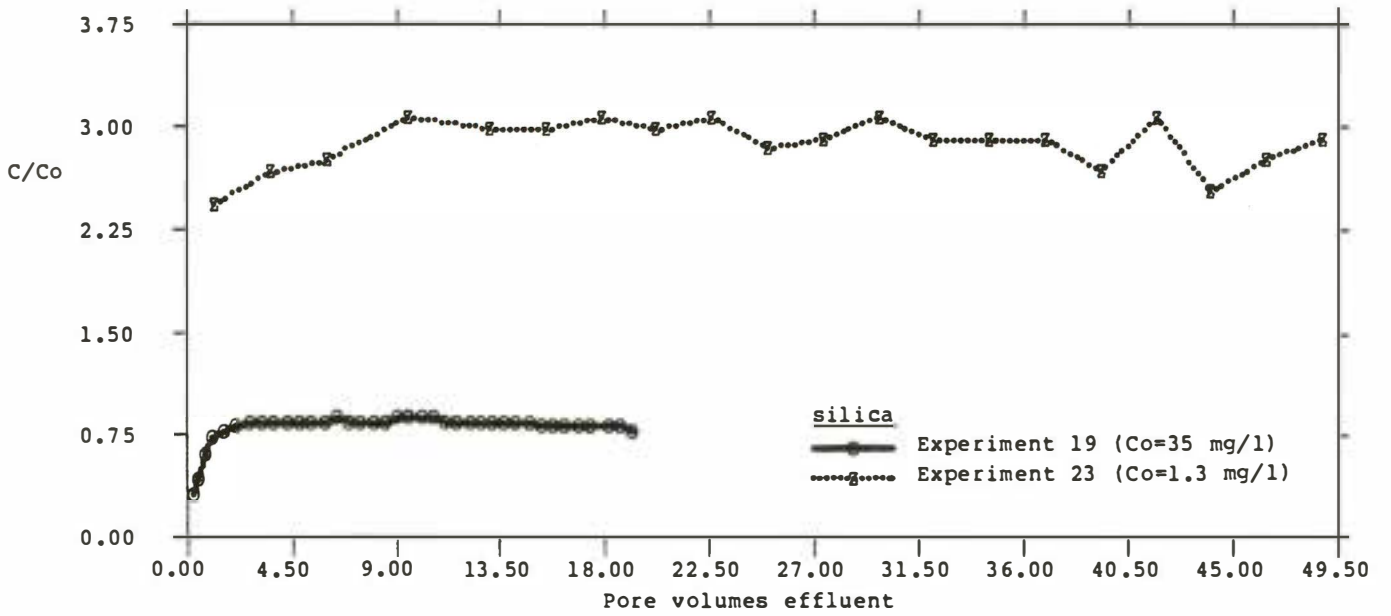

Figure 28. Breakthrough curves for silica. Experiment 19: Dilute synthetic raffinate. Constant acidic pH in effluent. Experiment 23: Alkaline tailings fluid. Effluent pH remained alkaline for entire run. See Figures 7 and 32B for details of pH variation.

Molybdenum

Concentrations of molybdenum are very high in many of the tailings fluids. For example, 170 mg/L are shown for the raffinate in Table 3. It is therefore appropriate to discuss molybdenum in the context of the major dissolved species.

Molybdenum behavior and retardation seems to be clearly related to pH. On the basis of experimental evidence, other workers (Jones, 1957; Kaback, 1977; LeGendre and Runnells, 1975) have proposed several mechanisms for attenuation of dissolved molybdenum from natural waters:

1) precipitation of a separate mineral phase;
2) sorption on clay minerals, by anion exchange with hydroxyl;
3) coprecipitation with, or sorption on, ferric oxyhydroxides.

The wide range in observed kd values for molybdenum (Table 4) is evidence of the complex behavior of this important component in the variety of test solutions.

The process of removal of molybdenum from solutions in contact with ferric oxyhydroxide is most effective between pH values of about 2 and 7 (Jones, 1957). This is the pH range in which bimolybdate ion, $HMoO_4^-$, predominates; it appears that hydrogen bonding between the bimolybdate and the hydroxyl ions within the solid may be a primary mechanism. Above a pH of about 7 molybdate ion, MoO_4^{--}, dominates, and below a pH of about 2 cationic species of molybdenum become important (Kaback, 1977).

Saturation indices, computed using WATEQFC, suggest that precipitation of a separate molybdenum mineral was highly unlikely in any of our experiments. However, we believe that adsorption, or coprecipitation, of molybdenum on iron oxyhydroxides is a very likely possibility. As discussed earlier, ferric oxyhydroxide was observed as a precipitate in many of our experiments, and in Experiment 6 (Fig. 29), in which the effluent pH fell from 8 to 1.5 (Fig. 5), the breakthrough curve for molybdenum closely resembles the curves given by LeGendre and Runnells (1975) for removal of molybdenum by ferric oxyhydroxide as a function of decreasing pH. In contrast, in those experiments in which a concentrated effluent raffinate remained alkaline, near pH 8, no retardation of molybdenum was detected (see, for example, Experiment 9, Figure 29).

Experiments 22, 23, and 24, summarized in Figure 30, exhibit a very clear-cut demonstration of the role of pH in controlling the mobility of molybdenum in our studies. In Experiment 22 of Figure 30, the effluent fluid was acidic, and molybdenum was strongly retarded. In Experiment 23, the solution was dilute alkaline tailings fluid, and the molybdenum was highly mobile. Finally, in Experiment 24 the dilute effluent changed from acidic to alkaline during the run, and the molybdenum went from immobile to mobile. These changes reflect very rapid reaction kinetics, relative to the rate of flow of the fluids.

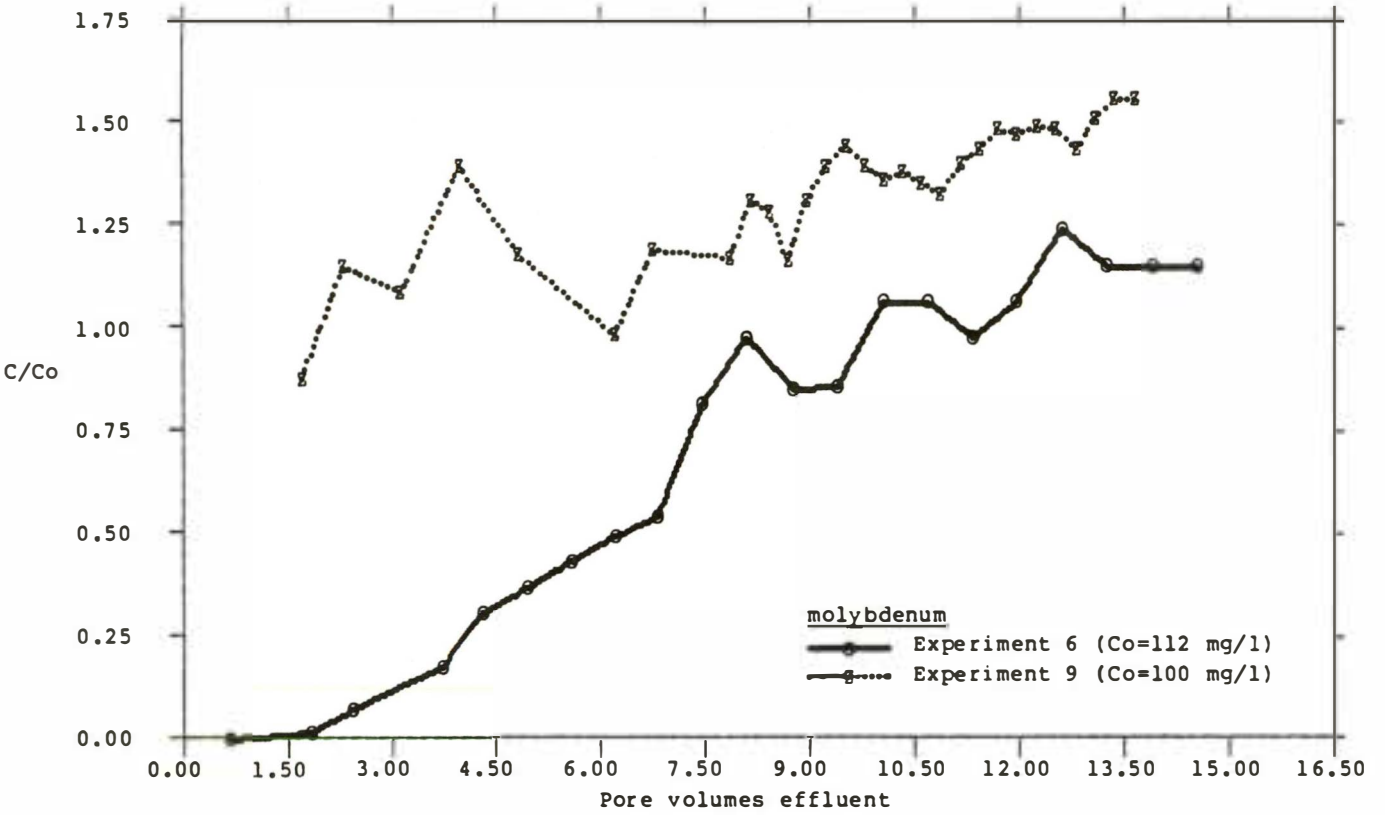

Figure 29. Breakthrough curves for molybdenum. Experiment 6: Concentrated synthetic raffinate. Effluent pH changed from alkaline to acidic. Experiment 9: Concentrated raffinate. Effluent remained alkaline for duration of run. See Figure 5 for details of pH.

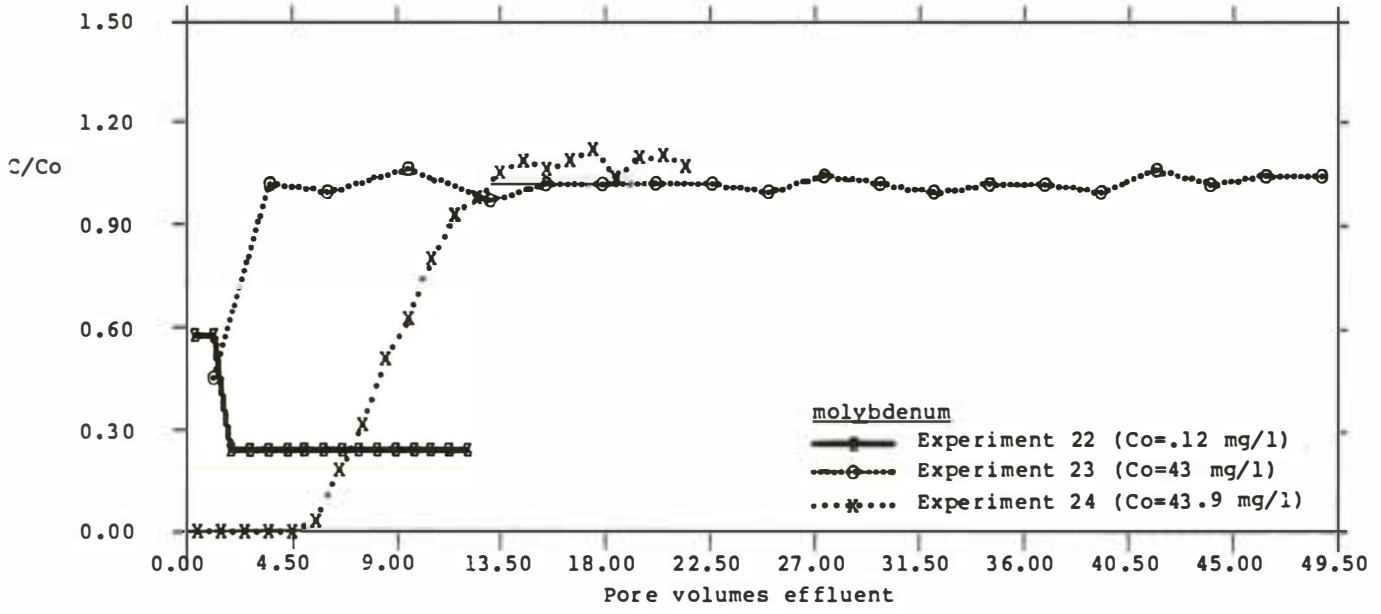

Figure 30. Breakthrough curves for molybdenum. Experiment 22: Dilute acidic raffinate. Constantly acidic effluent. Experiment 23: Dilute, alkaline tailings fluid. Constantly alkaline effluent. Experiment 24: Dilute alkaline tailings fluid. Effluent changed from acidic to alkaline during run.

Unfortunately, in addition to pH, other factors probably cloud the picture on molybdenum. There is almost certainly a role played by the absolute concentration of molybdenum in the fluid. For example, in Experiment 21, in which the effluent was constantly acidic, considerations of pH alone would lead us to predict that molybdenum would be strongly retarded upon passage through the core. However, as shown by the results summarized in Figure 31, molybdenum showed a significant degree of breakthrough, even in this acidic medium. We attribute this unexpected result to the very high initial concentration of molybdenum in the fluid, 125 mg/L, with the suggestion that the adsorption sites on the ferric oxyhydroxides in the rock were simply overwhelmed by the mass of molybdenum carried in by the fluid. In contrast, in Experiment 14 (Fig. 31), in which the effluent tailings fluid was constantly alkaline and the initial concentration of molybdenum was only 10 mg/L, a considerable degree of retardation of molybdenum took place; again, this is in direct opposition to the results that would be predicted on the basis of pH alone. The only explanation that we can offer for the observations in Experiment 14 is the possibility that an unknown mineral of molybdenum precipitated in the core.

Another factor that might be important in determining the mobility of molybdenum is the formation of stable aqueous complexes. It is well known, for example, that molybdenum and silica can combine under some conditions to form extremely stable complex ions in aqueous solution (Cotton and Wilkinson, 1972). In fact, such a reaction is the basis for one analytical procedure for measuring the concentration of dissolved silica in solution (American Public Health Association, 1980).

Our results for molybdenum strongly suggest that this component may not always be a good tracer for monitoring the escape of uranium-rich fluids from tailings ponds and in-situ mining operations. Factors such as pH, total concentration, and the availability of reactive substrates must all be considered in predicting the movement of molybdenum.

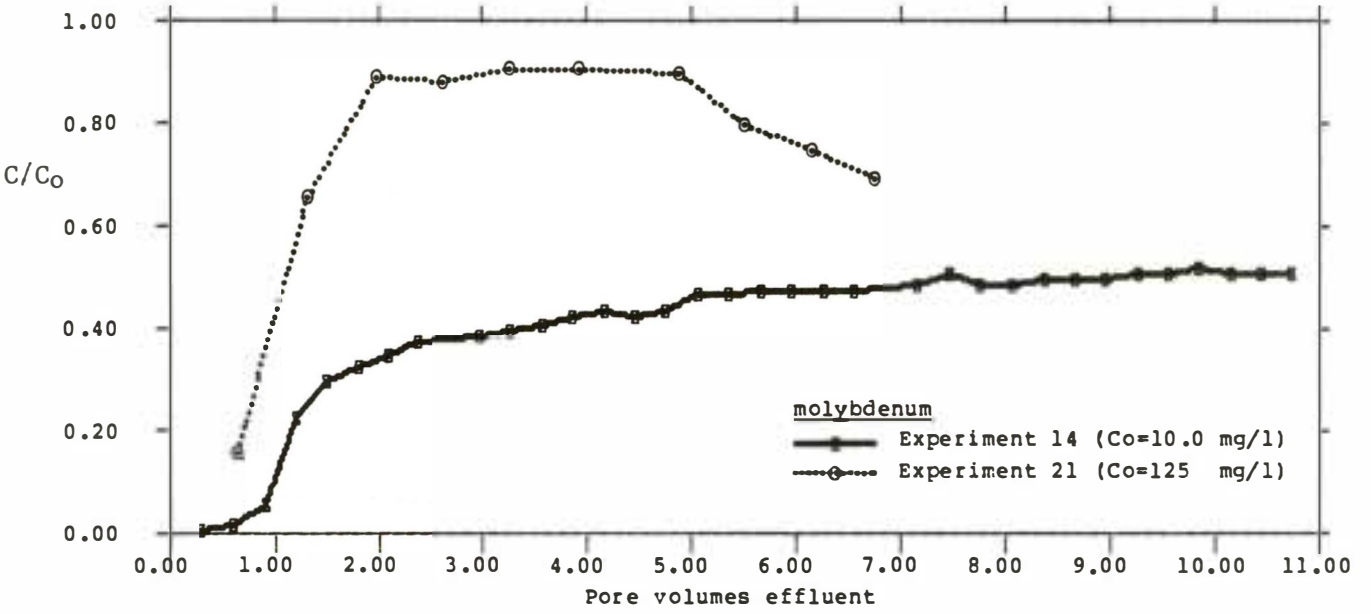

Figure 31. Breakthrough curves for molybdenum. Experiment 14: Dilute synthetic raffinate. Constantly alkaline effluent. Experiment 21: Concentrated synthetic raffinate. Constantly acidic effluent.

Statistics

Error bars are shown on several of the graphs in this report for the breakthrough of the major dissolved species. The uncertainty reflected in the error bars was obtained by the ratioing of one-sigma (67% confidence level) estimates of analytical errors, as outlined in the discussion in the remainder of this section (based on Dixon and Massey, 1957, and discussions with Professor John Andrews, Department of Geological Sciences, University of Colorado, Boulder).

The one-sigma analytical error over an infinite number of samples was estimated from the analyzed concentration, C, of each effluent aliquot, in which the error in C = $(\sigma)(1.960)$, or the detection limit = $(\sigma)(1.960)$, whichever is appropriate (1.960 is the coefficient for the 95% confidence level for an infinite number of samples, taken from Tables of Critical Values of Student's t-distribution; Rohlf and Sokal, 1969, p. 160-161). Therefore,

$$\sigma_C = 0.05C/1.960 \tag{7}$$

or

$$\sigma_C = \text{detection limit}/1.960. \tag{8}$$

Two or three samples of each test solution were analyzed prior to passage through a core. An estimate of σ for the original concentration, Co, of the test fluid was obtained by combining analytical error, A, and an estimate, B, for based on the range, W, of analyzed Co values:

$$\sigma_{Co} = (A^2 + B^2)^{0.5} \tag{9}$$

where $A = 0.05Co/1.960$

and $B = 0.886W$, for two Co values,
or $B = 0.591W$, for three Co values (Dixon and Massey, 1957).

The uncertainty range (UR) for breakthrough curves was then obtained by combining the errors on C and Co and by setting up ratios of the worst cases (Professor John Andrews, Department of Geological Sciences, University of Colorado, Boulder), as follows:

$$UR = (C - \sigma_C)/(Co + \sigma_{Co}) \text{ to } (C + \sigma_C)/(Co - \sigma_{Co}) \tag{10}$$

We have not had the opportunity to run the multiple chemical analyses that are required to determine error bars for the minor dissolved species in the tailings fluids. We hope to generate this information in the future. However, comparison of the results of Experiments 23 and 26, which were designed as duplicate runs, gives some idea of the total uncertainty in our experimental results for the minor and trace species.

Behavior of Minor Dissolved Species

Introduction

The work on minor dissolved species constitutes a somewhat independent study, done after completion of the experimental work on the major components in synthetic raffinates. The chief difference between the experimental approach used in the two studies is that the fluids used for the minor species were actual samples of alkaline and acidic tailings fluids, collected from the several ponds and the mill circuit at Canon City. The laboratory apparatus and approach used in the two programs were identical. We envision the study of the minor components as being built upon the foundation of results and understanding derived from the investigation of the major components.

pH and Eh

In the discussion which follows, emphasis is again placed on the role of pH in controlling the mobility of dissolved species. Experiments were run over a wide and variable range of pH. Attempts were also made to control Eh using various gases and chemical reagents, but the total range of Eh involved in the experiments is only about 0.3 volts.

Six of the experiments run in the study of the minor species, numbered 22 through 27, are summarized in Table 9. The rock samples came from two observation wells, OW-13 and OW-14. The initial pH values for the influent tailings fluids ranged from 2.3 to 8.3, and the initial Eh values ranged from (+)0.32 volts to (+)0.66 volts. Our lowest experimental value of Eh was about 0.2 volts above the value of 0.12 volts for the "natural" ground water from Canon City, which became available long after most of our experimental work had been completed (Table 7). This suggests that our experimental work probably represents conditions more oxidizing than those that might prevail in the deep ground water system near the mill at Canon City. Figures 32 and 33 summarize the values of Eh and pH measured in the effluent solutions during the course of Experiments 22 through 27.

Some of the pH values of the test solutions changed rather dramatically during the course of the experiments, as shown by Figures 32C, 33A, and 33C. In addition, in the case of Experiment 22 (Fig. 32A), the pH of the test fluid fell from an initial value of 6.0 in the influent solution to 3.7 in the first pore volume of effluent. We attribute the increasing pH values in the experimental runs to reaction with the calcite cement in the rock cores, and we believe that the decreasing pH values reflect rinse-out of acidic fluids that had contaminated the rocks before sampling.

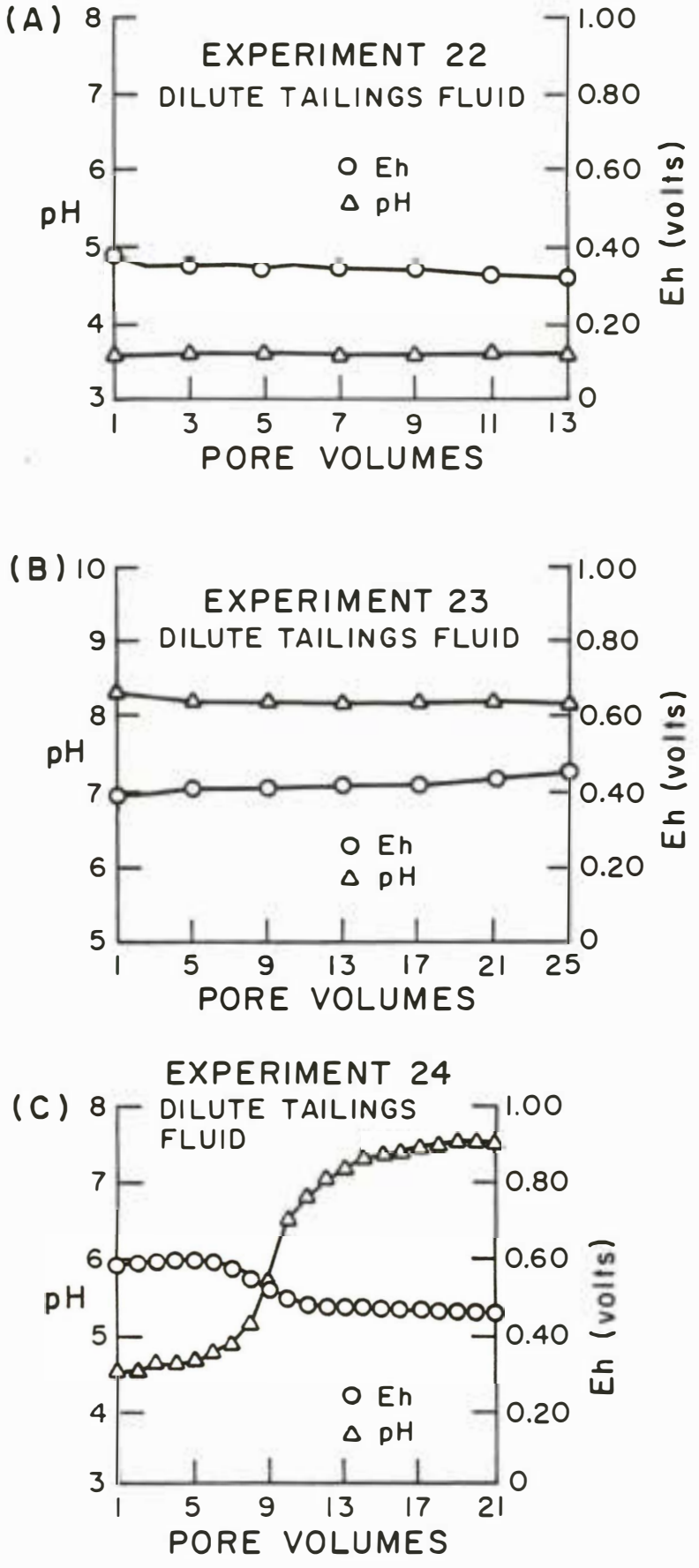

Figure 32. A. Observed Eh-pH values for effluent in Experiment 22. Dilute, acidic influent. B. Observed Eh-pH values for effluent in Experiment 23. Dilute, alkaline influent. C. Observed Eh-pH values for effluent in Experiment 24. Dilute, alkaline influent.

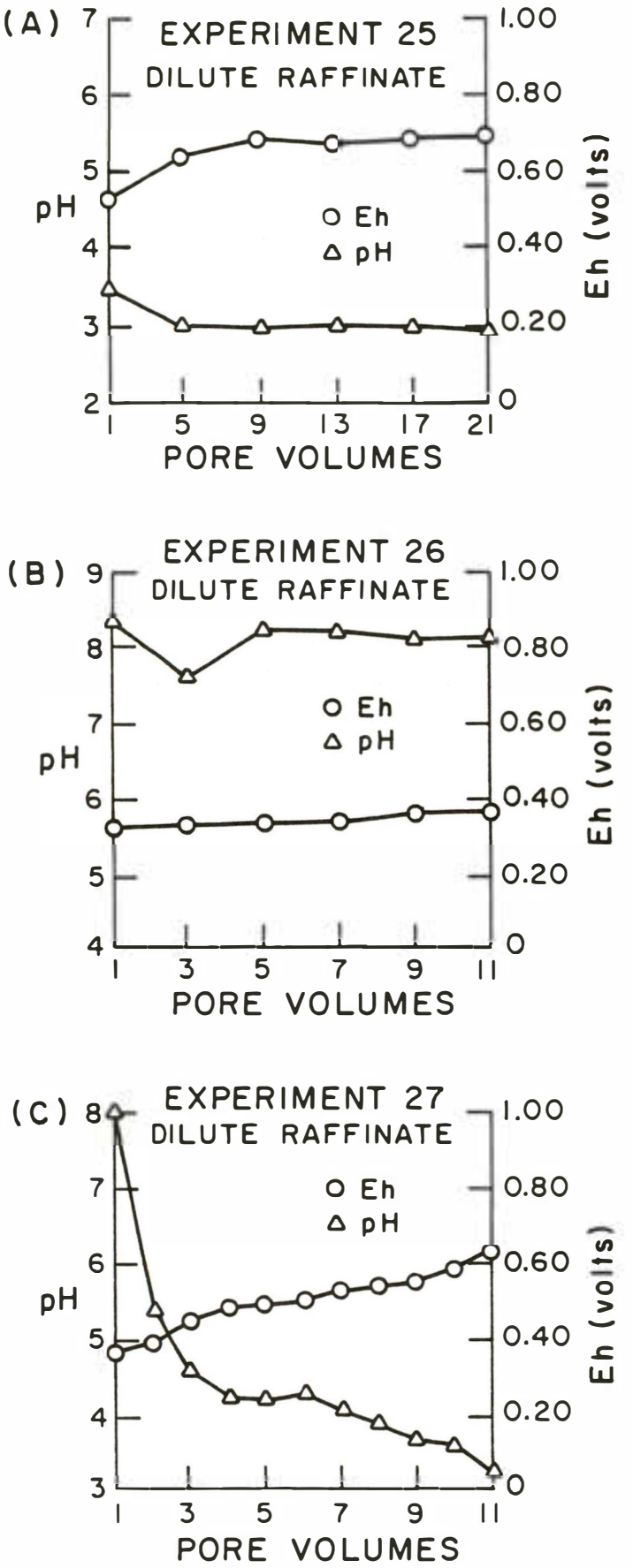

Figure 33. A. Observed Eh-pH values for effluent in Experiment 25. Dilute, acidic influent. B. Observed Eh-pH values for effluent in Experiment 26. Dilute, alkaline influent. C. Observed Eh-pH values for effluent in Experiment 27. Dilute, acidic influent.

Manganese

Figure 34 shows the stability fields of some manganese minerals and the theoretical equilibrium activities of dissolved species in the system $Mn-H_2O-S$, at $25^{o}C$ and 1 atmosphere total pressure. The total activity of the dissolved sulfur (10^{-1}; 9600 mg/l as sulfate) roughly corresponds to the values of dissolved sulfate that are observed in our tailings fluids. From the stability diagram we can predict that the absolute concentrations of dissolved manganese should be greatest in strongly acidic tailings fluids. Also, the values of C/Co should be lower for passage of alkaline tailings fluids through rock cores than for acidic fluids, simply because of the decreased solubility of manganese minerals at moderate pH values. A complicating factor in such simple predictions is the role of adsorption. Sung and Morgan (1981) show that significant adsorption of Mn^{++} occurs on solid ferric oxyhydroxide at elevated pH; as described earlier, we believe that the precipitation of ferric oxyhydroxide plays a dominant role in the observed chemical behavior of many of the dissolved species in the test fluids, probably including manganese.

In examining representative examples of our experimental data (Fig. 35) for manganese, we see that predictions based on the role of pH are generally supported by the results. For example, in comparing the breakthrough curves for three different experiments in Figure 35, the two experiments involving acidic tailings fluids (Experiments 22 and 25) both show significantly greater transport and mobility of manganese (C/Co > 1) than does the single curve for an alkaline fluid (Experiment 23). This is further supported by the results for Experiment 24 (Fig. 36), in which the pH of the effluent fluid went from acidic at the start of the experiment to alkaline at the end of the run (Figure 32C); in this experiment, manganese was mobile and strongly rinsed out of the core at the initially acidic values of pH, followed by immobility and removal of manganese from the fluid as the pH rose to alkaline values.

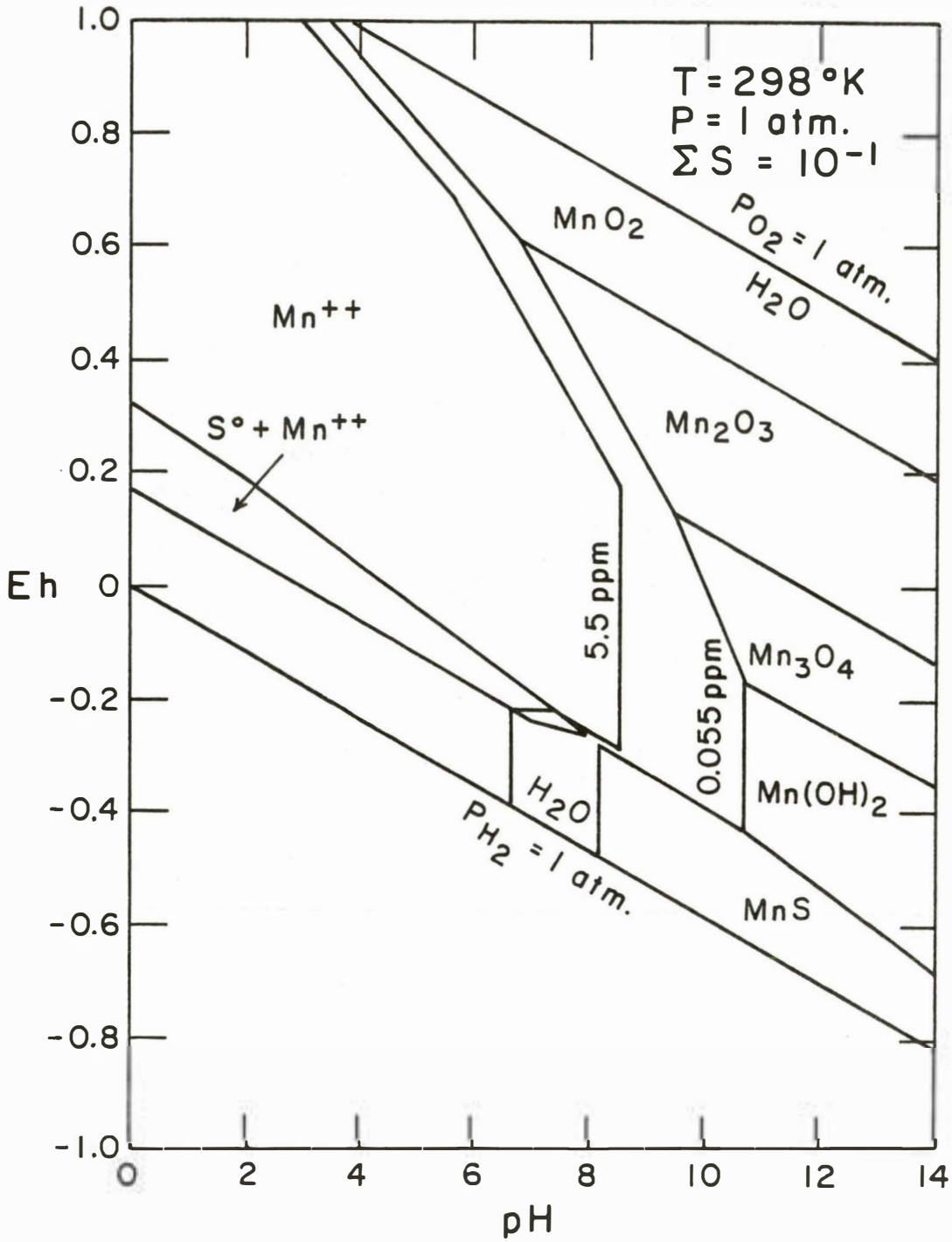

Figure 34. Thermodynamic stability relationships for the system Mn-H_2O-S. Total concentration of sulfur corresponds approximately to values of sulfate observed in tailings fluids (constructed from thermodynamic data in Garrels and Christ, 1965).

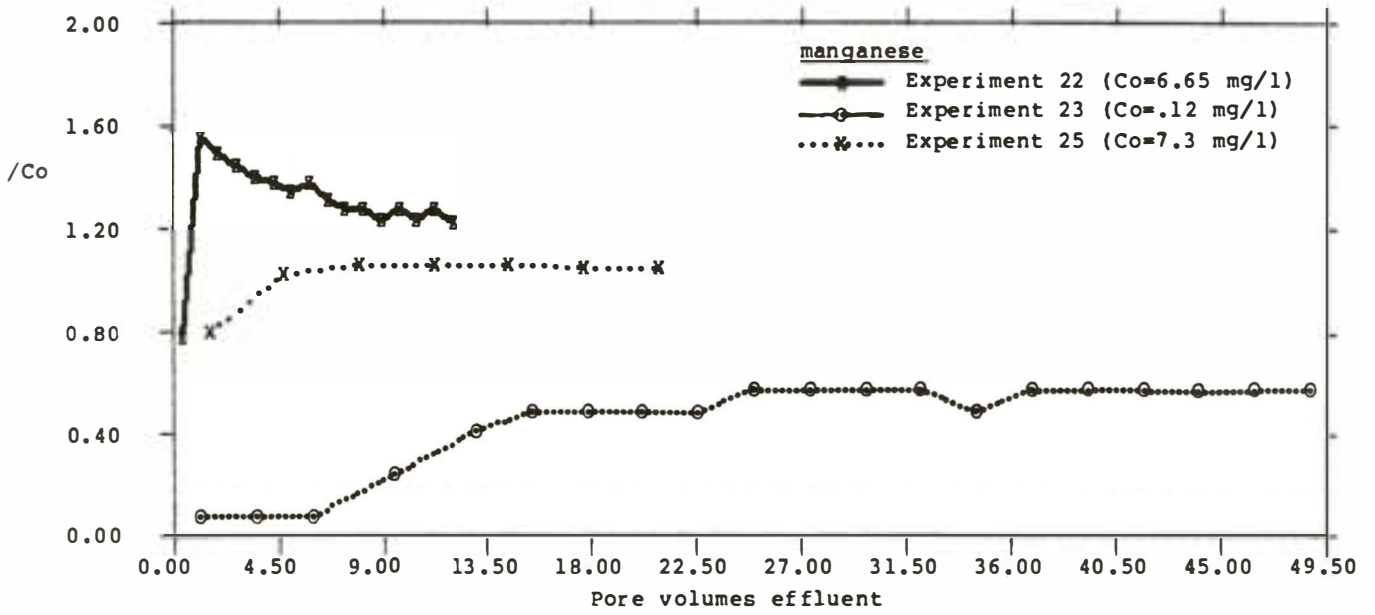

Figure 35. Breakthrough curves for manganese. Experiment 22: Dilute, acidic influent. Constantly acidic effluent. Experiment 23: Dilute, alkaline influent and alkaline effluent. Experiment 25: Dilute, acidic influent and acidic effluent. See Figures 32A, 32B, and 33A for Eh-pH values.

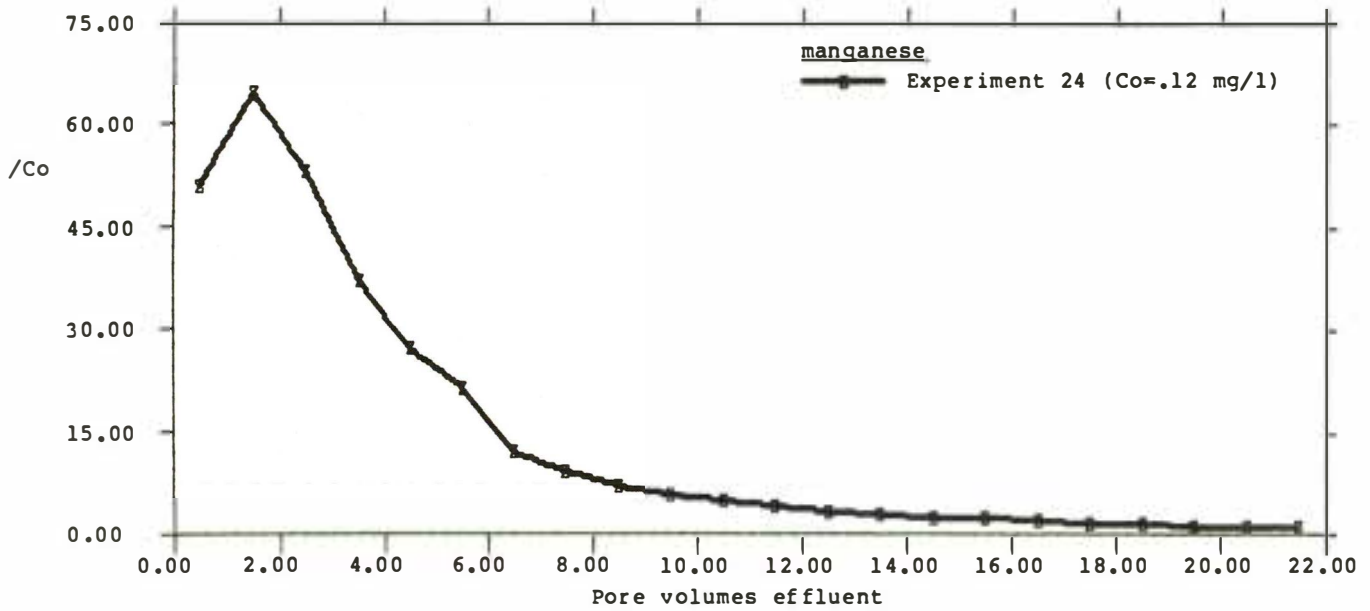

Figure 36. Rinse-out and breakthrough of manganese in Experiment 24. See Figure 32C for Eh-pH values. The initially alkaline influent was transformed into an acidic effluent upon passage through the core, then gradually became alkaline again. It appears that this sample of core, from a depth of 68 feet in OW-13, was contaminated in the field prior to collection.

Figure 36 summarizes the result of Experiment 24. In this experiment the original influent tailings fluid had a pH of 7.5 (Table 9). However, the effluent fluid was initially acidic (Fig. 32C), changing only gradually back toward the original alkaline value. The initially low pH of the effluent seems to represent rinse-out of an acidic fluid that contaminated the rock in the field prior to sampling. As discussed earlier, the contaminating fluid could have been used by the drillers in constructing the observation well, or it could have been an acidic tailings fluid that escaped from a pond.

Our conclusion regarding the mobility of manganese in tailings fluids in contact with bedrock is that it is strongly controlled by the pH, and that there is at least a suggestion that precipitation of solid manganese oxides or hydroxides may in some instances exert a control on the solubility of total dissolved manganese. The kinetics of the reactions involving manganese are very fast. We can expect manganese to move with the fluids from a tailings pond or from an in-situ leaching operations if the pH is low. In addition, we believe that in one of our experiments (Experiment 24), we can recognize pre-contamination of the rock by the shape of the rinse-out curve for manganese.

Cobalt and Nickel

Cobalt and nickel are both Group VIII metals in the periodic table, and according to Hem (1970) these two metals behave in a similar manner in aqueous solution. This is well illustrated by the results of our Experiment 22, Figure 37, in which cobalt and nickel show rapid breakthrough and mobility with similar values of C/Co under constantly acidic conditions (pH and Eh values for Experiment 22 shown in Fig. 32A). This behavior is in agreement with the known high solubilities and mobilities of cobalt and nickel under acidic, oxidizing conditions, as summarized in Figures 38A and 38B. Figures 38A and 38B show the stability of selected solid phases and the fields of predominance of aqueous species for cobalt and nickel as a function of Eh and pH. The key control on the solubility of these two components is pH, with free Ni^{++} and Co^{++} predominating in aqueous solution over a very broad range of Eh.

In Table 12 we have summarized the observed steady-state concentrations of total cobalt and nickel dissolved in the effluent solutions from four of our six experiments; the concentrations listed in Table 12 were relatively constant during the latter parts of the experimental runs. (Experiments 24 and 27 are omitted from Table 12 because of the variable pH values and variable concentrations of species observed in the experiments.) Also, note the similarity in C/Co values for cobalt and nickel in Table 12.

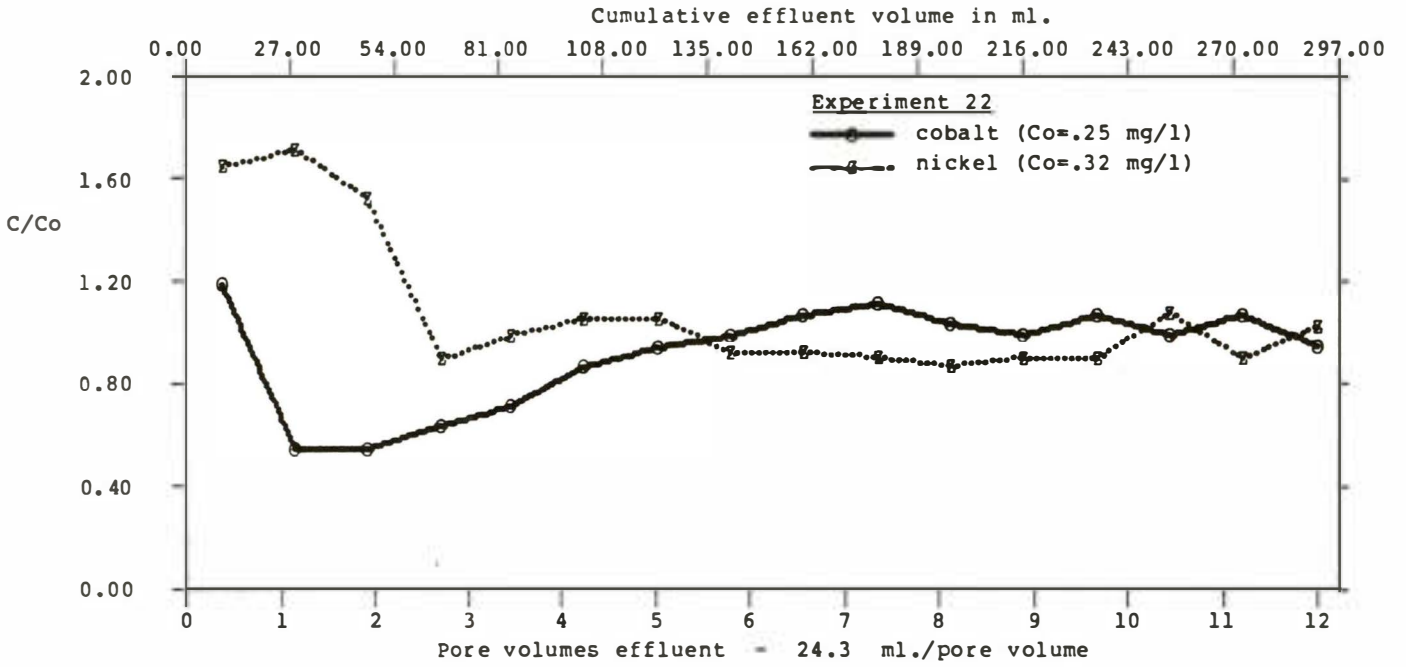

Figure 37. Breakthrough curves for cobalt and nickel in Experiment 22. Dilute raffinate influent. Constantly acidic effluent. See Figure 32A for Eh-pH values.

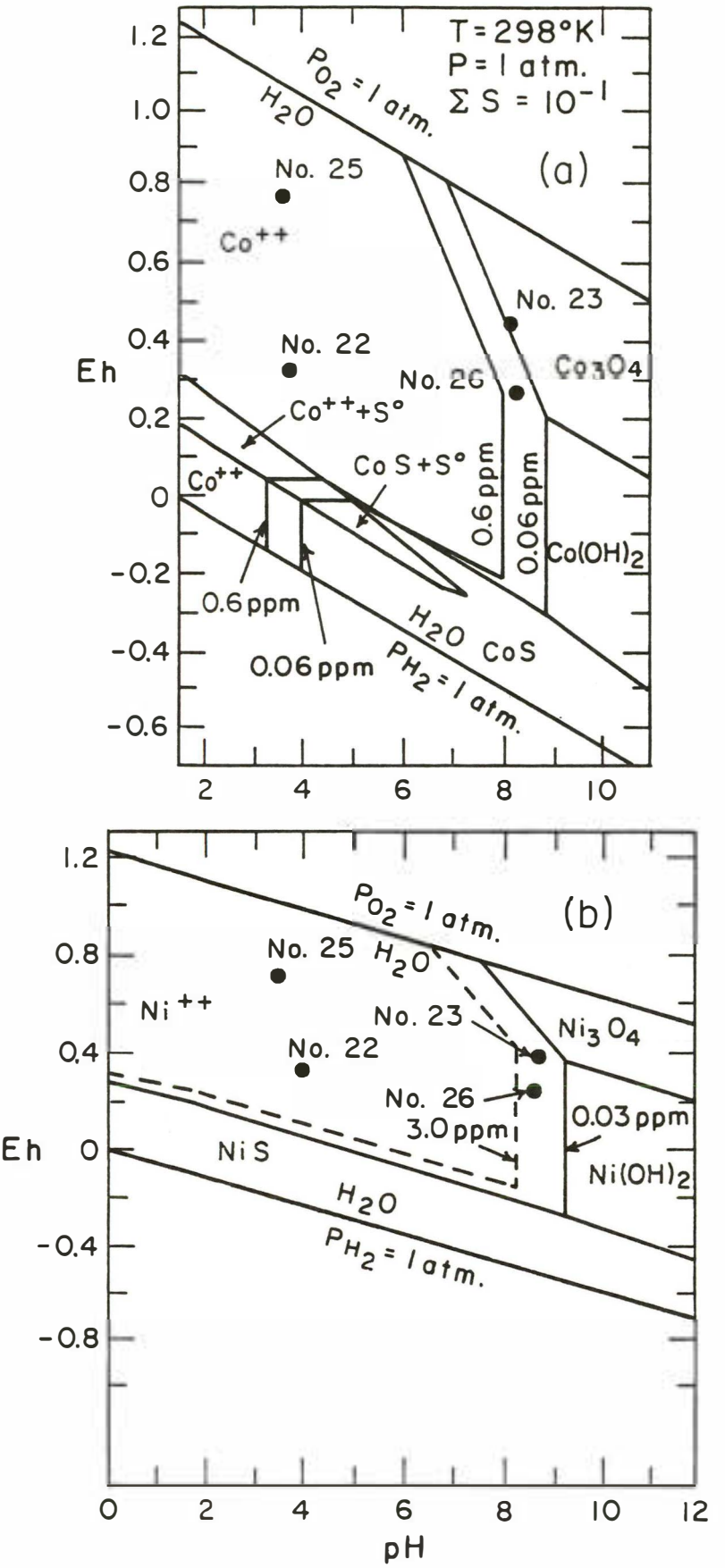

Figure 38A and 38B. Eh-pH stability diagrams for cobalt and nickel (constructed from thermodynamic data in Garrels and Christ, 1965).

Table 12. Observed values of C/Co and final effluent concentrations for cobalt and nickel in the four experiments that had relatively constant pH values. See Figures 32 and 33 for details of Eh and pH. Units in mg/l. ND = not determined.

Experiment	Equilibrium cobalt	Equilibrium C/Co	Equilibrium nickel	Equilibrium C/Co
22	0.25	1.0	0.32	1.0
23	0.05	1.6	0.10	2.5
25	0.35	1.2	0.30	1.5
26	<0.03	ND	<0.02	ND

The observed values of Eh and pH for the experiments in Table 12 have been used to plot the points in Figures 38A and 38B. As shown in Table 12, for cobalt in Experiments 23 and 26, the observed concentrations of 0.05 and <0.03 mg/l agree fairly well with the theoretical values of about 0.06 and 0.6 mg/l corresponding to the positions of the points in Figure 38A. However, for Experiments 22 and 25, the observed concentrations are far below those that should obtain for the Eh and pH conditions of the experiments. This apparent disagreement is probably due to the simple fact there was not enough cobalt present in the influent solution, or available in the rock, to satisfy the theoretical solubility requirements of Points 22 and 25 in Figure 38A.

In Figure 38B the plotted points for Experiments 23 and 26 represent theoretical activities of about 0.3 mg/l Ni^{++} in solution, compared to observed values of 0.10 and <0.02 mg/l in the effluent solutions (Table 12). As in the case of cobalt, the effluent solutions in Experiments 22 and 25 in Figure 38B contain far less than the theoretical equilibrium concentrations of nickel for the minerals considered.

The fact that the observed solubilities in Experiments 23 and 26 agree with the theoretical values (Figs. 38A and 38B) is permissive evidence that the precipitation of solid phases controls the mobility of Co and Ni, rather than ion-exchange and sorption.

In Experiment 24, Figure 39, cobalt and nickel behave in a very similar way to each other. In this experiment, both metals show rapid breakthrough and high initial rinseout, followed by a gradual decrease in C/Co to values near 1. During the course of Experiment 24 the pH of the effluent went from acidic (pH 4.5) to alkaline (pH 7.5). We earlier suggested that the rock core used in Experiment 24 had probably suffered contamination in the field prior to sampling. This suggestion is again strengthened by the very high C/Co values (about 9.0) observed in the initially acidic aliquots of effluent in Experiment 24. It seems probable that these high C/Co values result from rinseout of soluble salts of cobalt and nickel left on the surfaces of the mineral grains by the contaminating fluid.

From our results, it appears that cobalt and nickel are rapidly precipitated and would therefore not serve as effective tracers in alkaline fluids.

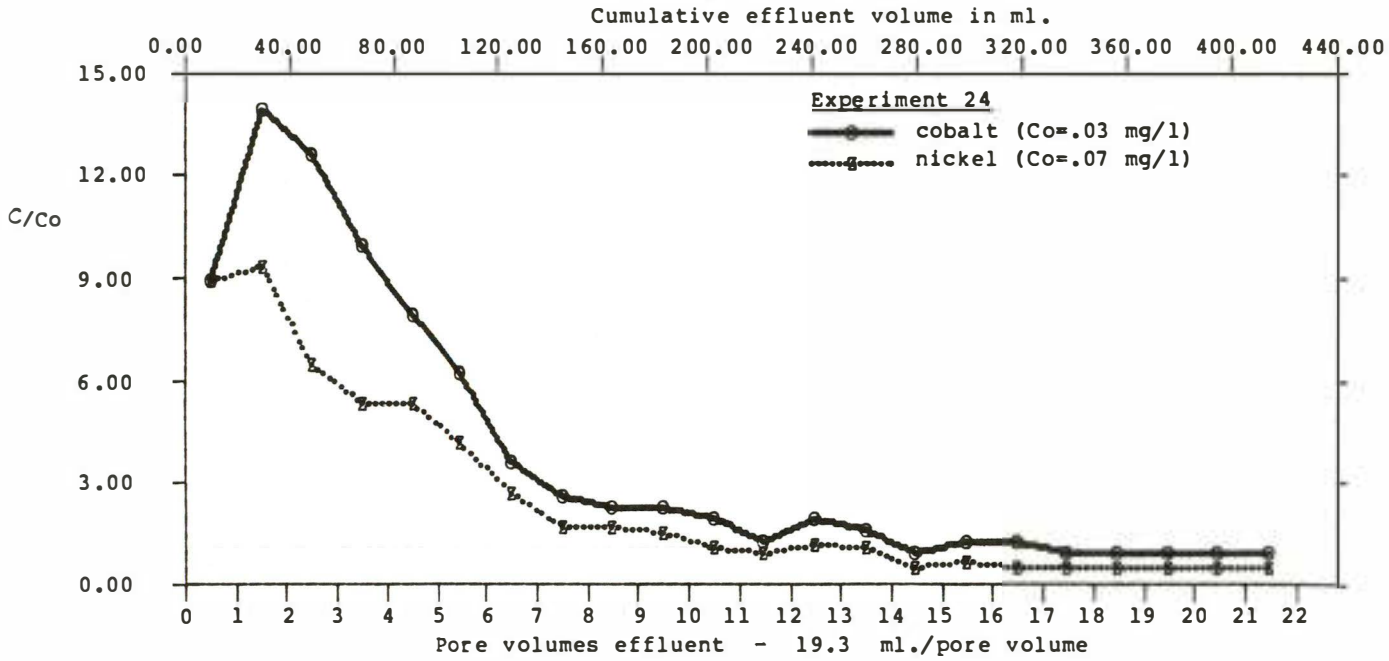

Figure 39. Breakthrough curves for cobalt and nickel. Experiment 24: Dilute, alkaline influent. Effluent changed from acidic to alkaline during run. See Figure 32C for Eh-pH values.

Copper

The mobility of copper appears to be controlled principally by pH, at least within the range of Eh values observed in our experiments (0.32 to 0.66 volts, Table 9). Figure 40 summarizes the results for copper from three experiments. The Eh-pH values for the experiments are summarized in Figures 32B, 33A, and 33C, and the flow rates are listed in Table 9. In Experiment 25 the influent fluid was dilute, acidic raffinate, and as shown in Figure 40, the copper was completely mobile (C/Co = 1). In Experiment 23 (Fig. 40), the solution was a dilute, alkaline tailings fluid, and copper was partially retarded for the entire length of the run (C/Co = 0.2 to 0.5). Because the average flow rates in Experiments 23 and 25 were very similar (20 ml/hr and 14 ml/hr, respectively), it is clear that pH was the major controlling parameter. The kinetics of the retarding reaction was rapid compared to the rate of flow of the fluids.

In Experiment 27, the effluent went from alkaline at the start of the run to acidic at the end (Fig. 33C), with a corresponding change from immobility to mobility for the copper (C/Co = 0.15 to 1.25).

The behavior of copper in our experiments agrees with known stability relationships, in which copper is highly soluble as free Cu^{++} ion under acidic, generally oxidizing conditions. We cannot identify any effects of aqueous complexes of copper in the results shown in Figure 47. Under alkaline conditions copper should precipitate as the solid oxide, hydroxide, or carbonate.

In addition to possible control by solid mineral phases of copper at elevated pH values, strong sorption of copper can also occur on iron oxyhydroxides. Swallow and others (1980) showed that essentially all of the dissolved copper (as cupric ion) in their studies, up to about 3 mg/l, was adsorbed on iron oxyhydroxides above a pH of about 6. The observed precipitation of iron oxyhydroxides in our experiments thus allows the interpretation that dissolved copper is scavenged from the migrating fluids under alkaline conditions by the precipitated iron compounds, in agreement with the observed rapid kinetics of removal. This is an example of our experimental results in which we cannot separate the effects of precipitation from those of ion-exchange and sorption.

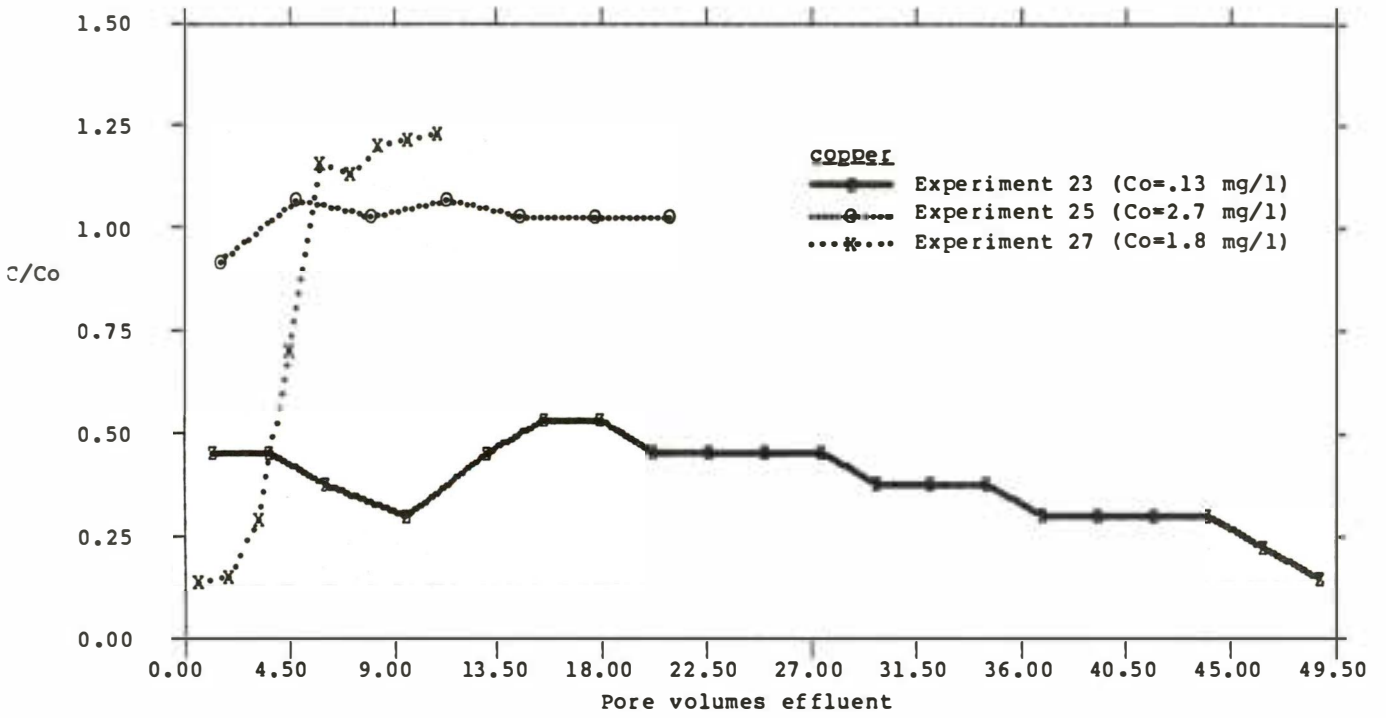

Figure 40. Breakthrough curves for copper. Experiment 23: Dilute, alkaline influent. Effluent remained alkaline. Experiment 25: Dilute, acidic influent. Effluent remained acidic. Experiment 27: Dilute, acidic influent. Effluent changed from alkaline to acidic during run. See Figures 32B, 33A, and 33C for Eh-pH values.

Zinc

Zinc is generally removed from the tailings fluids as they pass through the samples of bedrock under alkaline conditions, but it is mobilized and leached out of the rock under acidic conditions. Results that generally show this behavior are summarized for Experiments 22, 25, and 27 in Figure 41. The most reasonable explanation for this behavior is the probable precipitation of solid ZnO, or $Zn(OH)_2$, at elevated pH values, as shown by the theoretical stability relationships in Figure 42. In Experiment 24 (Fig. 43), in which the effluent fluid went from acidic (4.5) to alkaline (7.5), zinc showed a very great initial rinseout under acidic conditions (C/Co = 32), followed by diminished rinseout as the pH of the fluid became alkaline. The initially acidic pH of the effluent is consistent with our observation that this particular core had probably suffered contamination prior to sampling.

Figure 42 shows the theoretical stability relationships for zinc in the presence of 9600 mg/l dissolved sulfate ion. The observed concentrations of zinc in the steady-state effluent from Experiments 23 and 26 (0.25 mg/l and 0.01 mg/l, respectively) are consistent with a possible solubility control (at theoretical values of about 0.6 mg/l in Figure 42) by ZnO or $Zn(OH)_2$. However, the observed concentrations of 1.8 and 3.6 mg/l zinc in Experiments 22 and 25 are far below the theoretical concentrations that should obtain in the presence of ZnO at the measured values of Eh and pH, suggesting that inadequate zinc is present in the system to meet the theoretical solubility requirements.

We do not have an explanation for the long delay in breakthrough of zinc in Experiment 22 (Fig. 41). However, it may be related to the fact that the original pH of the influent test solution was near-neutral (Table 9), dropping rapidly to a pH of 3.7 in the first pore volume of effluent. The original high pH may have caused some initial precipitation of zinc, possibly followed by redissolution.

Zinc can also be strongly retarded by adsorption on iron oxyhydroxides, especially above pH values of about 5 (Jones and MacNaughton, 1977). Adsorption could therefore also have been an important factor in our experiments, which would be consistent with rapid kinetics of removal.

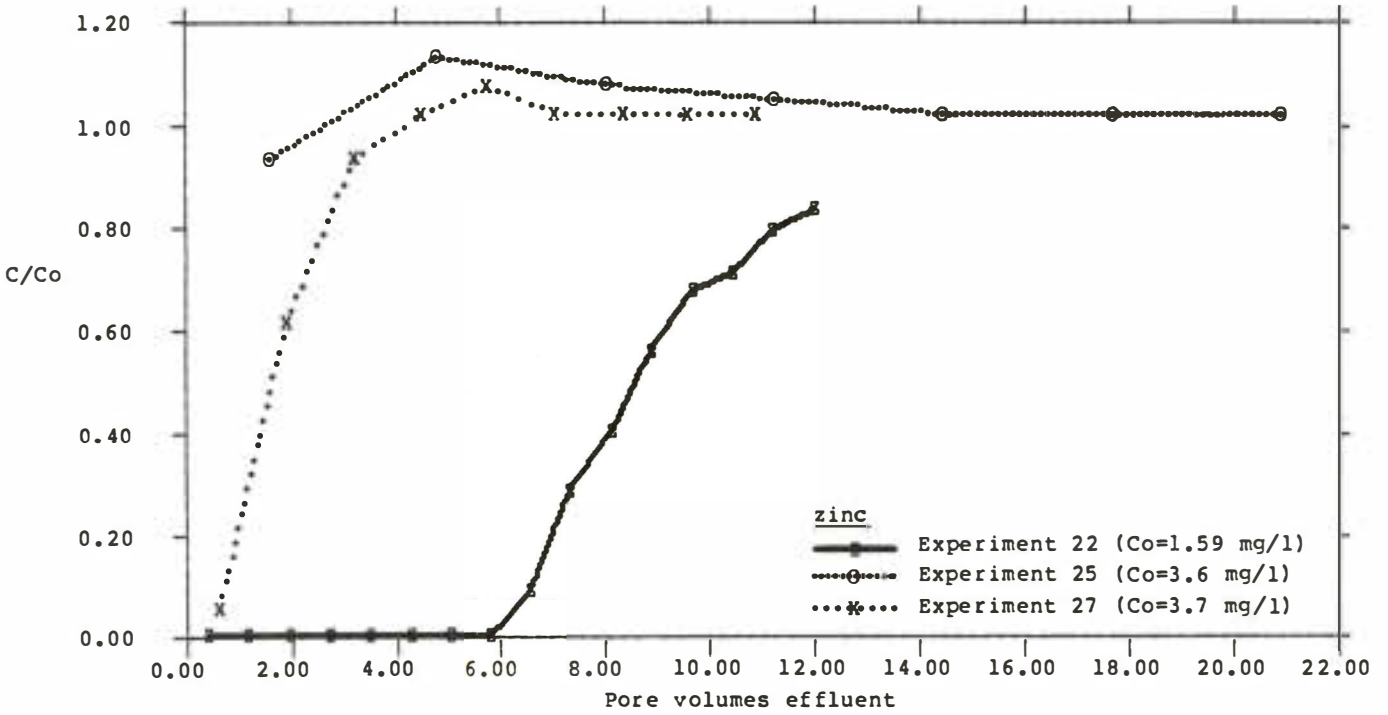

Figure 41. Breakthrough curves for zinc. Experiment 22: Dilute, acidic influent, with effluent becoming more acidic during run. Experiment 25: Dilute, acidic influent. Acidic effluent. Experiment 27: Dilute, acidic influent. Effluent changed from alkaline to acidic during run. See Figures 32A, 33A, and 33C for Eh-pH values.

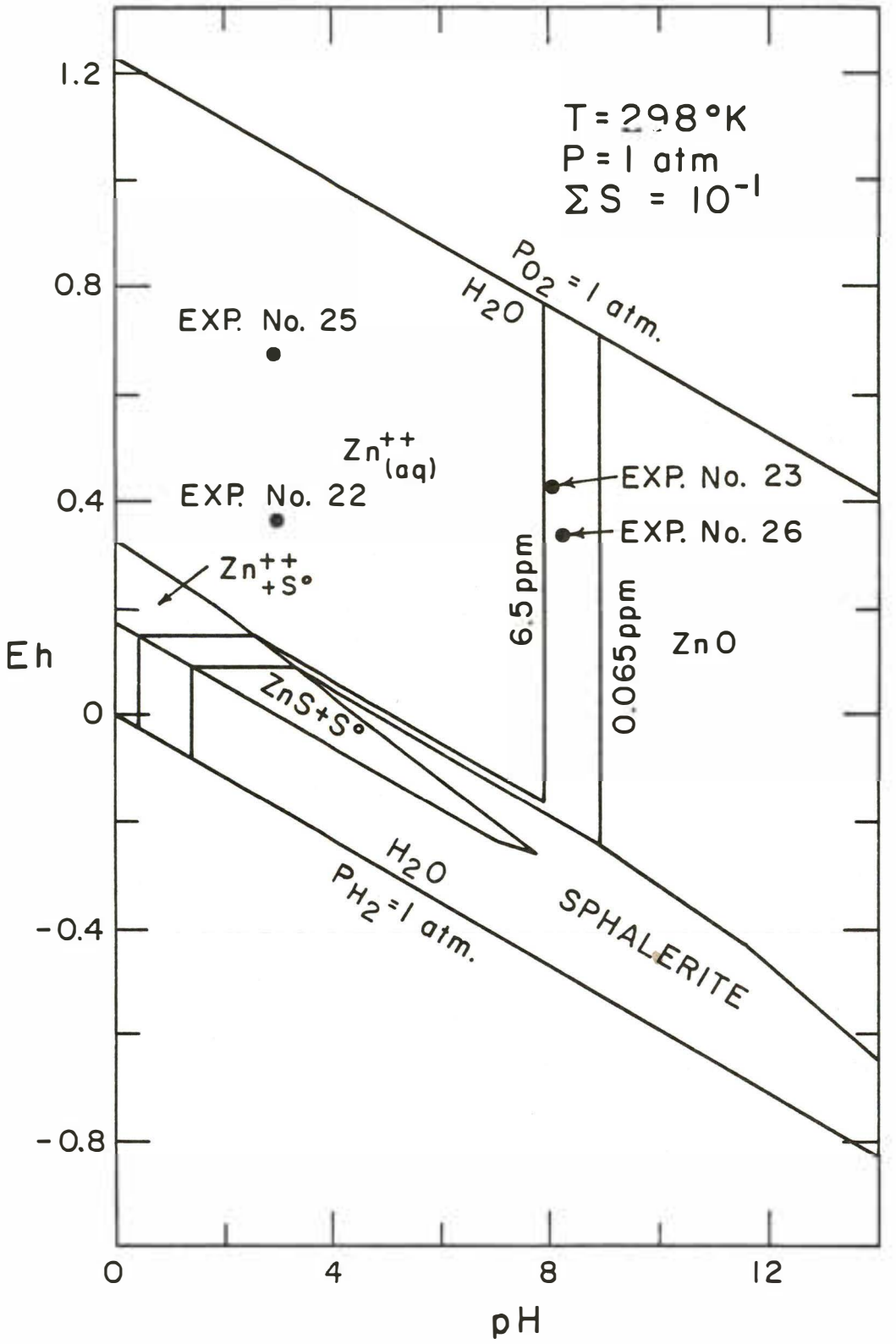

Figure 42. Theoretical stability relationships of zinc as a function of Eh and pH. Total dissolved sulfur = 10^{-1} (9600 mg/l SO_4) (constructed from data in Garrels and Christ, 1965).

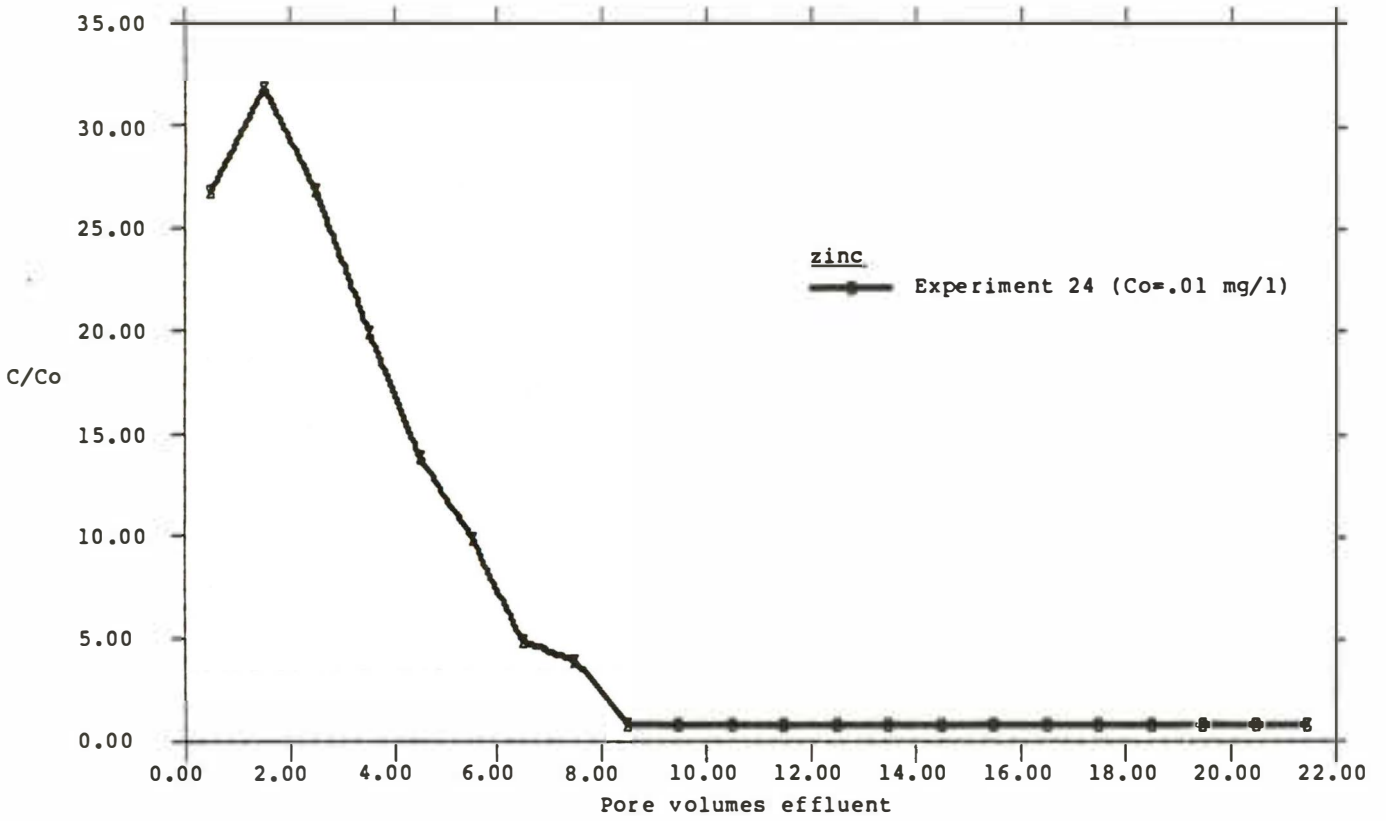

Figure 43. Breakthrough curve for zinc in Experiment 24. Dilute, alkaline tailings fluid. See Figure 32C for Eh-pH values. High initial C/Co values and initially acidic pH are consistent with the probability that this sample of core (68 foot depth in OW-13) was contaminated by subsurface fluids prior to sampling.

Uranium and Vanadium

Dissolved uranium was below the limits of detection of our analytical methods (Table 10) in Experiments 22, 24, and 25. The discussion which follows is therefore limited to Experiments 23, 26, and 27. Of the final steady-state effluent solutions from the latter three experiments, only Experiments 23 (alkaline) and 27 (acidic) contained detectable dissolved uranium.

Figure 44 shows the theoretical fields of stability of carnotite and uraninite, together with the predominant dissolved species of vanadium, as a function of Eh and pH. The concentrations of potassium and uranium chosen for the construction of this diagram are roughly those of the influent tailings fluids (activity $U = 10^{-5}$ (2.4 mg/l) and $K = 10^{-3}$ (39 mg/l)).

In Figure 45 the fields of carnotite and uraninite are again illustrated, but showing the fields of predominance of various ions of uranium instead of vanadium. This diagram was constructed to correspond to an average composition of the effluent fluids from the column experiments. The indicated pressure of carbon dioxide of 10^{-2} atmospheres is probably a reasonable approximation of the conditions that will exist within the pore spaces of the rock when an acidic raffinate solution reacts with the intergranular calcite cement. The activity coefficients used to plot the observed data points in these diagrams were computed using the Davies equation in WATEQFC (Runnells and Lindberg, 1981).

The observed values of Eh and pH were used to plot the observed experimental points for vanadium on Figure 44, with the initial observed concentrations of vanadium in each of the pond waters indicated beside the corresponding experimental point. With the exceptions of the high concentrations of 18.0 mg/l in Experiment 25 and 22.0 mg/l in Experiment 27, the initial observed concentrations of vanadium agree reasonably well with those that would be predicted from equilibrium with carnotite; this is at least permissive evidence that carnotite may be the solubility-limiting phase for total dissolved vanadium in some of the tailings ponds at Canon City.

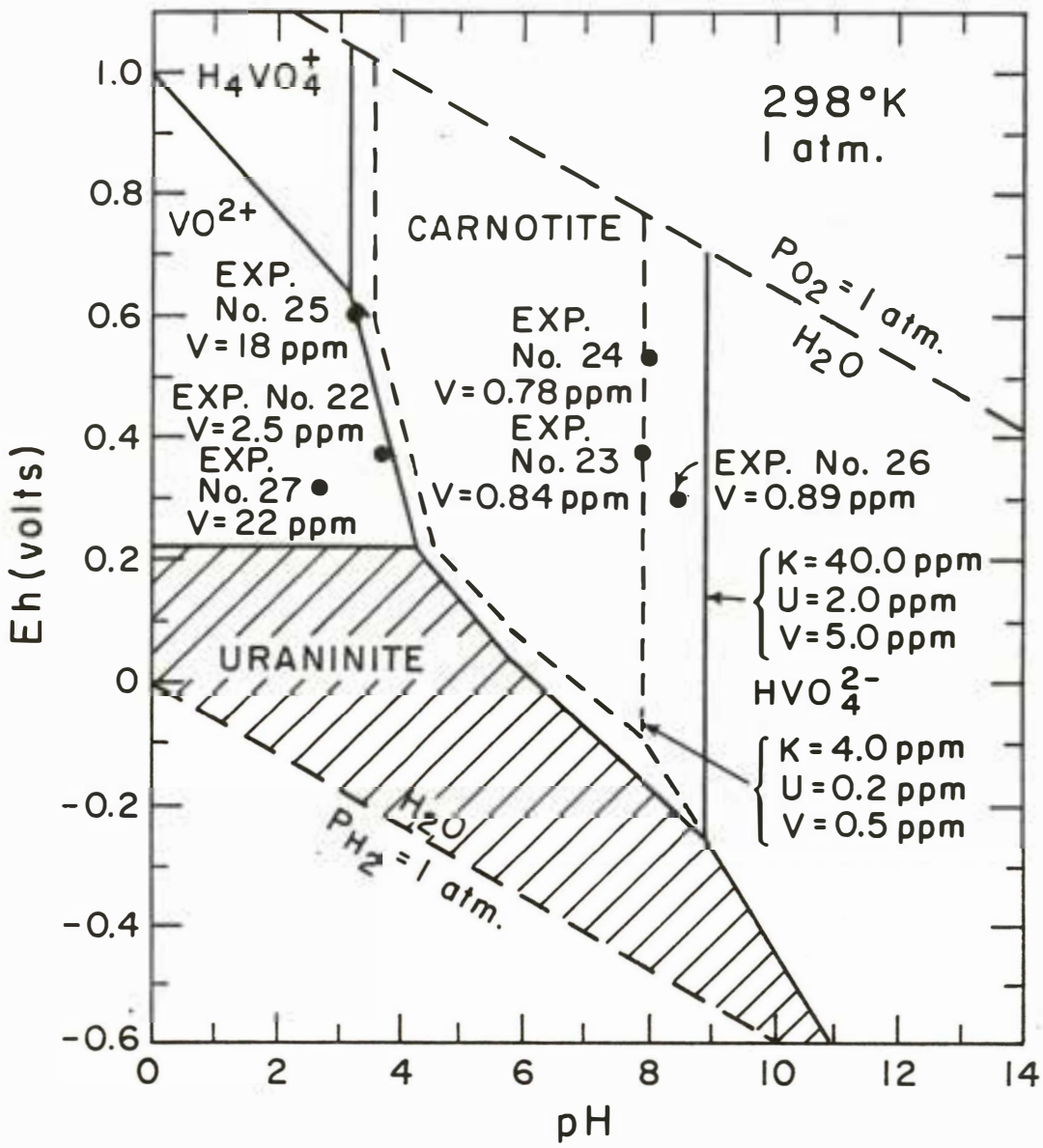

Figure 44. Stability relationships and predominant dissolved ions of vanadium in the system V-U-K-H_2O-CO_2 as a function of Eh and pH. Field of carnotite constructed for a typical range of concentrations of vanadium, uranium, and potassium present in sample tailings fluids from Canon City. Observed concentrations of vanadium shown below each experimental point (stability diagram constructed from thermodynamic data in Langmuir, 1978).

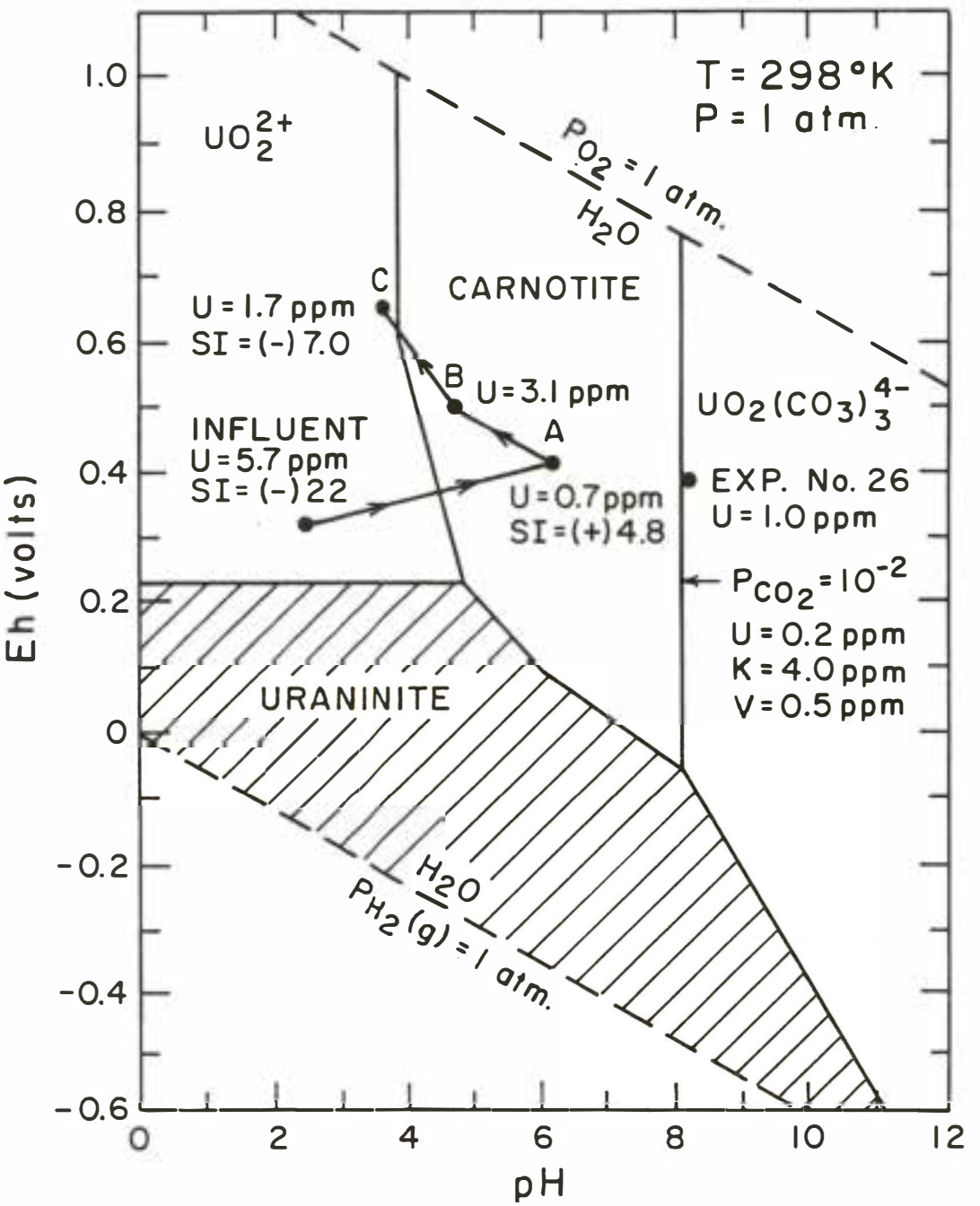

Figure 45. Stability relationships and predominant dissolved ions of uranium in the system U-V-K-H_2O-CO_2 as a function of Eh and pH. Field of carnotite constructed for "average" effluent values of K and V and partial pressure of carbon dioxide gas = 10^{-2} atmospheres. See text for details. Observed concentrations of uranium and computed saturation indices shown below each experimental point. (stability diagram constructed from thermodynamic data in Langmuir, 1978).

In Figure 45 we have plotted the observed conditions of Eh, pH, and dissolved uranium for the steady-state effluent solution in Experiment 26. We have also plotted the changing values of Eh and pH for the effluent from Experiment 27, as shown by the arrow A-B-C in Figure 45. (The Eh and pH data used in the plot can be read from Figure 32C.) As shown in Figure 45, as the experiment progressed from point A to point B to point C, the observed concentrations of uranium in the effluent solutions changed from 0.7 mg/l to 3.1 mg/l to 1.7 mg/l, respectively. A comparison between the observed values and the 0.2 mg/l contour for uranium at equilibrium with carnotite reveals that the agreement is very poor for the initial point at A. However, the observed and theoretical values at Points B and C differ only by a factor of 8 to 15, which we feel is good agreement. We take this to be at least permissive evidence that the precipitation of carnotite may control the amount of dissolved uranium moving through the experimental cores. If true, the precipitation would be kinetically fast.

Some additional consideration should be given to the aqueous species of uranium in solution. In Figure 45, for example, it can be seen that UO_2^{++} is the dominant aqueous species of uranium along the reaction path A => B -> C, and that $UO_2(CO_3)_3^{4-}$ is not an important species. However, as will be discussed later, and as summarized in Table 13, the aqueous species $UO_2SO_4^{o}$ is of importance in the path A -> B -> C in figure 45.

We have also investigated the state of saturation of the effluent solutions from Experiment 27 by computing the saturation indices (S.I.) for carnotite for Points A and C in Figure 45, using WATEQFC. The resulting S.I. values are shown on Figure 45 as (+)4.8 for Point A and (-)7.0 for Point C. These results mean that the effluent solution in Experiment 27 went from a state of apparent oversaturation with respect to carnotite at Point A to a condition of undersaturation at Point C. On Figure 45 the change from supersaturation to undersaturation with respect to carnotite is represented by the arrow crossing the reaction boundary between carnotite and UO_2^{++} at an activity of 10^{-6}(0.2 mg/l). This is to be expected as the solution changes from a near-neutral pH to acidic.

In Figure 46 we have plotted the results of column experiments 23, 26, and 27 for uranium. We believe that the lack of breakthrough for uranium in these experiments may reflect the precipitation of carnotite in the pore spaces of the cores. In many of our experiments we observed the formation of a light yellow precipitate, which may be carnotite. The alkaline fluids (Experiments 23 and 26) in Figure 46 show greater mobility of uranium than the acidic fluid (latter portion of Experiment 27).

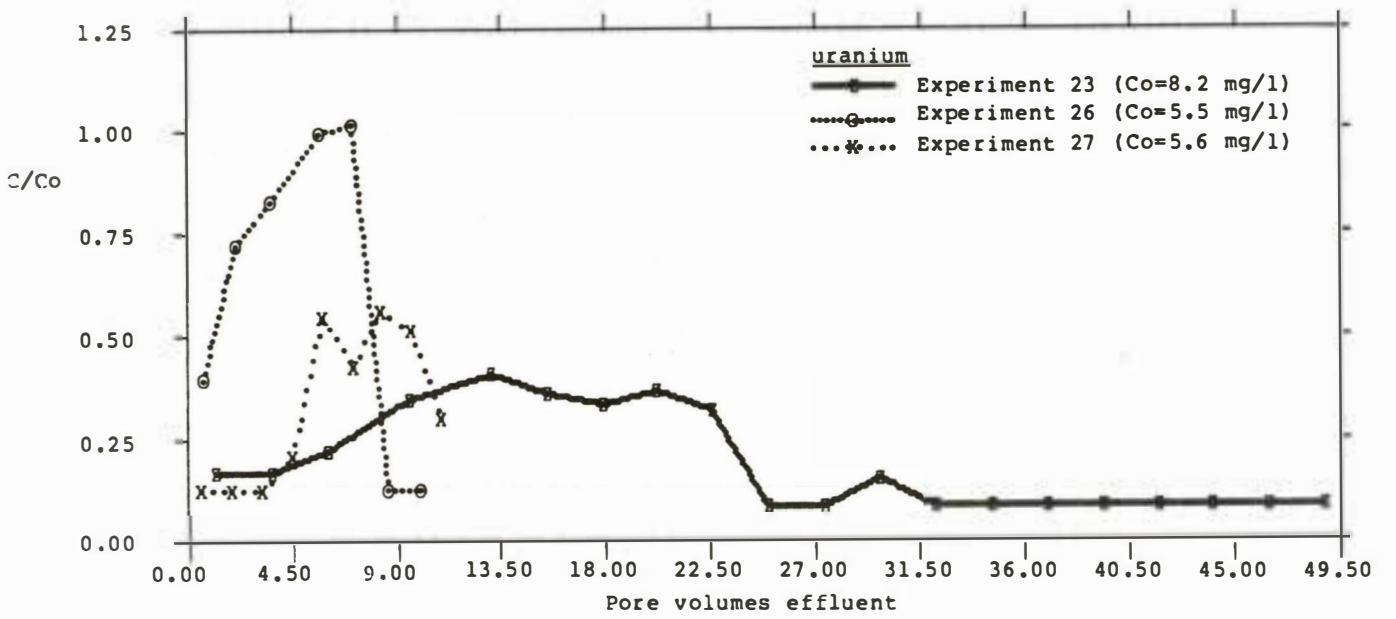

Figure 46. Breakthrough curves for uranium. Experiment 23: Dilute, alkaline influent and effluent. Experiment 26: Dilute, alkaline influent and effluent. Experiment 27: Dilute, acidic influent. Effluent changed from alkaline to acidic during run. See Figures 32B, 33B, and 33C for Eh-pH values.

None of the breakthrough curves in Figure 46 show C/Co values greater than 1.0, suggesting that there was no early rinse-out of indigenous uranium in the cores.

The breakthrough curves in Figure 46 are probably also influenced by adsorption reactions on ferric oxyhydroxide, in addition to whatever precipitation of uranium minerals may have occurred. Langmuir (1978) presents experimental data on the adsorption of uranium by ferric oxyhydroxides; his curves show that adsorption could play an important role in retarding the movement of uranium between pH values of about 5 and 7.5.

As noted earlier, our experiments were not designed to study kinetic effects. However, in Figure 46, it appears that the breakthrough curves for uranium in Experiments 26 and 27 level off at an earlier stage than Experiment 23. From data in Table 9 we see that the rate of flow through the core in Experiment 23 was approximately seven times as fast as the flow through the core of Experiment 27 (no data are available for Experiment 26). Thus, the difference in the number of pore volumes for the "leveling-off" positions in Figure 46 may well reflect the kinetics of the reactions. That is, the fluid in Experiment 23 required a larger number of pore volumes to reach the same stage of reaction simply because it was moving so much more rapidly than in the other experiments.

The mobilities of vanadium are illustrated in Figures 47 and 48 for four experiments. The breakthrough curve for Experiment 25 (Fig. 47) illustrates the relatively high mobility of vanadium in an acidic environment. This is in sharp contrast to the strong retardation shown for the alkaline portion of Experiment 27 (Fig. 47). In addition, in Experiment 25, the mobility of vanadium began to increase only when the pH and Eh conditions in the effluent coincided with the theoretical boundary between the carnotite field and the 5 ppm isopleth for VO^{++} (see Figure 44). Similarly, in Experiment 27 (Fig. 47), vanadium began to show significant mobility only toward the end of the experiment, when the solution became acidic. Referring to Figure 44, this behavior may again be explained as a function of the precipitation or dissolution of carnotite in the pore spaces of the rock, or possibly by adsorption of vanadium at elevated pH in a manner analogous to uranium. Unfortunately, we were not able to find any published data on the adsorption of vanadium by inorganic substrates.

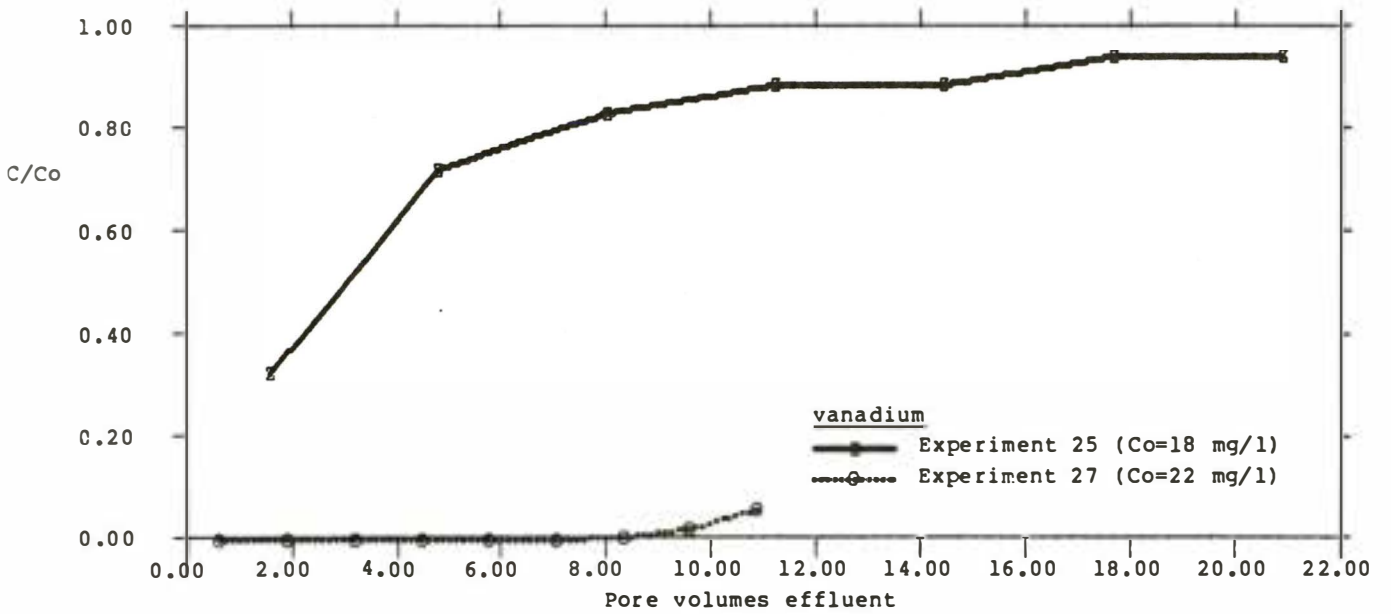

Figure 47. Breakthrough curves for vanadium. Experiment 25: Dilute, acidic influent. Acidic effluent. Experiment 27: Dilute, acidic influent. Effluent changed from alkaline to acidic during run. See Figures 33A and 33C for Eh-pH values.

In Experiments 22 and 26 (Fig. 48), we can clearly see the effect of pH on the mobility of vanadium in two solutions with approximately the same Eh (0.32 and 0.36 volts, respectively). The acidic solution (Experiment 22) in Figure 48 shows a much greater mobility of vanadium than does the alkaline fluid (Experiment 26).

In summary, based on a comparison between our experiments and theoretical stability diagrams, we believe that the precipitation of carnotite may be one important controlling mechanism in the mobility of dissolved uranium and vanadium as tailings fluids and fluids from in-situ mining operations migrate through sandstone bedrock. In our experiments, the role of pH was clearly dominant, and the kinetics of reaction were rapid relative to the rates of flow. Uranium and vanadium both showed minimal mobility at intermediate values of pH, with greatly enhanced mobility in strongly acidic solutions. Unfortunately, our experiments did not cover a wide enough range of Eh to clearly define the role of this parameter.

Selenium

Breakthrough curves are shown in Figure 49 for two representative experiments with selenium. In both of these experiments, one under relatively acidic conditions (Experiment 22) and the other under alkaline to acidic conditions (Experiment 27), selenium was highly mobile. We cannot recognize a pattern here that can be related to either solubility or adsorption controls.

Our experimental results are in agreement with the fact that selenium has been observed to be relatively mobile in the ground water at Canon City, with a plume of anomalous concentrations, up to approximately 50 ppb (10^{-6} molal), extending as far as 1.5 miles downgradient from the mill (Wahler, 1978b).

It appears that selenium is soluble and mobile over a rather broad range of pH conditions, at least for the range of relatively oxidizing conditions that obtained in our experiments. Early and others (1982) have suggested that selenium is also highly soluble under conditions of very low Eh, below (-)0.05 volts, in the form of HSe^- ion. Based on this information, plus the actual observed extent of migration of selenium in ground water at Canon City, we suggest that selenium may be very useful as a tracer of escaping fluids from tailings ponds and from in-situ mining operations. In the past (Wahler, 1978b) it has been suggested that molybdenum may be the best tracer for the fluids at Canon City; our work indicates that molybdenum may be misleading in some cases and that selenium may be more generally useful.

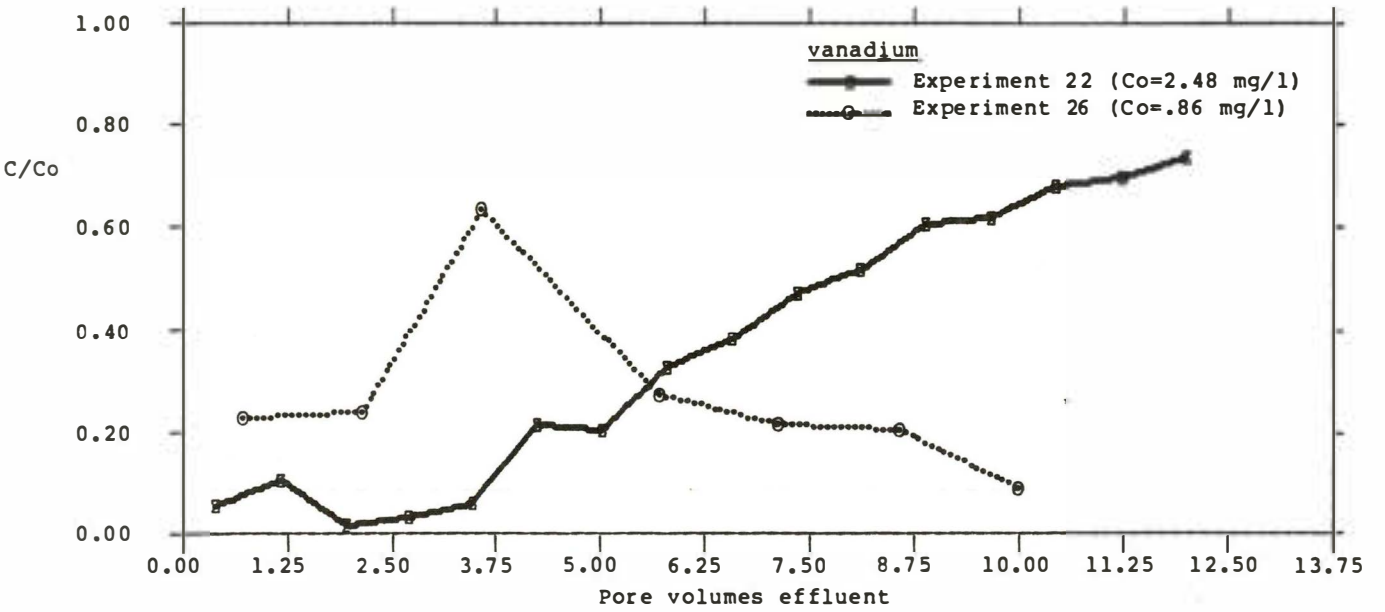

Figure 48. Breakthrough curves for vanadium. Experiment 22: Dilute, acidic influent. Effluent more strongly acidic. Experiment 26: Dilute, alkaline influent. Alkaline effluent. See Figures 32A and 33B for Eh-pH values.

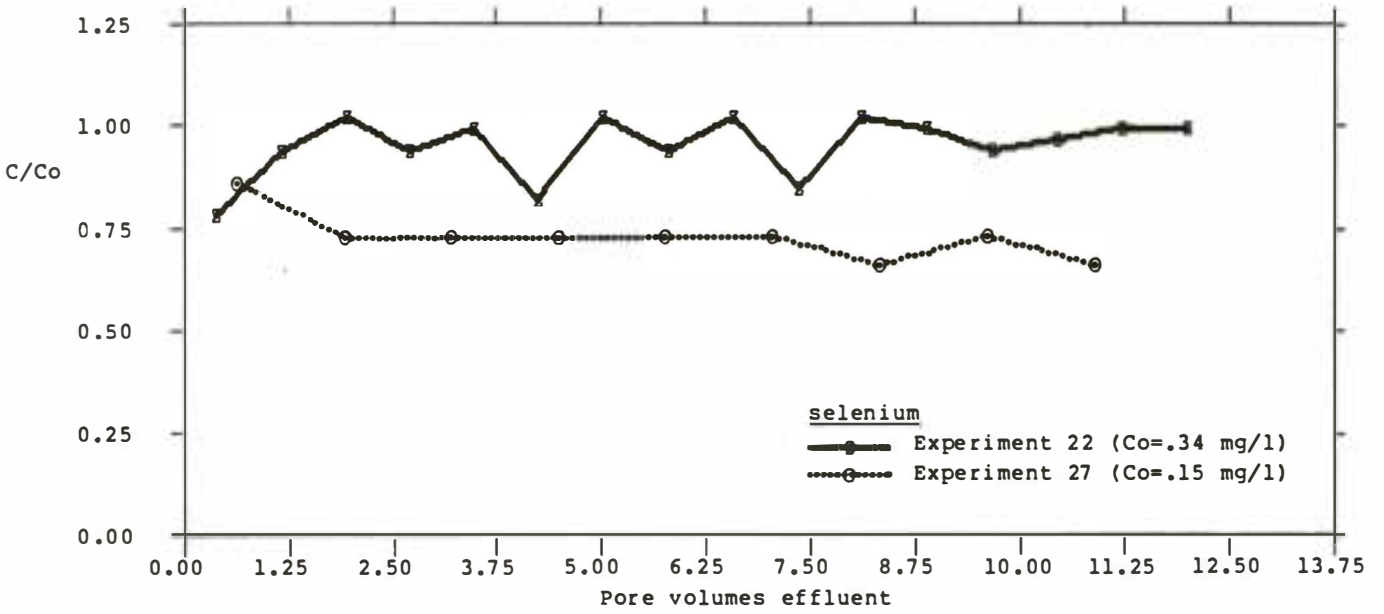

Figure 49. Breakthrough curves for selenium. Experiment 22: Dilute, acidic influent. Effluent more strongly acidic. Experiment 27: Dilute, acidic influent. Effluent changed from alkaline to acidic during run. See Figures 32A and 33C for Eh-pH values.

COMPUTER MODELING

We have used three computer models in our efforts to interpret and understand the chemical results of our experiments. These are WATEQFC (Runnells and Lindberg, 1981), EQ3/6 (Wolery, 1979), and PHREEQE (Parkhurst, Thorstenson, and Plummer, 1980). None of the models was initially fully appropriate for our work, and we have spent much time and effort in modifying them to better fit our needs. Unfortunately, after adapting EQ3/6 to run on the University of Colorado computer system we were forced to suspend work with that particular program because of its large size and the expense involved in running it. The appropriate adaptation and use of PHREEQE is now the primary objective of a Ph.D. Dissertation by Andy Davis, which should be completed in 1984.

In this report we present preliminary results and observations of tests of the models against our experimental results.

Distribution of Ionic Species in Solution

The ionic strength of the diluted tailings fluids used in the experiments on minor and trace species was about 0.1, which allowed us to use the Davies equation in WATEQFC to compute the appropriate activity coefficients.

Due to the large quantity of dissolved sulfate in the leachates (Table 3), it is reasonable to anticipate that sulfate ion pairs will dominate for most of the cations in solution. This is in fact demonstrated by the data in Table 13, representing the output of three runs with our equilibrium model, WATEQFC. The analyses used as input to the model represent the influent diluted tailings fluid for Experiment 27, plus two samples of the effluent solution after passage through the core. From Table 13, it is seen that sulfate complexes dominate for calcium, iron, zinc, and uranium, and are of major importance for manganese and vanadium. This information is important in attempting to understand how various metallic species might react and be retarded in their passage through bedrock.

The data for uranium in Table 13 show that the aqueous carbonate complexes are not important in the transport of uranium in these experiments, even for the intermediate stages of leaching in which pH is near-neutral (see point A in Figure 45 for a graphical representation of this). In other experiments, in which calcite was absent from the test cores (see Table 8, Experiments 17, 18, 19, 21, 24, and 25), the carbonate complexes would be even less significant.

Table 13. Principal aqueous ions along the reaction path of Experiment 27. Given as low (activity) units, as computed from equilibrium model WATEQFC. See Table 9 and Figure 33C for details of experimental parameters, Eh, and pH. Diluted raffinate influent.

Species	Acidic influent (initial)	Weakly acidic effluent species (early)		Strongly acidic effluent species (steady state)	
$CaSO_4^o$	-3.2	$CaSO_4^o$	-2.1	$CaSO_4^o$	-2.4
Ca^{++}	-3.5	Ca^{++}	-2.4	Ca^{++}	-2.7
$FeSO_4^o$	-2.8	$FeSO_4^o$	-3.5	$FeSO_4^o$	-3.0
Fe^{++}	-2.9	Fe^{++}	-3.7	Fe^{++}	-3.2
Mn^{++}	-4.0	Mn^{++}	-3.8	Mn^{++}	-3.9
$MnSO_4^o$	-4.4	$MnSO_4^o$	-4.2	$MnSO_4^o$	-4.3
MoO_2^+	-4.2	MoO_2^+	-5.4	MoO_2^+	-7.2
MoO_4^{--}	-10.7	$HMoO_4^-$	-6.4	$HMoO_4^-$	-5.6
H_2Se^o	-6.2	$HSeO_3^-$	-6.0	$H_2SeO_3^o$	-7.2
Se_2^{--}	-6.7	SeO_3^{--}	-8.3	$H_2SeO_4^o$	-15.0
VO^{++}	-3.9	$H_2VO_4^-$	-6.4	$H_2V_6O_{17}^{---}$	-6.2
$VOSO_4^o$	-4.1	$H_3V_2O_7^-$	-7.5	$H_3V_2O_7^-$	-6.7
$ZnSO_4^o$	-4.6	$ZnSO_4^o$	-4.8	$ZnSO_4^o$	-4.6
Zn^{++}	-5.0	Zn^{++}	-5.2	Zn^{++}	-5.0
$UO_2SO_4^o$	-5.0	$UO_2SO_4^o$	-6.3	$UO_2SO_4^o$	-5.4
UO_2^{++}	-5.6	UO_2^{++}	-6.9	UO_2^{++}	-6.0

Precipitation of Iron, Manganese, and Aluminum

In earlier sections of this report, we mentioned the probable importance of the precipitation of the oxyhydroxides of iron, and possibly of manganese and aluminum, in controlling the sorption, coprecipitation, and retardation of minor dissolved species. In order to properly interpret the breakthrough curves for all species, it is important for us to be able to recognize and predict when these solid sorbents may precipitate or dissolve in our experimental runs. And, for the larger picture, it is important to be able to transfer such predictions to situations in the field.

As part of our work on this topic, we have used the program PHREEQE to determine the state of saturation of the experimental fluids with respect to various minerals during the course of experimental runs. The results of the modeling of two such solutions involved in Experiment 27 are shown in Table 14. The data presented in Table 14 represent the saturation indices for a suite of potential mineral precipitates. The first column of data in Table 14 is the output from modeling the initial weakly acidic effluent solution. The second column of values in Table 14 represents the effluent after it turned more strongly acidic later in the experimental run (see Figure 33C).

Comparing the stages of evolution of the solution from Experiment 27, during the time when the fluid was only slightly acidic (first column in Table 14), PHREEQE predicted that amorphous ferric hydroxide, gibbsite, and kaolinite should all precipitate from solution. Later, when the buffering capacity of the rock was exhausted and the pH became more strongly acidic, essentially all minerals except quartz became theoretically undersaturated. These theoretical results agree rather well with our observed breakthrough curves for aluminum, iron, and manganese in Experiment 27 (Fig. 50). However, caution must be exercised when interpreting computed saturation indices. The computed values are based on equilibrium thermodynamics, telling us only what should happen in solution, not necessarily what will happen. Barriers to nucleation, for example, may allow metastable states of supersaturation to persist for long periods of time, despite the fact that the computed saturation indices are strongly positive. Further, because the saturation indices and the corresponding reaction kinetics depend on such a wide variety of factors, it is not possible to define a range of values for which the computed saturation indices might be most meaningful.

Table 14. Computer prediction of state of saturation of two effluent solutions in Experiment No. 27, with respect to several solid phases of interest. The model used was PHREEQE (Parkhurst and others, 1980). Results are expressed as saturation indices (S.I. values). Positive values suggest supersaturation, and negative values suggest undersaturation.

	Weakly acidic early effluent No. UW538	More strongly acidic later effluent No. UW545
observed pH	6.0	3.4
observed Eh (volts)	0.40	0.63
calcite	-4.7	-7.7
rhodochrosite	-4.0	-7.3
gypsum	+0.4	-0.2
fluorite	-0.6	-6.9
quartz	+0.9	+0.4
gibbsite	+0.03	-2.2
kaolinite	+4.7	-3.1
amorphous $Fe(OH)_3$	+3.2	-0.04
amorphous $Mn(OH)_2$	-11.	-15.
MnOOH	-7.0	-8.2

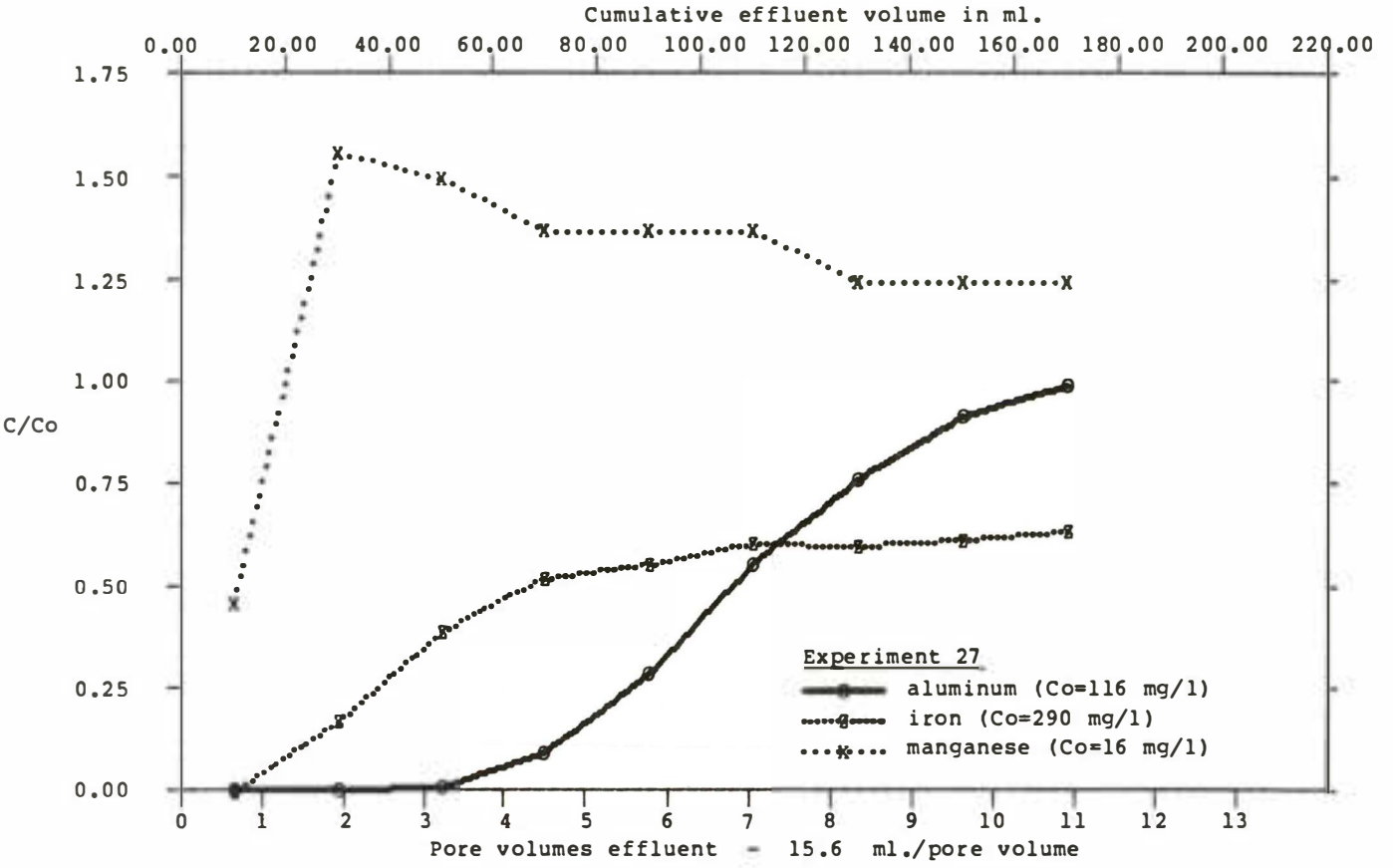

Figure 50. Breakthrough curves for iron, aluminum, and manganese in Experiment 27. Dilute, acidic influent. Effluent changed from alkaline to acidic during run. See S.I. values in Table 14. See Figure 33C for Eh-pH values.

Our interpretation of Figure 50, supported by the computer predictions, is that the initial low values of C/Co were caused by precipitation of ferric oxyhydroxide, gibbsite, and kaolinite. This interpretation is strongly supported by petrographic evidence, in which ferric oxyhydroxide can be seen as a precipitate next to a pore space after the tailings solution had passed through the rock (Fig. 24); microscopic study of the rock prior to the experimental run did not reveal any similar precipitates of ferric oxyhydroxide. The precipitation of ferric oxyhydroxide is obviously a very fast reaction relative to the rates of flow of our test solutions.

The computer model also predicts that manganese is undersaturated throughout the experimental run, as shown by the negative saturation indices in Table 14. This agrees well with the mobility of manganese revealed by the breakthrough curve for Experiment 27 in Figure 50.

In Table 15 we summarize the predicted states of saturation for a number of solid species in Experiment 23, in which the effluent solutions were always alkaline. The prediction by PHREEQE is that manganese is approximately at equilibrium with MnOOH (S.I. = (-)0.1) and iron should precipitate as amorphous ferric hydroxide. Again, excellent agreement is found for manganese and iron with the results from the column experiments (Fig. 51) in which C/Co was consistently less than 1. However, aluminum in Experiment 23 showed early and sustained mobility, in conflict with the predicted precipitation of gibbsite and kaolinite (Table 14). As noted earlier for the major-ion experiments, this may indicate that the kinetics of precipitation of aluminum compounds are slow relative to the rates of flow of the test fluids through the core.

In general, we are pleased that there is relatively consistent agreement, in a qualitative sense, between the computer predictions and the observed breakthrough curves for iron, manganese, and aluminum in two different experiments.

Table 15. Computer prediction of state of saturation of alkaline effluent from Experiment No. 23, with respect to several solid phases of interest. The model used was PHREEQE (Parkhurst and others, 1980). Results are expressed as saturation indices (S.I. values). Positive values suggest supersaturation, and negative values suggest undersaturation.

	Alkaline effluent No. UW538
observed pH	8.15
observed Eh (volts)	0.42
calcite	-3.6
rhodochrosite	-5.0
gypsum	-1.0
fluorite	+0.1
quartz	-0.2
gibbsite	+1.9
kaolinite	+4.0
amorphous $Fe(OH)_3$	+2.0
amorphous $Mn(OH)_2$	-6.6
MnOOH	-0.1

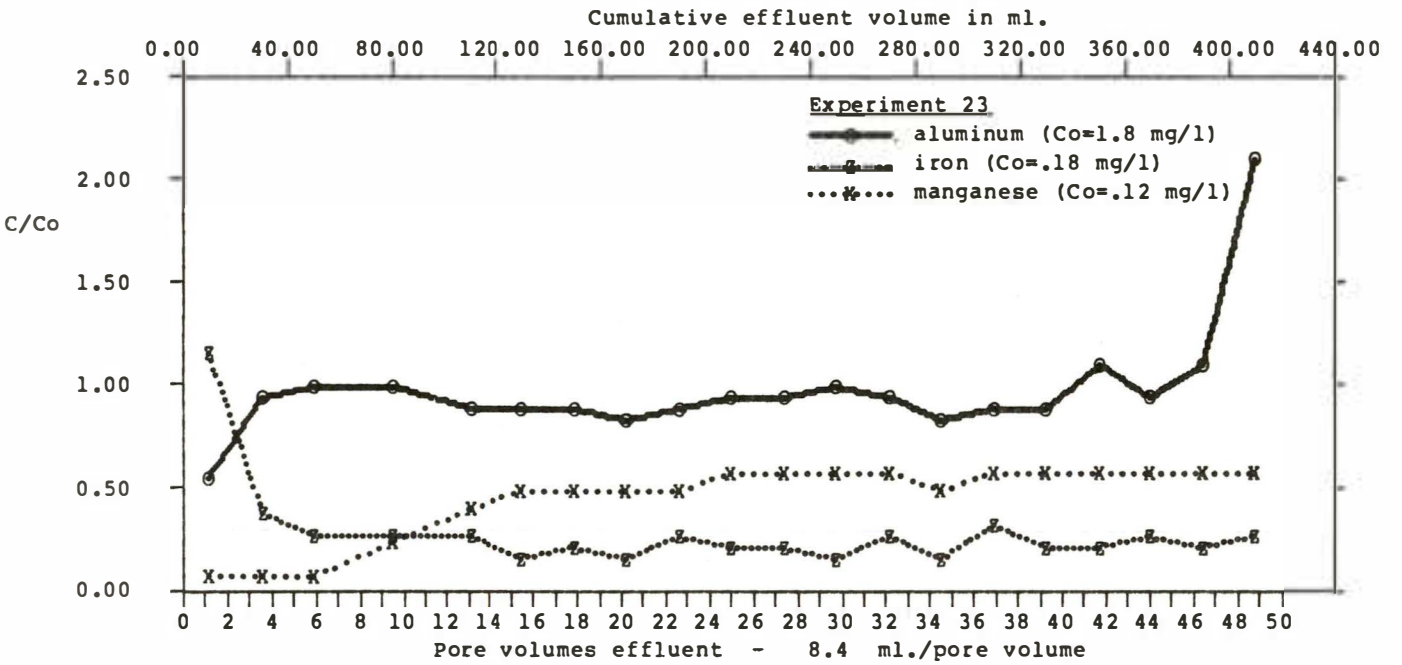

Figure 51. Breakthrough curves for iron, aluminum, and manganese in Experiment 23. Dilute, alkaline influent and effluent. See S.I. values in Table 15. See Figure 32B for Eh-pH values.

Equilibrium Composition of Effluents

PHREEQE was used to model the reaction between rock cores and influent tailings fluids for Experiments 22 and 27. The mineral assemblage for each core was established using electron microscopy and optical petrography. In Experiment 27 the major mineral assemblage consisted of clastic microcline, quartz, albite, and authigenic calcite. In Experiment 22 the same clastic minerals made up the bulk of the rock, but calcite cement was absent. Both cores also contain solid-solution minerals in the form of perthitic feldspar and clay minerals, but because PHREEQE will not yet accept non-integer stoichiometries we were forced to input idealized, stoichiometric compositions for the aluminosilicates.

Table 16 shows the results of the modeling of the chemical compositions of the solutions as compared to the actual, observed compositions. It is obvious from the comparative columns in Table 16 that whereas some species show reasonable agreement between theoretical and observed results, very serious disagreement exists for many other species. It must be emphasized that this is the aspect of our work which is not yet finished and which will be continued during 1984. We hope to improve PHREEQE by adding the appropriate adsorption isotherms, enlarging the data base, and adding the capability of dealing with non-stoichiometric phases.

Table 16. Observed and computer-predicted compositions of aqueous solutions from Experiments No. 27 and No. 22. Model used was PHREEQE (Parkhurst and others, 1980). Units in mg/l.

	Experiment 27		Experiment 22	
Component	Observed	Predicted	Observed	Predicted
Ca	393	1120	71	51
Na	660	10	4000	4350
K	40	0.04	99	16
Fe	185	210	1.3	5.1
Al	115	62	<0.3	5.4
Si	15	6	12	5.5
pH	3.4	6.1	3.6	5.5

CONCLUSIONS

Our study focused on the interaction of tailings fluids from ponds at Canon City, Colorado, with the arkosic sandstones that underlie the millsite. We constructed a special experimental apparatus and forced a series of actual and synthetic tailings fluids through samples of core taken from two observation wells near the mill at Canon City. Although our study was concerned only with uranium tailings fluids, we believe that the results may be usefully applied in other situations as well, such as the in-situ mining of stratabound uranium ore bodies. The average velocities of intergranular flow in our experiments were within the range from about 1 to 5 meters per day, which are realistic in comparison to natural ground waters.

Several of the core samples appear to have been contaminated by acidic subsurface fluids prior to collection. The contaminating fluids may have been used by the drillers when the wells were emplaced, or the acidic fluids may have leaked from the ponds.

Our laboratory experiments involved only intergranular flow of fluids through the rocks. However, in the field at Canon City the flow of ground water and of potentially escaping tailings fluids may be controlled by fracture permeability. Therefore, the degree of interaction and retardation of dissolved species from the fluids will be greater for our laboratory experiments than for the actual conditions in the field. In attempting to extrapolate and apply our laboratory results to the field, due consideration must be given to the type of flow to be expected in the field situation.

The most important chemical control on the mobility of dissolved species was the pH of the solution which, in turn, depended on the presence or absence of calcite cement in the rocks. In those cases in which calcite cement was present, it reacted with and neutralized the acidic raffinates. Upon neutralization, precipitation of iron oxyhydroxide rapidly took place in the pore spaces of the rock. In some samples we were able to identify precipitates of iron oxyhydroxide after passage of the experimental fluids. Other compounds, such as aluminum and manganese oxyhydroxides and carnotite, may also have precipitated as a result of the rise in pH. Minor dissolved components could then be sorbed and retarded by the freshly formed precipitates. The range of Eh in our experiments was not great enough to clearly define the role of this potentially important parameter.

We found that chloride, sulfate, and sodium were not retarded to any significant extent by reaction of the tailings fluids with the rocks in our experiments. Chloride and sulfate should therefore be useful as tracers of escaping and migrating fluids, either from tailings ponds or from in-situ mining operations. The concentrations of sodium are generally so high in the tailings fluids that the small amount which may be removed by ion-exchange does not significantly affect the composition

of the effluent solution for the short cores used in our experiments. Longer cores would be needed to characterize the exchange behavior of sodium.

The trace metals that were present in the tailings fluids, such as zinc, copper, cobalt, and nickel, all behaved in a generally similar fashion to each other. They all exhibit high solubility and mobility in strongly acidic solutions, with strong retardation under alkaline conditions.

Iron, aluminum, and manganese exhibited a very clear response to changing conditions of pH in the experiments. These three metals were all mobile under acidic conditions, becoming immobile to varying degrees under alkaline conditions. Only aluminum gave any indication of slow kinetics of precipitation relative to the velocities of the test fluids.

Calcium showed high initial mobility and rinseout in those experiments in which acidic tailings fluids reacted with calcite cement in the rocks. The reaction caused the dissolution of calcite, the release of dissolved calcium, and the neutralization of the acidic fluids. Calcium was also released from mineral surfaces by ion exchange with sodium and hydrogen ions. A halo of elevated concentrations of calcium in ground water might be expected to precede a migrating front of tailings fluid in the subsurface.

Magnesium was not retarded to any significant degree in the major-ion experiments involving concentrated raffinate. However, some retardation of magnesium did occur when the diluted raffinates passed through the test cores. The retarding mechanism for magnesium is probably ion-exchange and adsorption of the free Mg^{++} ion.

Potassium and ammonium showed very similar patterns of behavior, with moderate initial retardation, followed by early breakthrough and continued mobility. Our study of potassium and ammonium was restricted to acidic fluids.

Silica was moderately retarded relative to the flow of the bulk fluid in those experiments in which the initial concentration of silica was quite high, but in solutions in which the initial concentration was lower, the silica showed less retardation. This behavior appears to be nearly independent of the pH of the migrating fluid, but it may depend on the rate of flow. Silica is known to exhibit slow precipitation kinetics. Additional experiments would be necessary to define the role of the rate of flow in the behavior of dissolved silica, but it seems subordinate to the effect of the initial concentration.

Molybdenum was present in high concentrations in some of the solutions. The mobility of molybdenum was strongly dependent on the pH, with retardation at low pH and increased mobility under alkaline conditions. However, the original influent concentration of molybdenum was also an important factor. For solutions in which the original concentration of molybdenum was very high, the sites available in the rock

for adsorption and removal of the molybdenum appeared to be swamped, allowing the molybdenum to break through earlier than would otherwise have been expected. Due to the chemical reactivity of molybdenum, it is of questionable value as a tracer of escaping tailings fluids.

Selenium was highly mobile under all conditions of our experiments. It may be a very useful tracer for monitoring the escape and movement of fluids from uranium tailings ponds and from in-situ mining operations under relatively oxidizing conditions.

Uranium and vanadium were highly sensitive to changes in the pH of the migrating fluid, with high mobility only in acidic fluids. We found some evidence that the precipitation of carnotite exerted a control on the solubility of uranium and, possibly, of vanadium. The use of uranium as a tracer of migrating tailings fluids is of doubtful value, especially in calcite-rich rocks.

We collected one sample of native ground water from a depth of 100 meters adjacent to the tailings ponds at Canon City. The well was completed in the workings of an abandoned coal mine. The composition of the water suggests that it has been contaminated by reaction with the coal, but it gave no evidence of contamination by uranium tailings fluids. This casts serious doubt on the suggestion of a "deep flow path" for escaping tailings fluids at Canon City, in agreement with the conclusions of Murphy and others (1983).

The role of adsorption is no doubt of critical importance in controlling the mobility of dissolved species in migrating fluids. Unfortunately, we did not plan our experiments to separate the effects of adsorption and ion-exchange from those of precipitation and dissolution. This would be an obvious additional step in the research.

In general, the chemical changes observed in the experiments were indicative of kinetically fast reactions, relative to the rates of flow of the fluids. This suggests that, in some cases, sorption and ion-exchange reactions were probably important. Only silica and aluminum gave clear evidence of kinetic barriers.

The range of Eh involved in our experiments was not great enough to clearly define the role of this potentially important parameter. Future work might profitably investigate the role of Eh in controlling the mobility of the dissolved species.

Using a variety of computer models, we were able to interpret and predict which ionic species were probably predominant in the solutions. In addition, computation of the saturation indices for a wide variety of potential solid precipitates was helpful in arriving at plausible explanations for the behavior of some of the dissolved components in contact with the rock cores. We have begun to use a mass-transfer model, PHREEQE, to follow and to predict the path of reaction between the fluids and the rocks. Our initial tests of the model show both areas of

agreement and of disagreement with our experimental results. We intend to refine and enlarge PHREEQE, with the hope of being better able to predict what will happen when uranium-rich fluids pass through porous and reactive rocks.

REFERENCES

American Public Health Association, 1980, Standard methods for the examination of water and wastewater, 15th ed.:APHA-AWWA-WPCF, Washington, D.C., 1134 pp.

Benjamin, M.M. and Leckie, J.O., 1982, Effects of complexation by Cl, SO_4, and S_2O_3 on adsorption behavior of Cd on oxide surfaces: Environ. Sci. Technol., v. 16, p. 162-170.

Brierley, C. and Brierley, J., 1981, Contamination of ground and surface waters by uranium mining and milling: Volume I. Biological processes for concentrating trace elements from uranium mine waters: U.S. Bur. Mines Open File Report 128-82, 102 pp., available from National Technical Information Services, Springfield, VA 22161, NTIS No. PB 82-251992.

Carritt, D.E. and Goodgal, S., 1954, Sorption reactions and some ecological implications: Deep-Sea Research, v. 1, p. 224-243.

Cotton, F.A. and Wilkinson, G., 1972, Molybdenum and tungsten: in Advanced inorganic chemistry, a comprehensive text: Wiley-Interscience, N.Y., p. 844-861.

Davis, J.A., James, R.O., and Leckie, J.O., 1978, Surface ionization and complexation at the oxide/water interface: 1. Computation of electrical double layer properties in simple electrolytes: Jour. Colloid and Interface Sci., v. 63, p. 480-499.

Davis, J.A. and Leckie, J.O., 1978, Surface ionization and complexation at the oxide/water interface:2. Surface properties of amorphous iron oxyhydroxide and adsorption of metal ions: Jour. Colloid and Interface Sci., v. 67, p. 90-107.

_____, 1979, Speciation of adsorbed ions at the oxide/water interface: in Jenne, E.A., ed., Chemical modeling in aqueous systems, Amer. Chem. Soc., Washington, D.C., p. 299-317.

_____, 1980, Surface ionization and complexation at the oxide/water interface: 3. Adsorption of anions: Jour. Colloid and Interface Sci., v. 74, p. 32-43.

Dixon, W.J. and Massey, F.J., Jr.,1957, Introduction to statistical analysis, 2nd Edition: McGraw-Hill Book Co., Inc., New York, 488 pp.

Early, T.O., Drewes, D.R., Jacobs, G.K., and Routson, R.C., 1982, Geochemical controls on radionuclide releases from a nuclear waste repository in basalt: estimated solubilities for selected elements: Rockwell International Report RHO-BW-ST-39 P, Rockwell Hanford Operations, Energy Systems Group, Richland, Washington, 33 pp. plus appendices.

Fang, S.C, Nance, R.D., Chao, T.T., and Harward, M.E., 1962, A chromatographic approach to the determination of sulfate adsorption and exchange in less-retentive soils: Soil Science, v. 94, p. 14-18.

Freeze, R.A., 1972, Regionalization of hydrogeologic parameters for use in mathematical models of groundwater flow: 24th Intern. Geol. Congress Proc., Section 11, p. 177-190.

Freeze, R.A. and Cherry, J.A., 1979, Groundwater: Prentice-Hall, Inc., Englewood Cliffs, New Jersey, 604 pp.

Garrels, R.M. and Christ, C.L., 1965, Solutions, minerals, and equilibria: Harper and Row, New York, 450 pp.

Gerlitz, C.N., 1982, Chemical interaction between major dissolved components in acidic uranium tailings fluids and adjacent bedrock: M.S. Thesis, Department of Geological Sciences, University of Colorado, Boulder, Colorado, 141 pp.

Griffin, R.A., Cartwright, K., Shimp, N.F., Steele, J.D., Ruch, R.R., White, W.A., Hughes, G.M., and Gilkeson, R.H., 1976, Attenuation of pollutants in municipal landfill leachate by clay minerals, 1. Column leaching and field verification: Illinois State Geological Survey Environ. Geol. Notes, No. 78, 34 pp.

Grim, R.E., 1968, Clay Mineralogy, 2nd Edition: McGraw-Hill Book Company, New York, 596 pp.

Grisak, G.E., Cherry, J.A., Vonhof, J.A., and Bleumle, J.P., 1976, Hydrogeologic and hydrochemical properties of fractured till in the interior plains region: in Legget, R.F., ed., Glacial Till: Royal Soc. Canada Special Publ. No. 12, p. 304-305.

Harward, M.E, Chao, T.T., and Fang, S.C., 1962, Soil properties and constituents in relation to mechanisms of sulphate adsorption: Oregon Agricultural Exper. Station Misc. Paper 124, Oregon State University, Corvallis, Oregon, 18 pp.

Hem, J.D., 1970, Study and interpretation of the chemical characteristics of natural water: U.S. Geol. Survey-Supply Paper 1473, 2nd edition, 363 pp.

Hem, J.D. and Roberson, C.E., 1967, Form and stability of aluminum hydroxide complexes: U.S. Geol. Survey Water-Supply Paper 1827A, 55 pp.

Hingston, F.J., Posner, A.M., and Quirk, J.P., 1972, Anion adsorption by goethite and gibbsite. I. The role of the proton in determining adsorption envelopes: Jour. Soil Sci., v. 23, p. 177-191.

James, R.O. and MacNaughton, M.G., 1977, The adsorption of aqueous heavy metals on inorganic minerals: Geochim. et Cosmochim. Acta, v. 41, p. 1549-1555.

Jones, L. H. P.,1957, The solubility of molybdenum in simplified systems and aqueous soil suspensions: Jour. Soil Sci., v. 8, p. 313-327.

Kaback, D.S., 1977, The geochemistry of molybdenum in stream waters and sediments, central Colorado: Ph.D. Thesis, Department of Geological Sciences, University of Colorado, Boulder, 224 pp.

Ketelle, B.H. and Boyd, G.E., 1947, The exchange adsorption of ions from aqueous solution by organic zeolite, IV. the separation of the yttrium group of rare earths: Jour. Amer. Chem. Soc., v. 69, p. 2800-2812.

Krauskopf, K.B., 1979, Introduction to Geochemistry, 2nd Ed.: McGraw-Hill Book Co., New York, 617 pp.

Langmuir, D., 1978, Uranium solution-mineral equilibria at low temperatures with applications to sedimentary ore deposits: Geochim. et Cosmochim. Acta, v. 42, p. 547-569.

LeGendre, G.R. and Runnells, D.D., 1975, Removal of dissolved molybdenum from wastewaters by precipitates of ferric iron: Environ. Sci. and Technol., v. 9, p. 744-749.

Lindsay, W.L., 1979, Chemical Equilibria in Soils: John Wiley and Sons, Inc., New York, 449 pp.

Markos, G. and Bush, K.J., 1981, Contamination of ground and surface waters by uranium mining and milling: Volume II. Field sampling and empirical modeling: U.S. Bur. Mines Open File Report 19-83, 124 pp., available from National Technical Information Services, Springfield, VA 22161, NTIS No. PB 83-170688.

Morey, G.W., Fournier, R.O., and Rowe, J.J., 1964, The solubility of amorphous silica at 25°C: Jour. Geophys. Res., v. 69, p. 1995-2002.

Morgan, J., 1967, Applications and limitations of chemical thermodynamics in water systems: in Advances in Chem. Series 67, R.F. Gould, Ed., Amer. Chem. Soc., Washington, D.C., p. 1-29.

Murphy, J.R., Wilder, R.J., Goode, D.J., Huidobro, P., Kozik, M.O., Cogley, D.R., Krusell, N.H., Connolly, M.E., Limberakis, E.J., and Levin, A.W., 1983, Assessment of data concerning ground water contamination in the Lincoln Park section of Canon City, Colorado: Final Report, prepared for U.S. Environmental Protection Agency, Office of Waste Program Enforcement, No. GCA-TR-83-17-G: GCA Corporation, Bedford, Mass., 212 pp.

Naumov, G.G., Ryzhenko, B.N., and Khodakovsky, I.L, 1974, Handbook of thermodynamic data: Report No. USGS-WRD-70-001, 324 pp., available from National Technical Information Services, Springfield, VA 22161, NTIS No. PB 226-722.

Nightingale, E.R. Jr., 1959, Phenomenological theory of ion solvation: Effective radii of hydrated ions: Jour. Phys. Chem., v. 63, p. 1381-1387.

Osiensky, J., 1983, Ground-water withdrawal schemes for uranium mill waste disposal sites: Ground Water, v. 3, no. 1, p. 22-27.

Parkhurst, D.L., Thorstenson, D.C., and Plummer, L.N., 1980, PHREEQE, a computer program for geochemical calculations: U.S. Geol. Survey Water Res. Invest. 80-96, 210 pp.

Parks, G.A., 1965, The isoelectric points of solid oxides, solid hydroxides, and aqueous hydroxocomplex systems: Chem. Review, v. 65, p. 177-198.

Reardon, E.J., 1981, kd's--can they be used to describe reversible ion sorption reactions in contaminant migration?: Ground Water, v. 19, p.279-286.

Rohlf, F.J. and Sokal, R.R., 1969, Statistical tables: W.J. Freeman and Co., San Francisco, 253 pp.

Runnells, D.D., 1976, Wastewaters in the vadose zone of arid regions: geochemical interactions: Ground Water, v. 14, no. 6, p. 374-385.

_____, and Lindberg, R. L., 1981, Hydrogeochemical exploration for uranium ore deposits: use of the computer model WATEQFC: Jour. Geochem. Explor., v. 15, p. 37-50.

Scott, G.R., 1977, Reconnaissance geologic map of the Canon City quadrangle, Fremont County, Colorado: U.S. Geol. Survey Misc. Field Studies Map MF-892.

Stumm, W. and Morgan, J.J., 1981, Aquatic Chemistry, 2(nd) Ed.: John Wiley and Sons, Inc., New York, 780 pp.

Sung, W. and Morgan, J.J., 1981, Oxidative removal of Mn(II) from solution catalyzed by the gamma-FeOOH (lepidocrocite) surface: Geochim. et Cosmochim. Acta, v. 45, p. 2377-2383.

Swallow, K.C, Hume, D.N., and Morel, F.M.M., 1980, Sorption of copper and lead by hydrous ferric oxide: Environ. Sci. and Technol., v. 14, p. 1326-1341.

Tamura, T., 1972, Sorption phenomena significant in radioactive waste disposal, in Cook, T.D., ed., Underground waste management and environmental implications: Amer. Assoc. Petrol. Geol. Memoir 18, p. 318-330.

Todd, D.K., 1980, Groundwater Hydrology, 2nd edition: John Wiley and Sons, Inc., New York, 535 pp.

Valocchi, A.J., Roberts, R.P., Parks, G.A., and Street, R.L., 1981, Simulation of the transport of ion-exchanging solutes using laboratory-determined chemical parameter values: Ground Water, v. 19, p. 600-607.

van der Leeden, F. (ed.),1975, Water resources of the world: Water Information Center, Inc., Port Washington, N.Y., 568 pp.

Wahler, W.A., and Associates, Inc., 1978a, Site and laboratory investigation and definitive design report, Cotter Corporation uranium-vanadium tailings impoundment, Canon City, Colorado: Mountain States Mineral Enterprises, Inc., P. O. Box 17960, Tucson, AZ, 85731.

_____, 1978b, Investigations related to the migration of raffinates from the existing Cotter tailings impoundments: Cotter Corporation, P. O. Box 751, Canon City, Colorado.

Weast, R.C., ed., 1979, Chemical Rubber Company Handbook of Chemistry and Physics, 60th edition: CRC Press, Inc., Boca Raton, Florida, 2447 pp.

Wolery, T.J., 1979, Calculations of chemical equilibrium between aqueous solution and minerals:the EQ3/6 software package: Nat. Tech. Inform. Service, UCRL-52658.

APPENDIX ON ANALYTICAL PROCEDURES

by

Robert Meglen, Ph.D.
Glenda Swanson
Lynne Taylor
Robert Sistko
Robert McNelly

Analytical Laboratory
Center for Environmental Sciences
University of Colorado at Denver
Denver, Colorado 80202

1. INTRODUCTION

This report describes work done in the Analytical Laboratory of the Center for Environmental Sciences at the University of Colorado-Denver. This laboratory provided analytical services to the project investigators, G. Markos , D. D. Runnells, C. L. and J. A. Brierley under U. S. Bureau of Mines Contract # J0295033; "Contamination of Ground and Surface Waters Due to Uranium Mining and Milling." The services provided included development of accurate analytical procedures, routine analysis of samples, and computerized data interpretation techniques. A description of each of the following aspects of the progress achieved in this work is given in separate sections of this report.

Methods development work and evaluation of Inductively Coupled Plasma Atomic Emission Spectrometry (ICP-AES) was performed. Procedures were developed for the determination of twenty elements in solid and aqueous samples.

Procedures were developed for determining anionic species in aqueous samples by Ion Chromatography (IC).

Additional procedures using Atomic Absorption Spectrometry (AAS) and Colorimetric methods were used to supplement the primary methods of ICP-AES and IC.

A rigorous Quality Control (QC) protocol was designed and implemented for continuous monitoring of analytical performance (accuracy and precision).

Approximately 25,000 chemical determinations were performed on a variety of geological and aqueous sample materials.

2. ANALYTICAL METHODS

2.1 Inductively Coupled Plasma-Atomic Emission Spectrometry

Funds obtained through this contract and other sources were used to purchase a Model 35000C Bausch & Lomb sequential ICP spectrometer. A sequential (scanning) instrument was chosen because it affords operational flexibility that was deemed essential to the analysis of complex matrices encountered in this study. The spectrometer is fully automated and operates under the control of a dedicated Digital Equipment Corporation (DEC) PDP 11/03 computer. The only functions performed by the operator, after sample preparation, are lighting the argon torch, loading the automatic sampler and creation of analytical task files. These task files consist of a list of elements to be determined, the appropriate emission wavelengths for detection, on-line or off-line parameters for interelement interferences or background correction, and concentration of calibration standards. Correction parameters must be determined for each sample matrix prior to sample analysis. Since accuracy of the final analysis depends upon the proper selection of these parameters, a careful study of the anticipated sample matrix must precede routine application of this technique. This task is simplified by the versatile hardware and software configuration of the instrument purchased. Results of extensive spectral studies required for the selection of operating conditions are described in subsequent sections of this report. Once established, the operating parameters are stored on magnetic diskette for future use in routine analysis of samples. Task files were created for the analysis of dissolved solid tailings, acid and aqueous tailings leachates, raffinate and other aqueous samples.

The computer controls instrument performance and automates analyses by recalling the appropriate analytical task file, arranging the elements in order of increasing wavelength and executing the preselected protocol. Calibration solutions selected to cover the linear concentration range anticipated are then used to calibrate the instrument for quantification. Upon completion of the calibration for all elements (lines) in the task file, the analyst instructs the computer to perform the analysis of the quality control samples and unknowns. The results of the analyses are printed out in real-time and stored on magnetic diskette for later retrieval and final report preparation.

2.1.1 Selection of Instrument Parameters. While the ICP technique is less susceptible to the chemical interferences inherent in other analytical methods, the complex matrices encountered in this study require cautious application of sound analytical procedures if accurate results are to be obtained. The simultaneous occurence of potential chemical and spectral interferents with trace species requires special analyst attention. Three significant difficulties were encountered in the development of analytical procedures for this study.

Since the apparent concentration of an element depends upon the rate at which sample is delivered to the argon plasma, it is essential that a constant sample uptake rate be maintained. In addition, the uptake rate of sample and calibration standards must be equal. This requirement is easily attained for dilute aqueous samples. However, high concentrations of dissolved species present in tailings leachates and raffinates lead to reduced efficiency of analyte delivery to the plasma. Solution viscosity, density, and surface tension all affect nebulization efficency and uptake rate. Uptake rate variations of fifteen to forty percent have been observed in this study. Therefore, exact matrix matching of samples and standards is impractical. The appproach taken in this laboratory is to use internal standards to monitor uptake rates and to correct for variations among standards and samples. The flexibility afforded by the sequential ICP simplifies internal standard selection. Spectra of representative samples can be rapidly scanned in the emission region of the candidate internal standard element. If the samples do not contain the candidate element and the emission spectrum does not exhibit spectral interference from other sample components, one can exploit the utility of the internal standard method. **We strongly recommend the use of internal standards for the analysis of these materials.** Scandium and lanthanum have been used successfully as internal standards when they were absent from the original sample.

The ease with which multielement determinations can be performed by automated instruments should not be allowed to obscure the significance of individual element's chemical and physical characteristics. Distinctly different behavior among sample constituents may restrict the exploitation of multielement techniques. The "memory effect" of the ICP sample delivery system is one property that has been found to be element dependent. ("Memory" is the carry-over of analyte between samples that occurs when inadequate rinsing has been performed.) This effect is particulary important in ICP analysis because the technique has a wide dynamic concentration range. This characteristic permits single calibration analysis of samples that vary in concentration by four to five orders of magnitude. Failure of the instrument to return to baseline between samples leads to systematic errors. The magnitude of the memory effect is a function of nebulizer design. While this effect is well known among ICP users, it is not widely known that the effect is element dependent. Figure 2.1 shows the memory effect for several elements. Silicon and boron are shown to require longer rinse times before they return to baseline. Since samples are often randomized prior to analysis and the sample concentrations may vary widely, it is essential that adequate rinse times be provided for all sample species.

2.1.2 **Background correction.** High concentrations of several inorganic species in tailings related aqueous samples alters emission characteristics of the argon plasma. The continuum emission in the vicinity of a trace analyte peak may be enhanced by the presence of major sample constituents. Accurate determination of several elements in tailings matrices require **background (off-peak) correction.** Figure 2.2 shows the

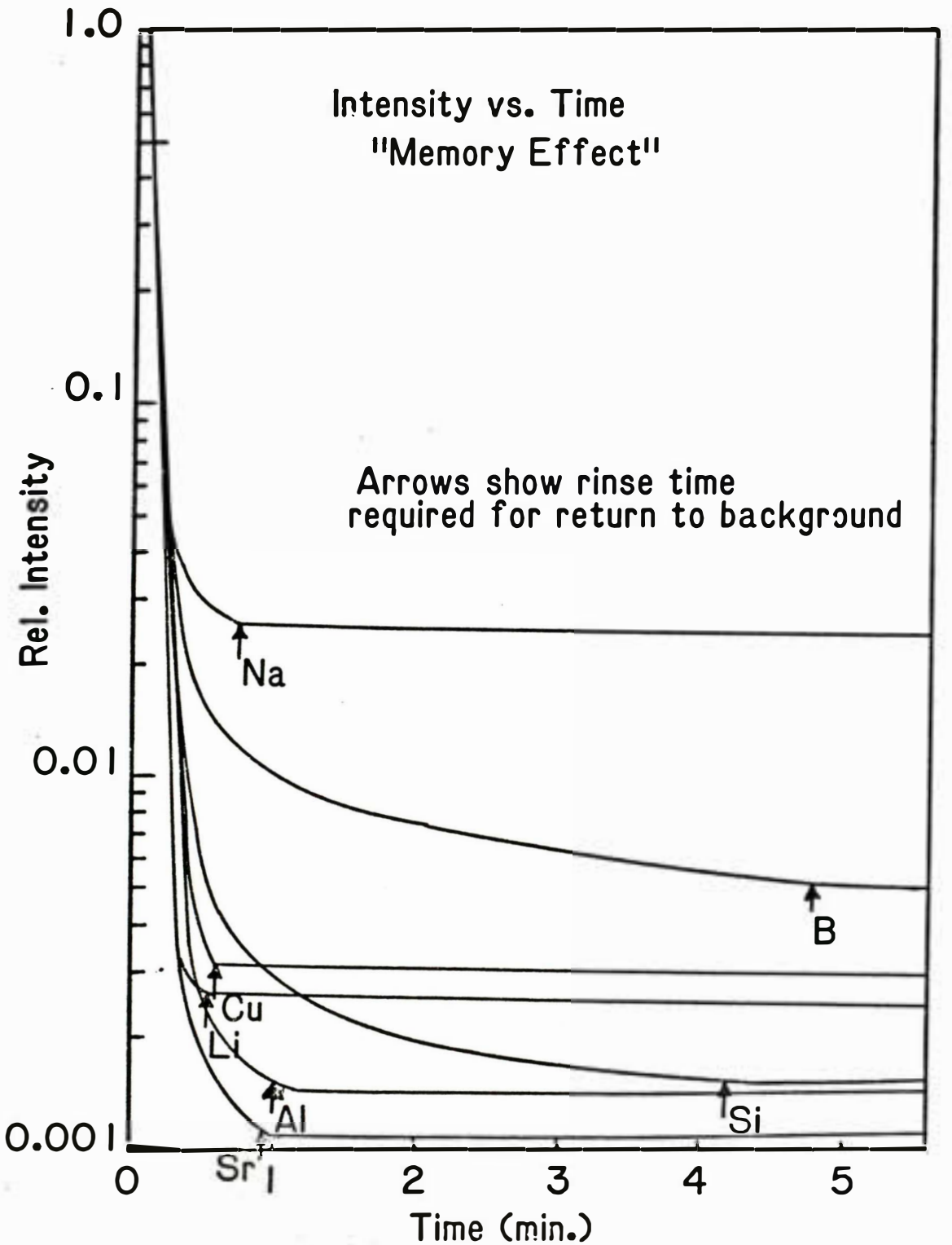
1.0
0.1
0.01
0.001
Rel. Intensity
Intensity vs. Time
"Memory Effect"
Arrows show rinse time
required for return to background
Na
B
Cu
Li
Al
Si
Sr
0
1
2
3
4
5
Time (min.)

Figure 2.1

emission spectrum of a typical raffinate sample in the vicinity of the Mo(281.6 nm) emission line. Failure to correct for the enhanced emission, above the blank baseline, would lead to a high bias. The magnitude of the bias is dependent upon the magnitude of the background emission relative to the analyte emission intensity. The illustrated case would lead to a ten percent error in reporting Mo. In other cases, where the Mo is present at much lower concentrations but the same matrix determined background emission exists, the apparent concentration could be orders magnitude in error. Since each matrix encountered presents different potential effect, careful case-by-case determination of appropriate background correction parameters is necessary.

2.1.3 **Spectral Overlap.** High concentrations of concomitant species can also lead to spectral overlap between analyte and interferent emission lines. An example of a spectral overlap interference of iron in the vicinity of Mo (202.0 nm) is shown in Figure 2.3. This problem is quite common when spectrally "rich" species are present at high concentrations. Uranium and vanadium represent two species that exhibit numerous secondary emission lines throughout the spectrum and lead to severe trace element interferences. These potential interferences can only be identified by examining the emission spectrum of representative samples. This task is simplified by the capability of a scanning ICP and it can be accomplished simultaneously with the examination of the background emission mentioned above. A scanning ICP affords two options in dealing with spectral overlap. The interferent's concentration dependent contribution to the analyte line may be determined simultaneously with emission intensity quantification and subtracted from the result. This **spectral overlap (on-peak) correction** can be automated and used to produce accurate determinations. However, some loss of precision ensues because two intensity measurements are required to produce the corrected result. The reduced precision is limiting only when the interferent intensity contribution is large relative to the analyte concentration. (This is the case for most of the sample matrices encountered in this study.) The alternative approach to the spectral overlap problem is to perform no correction, but to select an alternate analyte emission line for quantification. This option is readily exercised with a scanning ICP spectrometer. Lines that have sufficient sensitivity and are free of spectral interference can be identified during the initial spectral characterization described above. Any number of candidate analyte lines may be scanned prior to analysis. The Mo(281.615 nm) emission line shown in Figure 2.2 was chosen for Mo quantification of samples containing high concentrations of iron. This alternate line was free of the iron interference illustrated in Figure 2.3 and required only background correction.

By exploiting the scanning capability of the ICP it has been possible to tailor an analytical task file for each sample matrix. The protocol for task file creation incorporates the features described in the preceeding paragraphs. It consists of the following steps:

Several candidate emission lines are selected for each element to be

RAFFINATE SCAN FOR MO 2816.15

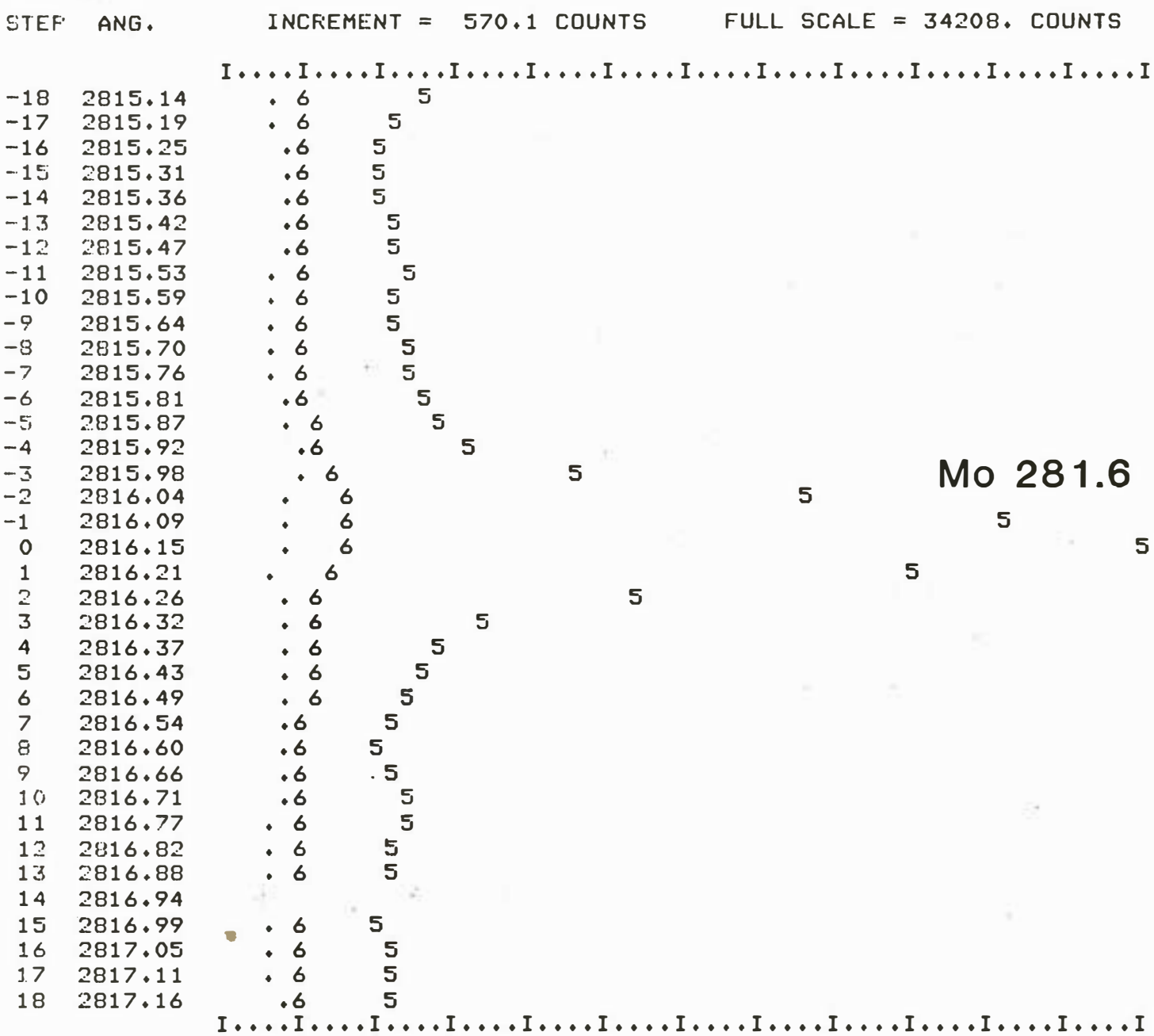

. = WATER BLANK

5 = RAFFINATE # 1X10

6 = RAFFINATE # 2X10

Figure 2.2

RAFFINATE SCAN FOR MO 2020.3

STEP ANG. INCREMENT = 48.6 COUNTS FULL SCALE = 2917.0 COUNTS

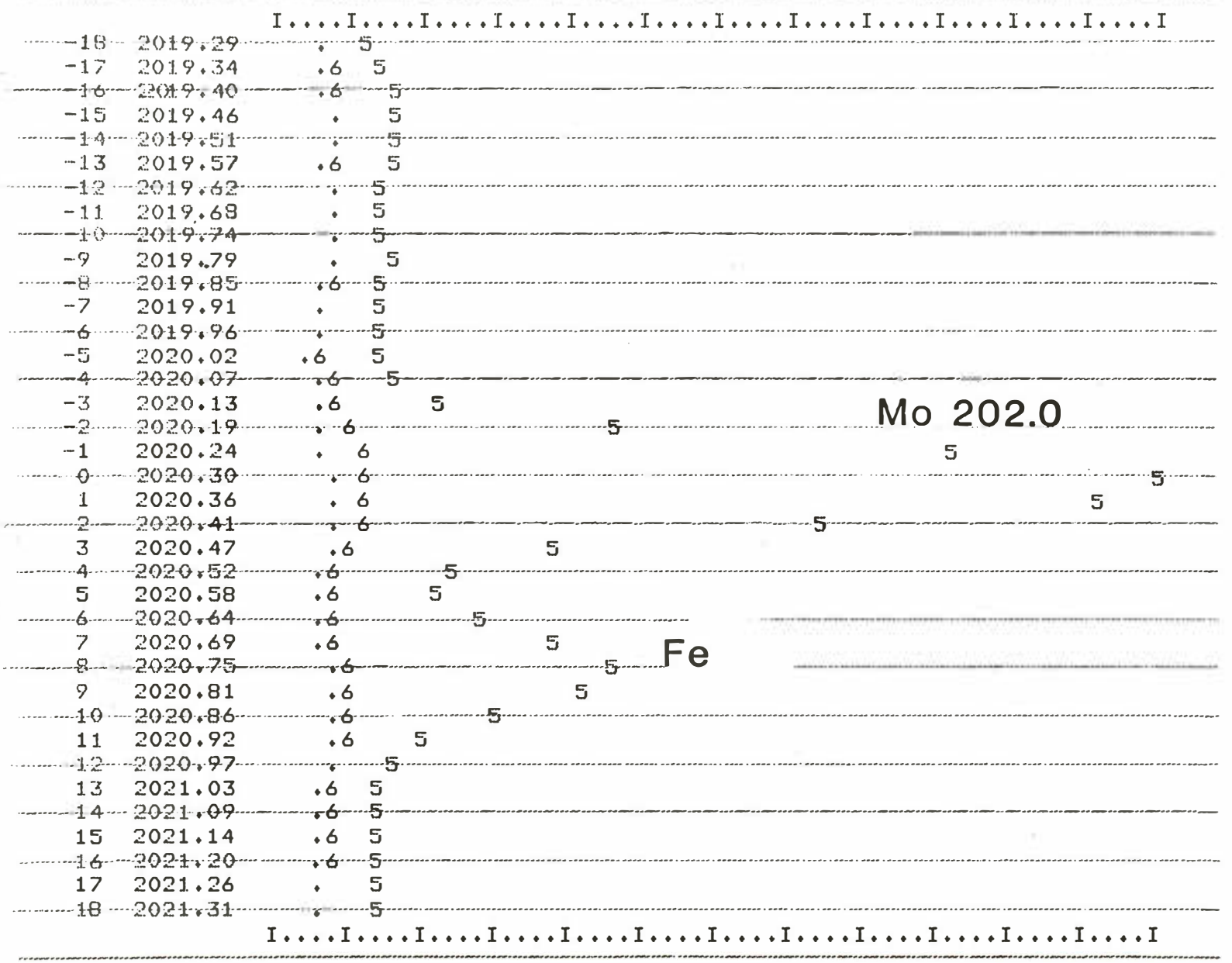

. =

5 = RAFFINATE #1X10

6 = RAFFINATE #2X10

Figure 2.3

determined.

A task file containing these lines is created and used to perform wavelength scans of a few "representative" samples of the matrix type under study.

The emission spectra are examined. Lines with severe spectral interferences are deleted. Additional candidate lines may be appended, if necessary.

The process is repeated in an iterative fashion until the lines that represent the optimum balance of sensitivity, detection limit, and freedom from severe spectral interference is achieved.

Two line selection criteria are applied during the evaluation of the emission scans.

Each element's concentration in the real samples must fall within the linear calibration range for the candidate emission line. An alternate line may be selected if an element's concentration is expected to exceed the linearity maximum or fall below the practical detection limit (determination limit). Sample dilution, to accommodate high concentration species, is avoided because it may reduce trace element contents below the determination limit.

Secondary emission lines of other sample constituents must be more than 0.025 nm distant from the candidate analyte line. The ICP peak seeking software would mistakenly identify interferent lines within this spectral window as analyte. Significant interferences outside the 0.5 nm window can be concentration corrected by the on-peak correction scheme as described above. However, on-peak correction is employed when no other candidate line can meet the specified criteria of sensitivity, detection limit and freedom from spectral interference.

2.1.4 **Finalizing Instrument Parameters.** After candidate lines have been examined the final selection of analytical parameters is completed. Appropriate chemical and electronic parameters for routine analysis are chosen and incorporated into the computer stored analytical task file. Attenuator settings, integration times, calibration standard concentrations and internal standards are selected by experimentation and past experience. Final selection of off-peak background correction parameters is accomplished by examining the emission scans of the representative sample matrix. The position of background correction points are stored in the task file as "step" numbers. The computer uses these numbers to instruct the emission grating stepper motor how many 0.005625 nm increments on either side of the emission line are to be executed before background intensities are to be measured. The software permits one, two or zero correction points to be specified. These points can be on either side of the analyte line. Criteria used for selecting these points are:

If the flat region on either side of the analyte line of a representative sample scan is offset relative to an aqueous calibration standard, background correction is required.

If the offset magnitude is equal on both sides of the analyte line, only one background correction point is necessary. If the offset varies with wavelength, two points that envelop the analyte peak are selected.

The background correction points are selected to accurately represent the spectral intensity characteristics of the vicinity. Regions exhibiting spectral structure are avoided.

While task file creation is time consuming, the ability to tailor the analytical parameters of line selection to the sample matrix provides distinct benefits in accuracy and precision. The optimal use of plasma emission spectroscopy for uranium tailing matrices required the examination more than 70 candidate emission lines and 700 emission spectra. A comprehensive spectral catolog has been compiled for use in this study. Its volume and limited general applicability to other studies precludes its inclusion in this report. However, "Operating Conditions for Analytical Methods" contains tables that summarize the general features of lines used in this study.

2.2 Ion Chromatography (IC)

While a variety of analytical techniques are available for inorganic anion determination, they are subject to severe interferences. In complex sample matrices, such as raffinates and tailings leachates, these techniques have limited reliability. When reliable methods can be found, complete anion characterization is accomplished only through the application of several methods. Each separate technique that must be developed adds to the cost of equipment and analyst time. Fortunately, since 1975, Ion Chromatography (IC) has been developed to assist the analyst in performing the difficult anion determinations. This technique has provided a sensitive and rapid method for determining anion species in complex sample matrices. Its advantage lies in the ability to utilize a single sample for the determination of several sample constituents. The intractable interferences that plague other anion detection techniques are avoided by employing classical ion exchange principles to effect a separation of anion constituents prior to detection and quantification. Ionic charge, size, hydrophobic and Van der Waals forces contribute to the selective interactions that effect separation of the various species. The technique permits determination of homologous oxy-anion species such as nitrate and nitrite, and sulfate, sulfite, thiosulfate etc. The ability to perform species selective determinations is an important addition to the analytical repertoire. The separated species emerging from the ion exchange column are detected and quantified by their conductivity or through coulometric titration. The power of the technique is also enhanced by the ease with which the analyses can be automated.

Through funds obtained from other sources we have aquired a Dionex Model 12-S automated Ion Chromatograph. We have exploited the advantages of this technique to improve the reliability of our analysis of uranium tailings related samples. A brief description of the significant achievements will be given here.

2.2.1 **Sulfate Determination.** Previous reports to USBM described difficulties encountered in the analysis of tailings extracts for anions. The principal difficulty was observed in the determination of sulfate by a colorimetric method that uses an indirect barium complexation reaction. While this method is reliable (a procedure accepted by EPA and USGS laboratories) for most natural waters, the chemically complex matrix represented by tailings leachates renders the method inaccurate. The inaccuracy was difficult to quantify since Standard Reference Materials (SRM's), which adquately represents the tailings extract matrix are not available. Preliminary indications of the colorimetric method's inaccuracy was indicated by a poor stoichiometric cation-anion balance. Confirmation of the sulfate inaccuracy was provided by Glenda Swanson in this laboratory through a series of standard addition and spike recovery tests. Further evidence of a systematic bias was obtained through application of two independent analytical techniques, Ion Chromatography and Inductvely Coupled Plasma Spectrometry. Swanson and McNelly studied 85 samples containing sulfate between 0 and 2.7 mg/mL. They established that the colorimetric sulfate procedure produced a low bias. A linear correction factor was obtained, validated and applied to the early colorimetric sulfate data. Figure 2.4 compares the sulfate results obtained by the two techniques. Comparisons between IC and ICP total sulfur determinations (Figure 2.5) show little "scatter". Thus, we conclude that the scatter in Figure 2.4 is the result of the colorimetric method's poor precision. Applying the valid correction factor permitted the "recovery" of previous inaccurate analyses. All subsequent sulfate determinations were performed using the accurate IC method.

2.2.2 **Other Anions.** Ion Chromatography was also used for the determination of chloride. The colorimetric chloride method was also shown to be unreliable when applied to some sample types. Since most aqueous tailings extracts were nitric acid preserved, nitrate, phosphate and bromide could not be determined. Fluoride was quantified routinely with little additional effort, but it was not requested and the results were stored but not reported. Nitrite was seldom seen and not quantified because its significance, in light of the preservation technique, could not be interpreted. A representative unacidified tailings leachate chromatogram is shown in Figure 2.6. A calibration chromatogram, at the top of the figure, is given for qualitative comparison. The dominant species are chloride and sulfate. Traces of fluoride and nitrate are also apparent. Detailed methods protocols are given in "Operating Conditions for Analytical Methods" of this report.

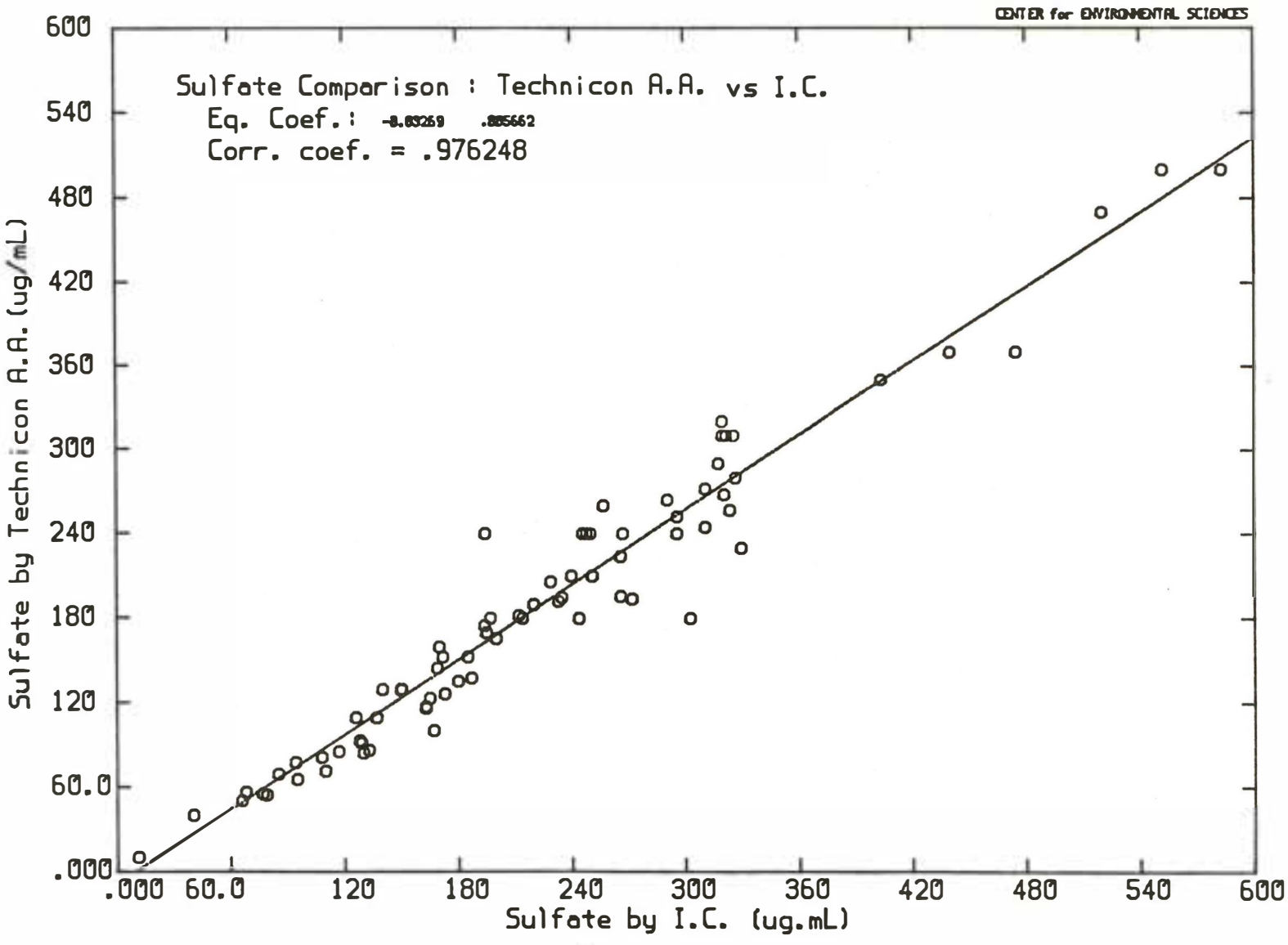
CENTER for ENVIRONMENTAL SCIENCES
Sulfate Comparison : Technicon A.A. vs I.C.
Eq. Coef.: -8.65269 .885662
Corr. coef. = .976248
Sulfate by Technicon A.A. (ug/mL)
Sulfate by I.C. (ug.mL)
.000
60.0
120
180
240
300
360
420
480
540
600

Figure 2.4

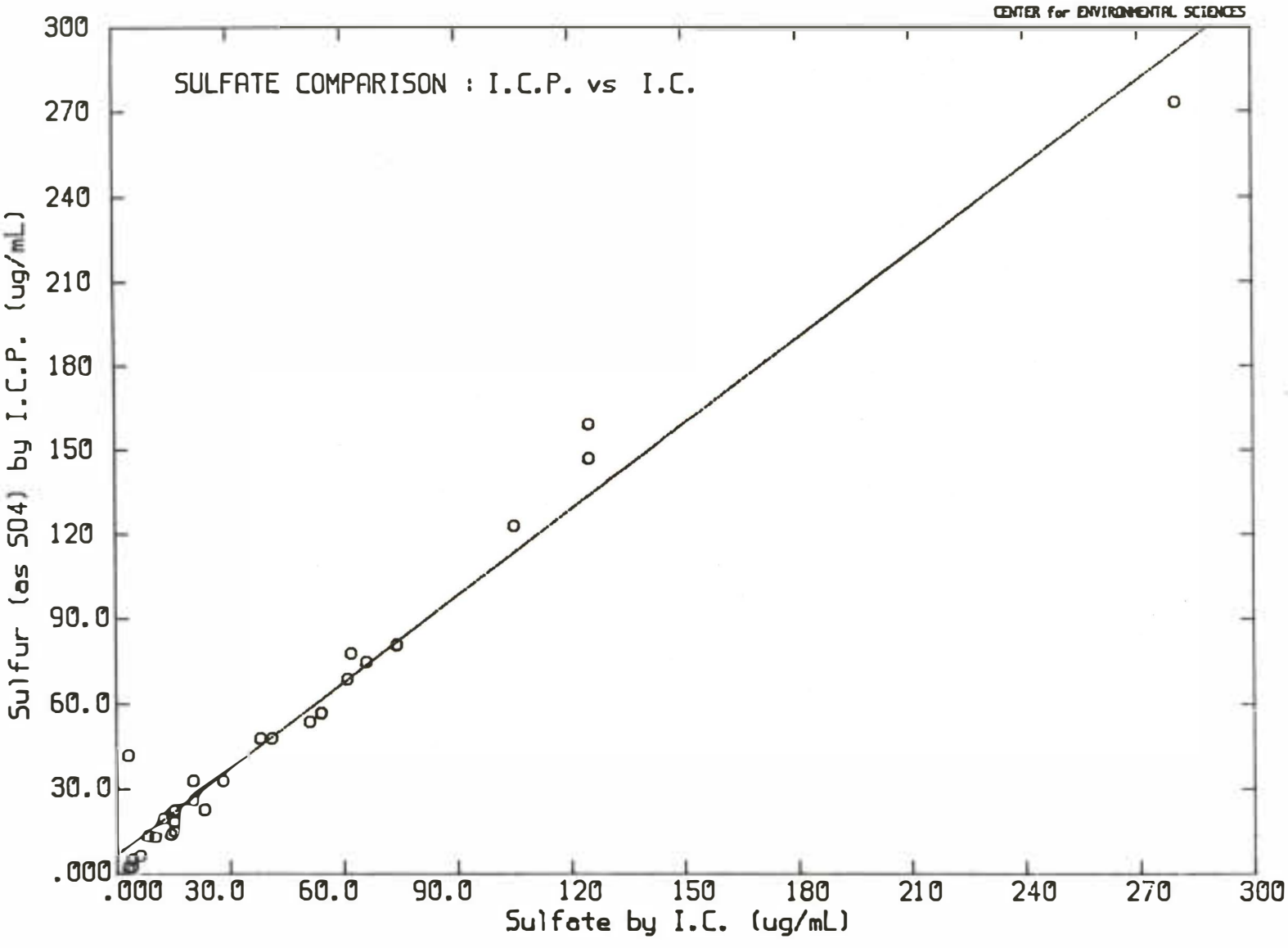
CENTER for ENVIRONMENTAL SCIENCES
SULFATE COMPARISON : I.C.P. vs I.C.
Sulfur (as SO4) by I.C.P. (ug/mL)
Sulfate by I.C. (ug/mL)
.000
30.0
60.0
90.0
120
150
180
210
240
270
300

Figure 2.5

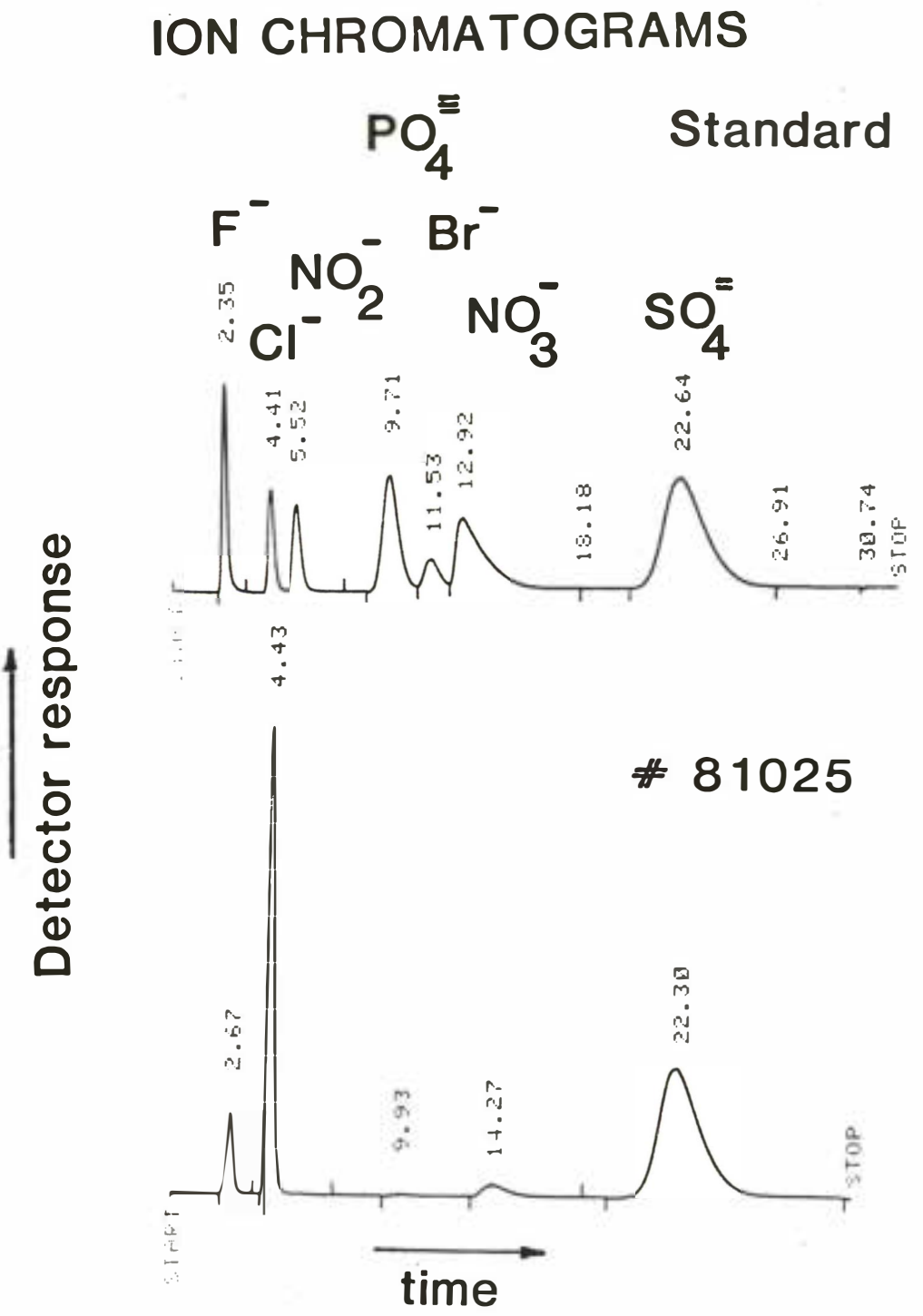
ION CHROMATOGRAMS
Standard
$PO_4^{\equiv}$
F^-
NO_2^-
Br^-
Cl^-
NO_3^-
$SO_4^{\equiv}$
2.35
4.41
5.52
9.71
11.53
12.92
18.18
22.64
26.91
30.74
STOP
4.43
81025
2.67
9.93
14.27
22.30
STOP
Detector response
time

Figure 2.6

2.3 Atomic Absorption Spectrophotmetry (AAS)

While most chemical determinations required for this project were performed with ICP and IC techniques, a few species were determined by Atomic Absorption Spectrophotometry (AAS). A Perkin-Elmer Model 5000 Atomic Absorption Spectrophotometer and Model 500 Heated Graphite Analyzer were used in this work. Both flame and furnace techniques were used to test accuracy of other techniques. (The role of independent methods testing is discussed in the quality control section of this report.) Graphite furnace AAS was used routinely for determining chromium, arsenic, selenium, silver, nickel, and lead. While ICP can be used for these species, they were present at low concentration in most of the samples. Since precise quantitative measurements can not be made near the instrumental detection limit, and these species were environmentally important, we developed procedures to perform the trace level determinations. Details of the procedures are found in "Operating Conditions for Analytical Methods" of this report. Additional information regarding the accuracy and precision of the methods is presented in Section 3 of the report.

3. QUALITY CONTROL

The quality control program employed in these studies consisted of two features. First the validity of the candidate method was established. A robust surveillance protocol was maintained to ensure the accuracy and precision of the analyses.

3.1 Estimation of Accuracy and Precision

While it is impossible to determine absolute accuracy, it is possible to obtain an estimate by using several techniques. Table 3.1 shows the principal techniques available for the estimation of an analytical method's accuracy and precision.

TABLE 3.1

Techniques for Estimating
Accuracy and Precision

	Method Used to Estimate **Accuracy**	Method Used to Estimate **Precision**
Primary:	1. Analysis of certified stds.	Replicates
	2. Independent methods	Replicates
	3. Collaborative tests	Replicates
Secondary:	1. Secondary (in-house) stds.	Replicates
	2. Spike recovery tests (inferential only)	Replicates

In the early stages of methods development a list of candidate methods was prepared. Representative samples of the anticipated matrices were analyzed by the candidate methods. Spike recovery tests and interference tests were performed to assess the need for matrix dependent methods modifications. Whenever possible, standard reference materials with similar matrix characteristics were also analyzed to determine the accuracy of the proposed methods. When no suitable standard reference material was available we relied upon analysis by independent methods and collaborative tests to assess accuracy. Examples of how these methods were used to assist in methods validation are given below.

3.1.1 **Determination of Accuracy.** Accuracy of trace analysis methods was evaluated by participating in large scale interlaboratory collaborative testing programs and analysis of certified standard reference materials. Aqueous samples of known composition were obtained from the U.S. Environmental Protection Agency. These samples simulate "natural" concentrations of several elements rather than the anomalous levels found in most of the study materials. However, when used in conjunction with the other accuracy tests described below, we were able to assess methods performance at drinking water standard levels. Table 3.2 shows the results of these tests. Periodic analysis of the same certified standards was used in conjunction with the formal routine surveillance protocol to establish a continuous time link between methods development and routine analysis.

Additional accuracy tests were performed by participating in a collaborative testing program (round-robin) conducted by the U. S. Geological Survey. Performance was judged by comparing results obtained in this laboratory with more than fifty other laboratories that used a variety of analytical procedures. Table 3.3 shows the results of the U.S.G.S. collaborative tests for very low levels (micrograms/liter) and trace levels (milligram/liter).

TABLE 3.2

Accuracy Tests on EPA Standard Reference Water #476E-2

Trace Metals in mg/L

Element	Accepted	Found	Std. Dev.
Mn	0.478	0.477	0.026
Fe	0.796	0.827	0.013
Cr	0.304	0.320	0.008
Cu	0.374	0.379	0.002
V	0.848	0.817	0.011
Zn	0.478	0.464	0.013

Accuracy Tests on EPA Standard Reference Water #476E-3

Trace Metals in mg/L

Element	Accepted	Found	Std. Dev.
Mn	0.047	0.045	0.009
Fe	0.078	0.076	0.006
Cr	0.065	0.076	0.009
Cu	0.037	0.035	0.009
V	0.470	0.442	0.012
Zn	0.026	0.048	0.020

TABLE 3.3

Accuracy Tests on USGS Reference Water #80
Concentration Units are mg/L

Analyte	USGS*	Found	Method
Alkalin.	123.1	120	Colorim.
Ca	50	52	ICP
Cl	31.9	32	IC
F	1.13	1.1	IC
K	4.36	4.9	ICP
Mg	12.3	13	ICP
Na	31.8	32	ICP
nitrate	0.546	0.70	IC
silica	5.41	3.0	ICP
sulfate	71.7	71	IC
Sp.Cond.	485.7	490	Wh.Bridg.
Sr	0.458	0.460	ICP

Accuracy Tests on USGS Reference Water #81
Concentration Units are mg/L

Analyte	USGS*	Found	Method
Al	0.104	0.200	ICP
As	0.018	0.024	HGA
Ba	0.240	0.240	ICP
Cd	0.009	0.006	HGA
Co	0.013	0.011	HGA
Cr	0.027	0.025	HGA
Cu	0.029	0.021	HGA
Fe	0.703	0.710	ICP
Li	0.509	0.580	ICP
Mn	0.546	0.550	ICP
Mo	0.038	0.042	HGA
Ni	0.010	0.042	HGA
Pb	0.004	0.002	HGA
Se	0.011	0.016	HGA
Sr	0.450	0.440	ICP
Zn	0.104	0.100	ICP

* Mean values reported by all participating Laboratories. (Consensus values only.)

Certified reference materials similar to the more complex matrices encountered in our studies were not available. Therefore, we relied upon in-house test materials prepared by homogenizing several aliquots of the sample matrix. These materials were subjected to analysis by candidate and independent methods. Independent methods included detection techniques that utilize different physical/chemical principles for analyte quantification. Figure 3.0 shows the results of a comparison between the candidate method (ICP) and a spectrophotometric method for determining boron. These two methods provided acceptable agreement to advance the candidate method to additional testing on other materials. Subsequent tests, and acceptable performance in an interlaboratory collaborative test (round-robin) showed that the ICP method was suitable for routine use. Similar tests were performed for most elemental determinations. Acceptance of a candidate method for routine use was predicated upon valid independent tests, performance in collaborative tests, and accuracy checks against standard reference materials.

No certified tailings or raffinate materials were available. Therefore, sample exchanges with other qualified laboratories were used to assess the accuracy of the candidate analytical methods. These collaborative tests are most useful when the participating laboratories use different methods of sample preparation and quantification. Table 3.4 shows the results of one collaborative test that was used to assess the performance of the candidate (ICP) method. Analysis by three outside laboratories using ICP and two laboratories using atomic absorption (AA) methods are shown here. This test, on a limited suite of elements, provided a basis for accepting the ICP method (for aqueous samples).

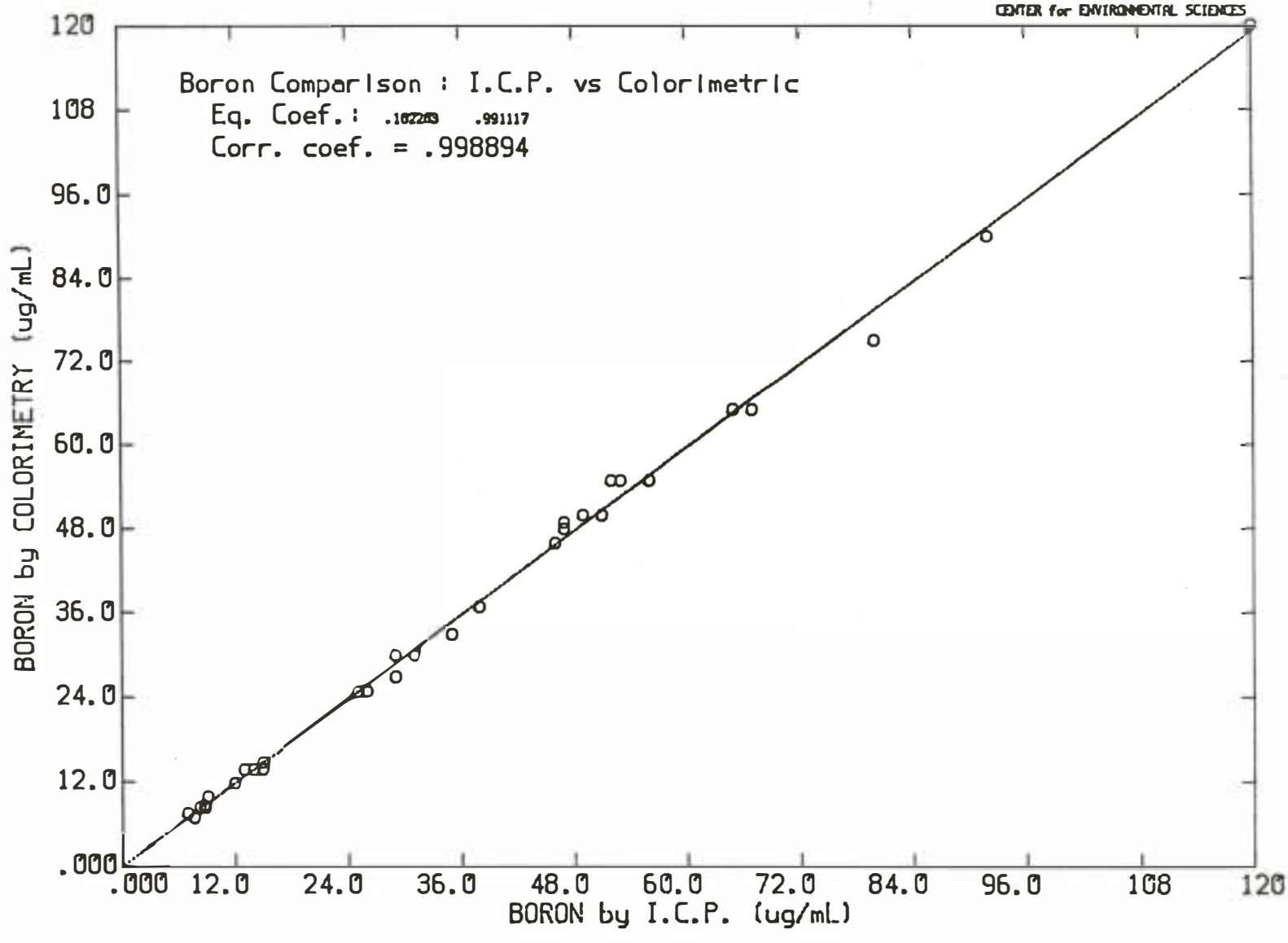
CENTER for ENVIRONMENTAL SCIENCES
Boron Comparison : I.C.P. vs Colorimetric
Eq. Coef.: .102203 .991117
Corr. coef. = .998894
BORON by COLORIMETRY (ug/mL)
BORON by I.C.P. (ug/mL)
.000
12.0
24.0
36.0
48.0
60.0
72.0
84.0
96.0
108
120

Figure 3.0

TABLE 3.4

Interlaboratory and Independent Methods
Accuracy Tests on
Trace Constituents in Waters

Concentration Units are mg/L
(Range in parentheses)

Analyte	Three Labs ICP	Two Labs AAS	This Lab ICP
Cd	0.088 (0.02)	0.079 (0.036)	0.091
Cr	0.27 (0.04)	0.23 (0.08)	0.26
Cu	0.34 (0.04)	0.36 (0.06)	0.36
Fe	0.88 (0.06)	0.98 (0.18)	1.04
Mn	0.45 (0.08)	0.52 (0.02)	0.52
Pb	0.39 (0.06)	0.47 (0.10)	0.47
Si	0.28 (0.04)	n.d.	0.36
V	n.d.	0.99 (0.12)	0.88
Zn	0.45 (0.08)	0.41 (0.08)	0.41

3.1.2 **Determination of Precision.** Precision of analytical methods is generally estimated by performing replicate determinations on samples. The ideal estimate would be obtained by performing replicate determinations on every sample. However, practical considerations limit the number of replicates that can be performed. When accuracy has been well established, a modified replicate analysis protocol can be substituted without sacrificing statistical rigor and the interpretive power of the results. The protocol adopted in this study was designed to maximize our ability to provide continuous performace surveillance and to minimize the labor associated with quality control monitoring. The precision estimates given here were obtained by applying a quality control protocol that will be described later.

Many of the studies performed by the project investigators involved sample collections over long time periods. This fact, and large numbers of samples, meant that analyses were performed over extended time periods. A quality control program was designed to monitor analytical performance daily so that consistency could be assured. Within run and between run variance measures are more important to that task than individual sample precision estimates. These variance measures were obtained by performing duplicate analyses on a single quality control sample (described later) with each analytical run of twenty four samples.

A quality control sample was placed at the beginning and end of each analytical run. This permitted us to "bracket" each set of unknowns with a performance check. Since the same Q.C. sample was used throughout the study it was possible to obtain estimates of the within run and between run variance for each analytical method over the duration of the project.

Since ICP was the principal analytical technique used, and because the scanning instrument performance had not been established, we performed extensive tests to assess its performance. An ICP task file of ten elements required approximately five minutes per sample. Therefore, a typical run of twenty four samples (including two Q.C. samples) required about two hours. Comparisons between the two Q.C. samples were used to determine whether any instrumental drift was occurring. Long term instrument peformance was monitored by computing the between run variances. Instrument precision is a complex function of the signal-to-noise ratio and sample matrix parameters. Each element, in a given matrix, will exhibit different precision characteristics. In order to illustrate the instrument performance on a specific matrix we have depicted the precision as relative standard deviations and plotted them against a parameter that reflects the concentration dependence of the precision. The parameter chosen is the logarithm of the actual concentration divided by the detection limit for that species. For example, a value of 1.0 means that the element is present at 10 times the detection limit; a value of 0.0 indicates analyte concentration equal to the detection limit. Figure 3.1 shows the plot of this precision function for the within run tests. At large multiples of the detection limit this function approaches an asymptote that reflects the optimal performance possible in this matrix. The residual noise is essentially element independent and reflects the "system noise". From this plot we can determine that the best precision to be expected in analyzing tailings leachates within a two hour period is about 2.0 percent. Precision gets poorer (imprecision increases) as the analyte concentration approaches the detection limit. (At the detection limit R.S.D. = 50%.) While each element ought to have its own characteristic curve, it is useful to depict all species on one plot to illustrate which elements in a given matrix are problematic. This plot shows that molybdenum and chromium determinations are less precise and barium is more precise than expected. Figure 3.2 shows the precision profile between runs. As expected, the high concentration asymptote is greater than we find within runs. This reflects the contribution of instrument recalibration imprecision. Between runs silicon precision is observed to get worse. Similar plots have been examined for the project duration. Additonal detailed element specific statistics provided by the Q.C. protocol provided an effective method to identify procedures that required improvement.

3.2 Principles of the Quality Control Surveillance Scheme

There are two types of errors associated with any chemical analysis; **systematic** (determinate) and **random** (indeterminate). Inaccurate results, consistently higher or lower than the "true" value, occur when systematic

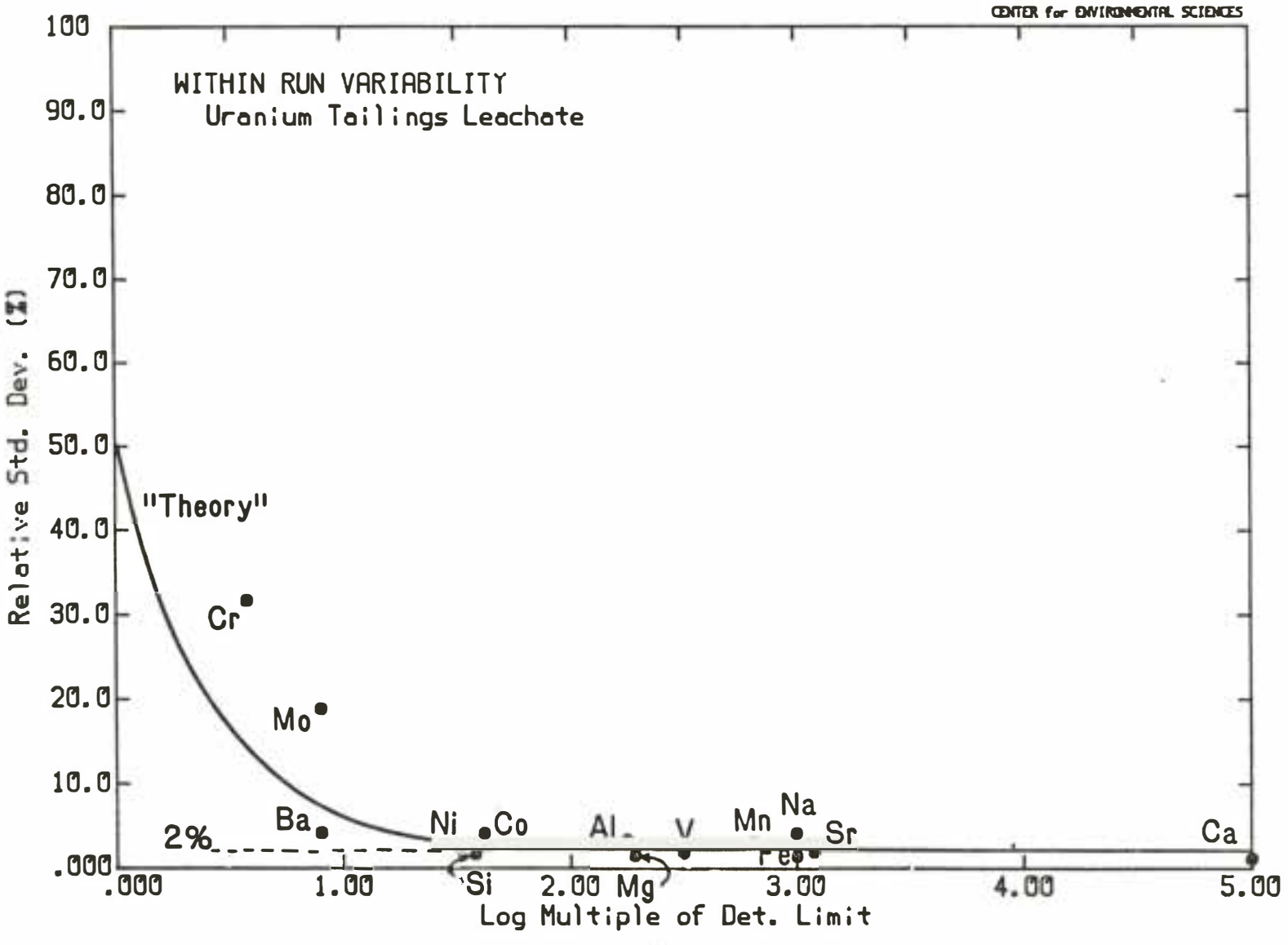
CENTER for ENVIRONMENTAL SCIENCES
WITHIN RUN VARIABILITY
Uranium Tailings Leachate
Relative Std. Dev. (%)
100
90.0
80.0
70.0
60.0
50.0
40.0
30.0
20.0
10.0
.000
"Theory"
Cr
Mo
Ba
2%
Ni
Co
Si
Al
Mg
V
Mn
Fe
Na
Sr
Ca
.000
1.00
2.00
3.00
4.00
5.00
Log Multiple of Det. Limit

Figure 3.1

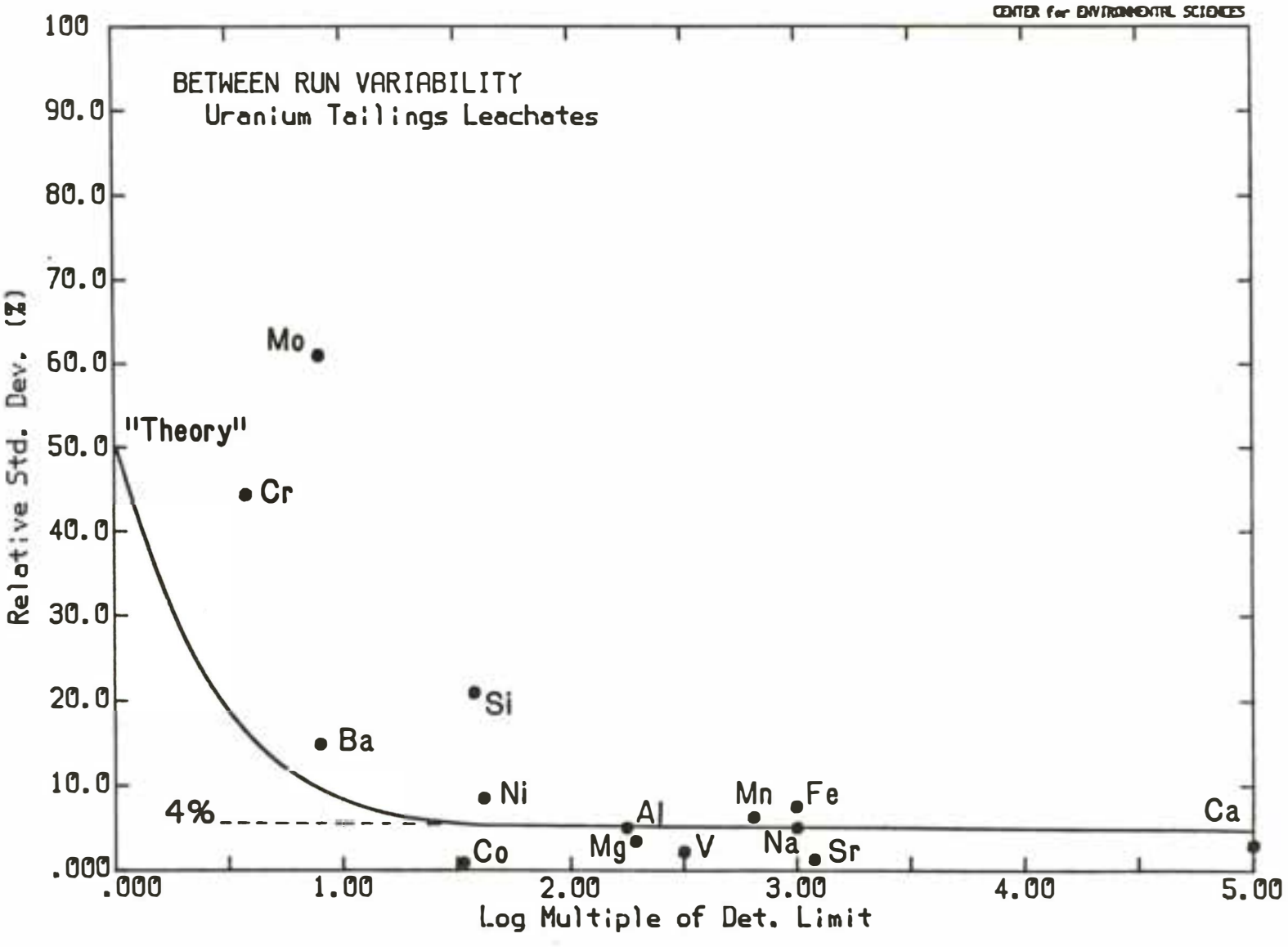
CENTER for ENVIRONMENTAL SCIENCES
BETWEEN RUN VARIABILITY
Uranium Tailings Leachates
Relative Std. Dev. (%)
100
90.0
80.0
70.0
60.0
50.0
40.0
30.0
20.0
10.0
.000
"Theory"
Mo
Cr
Si
Ba
Ni
4%
Co
Al
Mg
V
Mn
Fe
Na
Sr
Ca
.000
1.00
2.00
3.00
4.00
5.00
Log Multiple of Det. Limit

Figure 3.2

errors are present. Systematic errors tend to have the same algebraic sign and usually arise from erroneous calibration, instrumental drift, loss of analyte or contamination during sample preparation, failure to account for blank or background effects, etc. Through adequate testing procedures it is possible to determine the magnitude and source of this type of error (hence the term "determinate error"). The validation phase of methods development is designed to eliminate this source of error. Occasionally systematic errors appear after the method has been in use for some time. **An effective quality control scheme should permit early detection of systematic error and assist the analyst in diagnosing its cause.**

Random or indeterminate errors have a frequency of occurrence that is symmetrical. Small positive or negative errors have the highest probability of occurrence while very large positive or negative deviations are less probable. These errors are inherent in any measurement technique that is based on a continuous interval scale such as; reading peak heights or analog meters, determining mass, etc. While careful control of experimental variables can minimize the magnitude of these errors, they are always present. These errors define the precision of the measurements and establish the detection limit of the procedure. **An effective quality control scheme should permit early detection of any change in the magnitude of random errors and assist in diagnosing its cause.**

The ability to distinguish between random and systematic error contributions to measurements is an important prerequisite to problem diagnosis. The technique described by W. J. Youden (ref.1) was designed to identify and separate systematic and random errors that occur among laboratories participating in interlaboratory tests. The method has been extended and modified by Meglen (ref. 2) and King (ref. 3) for use within a single laboratory, intralaboratory testing. In this modification the results obtained from day-to-day are treated as if they were obtained in different laboratories. Two different plotting techniques are used to monitor the analytical performance. Following a brief description of the mathematical basis for this approach we will examine several example plots.

3.2.1 **Theory.** Assume that a single sample is split into two portions labeled A and B. A quantitative determination of some sample constituent should yield the "true" value X plus any systematic and random error contributions.

$$A = X + S + R \qquad (3\text{-}1)$$

$$X = B + S + R' \qquad (3\text{-}2)$$

Where S is the systematic error (bearing the same algebraic sign and having the same magnitude for each sample), and R and R' are the random errors (bearing potentially different algebraic signs and having different magnitudes for each sample). Recall that random error contribu-

tions for each sample have equal probability of being either positive or negative i.e. they are normally distributed and independently expressed. The sum of the results obtained for both splits will yield a number T that has twice the the true value and twice the systematic error of one sample.

$$T = (A + B) = 2X + 2S + R + R' \quad (3\text{-}3)$$

Since the random errors come from a symmetrical frequency distribution with both algebraic signs, R and R' will tend to cancel one another after many determinations. The average value of T, after many determinations, will contain only the systematic error contribution.

When the difference D between the results A and B is computed the systematic errors, which have the same magnitude and sign, will cancel. This leaves the sum of the two random error components, which do not necessarily cancel for a particular pair.

$$D = (A - B) = R + R' \quad (3\text{-}4)$$

By plotting the sum T and difference D in time ordered sequence the variation of random and systematic errors can be monitored between analytical runs.

The procedure used for day-to-day monitoring utilizes a single real sample (usually a composite of previously analyzed samples) split into two aliquots labeled A and B. These samples are carried though the analytical procedure together with the unknowns.

3.2.2 Quadrant Plots. The primary purpose of any quality control scheme is to identify (flag) significant changes in analytical performance. The Q. C. scheme described above is useful for identifying performance changes and systematic error components. However, rapid evaluation of a specific analytical run relative to previous data is also important. Graphical representations of these data provide an effective method for identifying anomalies. Two types of plots are used to depict analytical performance.

Consider a hypothetical case where an analytical method has been perfected and no systematic error is present. Random errors inherent in the determinations on the two samples (A and B) would exhibit the following deviations: i.e. both slightly low, both slightly high, or one slightly high and one slightly low.

SAMPLE A	SAMPLE B
+	+
-	-
+	-
-	+

All four possibilities are equally likely in an accurate method. The results from a series of paired determinations from the two identical samples (A and B) can be plotted on two axes. For any analytical run, the result of the determination on sample A is plotted against the result for B. For a large number of runs a vertical line is drawn through the average of the B results and a horizontal line through the average of the A results. The plot is therefore divided into four quadrants that correspond to the four outcomes enumerated above. (Upper right, lower left, upper left and lower left respectively.) If the only source of errors is truly random all four quadrants will be equally populated by points. (See Figure 3.3a.)

Consider the hypothetical non-random error case where both samples exhibit equivalent positive or negative (systematic) deviations. The point in the quadrant plot would be distributed along a 45 degree line with equal distribution of points in the upper right (++) and lower left (--) quadrants as shown in Figure 3.3b.

The two hypothetical cases , random error only and systematic error only, manifest themselves in qualitatively different behavior in the quadrant plots. Actual experience shows that random errors can be minimized, not eliminated. Figure 3.3c shows a more realistic representation of this. Figure 3.3d shows an ellipse which is drawn to enclose 95% of the results obtained in a hypothetical experiment that contains both random and systematic error components. The ellipse's major axis is equal to two standard deviations (determined from the total variance; between run), and the minor axis is equal to two times the random error standard deviation. The circle is drawn to enclose 95% of the random error results. Thus, points found in the region between the circle and the ellipse are from analyses that contain systematic error components. The adaptation of the Youden method to within laboratory evaluation derives its utility by incorporating time as a variable. Therefore, by connecting the points in time ordered sequence, it is possible to identify the time dependent varations within the systematic and random error domains. We will illustrate the utility of quadrant plots after a brief discussion of the second type of quality control plot.

3.2.3 **Time-Ordered Plots.** An additional type of time dependent plot provides complementary information for performance evaluation. Results of the determinations on A plus B (Totals, T) and A minus B (Differences, D) are plotted in time ordered sequence to facilitate the detection of time

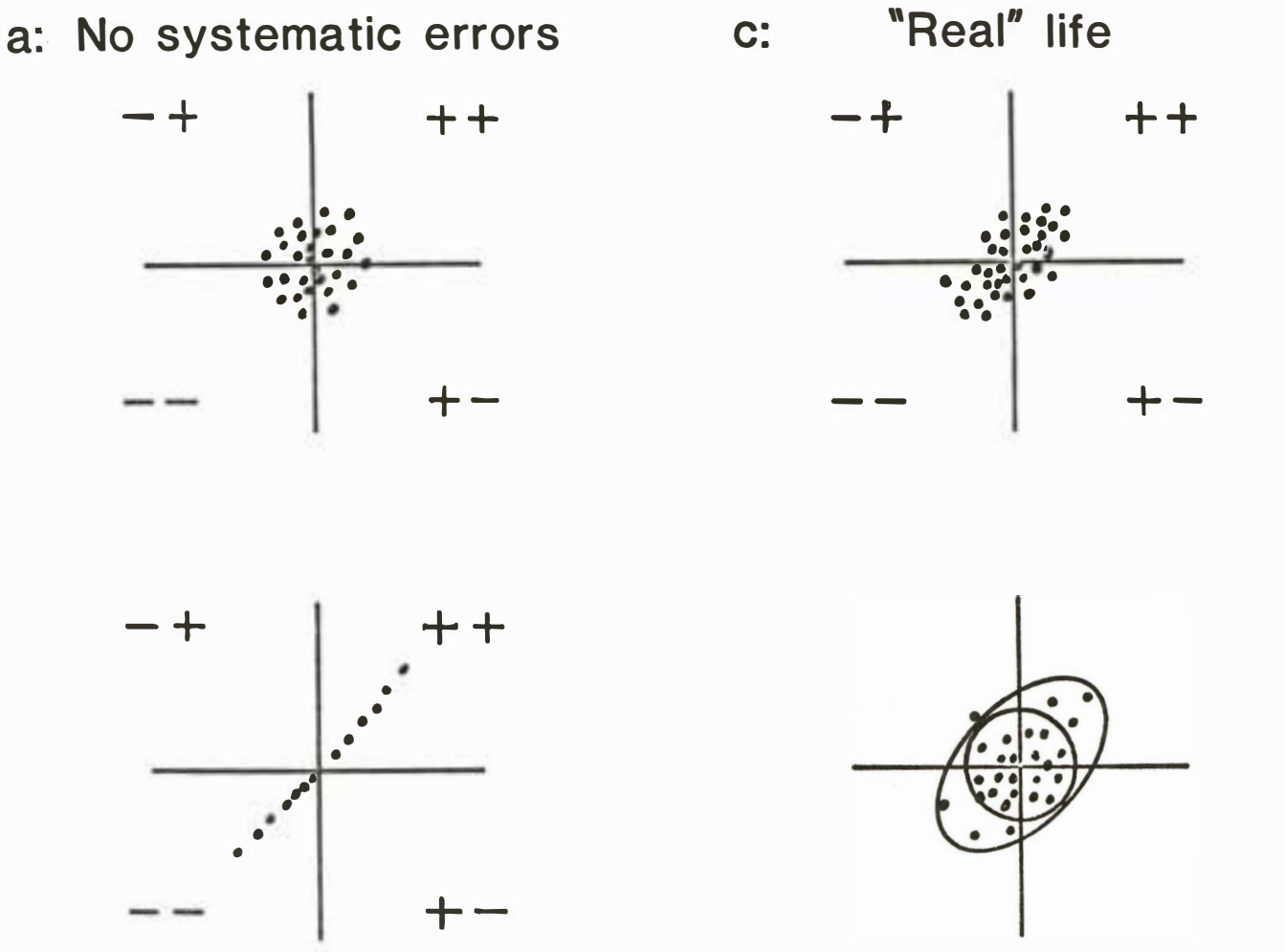
a: No systematic errors
c: "Real" life
−+
++
−−
+−
−+
++
−−
+−
−+
++
−−
+−
b: No random errors
d: random & systematic
error domains

FIGURE 3.3

dependent patterns or trends. The utility of these plots will be demonstrated with several examples from data obtained during routine quality control monitoring. Each of the following figures consists of three separate plots; "T"-plot, "D"-plot, and quadrant plot. The solid horizontal lines in the T and D plots are drawn through the mean of the totals (A + B) and differences (A - B) respectively. In the protocol adopted for this study, Q.C. sample A is the first sample and B is the last sample of twenty four analyzed in a given "run". If no systematic drift occurs during the run, the D plot mean should be 0.0 and the horizontal line should reflect this. The dashed horizontal lines indicate the quality control limits of plus and minus one standard deviation. Point-by-point comparisons of the T and D plots were made daily. Anomalies are identified and interpreted. All samples in an anomalous run are submitted for re-analysis. Long term patterns are used to diagnose the nature of the analytical difficulties. Seven basic patterns in T and D plots have been identified and are listed in "Quality Control Diagnostics". (Thirty five illustrative examples and their possible causes have been assembled for routine use.) The quadrant plot assists the analyst in identifying patterns and significant outliers. In principle, identical information is depicted in both time-ordered plots and quadrant plots. However, different aspects are emphasized by each.

Figure 3.4 shows a group of ICP sodium runs performed on a composited tailings extract. (The computer file name PYENA.2 used for storing the data identifies that the data were obtained by ICP [P=Plasma]; the composite matrix was a tailings extract [YE]; and the element being examined is sodium [NA].) The T plot shows no systematic error trend. However, the quadrant plot indicates that run # 19 contained systematic error beyond the historical precedent. The point lies in the systematic error quadrant (--) indicating that the result is biased on the low side. The same conclusion may be deduced from the fact the 19th run on the T plot is anomalously low. A corresponding large positive anomaly in the D plot indicates that the last Q.C. sample, B, was much lower than A. This observation is consistent with plasma nebulizer clogging during the run. The Q.C. plots for other elements in the plasma task file also show that run # 19 was anomalous. Therefore, all samples between the Q.C. samples were re-analyzed. The within run variability (RSD = 4.3%) and between run variability (RSD = 5.1%) are representative of performance obtained using ICP on this matrix type.

Figure 3.5 shows the Q.C. data for chromium in the same composite tailings extract. The large scatter in the T plot indicates that, in this matrix, plasma emission is too imprecise to permit quantitative measurement. The analyte concentration is too near the detection limit. Statistical analysis included in the plotting routine indicate that the between run variability (RSD = 45%) and the within run variability (RSD = 32%) support this conclusion. This difficulty lead to the selection of graphite furnace AAS for routine Cr determinations.

Figure 3.6 shows the Q.C. plots for sulfate determination on the tailings extract. All plots indicate that the Ion Chromatographic method is "under

control". No patterns or anomalies appear. Points lying outside the one standard deviation boundaries are not statistically significant (F-test). The quadrant plot shows a fairly tight random walk among the systematic and random error quadrants (note: circular error boundary). The statistical summary indicates that the within run RSD is 1.9% and the between run RSD is 2.0%. Similar precision values are observed for other IC determinations.

QUALITY CONTROL PLOTS

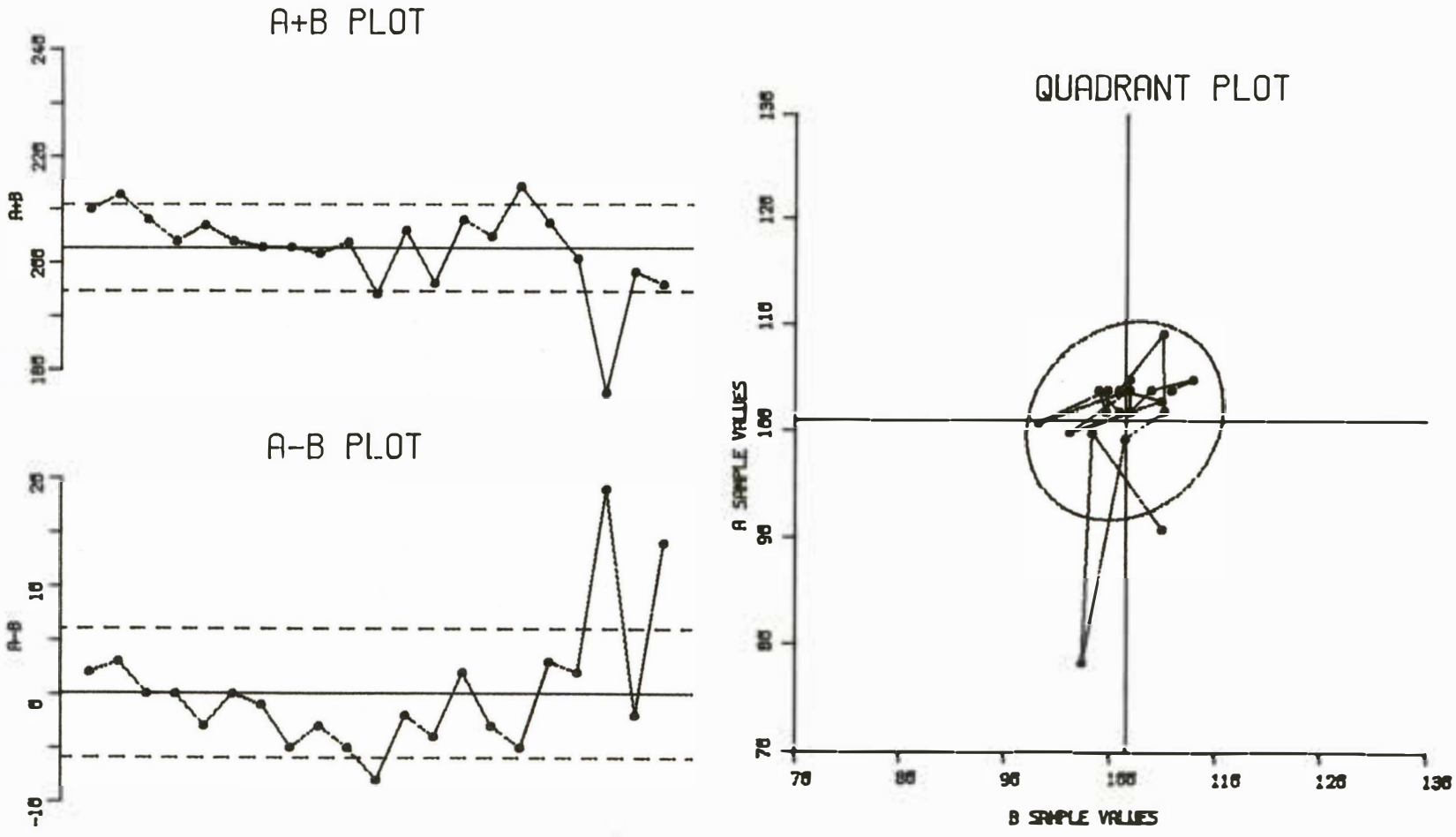

Figure 3.4 PYENA

QUALITY CONTROL PLOTS

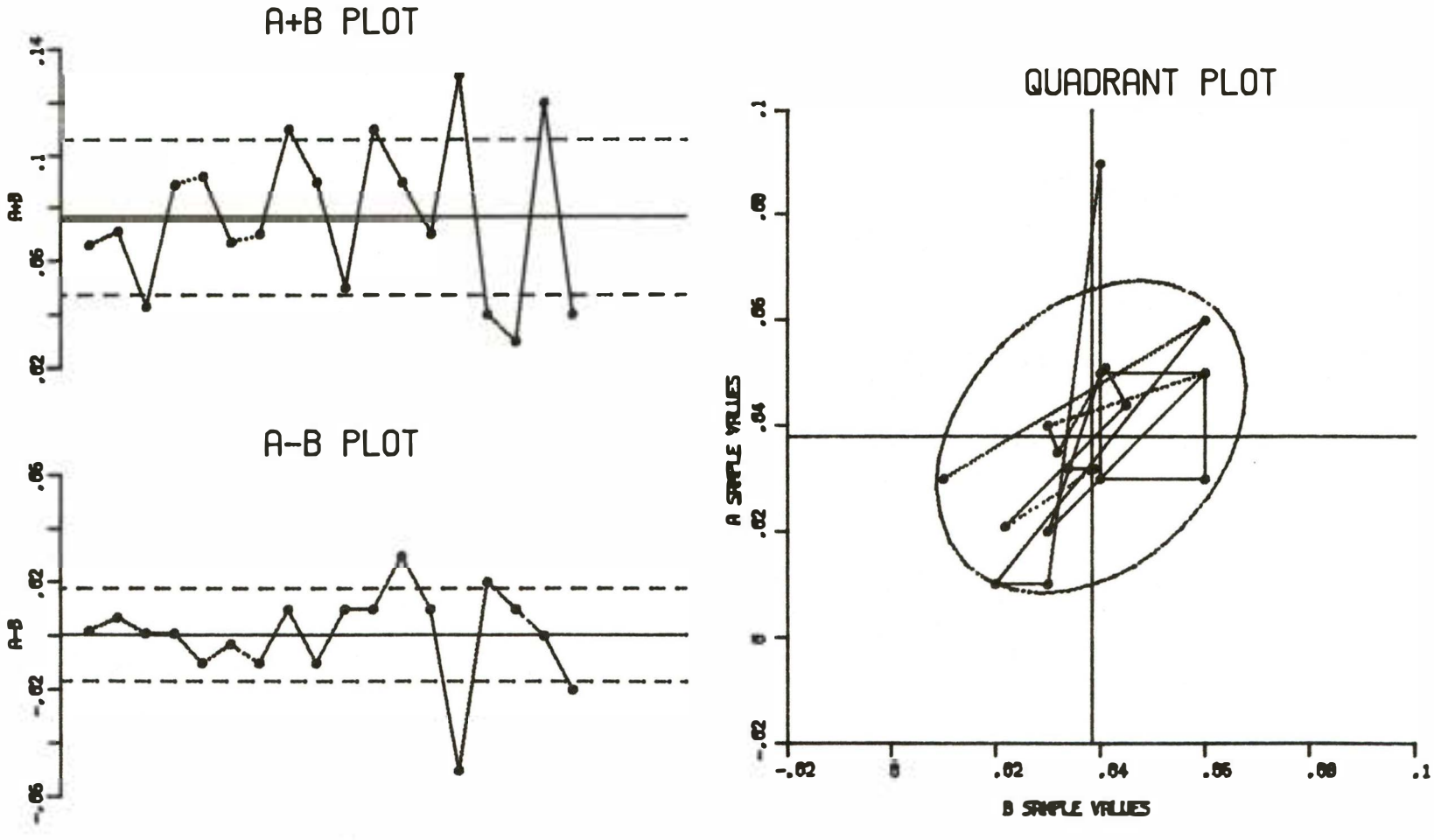

Figure 3.5 PYECR

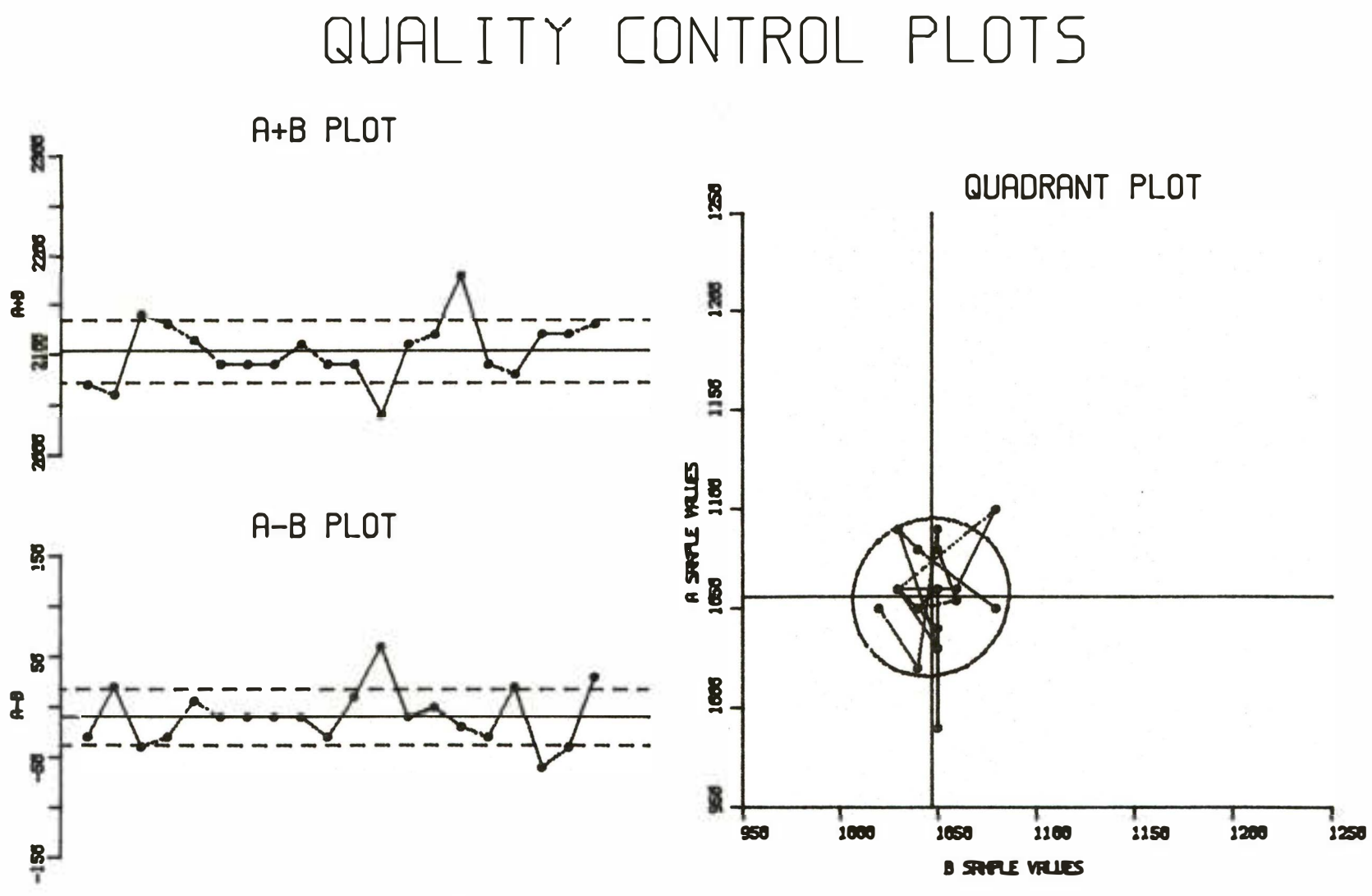

Figure 3.6 IYES04

4. OPERATING CONDITIONS FOR ANALYTICAL METHODS

4.1 ICP CONDITIONS

4.1.1 Nominal Wavelength Library. The Bausch & Lomb Model 35000 supporting software contains a wavelength library that contains suggested emission wavelegths that can be used for analyses. The supplied list has been augmented in this laboratory to contain additional lines that we have found useful for routine work. The abbreviated list of interferences has also been modified to reflect spectral interferences that we have found to be significant. The following list also contains a conservative estimate of the linear calibration range for each line. Estimates of the **determination limit** (the lowest concentration at wich quantitative measurements can be made) are also listed. Detection limits are approximately one fifth to one half of the determination limits.

WAVELENGTH LIBRARY

NO.	SYMBOL	WAVELENGTH	LO LIMIT	RANGE (PPM)	MAJOR INTERFS
1	AR	3554.31	0	0 - 0	
2	AR	3948.94	0	0 - 0	
3	AG	3280.68	.01	.01 - 200	
4	AG	3382.89	.05	.05 - 1000	
5	AL	3082.15	.15	.15 - 3000	
6	AL	3092.7	.25	.25 - 5000	
7	AL	3961.52	.075	.075 - 1500	CA
8	AS	1890.5	.2	.2 - 4000	
9	AS	1937.6	.125	.125 - 2500	AL
10	AS	1972.62	.2	.2 - 4000	
11	AU	2427.95	.05	.05 - 1000	MN
12	B	1825.9	.0005	.0005 - 10	
13	B	1826.4	.1	.1 - 2000	
14	B	2089.59	.02	.02 - 400	MO
15	B	2496.78	.0125	.0125 - 250	
16	B	2497.73	.01	.01 - 200	
17	BA	2335.27	.0015	.015 - 300	
18	BA	4554.03	.002	.002 - 40	
19	BE	2348.61	.001	.001 - 20	
20	BE	3130.42	.001	.001 - 20	V
21	BI	2230.61	.2	.2 - 4000	
22	BI	3067.72	.5	.5 - 10000	
23	C	1930.91	.5	.5 - 10000	
24	C	2478.56	1	1 - 20000	
25	CA	3179.33	.015	.015 - 300	
26	CA	3933.66	.00025	.00025 - 5	
27	CA	4226.73	.15	.15 - 3000	
28	CD	2144.38	.01	.01 - 200	PT
29	CD	2265.02	.015	.015 - 300	NI
30	CE	4137.65	.15	.15 - 3000	
31	CO	2286.16	.0125	.0125 - 250	
32	CO	2378.62	.01	.01 - 200	AL
33	CR	2055.52	.01	.01 - 200	
34	CR	2061.49	.02	.02 - 400	ZN BI PT
35	CR	2677.16	.015	.015 - 300	PT
36	CU	2247	.02	.02 - 400	
37	CU	3247.54	.01	.01 - 200	
38	FE	2599.4	.01	.01 - 200	
39	FE	2714.4	.5	.5 - 10000	

WAVELENGTH LIBRARY

NO.	SYMBOL	WAVELENGTH	LO LIMIT	RANGE (PPM)	MAJOR INTERFS
40	FE	2739.55	.02	.02 - 400	
41	GA	2943.64	.25	.25 - 5000	
42	GA	4172.1	.25	.25 - 5000	
43	GD	3422.47	.05	.05 - 1000	
44	GD	3549.36	.25	.25 - 5000	
45	GE	2094.26	.15	.15 - 3000	
46	GE	2651.18	.25	.25 - 5000	TA HF
47	HG	1849.57	0	0 - 0	
48	HG	1942.27	.05	.05 - 1000	V
49	HG	2536.52	.075	.075 - 1500	FE
50	I	1782.76	.175	.175 - 3500	P(BAD)
51	I	1830.4	.01	.01 - 200	
52	I	2062.4	3.2	3.2 - 64000	CU ZN
53	IN	2306.06	.25	.25 - 5000	
54	IR	2242.68	.075	.075 - 1500	CU
55	K	4047.2	20	20 - 400000	
56	K	7664.91	.5	.5 - 10000	CU
57	LA	3794.78	.0375	.0375 - 750	FE
58	LA	3988.5	.05	.05 - 1000	
59	LI	6707.8	.015	.015 - 300	
60	MG	2790.8	.25	.25 - 5000	TI
61	MG	2795.53	.0005	.0005 - 10	
62	MN	2576.1	.005	.005 - 100	
63	MN	2949.2	.025	.025 - 500	
64	MO	2020.3	.025	.025 - 500	FE
65	MO	2816.15	.02	.02 - 400	AL MG
66	NA	3302.37	10	10 - 200000	
67	NA	5895.92	.1	.1 - 2000	
68	NB	3094.2	.05	.05 - 1000	
69	NI	2216.47	.02	.02 - 400	CO W SI
70	NI	2270.21	.04	.04 - 800	
71	NI	2316.04	.02	.02 - 400	
72	OS	2255.85	.0025	.0025 - 50	FE
73	P	1782.87	.1	.1 - 2000	I(BAD)
74	P	2136.18	.1	.1 - 2000	CU
75	P	2149.14	.15	.15 - 3000	CU
76	PB	2169.99	.2	.2 - 4000	
77	PB	2203.53	.1	.1 - 2000	SN PD
78	PD	3634.7	.15	.15 - 3000	CO
79	PT	2659.45	.2	.2 - 4000	

WAVELENGTH LIBRARY

NO.	SYMBOL	WAVELENGTH	LO LIMIT	RANGE (PPM)	MAJOR INTERFS
80	RB	7800.23	2	2 - 40000	
81	RE	2275.25	.05	.05 - 1000	AG
82	RH	3434.89	.15	.15 - 3000	
83	S	1807.31	.125	.125 - 2500	
84	S	1820.37	.2	.2 - 4000	
85	SB	1871.15	0	0 - 0	
86	SB	2068.33	.2	.2 - 4000	CR MO GE
87	SC	3613.84	.005	.005 - 100	
88	SE	1960.9	.3	.3 - 6000	PD
89	SE	2039.85	.4	.4 - 8000	
90	SI	2124.12	.1	.1 - 2000	MO
91	SI	2516.11	.05	.05 - 1000	V MO
92	SI	2881.58	.1	.1 - 2000	
93	SN	1899.8	.15	.15 - 3000	TI
94	SN	2429.49	.4	.4 - 8000	
95	SR	3464.46	.1	.1 - 2000	
96	SR	4077.71	.001	.001 - 20	LA
97	TA	2400.6	.25	.25 - 5000	
98	TE	2142.75	.2	.2 - 4000	
99	TH	2837.3	.15	.15 - 3000	FE
100	TH	3741.2	.25	.25 - 5000	
101	TH	4019.1	.02	.02 - 400	
102	TI	3361.21	.01	.01 - 200	
103	TI	3372.8	.05	.05 - 1000	
104	TL	1908.64	.25	.25 - 5000	MO V
105	TL	3775.7	1	1 - 20000	
106	U	3670.07	.37	.37 - 7400	
107	U	3859.58	.5	.5 - 10000	FE ND
108	U	4090.14	.5	.5 - 10000	
109	U	4241.67	.75	.75 - 15000	
110	V	2924.02	.025	.025 - 500	
111	V	3110.7	.02	.02 - 400	
112	W	2079.11	.075	.075 - 1500	NI CU
113	W	2397.09	.1	.1 - 2000	
114	Y	3710.3	.01	.01 - 200	
115	ZN	2025.51	.0075	.0075 - 150	MG CU
116	ZN	2061.91	.01	.01 - 200	CR BI
117	ZN	2138.56	.005	.005 - 100	NI V
118	ZR	3438.23	.01	.01 - 200	HF
119	ZR	3496.21	.025	.025 - 500	

4.1.2 **Routine Wavelength Library.** The following subset of emission lines were examined for significant spectral interferences that are peculiar to the uranium tailings and raffinate matrices encountered in this study. Emission spectra of representative composites were obtained. By consulting published lines tables it was possible to identify most of the spectral interferences. The following candidate lines were then used to create analytical task files specific to each matrix type. The task files with minimal interferences are listed in section 4.1.4 .

CANDIDATE EMISSION LINES FOR URANIUM MATRICES

Elem.	Wavelength	Interferences	Elem.	Wavelength	Interferences
Al	3082.15	OH <	Mo	2020.3	Fe >
Al	3092.7	OH <,V >	Mo	2816.15	U p, Al p
Al	3961.52	bg	Na	5895.92	Fe p(low)
As	1890.5	bg	Ni	2216.47	V <,? <,U <
As	1937.6	V p,Fe p,Al <	Ni	2270.21	bg
As	1972.62	bg	Ni	2316.04	bg
Ba	2335.27	V p	Pb	2203.53	Al >,bg
Ba	4554.03	U p	Pd	3634.7	bg,Ar p(bad)
Ca	3179.33	bg	Re	2275.25	Re >
Ca	4226.73	bg	Rh	3434.89	U? <,bg
Cd	2144.38	Al >	S	1807.31	bg
Cd	2265.02	Fe <,Ni <	S	1820.37	U?p
Co	2286.16	bg	Sc	3613.84	bg
Co	2378.62	Al p	Se	1960.9	bg
Cr	2055.52	Fe <	Si	2881.58	bg
Cr	2061.49	? <	Sr	4077.71	U p (weak)
Cr	2677.16	? p	Th	2837.3	U p
Cu	3247.54	bg	Th	3741.2	bg,Fe >
Fe	2599.4	Mg p (low)	Th	4019.1	U? p
K	7664.91		U	3670.07	Fe <
La	3794.78		U	4090.14	V >
La	3988.5	Ca <,U >,Th >	V	3110.7	U ??
Mg	2790.8	U p(low)	Zn	2025.51	Mg >
Mn	2576.1	Fe <,Mg p	Zn	2061.91	bg
Mn	2949.2	U <, Fe <	Zn	2138.56	bg, V <

p = peak near
bg= continuum background
< = low wavelength overlap
> = high wavelength overlap

4.1.3 Task File Index. The following index gives the file names and usage for all matrices encontered in this study. Over the course of this project samples from the investigators varied in major components that could produce spectral interferences. Therefore several task files were tailored to the specific matrix. Thus, emission line selections are not consistent from matrix to matrix. (See the main body of this report for details of line selection and task file creation.

TASK FILE INDEX

MATRIX TYPE	APPLICATION	TASK FILE NAME
Dilute Aqueous	Natural Waters,low TDS (21 elem.)	$GW21
	Natural Waters,low TDS (Majors)	$GW1
	Natural Waters,low TDS (Traces)	$GW2
Uranium Raffinates	High TDS,sulfate,Acid,U,V(Majors)	$UR1
	High TDS,sulfate,Acid,U,V(Traces)	$UR2
	High TDS,sulfate,Acid,U,V(Traces)	$UR4
Tailings Extracts	Aqueous,dilute acid,High TDS(Majors)	XW1
	Aqueous,dilute acid,High TDS(Traces)	XW2
Tailings Leachates	Aqueous,High TDS. (Majors)	$UW1
	Aqueous,High TDS. (Traces)	$UW2
Mine Waters	Aqueous,Interm. TDS. (Traces 1)	$BW1
	Aqueous,Interm. TDS. (Traces 2)	$BW2
	Aqueous,Interm. TDS. (Traces 3)	$BW3
Tailings Solids	Lithium metaborate fusions (Majors)	XT1
	Lithium metaborate fusions (Minors)	XT2

4.1.4 Key to Task File Listings.

KEY TO TASK FILE LISTINGS

WAVELENGTH:	Wavelength in Angstroms
LOW LIMIT:	Determination limit (BEC/10 approx. 2 X Detection limit)
ATTEN:	Attenuator setting;PMT voltage increment (linear: 1=370v to 15=954v)
INTEG:	Integration time per scan step, 0.05625 A/step, 9 step integration
BCOR1: BCOR2:	Background correction points. (steps from emission max. 0.05625 A/step)

LISTING OF ANALYTICAL TASK FILE $GW21

NO.	ELEM	WAVELENGTH	LOW LIMIT	ATTEN	INTEG	BCOR1	BCOR2
1	AL	3961.52	.075	8	.5	0	0
2	B	2497.73	.01	9	.5	0	0
3	BA	4554.03	.002	7	.5	0	0
4	CA	3179.33	.015	8	.5	0	0
5	CD	2144.38	.01	11	.5	0	0
6	CO	2286.16	.0125	10	.5	0	0
7	CR	2055.52	.01	11	.5	0	0
8	CU	3247.54	.01	8	.5	0	0
9	FE	2599.4	.01	9	.5	0	0
10	K	7664.91	.5	12	.5	0	0
11	LI	6707.8	.015	12	.5	0	0
12	MG	2790.8	.25	9	.5	0	0
13	MN	2576.1	.005	8	.5	0	0
14	MO	2020.3	.025	12	.5	0	0
15	NA	5895.92	.1	12	.5	0	0
16	NI	2316.04	.02	10	.5	0	0
17	PB	2203.53	.1	12	.5	0	0
18	SC	3613.84	.005	8	.5	0	0
19	SI	2516.11	.05	8	.5	0	0
20	SR	4077.71	.001	6	.5	0	0
21	V	3110.7	.02	8	.5	0	0
22	ZN	2138.56	.005	10	.5	0	0

LISTING OF ANALYTICAL TASK FILE GW1

NO.	ELEM	WAVELENGTH	LOW LIMIT	ATTEN	INTEG	BCOR1	BCOR2
1	NA	5895.92	.2	10	1	0	0
2	K	7664.91	1	10	1	0	0
3	CA	3179.33	.03	6	1	0	0
4	MG	2790.8	.5	6	1	0	0
5	AL	3961.52	.15	6	1	0	0
6	CO	2378.62	.02	6	1	0	0
7	NI	2316.04	.04	6	1	0	0
8	BA	4554.03	.004	6	1	0	0
9	SR	4077.71	.002	6	1	0	0

LISTING OF ANALYTICAL TASK FILE GW2

NO.	ELEM	WAVELENGTH	LOW LIMIT	ATTEN	INTEG	BCOR1	BCOR2
1	PB	2203.53	.2	8	1	-7	0
2	CD	2144.38	.02	6	1	0	0
3	MN	2576.1	.01	6	1	0	0
4	FE	2599.4	.02	6	1	0	11
5	MG	2795.53	.001	6	1	0	0
6	MO	2816.15	.04	6	1	0	14
7	CR	2055.52	.02	6	1	0	13
8	SI	2516.11	.1	6	1	0	0
9	CU	3247.54	.02	6	1	0	11
10	V	3110.7	.04	6	1	0	11
11	ZN	2138.56	.01	6	1	0	0

LISTING OF ANALYTICAL TASK FILE $UR1

NO.	ELEM	WAVELENGTH	LOW LIMIT	ATTEN	INTEG	BCOR1	BCOR2
1	SE	1960.9	.3	12	1	0	12
2	NI	2316.04	.02	8	1	0	11
3	CO	2286.16	.0125	8	1	-11	0
4	AS	1890.5	.2	12	1	-13	7
5	TH	3741.2	.25	8	1	-16	0
6	CU	3247.54	.01	8	1	-8	0
7	SI	2881.58	.1	8	1	-9	0
8	CA	3179.33	.015	6	1	-14	0
9	S	1807.31	.125	10	1	-11	0
10	SR	4077.71	.001	5	1	-12	12

LISTING OF ANALYTICAL TASK FILE $UR2

NO.	ELEM	WAVELENGTH	LOW LIMIT	ATTEN	INTEG	BCOR1	BCOR2
1	MO	2020.3	.025	9	1	-10	0
2	CR	2055.52	.01	9	1	-10	10
3	ZN	2138.56	.005	8	1	0	0
4	CD	2144.38	.01	8	1	0	0
5	PB	2203.53	.1	10	1	-7	0
6	MN	2576.1	.005	6	1	-10	0
7	FE	2599.4	.01	6	1	-10	0
8	MG	2790.8	.25	7	1	-10	0
9	V	3110.7	.02	5	1	0	0
10	U	3670.07	.37	8	1	-7	0
11	AL	3961.52	.075	5	1	-10	0
12	NA	5895.92	.1	8	1	0	0
13	K	7664.91	.5	11	1	0	0

LISTING OF ANALYTICAL TASK FILE $UR4

NO.	ELEM	WAVELENGTH	LOW LIMIT	ATTEN	INTEG	BCOR1	BCOR2
1	S	1807.31	.125	10	1	0	0
2	AS	1890.5	.2	12	1	-10	0
3	SE	1960.9	.3	12	1	-7	0
4	CO	2286.16	.0125	8	1	-8	0
5	NI	2316.04	.02	8	1	0	12
6	SI	2881.58	.1	8	1	-8	0
7	V	2924.02	.025	6	1	0	0
8	CA	3179.33	.015	6	1	0	0
9	CU	3247.54	.01	8	1	-10	0
10	SR	4077.71	.001	5	1	0	0
11	LI	6707.8	.015	10	1	0	0

LISTING OF ANALYTICAL TASK FILE XW1

NO.	ELEM	WAVELENGTH	LOW LIMIT	ATTEN	INTEG	BCOR1	BCOR2
1	FE	2599.4	.02	8	1	0	0
2	MN	2576.1	.01	6	1	0	0
3	MG	2790.8	.5	8	1	0	0
4	CA	4226.73	.3	6	1	0	0
5	AL	3082.15	.3	8	1	0	0
6	SI	2881.58	.2	8	1	0	0
7	NA	5895.92	.2	12	1	0	0

LISTING OF ANALYTICAL TASK FILE XW2

NO.	ELEM	WAVELENGTH	LOW LIMIT	ATTEN	INTEG	BCOR1	BCOR2
1	CO	2286.16	.025	8	1	0	0
2	CR	2055.52	.02	8	1	0	0
3	SR	4077.71	.002	6	1	0	0
4	V	3110.7	.04	8	1	0	0
5	MO	2816.15	.04	8	1	-7	0
6	BA	4554.03	.004	8	1	0	0
7	AG	3280.68	.02	8	1	0	0
8	NI	2216.47	.04	8	1	0	0

LISTING OF ANALYTICAL TASK FILE $UW1

NO.	ELEM	WAVELENGTH	LOW LIMIT	ATTEN	INTEG	BCOR1	BCOR2
1	CA	3179.33	.015	6	1	0	0
2	MG	2790.8	.25	8	1	0	0
3	NA	5895.92	.1	12	1	0	0
4	FE	2599.4	.01	6	1	0	0
5	AL	3082.15	.15	8	1	0	0
6	SI	2881.58	.1	8	1	0	0
7	BA	4554.03	.002	5	1	0	0
8	SR	4077.71	.001	5	1	0	0

LISTING OF ANALYTICAL TASK FILE $UW2

NO.	ELEM	WAVELENGTH	LOW LIMIT	ATTEN	INTEG	BCOR1	BCOR2
1	MO	2816.15	.02	8	1	0	0
2	CR	2055.52	.01	8	1	0	0
3	CU	3247.54	.01	8	1	0	0
4	MN	2576.1	.005	8	1	0	0
5	V	3110.7	.02	8	1	0	0
6	ZN	2138.56	.005	8	1	0	0
7	CO	2286.16	.0125	8	1	0	0
8	NI	2216.47	.02	8	1	0	0
9	PB	2203.53	.1	10	1	0	0
10	CD	2265.02	.015	8	1	0	0
11	BA	4554.03	.002	5	1	0	0
12	AS	1890.5	.2	12	1	0	0
13	SE	1960.9	.3	12	1	0	0

LISTING OF ANALYTICAL TASK FILE $BW1

NO.	ELEM	WAVELENGTH	LOW LIMIT	ATTEN	INTEG	BCOR1	BCOR2
1	CR	2055.52	.01	9	.5	0	0
2	CO	2286.16	.0125	9	.5	0	0
3	NI	2316.04	.02	9	.5	0	0
4	MN	2576.1	.005	7	.5	0	0
5	FE	2599.4	.01	7	.5	0	0
6	MG	2790.8	.25	9	.5	0	0
7	MO	2816.15	.02	9	.5	-7	0
8	SI	2881.58	.1	9	.5	0	0
9	AL	3082.15	.15	8	.5	0	0
10	V	3110.7	.02	9	.5	0	0
11	CA	3179.33	.015	7	.5	0	0
12	AG	3280.68	.01	9	.5	0	0
13	SR	4077.71	.001	9	.5	0	0
14	BA	4554.03	.002	9	.5	0	0
15	NA	5895.92	.1	8	.5	0	0
16	K	7664.91	.5	12	.5	0	0

LISTING OF ANALYTICAL TASK FILE $BW2

NO.	ELEM	WAVELENGTH	LOW LIMIT	ATTEN	INTEG	BCOR1	BCOR2
1	S	1807.31	.125	12	1	0	0
2	AS	1890.5	.2	12	1	0	0
3	SN	1899.8	.15	12	1	0	0
4	C	1930.91	.5	12	1	0	0
5	HG	1942.27	.05	10	1	0	0
6	SE	1960.9	.3	12	1	0	0
7	ZN	2138.56	.005	8	1	0	0
8	PB	2203.53	.1	10	1	0	0
9	CD	2265.02	.015	8	1	0	0
10	B	2497.73	.01	8	1	0	0
11	CU	3247.54	.01	8	1	0	0
12	U	4090.14	.5	10	1	0	0
13	LI	6707.8	.015	10	1	0	0

LISTING OF ANALYTICAL TASK FILE $BW3

NO.	ELEM	WAVELENGTH	LOW LIMIT	ATTEN	INTEG	BCOR1	BCOR2
1	B	1825.9	.0005	12	1	0	0
2	B	1826.4	.1	12	1	0	0
3	B	2089.59	.02	10	1	0	0
4	B	2496.78	.0125	8	1	0	0
5	B	2497.73	.01	8	1	0	0
6	MO	2020.3	.025	10	1	0	0
7	LA	3988.5	.05	8	1	0	0
8	SC	3613.84	.005	8	1	0	0
9	CD	2144.38	.01	10	1	0	0
10	TH	4019.1	.02	8	1	0	0
11	TI	3361.21	.01	8	1	0	0
12	U	3670.07	.37	8	1	0	0
13	V	2924.02	.025	8	1	0	0
14	CE	4137.65	.15	10	1	0	0

LISTING OF ANALYTICAL TASK FILE XT1

NO.	ELEM	WAVELENGTH	LOW LIMIT	ATTEN	INTEG	BCOR1	BCOR2
1	FE	2599.4	.02	6	1	0	0
2	MN	2576.1	.01	6	1	0	0
3	CU	3247.54	.02	6	1	0	0
4	CR	2055.52	.02	8	1	0	0
5	MO	2816.15	.04	6	1	-6	5
6	AL	3082.15	.3	6	1	0	0
7	SI	2881.58	.2	6	1	0	0
8	V	2924.02	.05	6	1	0	0
9	U	4090.14	1	6	1	0	0

LISTING OF ANALYTICAL TASK FILE XT2

NO.	ELEM	WAVELENGTH	LOW LIMIT	ATTEN	INTEG	BCOR1	BCOR2
1	CA	4226.73	.3	4	1	0	0
2	MG	2790.8	.5	6	1	0	0
3	NA	5895.92	.2	10	1	0	0
4	K	7664.91	1	10	1	0	0
5	CD	2265.02	.03	6	1	0	0
6	BA	4554.03	.004	6	1	0	0

4.1.5 **Calibration Standards.** Multielement calibration standards are used to calibrate the instrument for concentration dependence of the intensity response. Calibration is performed only in each element's linear response range of the instrument or for the anticipated concentration range for the samples. Several calibration solutions are required for each task file since not all elements in a task file can be combined in a single calibration standard that is chemically stable.

STANDARDS USED FOR SPECTROSCOPIC CALIBRATION

ELEM.	CONC. mg/L	PREPARATION	PURITY/ SOURCE
Al	1000	Weigh out 1.000g of Al powder and place it in a 250mL beaker. Wet powder with a few mL DDI water. Slowly add 10 mL high purity HCl. (Have a cold water bath available to moderate the reaction.) Add two more 10 mL portions of HCl heating slightly if necessary. Dilute to 1.00 L with DDI water.	99.999*
Ag	1000	Weigh out 1.574g $AgNO_3$ and transfer to a 1.00L vol. flask. Dissolve in 50mL DDI water. Dilute to mark with 1v% HNO_3. Store in OPAQUE bottle.	RG
As	1000	Weigh out 1.5346g of As_2O_3 and place it in 250mL beaker. Add 20mL DDI water and 10mL high purity conc. HCl. After reaction subsides heat gently until dissolved. Dilute to 1.00 L with DDI water.	99.999#
B	1000	Weigh out 5.720g of H_3BO_3 and transfer to a 1.00 L vol. flask. Dissolve salt in 500mL DDI water. Dilute to 1.00L with DDI water.	99.999#
Ba	1000	Weigh 1.516g $BaCl_2$ and transfer to a 1.00L vol. flask. Dissolve salt and dilute to 1.00L with DDI water.	99.999#
Ca	10000	Weigh out 24.973g $CaCO_3$ and place in a 250mL beaker. Add about 100mL DDI water and gently swirl. Slowly add 40mL high purity conc. HNO_3. When dissolved transfer to a 1.00L vol. flask and dilute to mark with DDI water.	99.999*
Cd	1000	Weigh out 1.000g of Cd metal and place in a 150mL beaker. Add 20mL 1:1 aqueous HCl. Heat gently until dissolved. Transfer to a 1.00L vol. flask and dilute to mark with 1v% HCL.	99.9999#
Cu	1000	Weigh out 1.000g of Cu metal and place in a 150mL beaker. Add 10mL 1:1 HNO_3. Dissolve and transfer to a 1.00L vol. flask. Dilute to mark with 1v% HNO_3.	99.9999*
Co	1000	Weigh out 1.000g of Co metal and place in a 150mL beaker. Add 20mL 1:1 aqueous HCl. Heat gently until dissolved. Transfer to a 1.00L vol. flask and dilute to mark with 1v% HCL.	99.99#

All acids are high purity. DDI = distilled-deionized

* Aldrich Chemical Company,Inc. P.O. Box 355 Milwaukee, WI 53201

\# Spex Industries,Inc. Box 798, Metuchen, NJ 08840

ELEM.	CONC. mg/L	PREPARATION	PURITY/ SOURCE
Cr	1000	Weigh out 1.000g Cr metal and place in a 150mL beaker. Add 10mL conc. HCl and heat gently until dissolved. Transfer to a 1.00L vol. flask and dilute to mark with DDI water.	99.99#
Fe	1000	Weigh out 1.000g of Fe metal and place in a 250mL beaker. Add 50mL 1:1 HNO_3. Dissolve and transfer to a 1.00L vol. flask. Dilute to mark with DDI water.	99.999#
Hg	1000	Transfer 1.3535g HgCl2 to a 1.00L vol. flask and add 600mL DDI water. Dissolve salt and add 5.0mL conc. HNO_3. Dilute to mark with DDI water.	99.9999#
K	10000	Weigh 19.07g KCl and transfer to a 1.00L vol. flask. Dissolve salt in 500mL DDI water. Dilute to mark with DDI water.	99.999#
La	50000	Moisten 58.64g of La_2O_3 with 50mL of DDI water. Cautiously add 250mL conc. HCl. (Have a cold water bath ready to moderate the reaction.) When dissolved, dilute to 1.00L with DDI water.	99.99*
Li	1000	Transfer 6.108g of LiCl to a 1.00L vol. flask. Dissolve salt in 500mL DDI water. Dilute to mark with DDI water.	99.99*
Mg	1000	Weigh out 1.000g Mg metal and transfer to a 250mL beaker. Add sufficient 1:1 HCl to dissolve metal. Transfer to a 1.00L vol. flask and dilute to mark with DDI water.	RG
Mo	1000	Weigh 1.5003g MoO_3 and transfer to a 1.00L vol. flask. Moisten with a few mL DDI water. Add 20mL conc. ammonium hydroxide. Add 1 drop 1% phenolphthalein. Swirl to dissolve salt. Add conc. HNO_3 until color disappears (about 6 mL). Add 5mL excess HNO_3 and dilute to mark with DDI water.	99.999#
Mn	1000	Weigh out 1.000g Mn metal and transfer to a 250mL beaker. Add sufficient 1:1 HNO_3 to dissolve metal. Transfer to a 1.00L vol. flask and dilute to mark with 1v% HNO_3.	99.99#
Na	10000	Transfer 25.423g NaCl to a 1.00L vol. flask. Add 500ml of DDI water and swirl to dissolve salt. Dilute to the mark with DDI water.	99.999#

All acids are high purity. DDI = distilled-deionized

* Aldrich Chemical Company,Inc. P.O. Box 355 Milwaukee, WI 53201

\# Spex Industries,Inc. Box 798, Metuchen, NJ 08840

ELEM.	CONC. mg/L	PREPARATION	PURITY/ SOURCE
Pb	1000	Weigh out 1.000g Pb metal and transfer to a 250mL beaker. Add sufficient 1:1 HNO_3 to dissolve metal. Transfer to a 1.00L vol. flask and dilute to mark with 1v% HNO_3.	99.999#
Pd	1000	Weigh out 1.000g Pd metal and transfer to a 250mL beaker. Add sufficient aqua regia (1 HNO_3:3 HCl) and evaporate to near dryness. Add 5mL conc. HCl and 25mL DDI water and warm until solution is complete. Transfer to a 1.00L vol. flask and Dilute to the mark with DDI water.	99.999#
Re	1000	Weigh out 1.000g Re metal and transfer to a 250mL beaker. Add 20mL 1:1 HNO_3 to dissolve metal. (Have a cold water bath ready to moderate the Rxn.) Transfer to a 1.00L vol. flask and dilute to mark with DDI water.	99.99#
Sc	1000	Transfer 1.533g of Sc_2O_3 to a 150mL beaker. Add 10mL conc. HCL and heat gently to dissovle salt. Transfer to a 1.00L vol. flask and dilute to mark with DDI water.	99.999#
Se	1000	Transfer 1.000g Se metal to a 150mL beaker and add a sufficient volume of conc. HNO_3 to dissolve. Transfer to a 1.00L vol. flask and dilute to the mark with DDI water.	99.9999#
Si	1000	Weigh 6.342g of $(NH_4)_2SiF_6$ into a 1.00L PLASTIC vol. flask. Add 500mL DDI water and swirl to dissolve salt. Dilute to mark with DDI water.	99.9999#
Ti	1000	Transfer 1.000g of Ti metal to a 250mL beaker. Add 100mL 1:1 conc. HCl. Heat gently for 2 hrs. After dissolution, cool and transfer to a 1.00L vol. flask. Maintain 5% HCl concn. and dilute to volume.	99.9#
Zn	1000	Weigh out 1.000g Zn metal and transfer to a 250mL beaker. Add sufficient 1:1 HCl to dissolve metal. Transfer to a 1.00L vol. flask and dilute to mark with 1v% HCl.	99.9999#
Ni	1000	Weigh out 1.000g Ni metal and transfer to a 250mL beaker. Add sufficient 1:1 HNO_3 to dissolve metal. Transfer to a 1.00L vol. flask and dilute to mark with 1v% HNO_3.	99.99*

All acids are high purity. DDI = distilled-deionized

* Aldrich Chemical Company,Inc. P.O. Box 355 Milwaukee, WI 53201

\# Spex Industries,Inc. Box 798, Metuchen, NJ 08840

4.2 ION CHROMATOGRAPHY of Uranium Related Aqueous Samples

Ion chromatography was used to analyze several uranium related sample types; mine waters, tailings leachates, aqueous tailings extracts, raffinates and natural waters. Fluoride, chloride, nitrate and sulfate were determined by the following procedures. Note that nitric acid acidification of some aqueous samples (for preservation) and high sulfuric acid content of some process related samples (raffinates) precluded determination of bromide and phosphate.

INSTRUMENT:

Dionex Model 12-S Ion Chromatograph.
Hewlett-Packard 3385 Automation System.

STANDARD CONDITIONS:

Since many of the uranium related samples contained high anion concentrations, the following procedures use long (>500 mm), high capacity separation columns (Dionex S1) and fast eluent flow rates.

Columns: 3X500 mm Normal Anion Separator (Dionex 30170)
3X50 mm Normal Anion Precolumn (Dionex 30008)
Normal Anion Suppressor (Dionex 30828)

Eluent: 0.003M $NaHCO_3$ / 0.0024 M Na_2CO_3
Flow: 207 mL/hr. (pump rate 45%)
Injection loop: 0.100 mL
Suppressor Regenerant: 0.5 M H_2SO_4
Regenerant Flow: 207 mL/hr. (pump rate 45%)
Detector: Conductivity, typical settings 30,100,300 uMHOS/cm.

REAGENTS:

Eluent: 0.003 M $NaHCO_3$/0.0024 M Na_2CO_3

Transfer 12.6g of sodium hydrogen carbonate, $NaHCO_3$, and 12.72g of sodium carbonate, Na_2CO_3, to a 1.00L volumetric flask. Add 500mL of distilled-deionized water and swirl until the salt is dissolved. Dilute to volume, q.s., and filter through a 0.45 micrometer membrane filter. Store the sloution at 3 degrees C to prevent biological activity. Make a 0.003 M $NaHCO_3$/0.0024 Na_2CO_3 by diluting 80mL of the stock solution to 4.0L with distilled-deionized water.

To matrix match samples with eluent, add 0.10mL of stock solution to 5.0mL of samples and standards.

Regeneration Solution:

Cautiously add 111mL of concentrated H_2SO_4 to approximately 2L of distilled-deionized water and mix. Dilute to 4.0L, q.s.

4.2.1 Determination of Fluoride by IC.

STANDARDS:

Stock Standard: 1000 mg/L

Transfer 2.2100g of sodium fluoride, NaF, to a 1.00L volumetric flask. Add approximately 300mL of DDI (distilled-deionized) water and swirl until the salt is dissolved. Dilute to volume, q.s., with DDI water and store in a plastic container.

Prepare a 100mg/L standard by pipetting 25.00mL stock standard into a 250.0mL volumetric flask and dilute to volume with DDI water. STORE ALL STANDARDS IN PLASTIC CONTAINERS.

Prepare working standards with the following concentrations: 0.00, 0.50, 1.00, 3.00, 5.00, 10.0, 25.0 mg/L.

REAGENTS:

Eluent: 0.003 M $NaHCO_3$/0.0024 M Na_2CO_3 (See STANDARD CONDITIONS)
Regenerant: 0.5 M H_2SO_4 (See STANDARD CONDITIONS)

INTERFERENCES:

When using the standard conditions, any species that elutes in the void volume will interfere with the determination of fluoride. Co-eluting species include; organic acids, acetate, alcohols, ketones, iodate, some organic phosphonates.

N.B.: Extreme caution should be exercised in determining fluoride in complex matrices. The difficult problem of co-eluting species, particularily organic acids, renders unreliable results.

4.2.2 **Determination of Chloride by IC.**

STANDARDS:

Stock Standard: 1000 mg/L

Transfer 1.6485g of predried (104 degrees C) sodium chloride, NaCl, to a 1.00L volumetric flask. Add approximately 300mL of DDI (distilled-deionized) water and swirl until the salt is dissolved. Dilute to volume, q.s., with DDI water.

Prepare a 100mg/L standard by pipetting 25.00mL stock standard into a 250.0mL volumetric flask and dilute to volume with DDI water.

Prepare working standards with the following concentrations: 0.00, 1.00, 3.00, 5.00, 10.0, 50.0, 100 mg/L.

REAGENTS:

Eluent: 0.003 M $NaHCO_3$/0.0024 M Na_2CO_3 (See STANDARD CONDITIONS)
Regenerant: 0.5 M H_2SO_4 (See STANDARD CONDITIONS)

INTERFERENCES:

High concentrations of hypochlorite, carbonate, sulfide and nitrate interfere with the determination of chloride. Formate and other organic acids may also interfere. The principal difficulty encountered in chloride quantification is that the analyte may co-elute with the "carbonate/water dip". This produces severe variations in the analyte peak height and peak area of low concentration samples. This difficulty is more pronounced in acidic samples or samples that contain alcohols.

4.2.3 **Determination of Nitrate by IC.**

STANDARDS:

Stock Standard: 1000 mg/L

Transfer 1.3707g of anhydrous sodium nitrate, $NaNO_3$, to a 1.00L volumetric flask. Add approximately 300mL of DDI (distilled-deionized) water and swirl until the salt is dissolved. Dilute to volume, q.s., with DDI water.

Prepare a 100mg/L standard by pipetting 25.00mL stock standard into a 250.0mL volumetric flask and dilute to volume with DDI water.

Prepare working standards with the following concentrations: 0.00, 1.00, 3.00, 5.00, 10.0, 50.0, 100 mg/L.

REAGENTS:

Eluent: 0.003 M $NaHCO_3$/0.0024 M Na_2CO_3 (See STANDARD CONDITIONS)
Regenerant: 0.5 M H_2SO_4 (See STANDARD CONDITIONS)

INTERFERENCES:

High bromide concentrations will present a broad peak that interferes with nitrate determinations. Large sulfate peaks may "shift" sufficiently to interfere with nitrate peak quantification. Additonal interferences from chlorate, sulfite,and some organic acids have been observed.

4.2.4 Determination of Sulfate by IC.

STANDARDS:

Stock Standard: 1000 mg/L

Transfer 1.8142g of predried (104 degrees C) potassium sulfate, K_2SO_4, to a 1.00L volumetric flask. Add approximately 300mL of DDI (distilled-deionized) water and swirl until the salt is dissolved. Dilute to volume, q.s., with DDI water.

Prepare a 100mg/L standard by pipetting 25.00mL stock standard into a 250.0mL volumetric flask and dilute to volume with DDI water.

Prepare working standards with the following concentrations: 1.00,10.0,50.0, 150, 500, 1000 mg/L.

REAGENTS:

Eluent: 0.003 M $NaHCO_3$/0.0024 M Na_2CO_3 (See STANDARD CONDITIONS)
Regenerant: 0.5 M H_2SO_4 (See STANDARD CONDITIONS)

INTERFERENCES:

Oxalate and bisulfate may interfere with sulfate determinations.

4.3 ION SELECTIVE ELECTRODE Determination of Ammonium Ion

PROCEDURE:

Transfer approximately 5 mL of calibration standard or sample to a 7 mL capacity polystyrene cup (Microbeaker). Place a 3X10 mm. teflon coated stirring bar in the beaker. Place a weer paper towel, as a thermal balast, on a magnetic stirrer. Place the sample on the stirrer and adjust the stirring rate to give adequate mixing.

Position the ammonia electrode in the solution.

Add decomplexing agent in aliquots of approximately 0.06 mL until the pH tests greater than 10, as indicated by pH paper.

Turn pH meter (millivoltmeter) "on" and wait for a stable reading. Record the stable millivolt reading. Return the meter to "standby" and remove the sample.

Rinse the electrode with sufficient deionized water to prevent cross-contamination between sample readings.

Proceed to the next sample or calibration standard and repeat steps as described above.

CALIBRATION:

Plot a calibration curve using semi-log graph paper. (Ammonium concentrations should be plotted on the log axis and the millivolt readings on the linear axis.) The slope should be within 10% of 59 millivolts/log unit. Read sample concentrations directly from the plotted curve.

STANDARDS:

Prepare a stock standard containing 1000 mg/L ammonium ion by weighing 2.965g ammonium chloride and transfering to a 1.00 L volumetric flask. Add 500 mL deionized water and swirl until the salt is completely dissolved. Dilute to the mark with deionized water.

Working standards are prepared to span the optimum calibration range between 10 and 300 mg/L. (2.00, 3.00, 5.00, 10.0, 20.0, 60.0, 100, 200, 300, 500 mg/L)

INSTRUMENT:

Corning Model 130 Digital pH Meter

Electrode; Ammonia Sensor, Altex 531254

4.4 COLORIMETRIC METHODS

Colorimetric (spectrophotometric) methods were used for a variety of chemical species. While not the primary methods of analysis, they were used to provide an independent check of other analytical procedures. The complexity of uranium related matrices can render some of the procedures unreliable, as indicated in the main body of this report. The following procedures are given with the implicit understanding that they are subject to restricted use on complex matrices.

4.4.1 **Determination** of Chloride by Colorimetric Method.

INSTRUMENT:

Sargent-Welch Model SD
Phototube: Blue Sensitive
Wavelength: 480 nm.

STANDARDS:

Stock Standard: 1000 mg/L

Transfer 1.6485g of sodium Chloride, NaCl, to a 1.00 L volumetric flask. Add approximately 300 mL of DDI (distilled-deionized) water and swirl until the salt is dissolved. Dilute to volume, q.s., with DDI water.

Prepare a 100 mg/L standard by pipetting 25.00 mL of stock standard into a 250.0 mL volumetric flask and dilute to volume, q.s., with DDI water.

Prepare working standards with the following concentrations: 0.00, 5.00, 10.0, 20.0, 50.0, 100, 250 mg/L.

REAGENTS:

Prepare a saturated mercuric thiocyanate, $Hg(SCN)_2$, solution by dissolving 5.0g of reagent grade $Hg(SCN)_2$ in 1.0 L of DDI water. (Weights and volumes need not be determined accurately because a saturated solution is all that is necessary.) Decant and filter a portion of this solution sufficient for use with all samples and calibration standards (about 0.6 mL per sample).

Prepare a ferric ammonium sulfate solution by dissolving 60g of $FeNH_4(SO_4)_2 * 12H_2O$ in approximately 500 mL DDI water. Cautiously add 355 mL of concentrated nitric acid. Mix thoroughly and dilute to 1.0 L with DDI water, filter and store.

PROCEDURE:

Transfer 1.00 mL of standards and samples to a 20 mL test tube and add 4.0 mL of DDI water to each tube.

Add 1.6 mL of the ferric iron / acid solution and stir.

Add 0.6 mL of the saturated mercuric thiocyanate solution and stir. Allow reaction to proceed for 15 minutes.

Read the absorbance of the standards and samples against a blank at 480 nm. Prepare an absorbance versus concentration calibration curve. Obtain the sample concentrations from the plotted curve or a

linear regression computation.

REFERENCE:

"EPA Methods for Chemical Analysis of Water and Wastes."; EPA-600/4-79-020. March, 1979. Chloride method 325.1 (Colorimetric, Automated Ferricyanide AA I)

4.5 AUTOMATED COLORIMETRIC METHOD

4.5.1 **Determination of Sulfate by Methylthymol Blue.**

SAMPLE PREPARATION:

Aliquot 3.0 mL each of calibration standards and samples into 4 mL polystyrene autosampler cups. Add approximately 0.05g BIOREX 70 cation exchange resin (20-50 mesh). Place plastic caps on the cups and agitate the samples for 30 seconds each. Remove caps and place the samples in the Technicon autosampler tray.

LINEARIZATION by MEASUREMENT:

Because the methylthymol blue (MTB) dye varies in purity, experimental adjustment of quantity is required. The following paper describes a prcedure to improve the performance and reliability of the method.

Colouos, George, Panesar, Martha R and Perry, Edward P.; "Linearizing the Calibration Curve in Determination of Sulfate by the Methylthymol Blue Method."; Anal. Chem. 48: (1976)pp.1693-1696.

PROCEDURE:

Follow the precedure described in the Technicon Manual and the linearization procedure referenced above.

REFERENCE:

"Sulfate in Water and Wastewater"; Industrial Method No. 118-71W/Preliminary.

4.6 ATOMIC ABSORPTION METHODS

4.6.1 Determination of Arsenic by Furnace AAS.

SPECTROPHOTOMETER CONDITIONS:

Instrument: Perkin-Elmer Model 5000 AAS
Slit : 0.7 nm. High
Lamp : As Electrodeless Discharge Lamp.... 8 watts
Wavelength: 193.7 nm
Mode : AA-BG (background subtraction)
: Absorbance
: Peak height 5 sec.

GRAPHITE FURNACE CONDITIONS:

Instrument: Perkin-Elmer Model 500 HGA
: Autosampler AS-40
: 20 uL sample with 20 uL 1% Ni

Program Step	1	2	3	4	5
Temperature (C)	110	1000	2700		
Ramp Time (sec.)	15	15	0		
Hold Time (sec.)	20	15	8		
Read Time (sec.)			-2		
Ar Flow (mL/min)	300	300	30		

REAGENTS:

Prepare a 1.0% Ni solution by weighing 5.0g Ni metal and place in a 250mL beaker. Add 20mL of concentrated nitric acid and heat gently until metal dissolves. Dilute to 500mL with distilled deionized water.

STANDARDS:

Low Range: 0.00, 10.0, 30.0, 50.0, ug/L
High Range: 0.00, 100, 200, 300 ug/L

4.6.2 **Determination of Selenium by Furnace AAS.**

SPECTROPHOTOMETER CONDITIONS:

Instrument: Perkin-Elmer Model 5000 AAS
Slit : 0.7 nm. High
Lamp : Se Electrodeless Discharge Lamp.... 6 watts
Wavelength: 196.0 nm.
Mode : AA-BG (background subtraction)
: Absorbance
: Peak height 5 sec.

GRAPHITE FURNACE CONDITIONS:

Instrument: Perkin-Elmer Model 500 HGA
: Autosampler AS-40
: 20 uL sample with 20 uL 1% Ni

Program Step	1	2	3	4	5
Temperature (C)	110	1000	2700		
Ramp Time (sec.)	15	15	0		
Hold Time (sec.)	20	15	8		
Read Time (sec.)			-2		
Ar Flow (mL/min)	300	300	30		

REAGENTS:

Prepare a 1.0% Ni solution by weighing 5.0g Ni metal and place in a 250mL beaker. Add 20mL of concentrated nitric acid and heat gently until metal dissolves. Dilute to 500mL with distilled deionized water.

STANDARDS:

Low Range: 0.00, 10.0, 30.0, 50.0, ug/L
High Range: 0.00, 100, 200, 300 ug/L

4.6.3 **Determination of Lead by Furnace AAS.**

SPECTROPHOTOMETER CONDITIONS:

Instrument: Perkin-Elmer Model 5000 AAS
Slit : 0.7 nm. Low
Lamp : Pb Hollow Cathode Lamp.... 8 ma.
Wavelength: 217.0 nm.
Mode : AA-BG (background subtraction)
: Absorbance
: Peak height 2 sec.

GRAPHITE FURNACE CONDITIONS:

Instrument: Perkin-Elmer Model 500 HGA
: Autosampler AS-40
: 20 uL sample

Program Step	1	2	3	4	5
Temperature (C)	110	600	2300	2500	30
Ramp Time (sec.)	10	15	1	0	1
Hold Time (sec.)	15	10	2	2	2
Read Time (sec.)			0		
Baseline Time(sec.)			-3		
Ar Flow (mL/min)	300	300	30		

STANDARDS:

Low Range: 0.00, 5.00, 10.0, 25.0, 50.0, ug/L
High Range: 0.00, 100, 200, 300 ug/L

4.6.4 **Determination of Cadmium by Furnace AAS.**

SPECTROPHOTOMETER CONDITIONS:

Instrument: Perkin-Elmer Model 5000 AAS
Slit : 0.7 nm. Low
Lamp : Cd Hollow Cathode Lamp.... 6 ma.
Wavelength: 228.8 nm.
Mode : AA-BG (background subtraction)
: Absorbance
: Peak height 3 sec.

GRAPHITE FURNACE CONDITIONS:

Instrument: Perkin-Elmer Model 500 HGA
: Autosampler AS-40
: 10 uL sample

Program Step	1	2	3	4	5
Temperature (C)	110	450	2100	2300	30
Ramp Time (sec.)	10	15	1	0	1
Hold Time (sec.)	15	10	3	3	2
Read Time (sec.)			0		
Baseline Time(sec.)			-3		
Ar Flow (mL/min)	300	300	100		

STANDARDS:

Low Range: 0.00, 1.00, 2.00, 5.00, 10.0, 20.0 ug/L
High Range:

4.6.5 **Determination of Chromium by Furnace AAS.**

SPECTROPHOTOMETER CONDITIONS:

Instrument: Perkin-Elmer Model 5000 AAS
Slit : 0.7 nm. High
Lamp : Cr Hollow Cathode Lamp.... 10 ma.
Wavelength: 357.9 nm.
Mode : AA-BG (background subtraction)
: Absorbance
: Peak height 2 sec.

GRAPHITE FURNACE CONDITIONS:

Instrument: Perkin-Elmer Model 500 HGA
: Autosampler AS-40
: 20 uL sample

Program Step	1	2	3	4	5
Temperature (C)	110	1000	2700	2800	
Ramp Time (sec.)	15	10	1	1	
Hold Time (sec.)	20	15	2	1	
Read Time (sec.)			0		
Baseline Time(sec.)					
Ar Flow (mL/min)	300	300	100	300	

STANDARDS:

Low Range: 0.00, 5.00, 10.0, 100.0, ug/L
High Range: 0.00, 100, 200, 300 ug/L

4.6.4 Determination of Cadmium by Furnace AAS.

SPECTROPHOTOMETER CONDITIONS:

Instrument: Perkin-Elmer Model 5000 AAS
Slit : 0.7 nm. Low
Lamp : Cd Hollow Cathode Lamp.... 6 ma.
Wavelength: 228.8 nm.
Mode : AA-BG (background subtraction)
: Absorbance
: Peak height 3 sec.

GRAPHITE FURNACE CONDITIONS:

Instrument: Perkin-Elmer Model 500 HGA
: Autosampler AS-40
: 10 uL sample

Program Step	1	2	3	4	5
Temperature (C)	110	450	2100	2300	30
Ramp Time (sec.)	10	15	1	0	1
Hold Time (sec.)	15	10	3	3	2
Read Time (sec.)			0		
Baseline Time(sec.)			-3		
Ar Flow (mL/min)	300	300	100		

STANDARDS:

Low Range: 0.00, 1.00, 2.00, 5.00, 10.0, 20.0 ug/L
High Range:

5. QUALITY CONTROL DIAGNOSTICS

5.1 Patterns in the Quality Control Plots

5.1.1 **Patterns in the Systematic Error.** The simulated data shown in these plots illustrate the basic patterns in the systematic error that have been observed in actual laboratory situations. The magnitude of the effects have been exagerated so that the essential features of the interpretation may be illustrated.

NONE - No systematic error is present. The only error contribution is the result of random deviations in the results obtained for the two quality control samples, A and B.

FREAKS - Systematic error is present, but it does not follow a simple functional relationship with time. This case is simulated by the occurence of a large systematic error component (greater than three standard deviations from the mean) which appears without warning.

SHIFT - The systematic error contribution obeys a step function. The absence of any systematic bias during the early time period is followed by a sudden appearance of a large constant sytematic error (either positive or negative).

TREND - The systematic error contribution increases or decreases monotonically with increasing time.

PLATEAU - The systematic error contribution increases or decreases rapidly with time, but finally levels off to a constant value. This behavior is similar to, but less precipitous than, the step function exhibited by the SHIFT.

CYCLE - The magnitude of the systematic error contribution changes continuously with time, but it follows a definite cyclic pattern that repeats itself periodically. (This case is simulated here as a sine wave.)

BUNCHING - The sytematic error contribution undergoes several successive "quantized" magnitude changes. It is similar to several successive SHIFTs.

5.1.2 Example Q.C. Plots. The example plots generated from the hypothetical data illustrate the systematic error patterns described above. These hypothetical data were computer generated such that the "true" value of A and B should be 100 units. The random error contribution was generated such that each simulated measurement was taken from a normally distributed error population with a standard deviation of 5 units. Additional combinations of patterns (28) in both systematic and random error components are not shown here.

COMMENTARY on FIGURE 5.1 (NONE)

Q Plot:

The shape of the distribution is circular with lines of equal lengths at random angles. There is an equal distribution of points among the four quadrants. (Normally distributed; dense in the center, sparse in the outer region.) No systematic error is detected.

T Plot:

Spurious high and low points corresponding to small errors in the D plot suggest possible systematic errors. However, this is also consistent with normally distributed errors.

D Plot:

Normally distributed random errors are shown with no apparent trend.

Total	RSD = 5.1 %
Random	RSD = 4.8 %
Systematic	RSD = 1.5 %

QUALITY CONTROL PLOTS

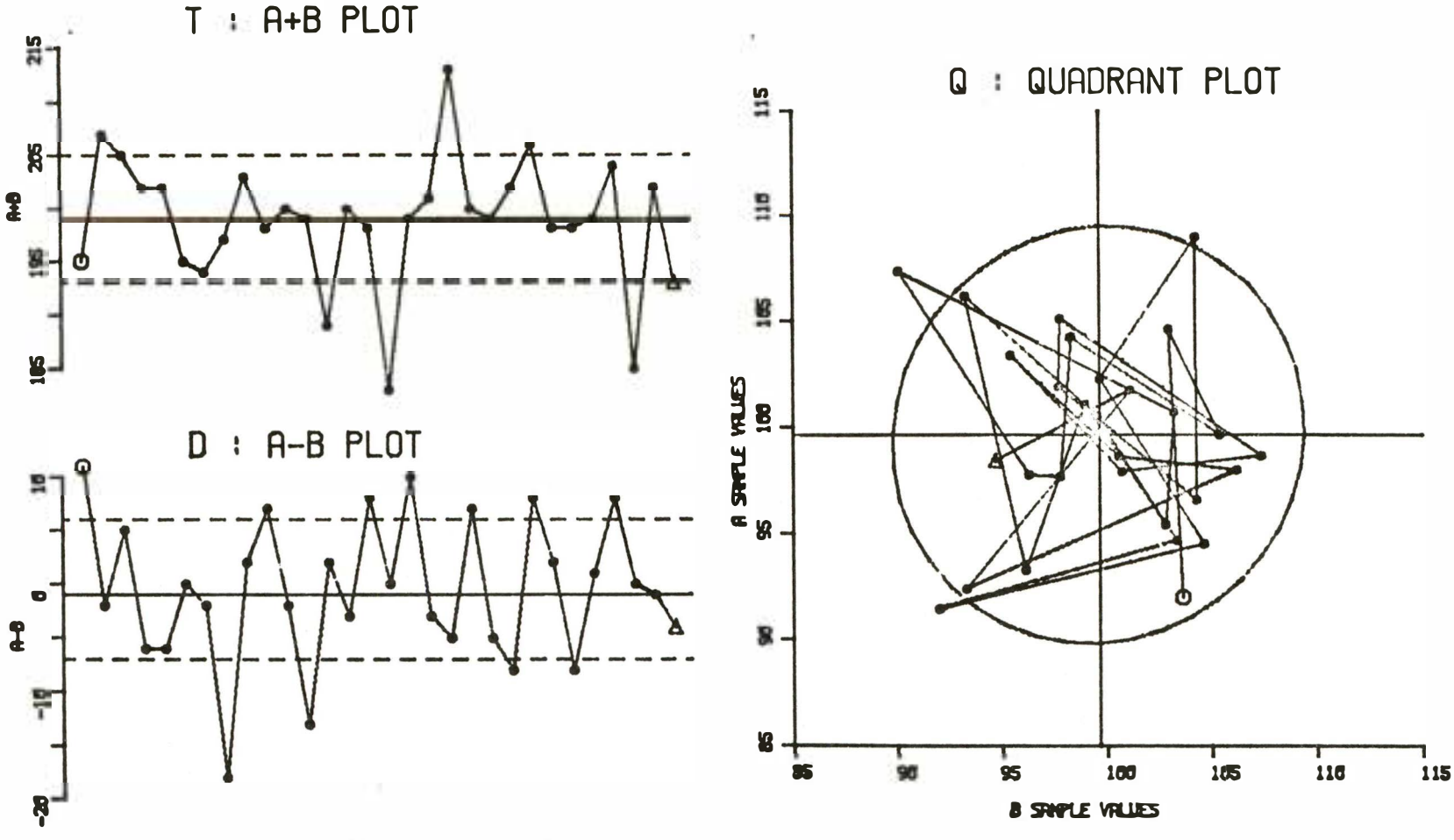

Figure 5.1

SYSTEMATIC ERROR PATTERN : NONE
RANDOM ERROR PATTERN : NONE

COMMENTARY on FIGURE 5.2 (FREAKS)

Q Plot:

An elliptical distribution indicates that systematic error is detected. Long line segments at 45 degrees deviate from an otherwise random direction and equal placement among the four quadrants. Anomalous points are well outside of the ellipse in the systematic error quadrants. The points are otherwise normally distributed.

T Plot:

No systematic pattern appears. Only spurious high and low points are seen.

D Plot:

An absence of large random error contribution corresponding to anomalous points in the T plot shows that they are in the systematic error domain. (This is more readily seen in the Q plot.)

Total RSD = 6.7 %
Random RSD = 3.9 %
Systematic RSD = 5.5 %

QUALITY CONTROL PLOTS

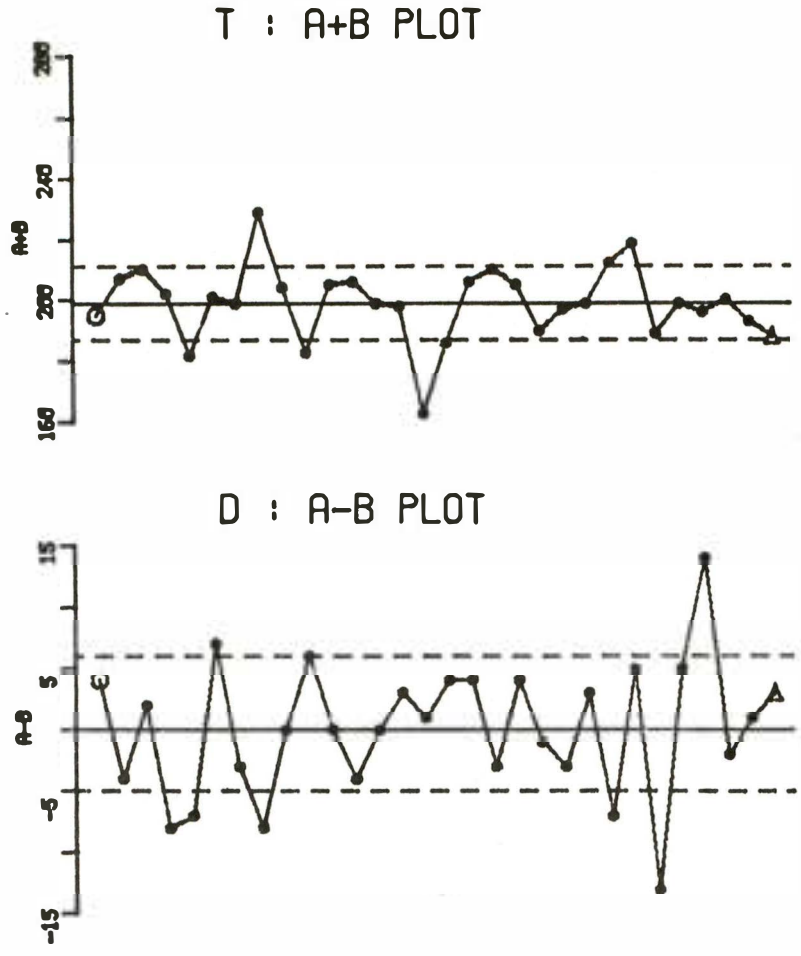

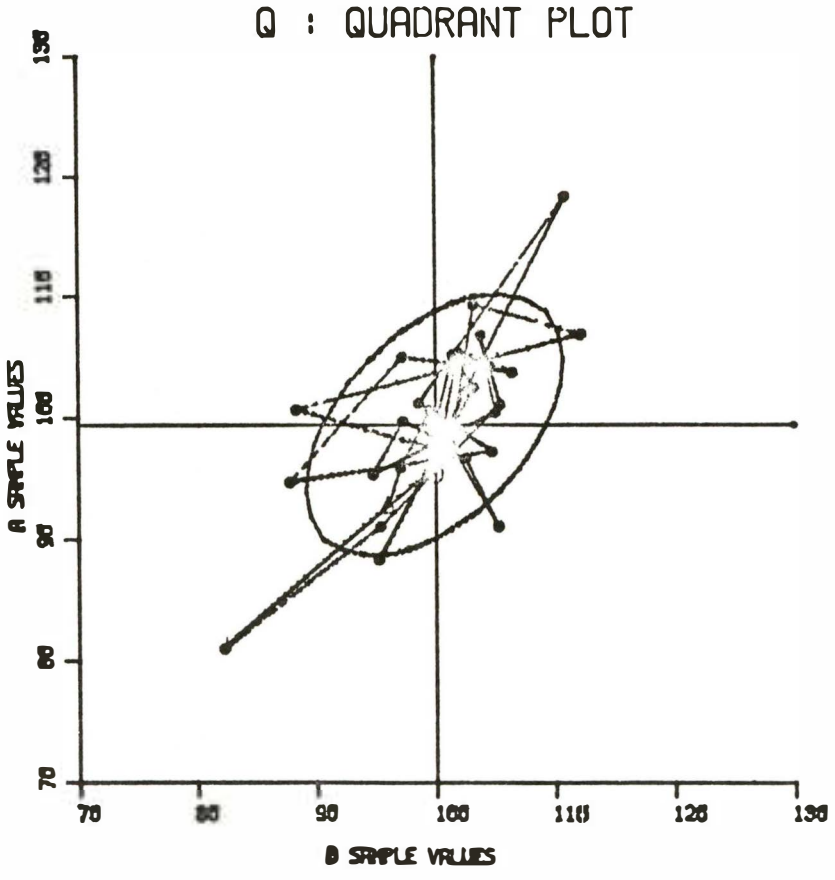

Figure 5.2

SYSTEMATIC ERROR PATTERN : FREAKS
RANDOM ERROR PATTERN : NONE

COMMENTARY on FIGURE 5.3 (SHIFT)

Q Plot:

The elliptically shaped distribution shows that systematic errors are detected. Two distributions are seen; each characterized by randomly directed short line segments. One long line segment at 45 degrees between systematic error quadrants signals the sudden systematic shift.

T Plot:

Points form a step function with a sudden increase (or decrease).

D Plot:

No apparent pattern appears, and the points are normally distributed about zero.

Total RSD = 8.4 %
Random RSD = 4.6 %
Systematic RSD = 7.1 %

QUALITY CONTROL PLOTS

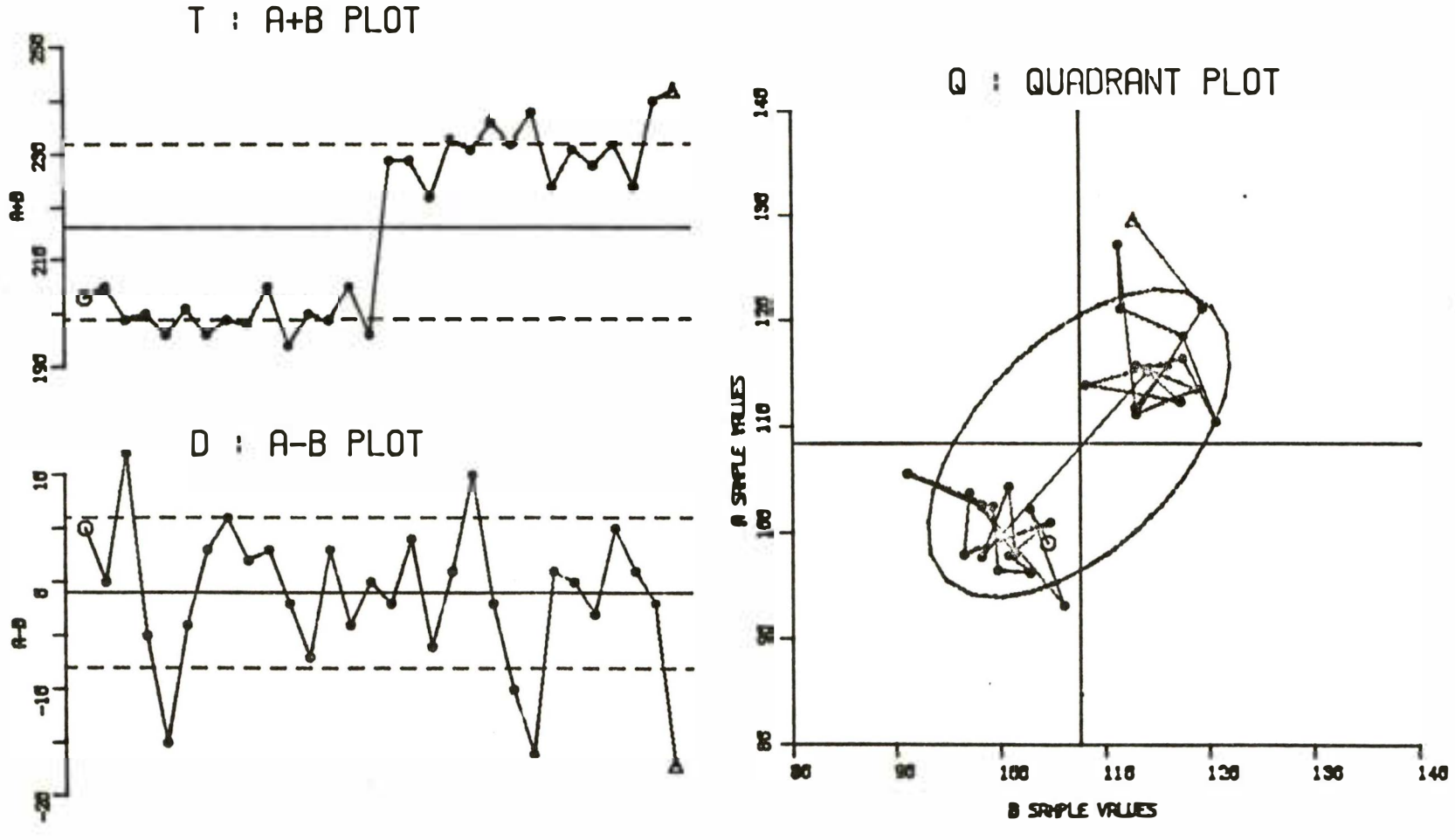

Figure 5.3

SYSTEMATIC ERROR PATTERN : SHIFT
RANDOM ERROR PATTERN : NONE

COMMENTARY on FIGURE 5.4 (TREND)

Q Plot:

An elliptical distribution indicates that systematic errors are present. Short line segments connect the points. They move monotonically from one systematic error quadrant to the other. There is an insufficient density of points in the middle of the ellipse and in the random error quadrants for this to be a normal distribution of errors.

T Plot:

The time sequence of points have non-zero slope, i.e. the absolute value of T changes with increasing time.

D Plot:

Points and normally distributed about zero, no pattern appears.

Total	RSD = 12.2 %
Random	RSD = 3.5 %
Systematic	RSD = 11.7 %

QUALITY CONTROL PLOTS

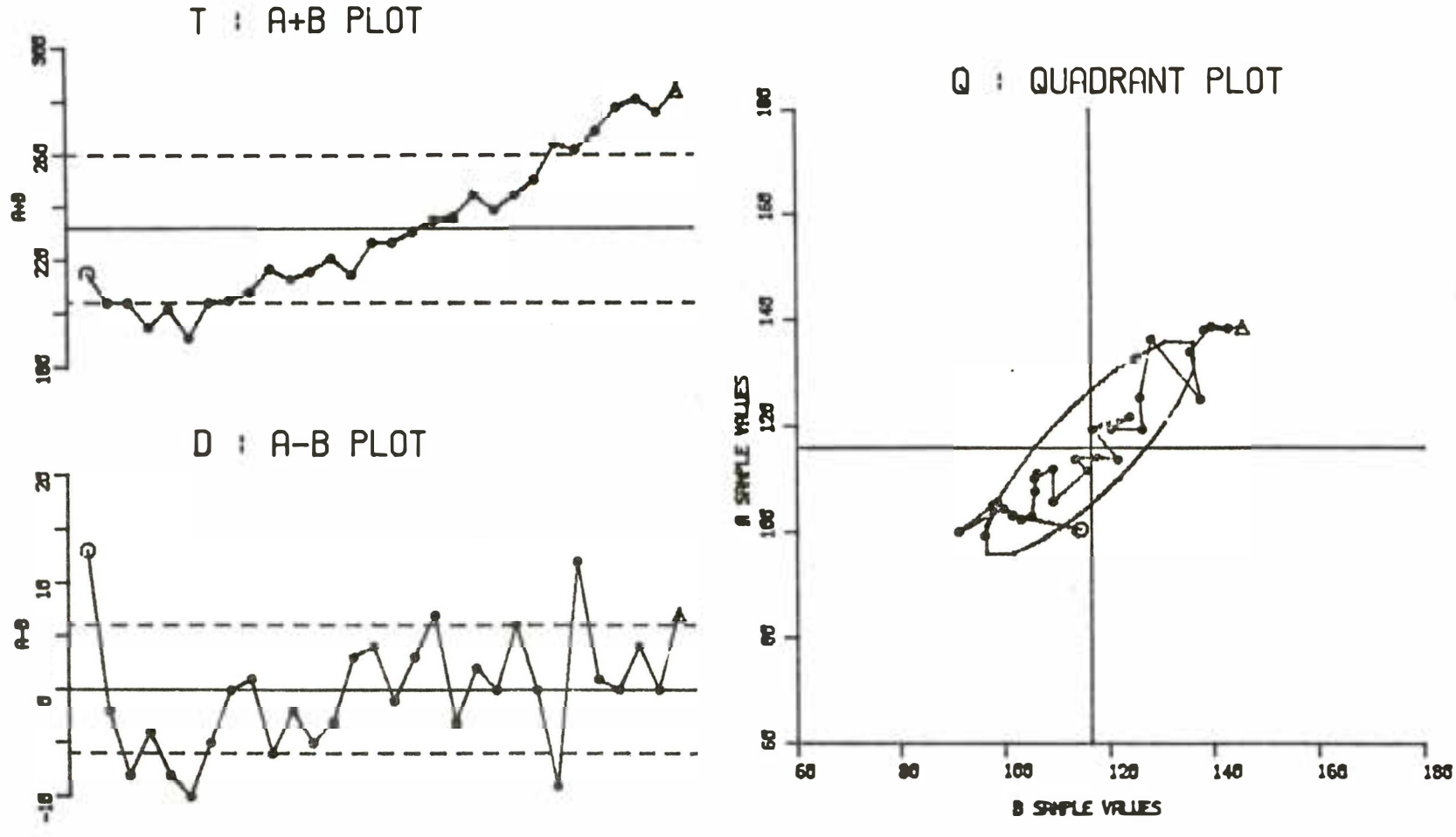

Figure 5.4

SYSTEMATIC ERROR PATTERN : TREND
RANDOM ERROR PATTERN : NONE

COMMENTARY on FIGURE 5.5 (PLATEAU)

Q Plot:

An elliptical distribution indicates that systematic errors are present. The pattern is similar to Figure 5.4; however, the line segments are longer and too many points lie at the ellipse extrema. This indicates two "level" regions in the T plots (early and late). The time sequence connected points show movement from the systematic low quadrant to the systematic high quadrant.

T Plot:

The plot shows a rapid increase followed by a slower upward trend which levels off later in the chart.

D Plot:

Normally distributed random errors are shown with no apparent trend.

Total	RSD =	10.2 %
Random	RSD =	6.6 %
Systematic	RSD =	7.8 %

QUALITY CONTROL PLOTS

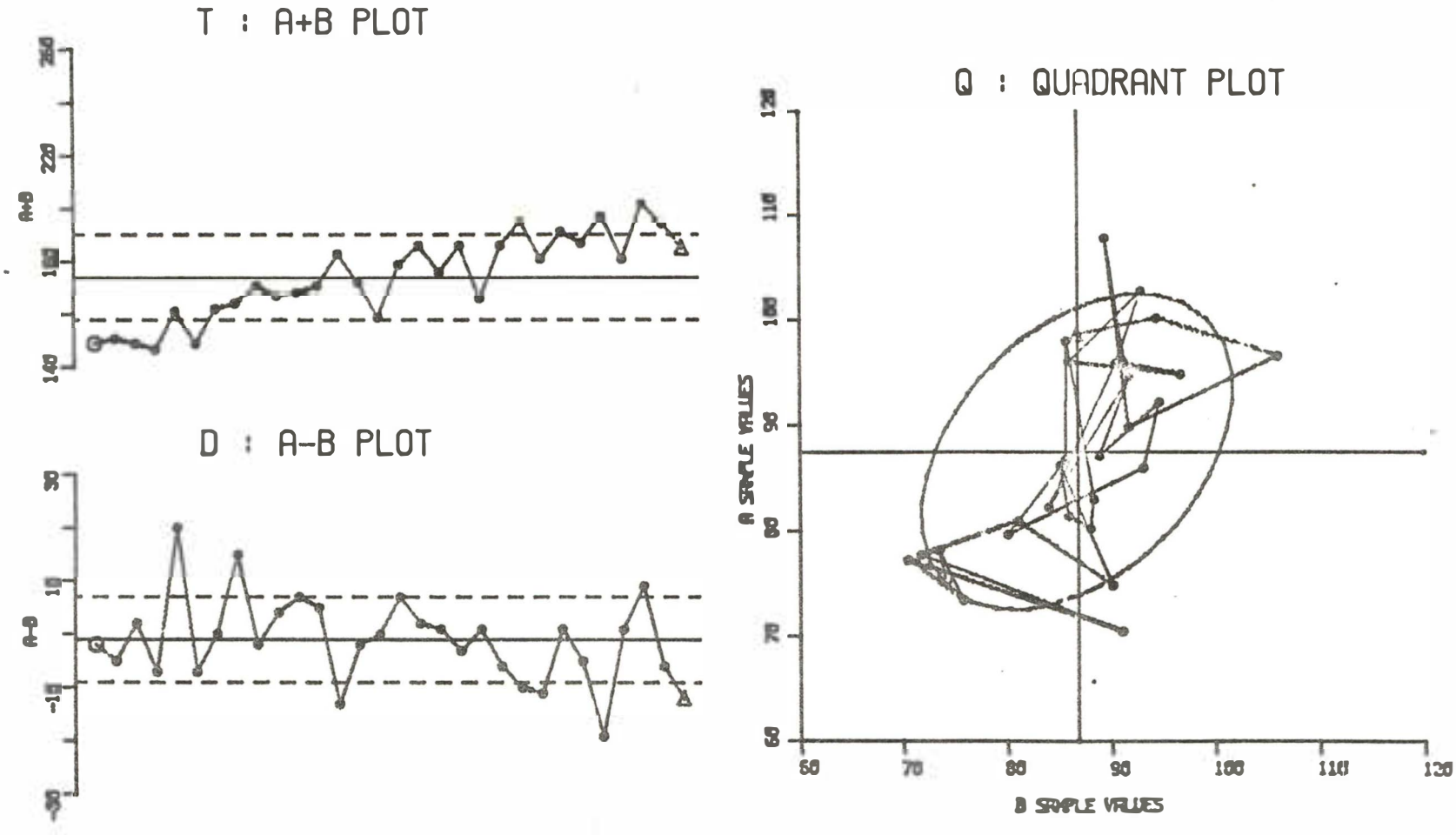

Figure 5.5

SYSTEMATIC ERROR PATTERN : PLATEAU
RANDOM ERROR PATTERN : NONE

COMMENTARY on FIGURE 5.6 (CYCLE)

Q Plot:

Systematic error is evident in the clear ellipticity of the distribution. The time ordered sequence shows a non-random "walk" between systematic error quadrants. An excursion from one systematic quadrant to another and a subsequent return is evident. The distribution is non-normal, with too few points in the central region.

T Plot:

Sinusoidal fluctuation shows clear periodic behavior in the systematic error domain.

D Plot:

Normal distribution of random errors is shown.

Total	RSD = 11.8 %
Random	RSD = 4.5 %
Systematic	RSD = 9.8 %

QUALITY CONTROL PLOTS

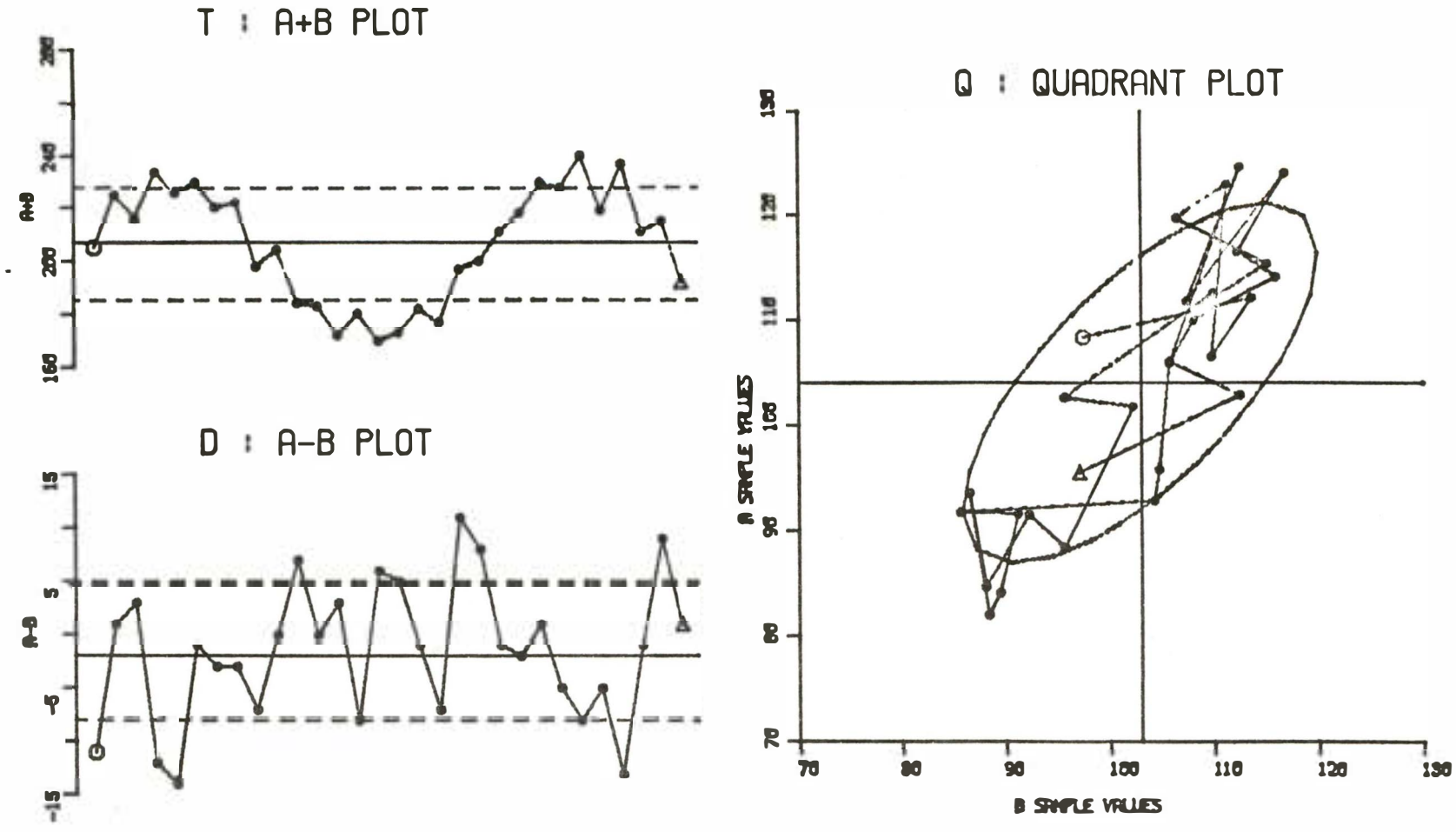

Figure 5.6

SYSTEMATIC ERROR PATTERN : CYCLE
RANDOM ERROR PATTERN : NONE

COMMENTARY on FIGURE 5.7 (BUNCHING)

Q Plot:

The elliptical distribution shows the presence of systematic error. Three dense sub-clusters distinguish this behavior from TREND (Figure 5.4). Note the long 45 degree segments along the systematic error directions. Bunching is characterized by multimodal behavior with fairly dense sub-clusters. The SHIFT shown in Figure 5.3 is a special case of bunching, but a SHIFT generally exhibits only one step change. True bunching behavior tends to reoccur but without the predictable periodicity which characterizes CYCLES. CYCLES do not exhibit the long line segments seen in this plot.

T Plot:

Randomly reoccurring stratification of results about different localized means characterize this plot.

D Plot:

No apparent patterns appear and a random normal distribution is seen.

Total	RSD = 13.2 %
Random	RSD = 4.2 %
Systematic	RSD = 12.5 %

QUALITY CONTROL PLOTS

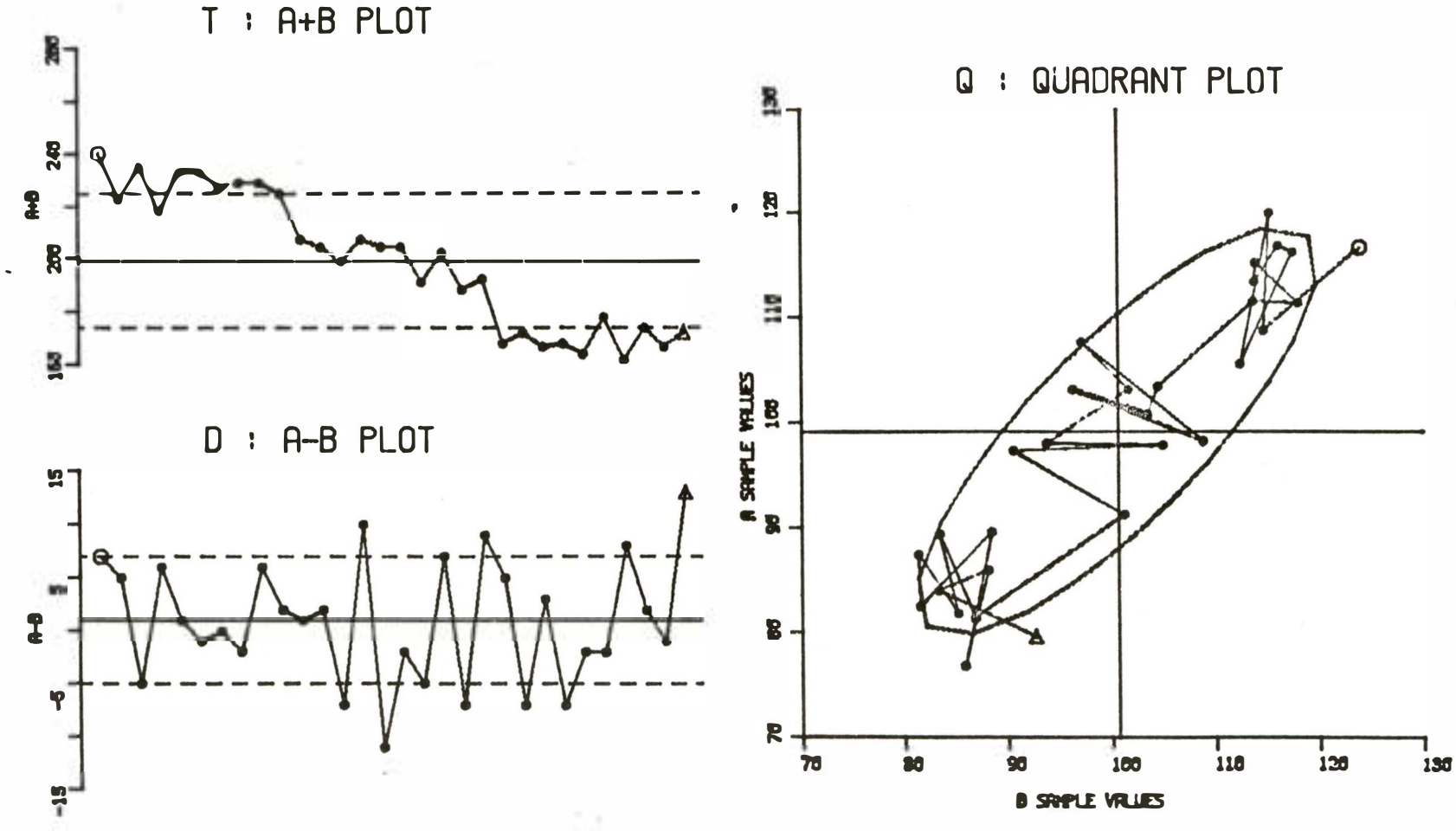

Figure 5.7

SYSTEMATIC ERROR PATTERN : BUNCHING
RANDOM ERROR PATTERN : NONE

5.1.3 **Diagnostic Aides.** Once identified, patterns in the quality control plots can be used to assist in the diagnosis of a problem. Patterns of behavior in the systematic error contribution are more frequent and easy to diagnose. However, pattern complications in both error domains are observed and simultaneous events in both T and D plots can help to isolate the problems. Point-by-point comparisons of T and D plots should be made daily (immediately after the data are generated). Early detection of abnormal behavior reduces the possibility that large numbers of samples will require re-analysis.

T PLOT DIAGNOSTIC AIDS:

FREAKS: Freaks in the T charts generally occur simultaneously with freaks in the D plots. They are generally caused by sudden introduction of bias such as; sample contamination, loss of analyte, calibration standards or reagents gone bad, carelessness or failure to control operating parameters. Some freaks are to be expected in any stochastic process. However, frequently reoccuring anomalies suggest a systematic source for the bias. Carefull scrutiny of operations often reveals an underlying pattern that leads to recurrent freaks (e.g all freaks are produced by a single operator; or all freaks occur on a particular work day, implying an environmental factor.)

SHIFT: Sudden shifts to lower or higher values in the T plot are generally operator related. Different operators may use slightly different procedures that lead to bias. New reagent lots may introduce systematic error through blank contamination or different potency. Sudden undocumented environmental events may change the operational characteristics of the instrument (physical abuse or movement of optically sensitive instruments by janitorial staff has been encountered in some laboratories.)

TREND: Monotonic increases or decreases in the T plot are generally related to changes in calibration standards, or the Q.C. samples themselves. Failure to adequately preserve stored standards or samples will lead to this pattern. Slow constant reagent degradation can also produce the TREND pattern.

PLATEAU: Slow change to higher or lower values in the T plots, with subsequent leveling off to a constant value characterize this pattern. This behavior usually suggests the slow attainment of an equilibrium value. Inadequately stabilized and equilibrated calibration standards or Q.C. samples will lead to this pattern in the T plot. Such patterns are seldom the result of instrumental changes unless the D plot shows a corresponding change in magnitude.

CYCLES: Slow periodic variation of the T plot are usually the result of uncontrolled environmental factors. Seasonal variations related to poor laboratory temperature control have been frequently identified by this pattern. Instruments are seldom sensitive to small ambient temperature changes. However, if an instrument is operating near its suggested

nominal operating temperature; short term excursions from this temperature can affect both accuracy and precision. CYCLES in the T plots are usually accompanied by similar behavior in the D plots.

BUNCHING: The bunching pattern in T plots differ from cycles in two respects; in bunching, the changes precipitous, and they do not have a characteristic repetition frequency. The sudden syatematic error shifts are due to apparently random events. These events are most commonly associated with calibration errors and/or operator technique. Rotation of laboratory personnel can produce this pattern if the individuals follow different procedures. Operator related systematic errors can be detected by plotting points with separate symbols for different operators. Bunching may also appear when reagent lots are changed.